



**KINEMATIC CONTROL BASED ON DUAL QUATERNION ALGEBRA  
AND ITS APPLICATION TO ROBOT MANIPULATORS**

**LUIS FELIPE DA CRUZ FIGUEREDO**

**TESE DE DOUTORADO EM ENGENHARIA ELÉTRICA  
DEPARTAMENTO DE ENGENHARIA ELÉTRICA**

**FACULDADE DE TECNOLOGIA  
UNIVERSIDADE DE BRASÍLIA**



UNIVERSIDADE DE BRASÍLIA  
FACULDADE DE TECNOLOGIA  
DEPARTAMENTO DE ENGENHARIA ELÉTRICA

**KINEMATIC CONTROL BASED ON DUAL QUATERNION ALGEBRA  
AND ITS APPLICATION TO ROBOT MANIPULATORS**

**CONTROLE CINEMÁTICO  
BASEADO NA ÁLGEBRA DE QUATÉRNIOS  
DUAIS E SUA APLICAÇÃO PARA ROBÔS MANIPULADORES**

**LUIS FELIPE DA CRUZ FIGUEREDO**

ORIENTADOR: PROF. JOÃO YOSHIYUKI ISHIHARA  
CO-ORIENTADOR: BRUNO VILHENA ADORNO

TESE DE DOUTORADO EM ENGENHARIA  
DE SISTEMAS ELETRÔNICOS E DE AUTOMAÇÃO

PUBLICAÇÃO: PPGEA.TD-110/16

BRASÍLIA/DF: JULHO - 2016

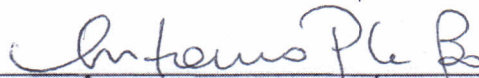
UNIVERSIDADE DE BRASÍLIA  
FACULDADE DE TECNOLOGIA  
DEPARTAMENTO DE ENGENHARIA ELÉTRICA

KINEMATIC CONTROL BASED ON DUAL QUATERNION ALGEBRA  
AND ITS APPLICATION TO ROBOT MANIPULATORS

LUIS FELIPE DA CRUZ FIGUEREDO

TESE DE DOUTORADO SUBMETIDA AO DEPARTAMENTO DE ENGENHARIA ELÉTRICA DA  
FACULDADE DE TECNOLOGIA DA UNIVERSIDADE DE BRASÍLIA, COMO PARTE DOS  
REQUISITOS NECESSÁRIOS PARA A OBTENÇÃO DO GRAU DE DOUTOR.

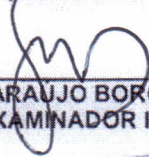
APROVADA POR:



ANTÔNIO PADILHA LANARI BÓ, Dr., ENE/UNB  
(PRESIDENTE)



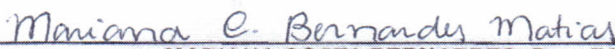
BRUNO VILHENA ADORNO, Dr., UFMG  
(CO-ORIENTADOR)



GEOVANY ARAUJO BORGES, Dr., ENE/UNB  
(EXAMINADOR INTERNO)



FERNANDO CESAR LIZARRALDE, Dr., UFRJ  
(EXAMINADOR EXTERNO)



MARIANA COSTA BERNARDES, Dra., FGA/UNB  
(EXAMINADORA EXTERNA)

EDUARDO STOCKLER TOGNETTI, Dr., ENE/UNB  
(SUPLENTE)

Brasília, 14 de julho de 2016.

## FICHA CATALOGRÁFICA

FIGUEREDO, LUIS FELIPE CRUZ

Kinematic control based on dual quaternion algebra and its application to robot manipulators [Distrito Federal] 2016.

xi+182 p., 210 x 297 mm (ENE/FT/UnB, Doutor, Engenharia Elétrica, 2016).

Tese de doutorado – Universidade de Brasília, Faculdade de Tecnologia.

Departamento de Engenharia Elétrica

1. Dual quaternions

3. Optimal robot manipulation

I. ENE/FT/UnB

2. Robust  $H_{\infty}$  robot manipulation

4. Hybrid controller

II. Título (série)

## REFERÊNCIA BIBLIOGRÁFICA

FIGUEREDO, L. F. C. (2016). Kinematic control based on dual quaternion algebra and its application to robot manipulators, Tese de doutorado, Publicação PPGEA.TD-110/16, Departamento de Engenharia Elétrica, Universidade de Brasília, Brasília, DF, xi+182.

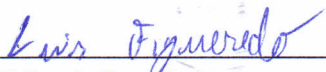
## CESSÃO DE DIREITOS

AUTOR: Luis Felipe da Cruz Figueredo

TÍTULO: Kinematic control based on dual quaternion algebra and its application to robot manipulators.

GRAU: Doutor ANO: 2016

É concedida à Universidade de Brasília permissão para reproduzir cópias desta tese de doutorado e para emprestar ou vender tais cópias somente para propósitos acadêmicos e científicos. O autor reserva outros direitos de publicação e nenhuma parte dessa tese de doutorado pode ser reproduzida sem autorização por escrito do autor.



Luis Felipe da Cruz Figueredo

Departamento de Eng. Elétrica (ENE) - FT

Universidade de Brasília (UnB)

Campus Darcy Ribeiro

CEP 70919-970 - Brasília - DF - Brasil

*To Marina, Maurilio, Jacinta, Ana and Gustavo*

## ACKNOWLEDGMENTS

*This thesis is the result of a long period of work carried out under the guidance, inspiration and support of many. To express my sincere gratitude to the people who during this venture have helped me mold this thesis into a gratifying experience is a great pleasure and the most fulfilling task.*

*First, I would like to express my utter gratitude to Prof. João Y. Ishihara and to Prof. Bruno V. Adorno. I have been fortunate to have, not only one, but two outstanding advisors and its privilege to acknowledge their support and guidance. To João, I am thankful for all the encouragement, knowledge and mostly for the autonomy and confidence placed in me and in my work whilst also being solicitous and supportive. To Bruno, I am foremost grateful for his guidance through the world of robotics and dual quaternions which has led to a paradigm shift in my professional life. I am indebted for his wisdom, friendship and uncountable advices. Both João and Bruno are great sources of inspiration for me. A special thanks goes also for Prof. Adolfo Bauchspiess for introducing me to the world of research.*

*I extend my gratitude towards the members of my thesis committee: Prof. Fernando C. Lizarralde for showing roboticists like myself the practicability of a good theory and for the hard questions which prompted me to widen my research; Prof. Mariana C. Bernardes for her generosity, friendship and insightful comments. Prof. Antonio P. L. Bó for his keen advices on the importance of real-world applications which found their way into the pages of this thesis; and Prof. Geovany A. Borges for his wisdom and, most important, for his arduous work to provide the best possible work conditions for all fellow researches at LARA. I'm also indebted to him for all the opportunities that led me to grow as a researcher.*

*Also, it gives me immense pleasure to thank Prof. Brian C. Williams. First, for accepting me at his group at MIT, but foremost for the wisdom, support and opportunity to work together. The time I spent with the group was essential for my academic and personal growth, and I must also thank Dr. Andreas Hofmann and my fellow colleagues at MERS for this experience—particularly, Dr. Erez Karpas for the encouragement and Pedro Santana for his friendship and willingness to help. Everyone in the group is a little bit responsible for making the Cambridge feel like a second home to me.*

*Moreover, I am very grateful to my fellow labmates at LARA for the stimulating discussions—and, also, for the meaningless—for their fellowship, support and for making the lab a more pleasant and productive place. I thank them also for the short but important moments of procrastination and for the companionship during all nighters before deadlines. Particularly, I would like to mention and thank João V. C. Vilela, Murilo M. Marinho and Hugo T. Kussaba (fellow grad students of mine) for their collaboration in different academic ventures. Also, I thank Hugo for the proofreading assistance on group theory.*

*For their financial support to this thesis, I would also like to thank The Cordenção de Aperfeiçoamento de Pessoal de Nível Superior (CAPES) and The Brazilian National Council for Scientific and Technological Development (CNPq).*

*A special thanks goes to all my friends for understanding my absence and for showing me that there is more to life than control, automation and robotics. Particularly, I am grateful to my dear friends Luis, Fernando, Pedro and Guilherme for their invaluable friendship and for their importance in my life.*

*Finally, but not the least, I would like to thank my amazing family for their love and encouragement. A special thanks goes to my warmhearted beloved parents: Maurilio and Jacinta, and to my loving sister and brother-in-law: Ana and Gustavo for their unconditional love and friendship which undoubtedly shaped me into the person I am today, and for their unrestrictive support which comforted and heartened me during good and harsh times alike. Foremost, I am most grateful to my lovely friend and partner Marina Baldoni Amaral for being always with me, for the adventures and happiness we shared, and for the love and affection which have been paramount for me to achieve my endeavors and for making me feel fulfilled.*



# ABSTRACT

**Title:** Kinematic control based on dual quaternion algebra and its application to robot manipulators

**Author:** Luis Felipe da Cruz Figueredo

**Supervisor:** Prof. João Yoshiyuki Ishihara

**Co-Supervisor:** Prof. Bruno Vilhena Adorno

**Keywords:** *Dual quaternion algebra, Kinematic control, Robust manipulation,  $H_\infty$  control, Optimal manipulation, Task-space optimization, Singularity avoidance, Hybrid systems, Switched systems.*

In the light of the ongoing effort to improve the state-of-the-art in robotics, this thesis's main goal is to contribute to the understanding and advancement of control techniques for robot manipulators. In this context, the present work provides solutions to a number of relevant and challenging task-space kinematic control problems for robot manipulators in the sense of accuracy, robustness, optimality and flexibility. These are cornerstone features required to unfold tools for robots to execute sophisticated tasks deployed at increasingly less controlled scenarios. To support the theory presented herein, this thesis exploits the advantages of the dual quaternion algebra to model and control the robot coupled translation and rotation kinematics.

First, to address the manipulator liability to modeling errors, uncertainties, exogenous disturbances, and their influence upon the robot orientation and translation kinematics, we adapt  $H_\infty$  techniques—suitable solely for additive noises—to dual quaternion algebra. In this sense, we provide an intuitive and elegant connection between performance effects over the end-effector trajectory and different sources of uncertainties and disturbances while satisfying disturbance attenuation properties with minimum instantaneous control effort.

Sharing the dual quaternion advantages, we also propose novel optimal control strategies in dual quaternion task-space. In contrast to standard optimal control techniques, herein, we focus on optimizing task-space variables. In addition to preventing drifts and overshoots, the analysis is particularly relevant to address the challenges for increasing accuracy in scenarios that require precise and safe interaction in contrast to convergence speed—for instance, compliant robots, multiple arms and human-robot interaction where literature shows that controlled speed at task-space largely influences the human acceptance of the contact.

Finally, to cope with reactivity requirements, we introduce a new criterion to enrich the self-motions of robot manipulators. Using a switching control technique, we relax particular task specifications in order to control fewer degrees of freedom while maintaining the end-effector within desired subspaces. As a consequence, the Jacobian nullspace is enlarged with more degrees of freedom to perform additional self-motion tasks.

Departing from the requirements for robustness, optimality and reactivity, this thesis also aims at ensuring proper manipulation throughout the workspace. Singularities intrinsic to the kinematic modeling are addressed both by means of self-motion—which is shown to be valid within the dual quaternion formalism—and using a novel avoidance strategy based on the  $H_\infty$  criteria. The novel solution is suitable for dual quaternion manifold and explicitly regulates the trade-off between exactness and effort of avoiding inescapable singularities. Finally, we also approach the topological obstruction to global stabilization using continuous feedback—inherent to all rigid body representations. In the case of unit dual quaternions, the obstruction is reflected by the unwinding phenomenon that stems from the group double cover. Herein, we propose a switching control law with hysteresis that ensures robust global asymptotic stability within dual quaternion space.

An extensive collection of examples, simulations and experiments are performed to illustrate the effectiveness and relevance of our results. Most important, all the proposed results are supported by rigorous mathematical evidence to ensure accuracy and proper synthesis with practical applications. Therefore, we believe the approaches herein formalize the control theory within unit dual quaternions and improve the state-of-the-art in control of manipulators—contributing to the ongoing effort of unfolding tools for the future of robotics.

## RESUMO

**Título:** Controle cinemático baseado na álgebra de quatérnios duais e sua aplicação para robôs manipuladores

**Autor:** Luis Felipe da Cruz Figueredo

**Orientadore:** Prof. João Yoshiyuki Ishihara

**Co-Orientador:** Prof. Bruno Vilhena Adorno

**Keywords:** *Quatérnios duais, Controle cinemático, Manipulação robusta, Controle  $H_\infty$ , Controle ótimo, Otimização em espaço de tarefas, Prevenção de singularidades, Sistemas híbridos, Controle chaveado.*

O objetivo principal deste trabalho é contribuir para a compreensão e para o avanço das técnicas de controle para robôs manipuladores no contexto de aprimorar o estado-da-arte em robótica. O presente trabalho fornece soluções para uma série de problemas relevantes e desafiadores com ênfase na precisão, robustez, otimização e flexibilidade do controle cinemático no espaço de tarefas. Estas características são essenciais para o desenvolvimento de ferramentas que permitam robôs executarem tarefas sofisticadas em cenários cada vez menos controlados. As contribuições são obtidas a partir da exploração da álgebra de quatérnios duais que é a abordagem escolhida para a modelagem e o controle da cinemática acoplada dos robôs manipuladores.

A fim de defrontar a suscetibilidade de manipuladores com respeito a erros de modelagem, incertezas, distúrbios exógenos e a influência destes na pose do efetuador, adaptamos técnicas de controle  $H_\infty$ —válidas apenas para perturbações aditivas—para a álgebra de quatérnios duais. Assim, obtemos um vínculo intuitivo e elegante entre o desempenho sobre a trajetória do efetuador e diferentes fontes de incertezas e perturbações, ao mesmo tempo que atenuamos perturbações no sentido  $H_\infty$  com o mínimo esforço de controle instantâneo.

A partir da álgebra de quatérnios duais, também propomos novas estratégias de controle ótimo para manipuladores. Em contraste a técnicas clássicas, a otimização foca-se em variáveis do espaço de tarefas. Além de prevenir derrapagens e sobrepassos, esta nova estratégia é particularmente relevante ao lidarmos com os desafios inerentes a cenários que requerem maior precisão e segurança de interação em contraste com velocidade de convergência—é o caso, por exemplo, de robôs complacentes, múltiplos braços e interação homem-robô, onde a velocidade no espaço de tarefas é fator que influencia largamente a aceitação humana ao contato.

A fim de aprimorar a reatividade do manipulador, introduzimos um novo critério que enriquece movimentos no espaço nulo. Utilizando controle chaveado, relaxamos determinadas especificações reduzindo o número de graus de liberdade controláveis, mas mantendo o efetuador dentro de subespaços desejados. Assim, o espaço nulo da Jacobiana é ampliado com mais graus de liberdade possibilitando a execução de tarefas adicionais.

Aparte destes requisitos, visamos igualmente assegurar a manipulação adequada em toda a área de trabalho. Singularidades intrínsecas à cinemática são defrontadas tanto por meio de movimentos no espaço nulo—que mostramos ser válidos no formalismo de quatérnios duais—como através de uma nova estratégia de prevenção com base em critérios  $H_\infty$ . A solução é adequada para a variedade de quatérnios duais e regula explicitamente a compensação entre a exatidão e esforço de prevenção de singularidades inevitáveis. Finalmente, também abordamos a obstrução topológica referente a estabilização global a partir de controladores contínuos—restrição válida para todas as representações de corpos rígidos. No caso de quatérnios duais unitários, a obstrução é representada pela problema de cobertura dupla inerente ao grupo. Neste trabalho, propomos uma lei de controle chaveada com histerese que assegura a estabilidade global robusta e assintótica no espaço de quatérnios duais.

Uma extensa coleção de exemplos, simulações e experimentos são realizados para ilustrar a eficácia e relevância dos resultados. Ademais, e mais importante, os resultados propostos são validados por uma exploração matemática rigorosa a fim de garantir precisão e síntese adequada para aplicações práticas. Assim, o trabalho formaliza a teoria de controle na álgebra de quatérnios duais e aprimora o estado-da-arte de controle para manipuladores—contribuindo com o esforço contínuo para o desenvolvimento da robótica do futuro.

## CONTENTS

---

<b>1</b>	<b>INTRODUCTION</b>	<b>1</b>
1.1	CONTRIBUTIONS	3
<b>2</b>	<b>FUNDAMENTALS FOR KINEMATIC MODELING AND CONTROL OF ROBOT MANIPULATORS</b>	<b>6</b>
2.1	COMPLEX NUMBERS IN GEOMETRY	6
2.1.1	MOST GENERAL COMPLEX NUMBERS	8
2.1.2	DUAL NUMBERS	8
2.2	QUATERNIONS	10
2.2.1	VECTOR ISOMORPHISM AND HAMILTON OPERATORS FOR QUATERNIONS	13
2.3	DUAL QUATERNIONS	14
2.3.1	VECTOR ISOMORPHISM AND HAMILTON OPERATORS FOR DUAL QUATERNIONS	17
2.4	RIGID BODY ATTITUDE	19
2.4.1	ROTATION GROUP $SO(3)$	19
2.4.2	UNIT QUATERNIONS	20
2.5	RIGID BODY POSE REPRESENTATION	24
2.5.1	UNIT DUAL QUATERNIONS	24
2.5.2	THEORETICAL LIMITATIONS FOR GLOBAL STABILITY	27
2.6	RIGID BODY KINEMATICS	28
2.6.1	RIGID BODY ATTITUDE KINEMATICS USING UNIT QUATERNIONS	28
2.6.2	RIGID BODY KINEMATICS USING UNIT DUAL QUATERNIONS	30
2.7	ROBOTIC MANIPULATOR KINEMATICS	30
2.7.1	DUAL QUATERNION FORWARD KINEMATIC MODEL (DQ-FKM)	31
2.7.1.1	D-H CONVENTION TO DUAL QUATERNION FKM	31
2.7.1.2	DIFFERENTIAL FORWARD KINEMATICS USING D-H CONVENTION	32
2.7.1.3	MODIFIED D-H CONVENTION TO DUAL QUATERNION FKM	33
2.7.1.4	DIFFERENTIAL FORWARD KINEMATICS USING MODIFIED D-H CONVENTION	34
2.7.2	DUAL QUATERNION BASED END-EFFECTOR POSE JACOBIAN ( $J_{vec}$ )	35
2.7.3	DUAL QUATERNION JACOBIAN ( $J_{qu}$ )	36
2.7.4	JACOBIAN MATRICES COMPARISON AND KINEMATIC SINGULARITIES	37
2.8	THEORETICAL BACKGROUND ON CONTROL	38
2.8.1	STABILITY ANALYSIS	38
2.8.1.1	EQUILIBRIUM POINTS	38
2.9	LITERATURE REVIEW ON DUAL QUATERNION BASED KINEMATIC CONTROLLERS	41
2.9.1	IN THE CONTROL POINT OF VIEW: DIFFERENCES BETWEEN QUATERNIONS AND DUAL QUATERNIONS	42
<b>3</b>	<b>DUAL QUATERNION BASED ROBUST <math>H_\infty</math> KINEMATIC CONTROL OF MANIPULATOR ROBOTS</b>	<b>44</b>
3.1	MODELING WITH UNCERTAINTIES AND ERROR DEFINITION	45
3.1.1	MANIPULATOR KINEMATIC MODEL WITH UNCERTAINTIES AND EXOGENOUS DISTURBANCES	46

3.1.2	ERROR DEFINITION AND PROBLEM STATEMENT .....	47
3.2	DUAL QUATERNION BASED $H_\infty$ CONTROLLER IN $\mathbb{R}^8$ MANIFOLD .....	48
3.2.1	CONTINUOUS-TIME DUAL QUATERNION BASED $H_\infty$ CONTROLLER IN $\mathbb{R}^8$ MANIFOLD ..	49
3.2.2	DISCRETE-TIME DUAL QUATERNION BASED $H_\infty$ CONTROLLER IN $\mathbb{R}^8$ MANIFOLD .....	53
3.3	$H_\infty$ CONTROLLER IN DUAL QUATERNION SPACE .....	61
3.3.1	DUAL QUATERNION $H_\infty$ CONTROLLER .....	62
3.3.2	DUAL QUATERNION $H_\infty$ TRACKING CONTROLLER .....	65
3.4	NUMERICAL EXAMPLES AND SIMULATIONS .....	66
<b>4</b>	<b>DUAL QUATERNION BASED OPTIMAL CONTROLLER FOR TRAJECTORY TRACK- ING OF ROBOT MANIPULATORS .....</b>	<b>76</b>
4.1	OPTIMAL DUAL QUATERNION BASED CONTROLLER IN $\mathbb{R}^8$ MANIFOLD .....	78
4.2	OPTIMAL QUADRATIC CONTROLLER IN DUAL QUATERNION SPACE .....	82
4.3	COMPUTATION AND PARAMETER SELECTION .....	86
4.4	NUMERICAL EXAMPLES AND SIMULATIONS .....	87
4.4.1	NUMERICAL EXAMPLE: COMAU SMART SIX ROBOT USING MATLAB .....	87
4.4.2	SIMULATED SCENARIO: KUKA LBR IIWA USING V-REP .....	89
4.5	REAL ROBOT EXPERIMENTS .....	94
<b>5</b>	<b><math>H_\infty</math> SINGULARITY AVOIDANCE TECHNIQUE USING DUAL QUATERNIONS.....</b>	<b>102</b>
5.1	SINGULARITY CLASSIFICATION AND EXISTING AVOIDANCE TECHNIQUES .....	103
5.1.1	OVERVIEW ON SINGULARITY AVOIDANCE STRATEGIES .....	105
5.1.1.1	SINGULARITY AVOIDANCE BY SELF-MOTION .....	105
5.1.1.2	PLANNING SINGULARITY FREE TRAJECTORIES.....	106
5.1.1.3	TRAJECTORY MODIFICATION.....	106
5.1.1.4	OTHER SINGULARITY AVOIDANCE STRATEGIES .....	109
5.2	DUAL QUATERNION $H_\infty$ SINGULARITY AVOIDANCE CONTROL .....	110
5.2.1	REDUNDANT ARMS .....	110
5.2.2	NON-REDUNDANT ARMS AND INESCAPABLE SINGULARITIES .....	111
5.3	SIMULATIONS .....	113
<b>6</b>	<b>HYBRID ROBUST KINEMATIC CONTROL FOR GLOBAL STABILITY USING DUAL QUATERNIONS .....</b>	<b>115</b>
6.1	DUAL QUATERNION BASED DISCONTINUOUS CONTROL LAW FOR POSE STABILIZATION ...	116
6.2	HYBRID CONTROL LAW FOR ROBUST GLOBAL RIGID BODY STABILIZATION .....	117
6.2.1	HYBRID CONTROL LAW APPLIED TO ROBOT MANIPULATORS .....	122
6.3	NUMERICAL SIMULATIONS .....	124
<b>7</b>	<b>SWITCHING STRATEGY FOR FLEXIBLE TASK EXECUTION AND ITS APPLICA- TIONS TO BIMANUAL MANIPULATION WITHIN THE COOPERATIVE DUAL TASK- SPACE .....</b>	<b>127</b>
7.1	COOPERATIVE DUAL TASK-SPACE: DESCRIPTION AND CONTROL .....	128
7.1.1	PRIMITIVE CONTROLLABLE SETS .....	130
7.1.2	TASK PRIMITIVE STABILITY .....	132
7.2	SWITCHING CONTROL SCHEME FOR FLEXIBLE COOPERATIVE TASK EXECUTION .....	133
7.2.1	LESS RESTRICTED CONTROLLER DESIGN .....	133

7.2.2 HYSTERESIS-BASED SWITCHING STRATEGY .....	135
7.3 NUMERICAL EXAMPLES.....	137
<b>8 CONCLUSIONS.....</b>	<b>140</b>
<b>A RESUMO ESTENDIDO EM LÍNGUA PORTUGUESA .....</b>	<b>143</b>
<b>B SUMMARY OF DUAL QUATERNION BASED CONTROLLERS.....</b>	<b>148</b>
B.1 CLASSIC CONTROL SOLUTIONS .....	148
B.2 DUAL QUATERNION BASED $H_\infty$ CONTROL SOLUTIONS .....	149
B.3 DUAL QUATERNION BASED OPTIMAL CONTROL SOLUTIONS .....	152
B.4 SWITCHING STRATEGY FOR FLEXIBLE TASK EXECUTION .....	155
<b>C GENERAL PROOFS AND DEFINITIONS.....</b>	<b>157</b>
C.1 GENERAL LYAPUNOV CANDIDATE FUNCTION DERIVATIVE.....	157
C.2 LYAPUNOV CANDIDATE FUNCTION DERIVATIVE IN THE PRESENCE OF DISTURBANCES .....	159
<b>D TABLE OF RESULTS .....</b>	<b>160</b>
D.1 TABLE FROM V-REP SIMULATION USING DUAL QUATERNION OPTIMAL CONTROL THEORY— SUBSECTION 4.4.2 .....	160
<b>E BASIC ALGEBRAIC STRUCTURES .....</b>	<b>163</b>
E.1 ALGEBRAIC PROPERTIES FROM MOST USED SETS AND GROUPS .....	167
<b>F PUBLICATIONS .....</b>	<b>169</b>
<b>G SYSTEM DEMONSTRATIONS - AWARDS.....</b>	<b>171</b>
<b>BIBLIOGRAPHY.....</b>	<b>173</b>

## List of Figures

---

1.1	A demonstration and an illustration of the proposed robust robotic manufacturing assembly concept with a Baxter robot and two Wam arms.....	2
2.1	Denavit-Hartenberg parameters: (a) standard and (b) modified conventions (figure extracted from [1]). .....	32
2.2	Trajectory of the state $x$ over time (dashed line) for an stable equilibrium point (solid green line) [2]......	39
2.3	Geometric representation of the level curves of a Lyapunov function [3]. .....	40
2.4	System with stable equilibrium point $x_e = 0$ in the Lyapunov sense [3]. .....	41
2.5	System with asymptotically stable equilibrium point $x_e = 0$ in the Lyapunov sense [3]. .....	41
3.1	<i>[Example 3.1]</i> Exogeneous disturbance ( <i>green dashed curve</i> ), desired dual quaternion coefficient ( <i>red dash-dotted curve</i> ), and measured dual quaternion coefficient ( <i>black solid curve</i> ). .....	67
3.2	<i>[Example 3.1]</i> Three dimensional position: reference ( <i>black dashed curve</i> ) and measured value ( <i>solid green</i> ).....	67
3.3	<i>[Example 3.1]</i> Plot (a) shows the error norm compared to the exogenous disturbances whereas in (b) it is shown the control effort from the controller compared to a random gain $K$ with similar error norm. ....	68
3.4	<i>[Example 3.2]</i> Setpoint error norm (a) and control effort (b). .....	68
3.5	<i>[Example 3.2]</i> Three-dimensional position and quaternion orientation: reference ( <i>red dashed curve</i> ), measured values from manually chosen controller ( <i>green</i> ) and from Theorem 3.6 ( <i>black</i> ). .....	69
3.6	<i>[Example 3.2]</i> Cartesian position: tracking reference ( <i>red dashed curve</i> ) and measured positions from Theorem 3.6 without the feedforward term, i.e., setpoint control ( <i>green</i> ) and from Theorem 3.6 considering the feedforward term, that is, tracking controller ( <i>black</i> ). .....	69
3.7	<i>[Example 3.3]</i> Screenshot from the simulated task (V-REP platform). .....	70
3.8	<i>[Example 3.3]</i> Setpoint control error.....	71
3.9	<i>[Example 3.3]</i> End-effector translation and orientation for setpoint control: Theorem 3.7 (solid black line), decoupled controller (orange dotted-line), controller from [4] (green dashed line) and from Theorem 3.3 (magenta point-dashed line). .....	72
3.10	<i>[Example 3.3]</i> Tracking error along time: Theorem 3.8 (solid black line), controller from [4] (green dashed line) and from Theorem 3.3 (magenta point-dashed line). .....	73
3.11	<i>[Example 3.3]</i> Joint velocity comparison. ....	73
3.12	<i>[Example 3.4]</i> Screenshot from the simulated task (V-REP platform). .....	73
3.13	<i>[Example 3.4]</i> Control error from Theorem 3.7 for different values of the noise-to-error prescribed upper bound $\gamma$ .....	74
3.14	<i>[Example 3.4]</i> Pose error subjected to multiple disturbances.....	75
4.1	<i>[Numerical example]</i> End-effector translation ( <i>left</i> ) and orientation ( <i>center</i> ), the control effort ( <i>top-right</i> ), and end-effector trajectory ( <i>bottom-right</i> ); using the optimal controller from Theorem 4.1 with different control parameters. The trade-off between error and control effort is noticeable, and the end-effector motion shows no steady-state phase shift in relation to the reference. ....	88

4.2	[Numerical example] End-effector translation ( <i>left</i> ) and orientation ( <i>center</i> ), the control effort ( <i>top-right</i> ), and end-effector trajectory ( <i>bottom-right</i> ); comparing the optimal quadratic controller from Theorem 4.1 with the proportional gain controllers. The initial peak velocity using the proportional controllers is noticeable. Moreover, without the prediction term, the proportional controller has an inherent phase shift in relation to the desired trajectory. ....	89
4.3	[V-REP Simulation] Screenshot of the simulated circular task trajectory using KUKA LBR iiwa.	90
4.4	[V-REP Simulation] Comparison of the error norm between classic proportional (red line) and proportional with feedforward term (green line), and the dual quaternion based optimal controllers from Theorem 4.1 (blue line) and Theorem 4.3 (dark blue line). ....	91
4.5	[V-REP Simulation] Comparison of the control effort as the joint velocity norm between classic proportional (red line) and proportional with feedforward term (green line), and the dual quaternion based optimal controllers from Theorem 4.1 (blue line) and Theorem 4.3 (dark blue line). ....	92
4.6	[V-REP Simulation] Comparison of the control effort in task-space, that is, the norm of the end-effector velocities between classic proportional (red line) and proportional with feedforward term (green line), and the dual quaternion based optimal controllers from Theorem 4.1 (blue line) and Theorem 4.3 (dark blue line). ....	92
4.7	[V-REP Simulation] Comparison of the accelerations norm of the end-effector trajectory between classic proportional (red line) and proportional with feedforward term (green line), and the dual quaternion based optimal controllers from Theorem 4.1 (blue line) and Theorem 4.3 (dark blue line). ....	93
4.8	[V-REP Simulation] Trajectory error norm along time for different Theorem 4.3 dual quaternion optimal control parameters $q$ and $r$ for $\mathbf{Q} = q\mathbf{I}$ , $\mathbf{R} = r\mathbf{I}$ , and $\mathbf{S} = \mathbf{0}$ . ....	93
4.9	[Real robot experiment] Meka A2 compliant arm with seven degrees of freedom (DOF) from Meka Robotics. ....	95
4.10	[Real robot experiment] Control effort: norm of joint velocities (a) and norm of the control signal (b) for the circular trajectory with $r = 0.01$ , $q = 20$ . ....	97
4.11	[Real robot experiment] End-effector three-dimensional translational (a) and quaternion rotational ( $\mathbf{r} = \eta + \mu_1\hat{i} + \mu_2\hat{j} + \mu_3\hat{k}$ ) (b) trajectory along time for the circular trajectory with $r = 0.5$ and $q = 350$ . ....	97
4.12	[Real robot experiment] Control effort: norm of joint velocities (a) and norm of the control signal (b) for the circular trajectory with $r = 0.5$ and $q = 350$ . ....	98
4.13	[Real robot experiment] Control effort in task-space: norm of end-effector velocities (a) and norm of its accelerations (b) for the circular trajectory with $r = 0.5$ and $q = 350$ . ....	98
4.14	[Real robot experiment] Comparison of the error norm between classic proportional (red line) and proportional with feedforward term (green line) with the optimal controller in dual quaternion space from Theorem 4.3 (dark blue line). ....	99
4.15	[Real robot experiment] Comparison of the control effort: joint velocity norm between classic proportional (red line) and proportional with feedforward term (green line) with the optimal controller in dual quaternion space from Theorem 4.3 (dashed dark blue line). ....	100
4.16	[Real robot experiment] Comparison of the control effort in task-space, that is, the norm of the end-effector velocities between classic proportional (red line) and proportional with feedforward term (green line) with the optimal controller in dual quaternion space from Theorem 4.3 (dashed dark blue line). ....	101

4.17	[Real robot experiment] Comparison of the accelerations norm of the end-effector trajectory between classic proportional (red line) and proportional with feedforward term (green line) with the optimal controller in dual quaternion space from Theorem 4.3 (dashed dark blue line). . .	101
5.1	Comparison between singularities and a nonsingular configuration (d) for a 3-DOF manipulator (only 2-D position control): the boundary singularity in (a) prevents movements in self-motion since any joint will displace the end-effector pose; the joint configuration in (b) permits different joints movements without perturbing the end-effector position (that coincides with the base) but the movements are performed along the singular region; the manipulator configuration in (c) can be reconfigured via the self- motion. ....	104
5.2	A comparison of the damped and undamped least-square solutions as a function of the singular value showing the norm of the joint velocity for a component in the direction for the singular vector associated with the plotted singular value. ....	108
5.3	Joint velocities for a trajectory in the presence of singularities: controller from Theorem 3.3 and Corollary 3.1 without singularity avoidance consideration (green dashed and orange point-dashed lines) compared to Theorem 5.1 (solid black line). ....	113
5.4	Joint velocities for a trajectory in the presence of singularities: controller from Theorem 3.3 with adaptive SRI from [5, 6] (magenta dashed line) compared to Theorem 5.1 (solid black). ....	114
6.1	(a) Trajectory of the rotation unit quaternion $\mathbf{r}$ in terms of $\eta$ and $\boldsymbol{\mu}$ (dashed line) with switches along time between the control laws in (6.2) represented by $s(t)$ . (b) Trajectory of the three-dimensional translation elements $\mathbf{p} = p_1\hat{i} + p_2\hat{j} + p_3\hat{k}$ . ....	117
6.2	(a) Trajectory of the rotation unit quaternion $\mathbf{r}$ in terms of $\eta$ and $\boldsymbol{\mu}$ (dashed line). (b) Trajectory of the three-dimensional translation elements $\mathbf{p} = p_1\hat{i} + p_2\hat{j} + p_3\hat{k}$ . ....	124
6.3	Trajectory of $\eta$ with hybrid feedback controller (6.4) and discontinuous controller (6.2) over time. ....	125
6.4	The number of switches with regard to the hysteresis parameter $\delta$ is shown in (a), while the switches along time $s(t)$ are illustrated in (b) for different values of $\delta$ . ....	125
6.5	Influence of the hysteresis parameter $\delta$ on unwinding— $\eta$ converges to the farther stable point. ....	126
7.1	Cooperative dual task-space representation: the absolute and relative dual positions $\underline{\mathbf{x}}_a$ and $\underline{\mathbf{x}}_r$ completely describe the manipulation task [1]. ....	129
7.2	Illustration of controllable sets from primitive tasks. ....	134
7.3	Given a task defined through the regions of interest, $\mathcal{I}_i, \mathcal{I}_j$ , the valid region (in blue) is amid $\mathfrak{R}_i \cup \mathfrak{R}_j$ . For example, if the initial pose satisfies only $\mathcal{I}_i$ (as in pose C), the active task primitive must be controllable at $\mathfrak{R}_j$ , but may relax the constraint upon $\mathfrak{R}_i$ which can be optimized within the nullspace. ....	136
7.4	Evolution of the error norm for the switched main task $e_i$ . ....	138
7.5	Evolution of the error norm for the secondary task (7.18) using self-motion dynamics (traditional controller in <i>dashed-red</i> and switched scheme in <i>solid-blue</i> ). ....	139
7.6	Evolution of the angle $\beta$ for the cone in (7.17) with switching rule. ....	139
G.1	<i>Outstanding System Demonstration – Honorable Mention ICAPS 2014</i> (June, 2014). ....	171
G.2	<i>Winner of Rethink Robotics Contest for IROS 2014</i> (Sept, 2014).....	172



## List of Tables

---

3.1	<i>[Example 3.3]</i> Percentage of successfully completed tracking task from fifty trials per controller	71
3.2	<i>[Example 3.4]</i> Comparison between theoretical upper bound for the $H_\infty$ performance $(\gamma_\tau, \gamma_o)$ with the numerically calculated noise-to-error attenuation from simulation $(\gamma_{\tau sim}, \gamma_{o sim})$ .....	74
4.1	<i>[V-REP Simulation]</i> Comparison of integral norm ( $\times 10^{-3}$ ) of the trajectory error, joint velocity, and end-effector translation and rotational velocities and accelerations between classic proportional and proportional with feedforward term, and optimal controllers: Theorems 4.1 and 4.3 .....	90
4.2	<i>[Real robot experiment]</i> Comparison of integral norm of the trajectory error, control signal, joint velocity, and end-effector velocities and accelerations between classic proportional and proportional with feedforward term, decoupled controller and dual quaternion based optimal controller from Theorem 4.1—experimental results obtained from the Meka A2 arm for the circular trajectory .....	96
4.3	<i>[Real robot experiment]</i> Comparison of integral norm of the trajectory error, control signal, joint velocity, and end-effector velocities and accelerations between classic proportional and proportional with feedforward term, decoupled controller and dual quaternion based optimal controller from Theorem 4.1—experimental results obtained from the Meka A2 arm for the squared trajectory .....	96
4.4	<i>[Real robot experiment]</i> Comparison of integral norm of the trajectory error, joint velocity, and end-effector velocities and accelerations between classic proportional and proportional with feedforward term, and dual quaternion based optimal controller from Theorem 4.1—experimental results obtained from the Meka A2 arm .....	99
7.1	Control primitives and correspondent task Jacobians .....	130
7.2	Summary of tasks primitives and the corresponding controllable sets .....	132
D.1	Integral norm of the end-effector trajectory error .....	160
D.2	Integral norm of the joint velocity vector .....	160
D.3	Integral norm of the end-effector translational velocity .....	161
D.4	Integral norm of the end-effector rotation velocity .....	161
D.5	Integral norm of the end-effector translational acceleration .....	162
D.6	Integral norm of the end-effector rotation acceleration .....	162
E.1	Summary of algebraic properties from sets and unit groups used in this thesis .....	168

## List of Acronyms and Abbreviations

---

CSAIL	Computer Science and Artificial Intelligence Laboratory
D-H	Devavit-Hartenberg
DOF	Degrees of Freedom
FKM	Forward Kinematics Model
IK	Inverse Kinematics
LARA	Laboratório de Automação e Robótica
MACRO	Mechatronics, Control, and Robotics group
MERS	Model-based Embedded and Robotic Systems group

## List of Symbols and Notations

---

### Basic symbols and notations

In this thesis, the following notation is employed for scalar, vectors and matrices elements:

$a, b, c, \dots$	scalars are represented by lowercase plain letters;
$\mathbf{a}, \mathbf{b}, \mathbf{c}, \dots$	vectors are represented by lowercase bold letters;
$\mathbf{A}, \mathbf{B}, \mathbf{C}, \dots$	matrices are represented by uppercase bold letters.

The only exceptions lie with respect to cost functions, represented by uppercase plain letters  $F$  and  $H$ , and to Lyapunov function candidates, represented by uppercase plain letter  $V$ .

Moreover, throughout the thesis we use the following notation:

$\text{sgn}(\bullet)$	the signal of a given scalar;
$\ \bullet\ $	a generic norm of a function;
$\ \bullet\ _2$	the induced norm $p=2$ of a function (also called, the Euclidean norm);
$\langle \bullet, \bullet \rangle$	the inner product;

### Symbols and notations for vectors and matrices

The regular notation related to vectors and matrices are

$\bullet \times \bullet$	the outer product (also known as the cross-product) between two three-dimensional vectors, or two pure quaternions;
$\{\bullet\}^\times$	the skew symmetric matrix representation for a given vector, such that, $\{\mathbf{v}\}^\times \mathbf{u} = \mathbf{v} \times \mathbf{u}$ and $-\{\mathbf{v}\}^\times = \{\mathbf{v}\}^{\times T}$ , for any given vectors $\mathbf{v}, \mathbf{u}$ ;
$\mathbf{I}$	the identity matrix with appropriate dimensions;
$\mathbf{A}^T$	the transpose of matrix $\mathbf{A}$ ;
$\mathbf{A}^+$	the Moore-Penrose pseudoinverse of matrix $\mathbf{A}$ ;
$\text{tr}(\mathbf{A})$	the trace of matrix $\mathbf{A}$ ;
$\text{diag}(a_1, a_2 \dots, a_n)$	diagonal matrix with the diagonal elements being the scalars $a_1, a_2 \dots, a_n$ ;
$\text{diag}(\mathbf{A}_1, \mathbf{A}_2 \dots, \mathbf{A}_n)$	block diagonal matrix with the diagonal elements being the matrices $\mathbf{A}_1, \dots, \mathbf{A}_n$ ;
$\ \mathbf{v}\ _2$	the induced norm $p=2$ of a vector, known as the Euclidean norm, defined by the square root of the inner product of the vector with itself;
$\ \mathbf{A}\ _2$	the induced norm $p=2$ of a matrix, known as the Euclidean norm, defined by its largest singular value, i.e., the square root of the largest eigenvalue of $\mathbf{A}^T \mathbf{A}$ ;
$\ \bullet\ _F$	the Frobenius norm of a matrix;
$\sigma_m\{\mathbf{A}\}$	the minimum singular value of a matrix $\mathbf{A}$ .

## Quaternion and dual quaternions symbols and notations

The variables  $\hat{i}$ ,  $\hat{j}$  and  $\hat{k}$  denote ordinary complex imaginary units (also known as quaternionic units), whereas the variable  $\varepsilon$  is reserved to denote the nilpotent dual unit.

Similarly to vectors, in this thesis we represent quaternions using lowercase bold letters, whereas dual quaternions are represented by underlined bold variables, that is,

$\mathbf{a}, \mathbf{b}, \mathbf{c}, \dots$	quaternions and pure quaternions are represented by lowercase bold letters;
$\underline{\mathbf{a}}, \underline{\mathbf{b}}, \underline{\mathbf{c}}, \dots$	dual quaternions and pure dual quaternions are represented by lowercase bold underlined letters;
$\mathbf{a}^*$ and $\underline{\mathbf{a}}^*$	the conjugate of quaternion $\mathbf{a}$ and dual quaternion $\underline{\mathbf{a}}$ , respectively;

A set of operators for quaternions and dual quaternions employed throughout this thesis is also represented as follows:

$\text{Re}(\mathbf{a}), \text{Im}(\mathbf{a})$	the real and imaginary components of the quaternion $\mathbf{a}$ , such that, $\mathbf{a} = \text{Re}(\mathbf{a}) + \text{Im}(\mathbf{a})$ ;
$\text{Re}(\underline{\mathbf{a}}), \text{Im}(\underline{\mathbf{a}})$	the real and imaginary components of the dual quaternion $\underline{\mathbf{a}}$ ;
$\mathcal{P}(\underline{\mathbf{a}}), \mathcal{D}(\underline{\mathbf{a}})$	the primary and secondary parts of the dual quaternion $\underline{\mathbf{a}}$ , such that, $\underline{\mathbf{a}} = \mathcal{P}(\underline{\mathbf{a}}) + \mathcal{D}(\underline{\mathbf{a}})\varepsilon$ ;
$\text{vec}_3 \mathbf{a}$ and $\text{vec}_4 \mathbf{a}$	the vector space isomorphism mapping from pure quaternions and quaternions to $\mathbb{R}^3$ and $\mathbb{R}^4$ , respectively;
$\text{vec}_6 \underline{\mathbf{a}}$ and $\text{vec}_8 \underline{\mathbf{a}}$	the vector space isomorphism mapping from pure dual quaternions and dual quaternions to $\mathbb{R}^6$ and $\mathbb{R}^8$ , respectively;
$\text{vec}$	the inverse vector space mapping from $\mathbb{R}^n$ ;
$\overset{+}{\mathbf{H}}_4(\mathbf{a}), \overset{-}{\mathbf{H}}_4(\mathbf{a})$	the Hamilton operator (matrix form of the algebra product) for a quaternion $\mathbf{a}$ , such that $\text{vec}_4(\mathbf{ab}) = \overset{+}{\mathbf{H}}_4(\mathbf{a}) \text{vec}_4 \mathbf{b} = \overset{-}{\mathbf{H}}_4(\mathbf{b}) \text{vec}_4 \mathbf{a}$ ;
$\overset{+}{\mathbf{H}}(\underline{\mathbf{a}}), \overset{-}{\mathbf{H}}(\underline{\mathbf{a}})$	the Hamilton operator (matrix form of the algebra product) for a dual quaternion $\underline{\mathbf{a}}$ , such that $\text{vec}_8(\underline{\mathbf{ab}}) = \overset{+}{\mathbf{H}}(\underline{\mathbf{a}}) \text{vec}_8 \underline{\mathbf{b}} = \overset{-}{\mathbf{H}}(\underline{\mathbf{b}}) \text{vec}_8 \underline{\mathbf{a}}$ .

## Symbols and notations related to sets

$\mathbb{R}$	the set of real numbers;
$\mathbb{R}^n$	the set composed of $n$ -tuples of real numbers $(x_1, x_2, \dots, x_n)$ for $x_i \in \mathbb{R}$ , $i = \{1, \dots, n\}$ . In vector matrix notation, it can be written as $[x_1 \ x_2 \ \dots \ x_n]^T$ ;
$\mathbb{C}$	the set of ordinary complex numbers;

$\mathbb{D}$	the set of dual numbers;
$\mathbb{H}$	the set of quaternions;
$\mathbb{H}_0$	the set of pure quaternions;
$\mathcal{S}^n$	the unit hyper-sphere belonging to $\mathbb{R}^{n+1}$ ;
$\mathcal{S}^3$	the set of quaternions with unit norm, i.e. the unit 3-sphere;
$\mathbb{H} \otimes \mathbb{D}$	the set of dual quaternions;
$\mathbb{H}_0 \otimes \mathbb{D}$	the set of pure dual quaternions;
$\underline{\mathcal{S}}$	the set of dual quaternions with unit norm;
$\mathbb{B}$	the closed unit ball in the Euclidean norm of appropriate dimension;

### Symbols and notations related to groups and algebras

$GL(n, \mathbb{R})$	the $n$ -dimensional general linear group over the field $\mathbb{R}$ ;
$SL(n, \mathbb{R})$	the $n$ -dimensional special linear group over the field $\mathbb{R}$ ;
$SE(n)$	the $n$ -dimensional special Euclidean group;
$SO(n)$	the $n$ -dimensional special orthogonal group;
$SE(3)$	the group of rigid body motions, i.e., the tridimensional special Euclidean group;
$SO(3)$	the group of rigid body rotations, i.e., the tridimensional special orthogonal group;
$\mathfrak{gl}(n, \mathbb{R})$	the Lie algebra associated to the group $GL(n, \mathbb{R})$ ;
$\mathfrak{sl}(n, \mathbb{R})$	the Lie algebra associated to the group $SL(n, \mathbb{R})$ ;
$\mathfrak{se}(n)$	the Lie algebra associated to the group $SE(n)$ ;
$\mathfrak{so}(n)$	the Lie algebra associated to the group $SO(n)$ ;

The Lie group of unit quaternions and unit dual quaternions are denoted by  $\text{Spin}(3)$  and  $\text{Spin}(3) \times \mathbb{R}^3$ .

### Additional symbols and notations

Matrices corresponding to task Jacobians are represented by  $\mathbf{J}$ . Particularly, the task Jacobian that maps the joint velocity vector to an  $\mathbb{R}^8$ -representation of the end-effector pose is denoted by  $\mathbf{J}_{\text{vec}}$  whereas the task Jacobian that maps the joint velocity vector to the unit dual quaternion twist is denoted by  $\underline{\mathbf{J}}_{\underline{\mathbf{q}}}$ .

The variable  $\gamma$  is reserved to denote the upper bound of the  $H_\infty$  induced norm. Particularly,  $\gamma_{\mathcal{O}}$  and  $\gamma_{\mathcal{T}}$  are used to denote the noise-to-error upper bound in the  $H_\infty$  sense for the rotation and translational errors, respectively.

# 1

## INTRODUCTION

---

The ongoing research on control, cybernetics and automation brought the robotics field to the edge of a paradigm revolution. The future of robotics is being studied today and moves towards releasing robots from mostly repetitive tasks and bringing them to close, fluid and robust interaction with other robots and humans in less constrained environments.

Since the 18th century industrial revolution to current day, human relation to machinery changed quickly and deeply. From the first digitally operated and programmable robots from Unimation in the fifties and up to complex service and state-of-the-art robots of today, robotics played a significant role in this attitude shift that brought machines closer to humans. With the advance of Lyapunov's control and Kalman's estimation theories, and the development of feedback systems and Wiener's cybernetics systems, robotics flourished as a science of perceiving and manipulating the physical world with computer-based mechanical devices.<sup>1</sup>

There is still plenty to be done in robotics and we are far from the futuristic scenario envisioned by Karel Čapek and Isaac Asimov,<sup>2</sup> but it is a field with enormous potential to change the way we interact with the world and with ourselves. Due to its life-changing characteristics, robotics has increasingly become an interdisciplinary and multidisciplinary field of study, attracting and stimulating research from engineers—control, automation, mechanical, computer, electric, cybernetics, and others engineers—scientists, mathematicians, physicians, psychologists, among others. Despite being a relatively new field of study, robots are currently present in various aspects of the construction of modern life, whether for industrial manufacturing, service robotics, autonomously driven cars, actuated arms that assist surgeons and other medical robotic devices, or robotic platforms for aquatic and planetary exploration.

However, most applications involving robots—particularly, in manufacturing environments—are still generally limited by the following key features: for safety, robots work isolated from humans, they operate in environments that are well structured and fully known, and robots are constrained to performing simple repetitive tasks.

In contrast, robots of tomorrow are expected to execute tasks deployed at increasingly less controlled scenarios where robustness and flexibility become crucial features. In this scenario, robots are supposed to understand different scenes and contexts, navigate in populated and unstructured environments, and work with other robots and with humans. Taking a closer look at the aforementioned problems, even seemingly simple subproblems such as the interpretation of range measurements from a precise laser sensor are often hard to solve due to the complexity of realistic environments and the inherent uncertainties. These uncertainties are propagated to decision, planning and control problems requiring robust responses from each solution.

Motivated by the new challenges that arise from the envisioned scenario and the considerable amount of work to be done to achieve such features, this thesis was developed within the context of the *Towards Robust Robotic Manufacturing* project from the Model-based Embedded and Robotic Systems group (MERS) from the Computer Science and Artificial Intelligence Laboratory (CSAIL) at the Massachusetts Institute of Technology (MIT) in partnership with the Mechatronics, Control, and Robotics research group (MACRO) at the Federal

---

<sup>1</sup>This particular concept of robotics is introduced by Thrun et al. [7]

<sup>2</sup>The term "robot" was first used in a play called "Rossum's Universal Robots" by the Czech writer Karel Čapek to describe intelligent machines that resemble humans and execute complex and undesired tasks. In the forties, Asimov coined the term "robotics" and postulated the famous three laws of robotics.

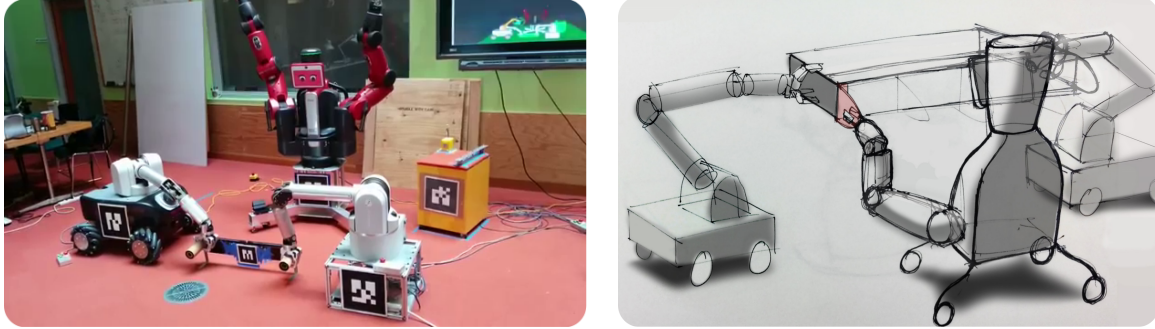


Figure 1.1: A demonstration and an illustration of the proposed robust robotic manufacturing assembly concept with a Baxter robot and two Wam arms.

University of Minas Gerais (UFMG) and the Automation and Robotics Laboratory (LARA) at the University of Brasília. The project and the partnership, funded by Boeing and CNPq-MIT MISTI Global Seed Funds, aimed at pushing the state-of-the art in robotics and developing tools to unfold tomorrow's robotic manufacturing environment. In this framework, teams of robots are expected to collaborate together as peers to leverage their different abilities in order to perform elaborate tasks robustly and efficiently within a semi-structured workplace and likewise to be able to perform tasks with human help. This scenario as depicted in Figure 1.1 highlights task execution that is quite fluid from the robot point of view.

Among the multiple dimensions of this project, this thesis's goal is to contribute to the understanding and advancement of control techniques for robot manipulators in the sense of robustness, optimality and flexibility—cornerstone features for the required level of performance and robotic autonomy. Because the robots must operate in different conditions executing complex and time-varying tasks, the control strategies should allow reactivity. Hence, the present work focused on kinematic control strategies in task-space. Moreover, due to the environment and tasks uncertainties, accurate, optimal, robust and flexible task execution have been the central to this thesis. Supporting this level of robot manipulation still poses challenges and is essential to disclose the envisioned robust robot scenario.

Moreover, to cope with the challenges arising from robust, optimal and flexible control of robot manipulators in the task-space, this thesis exploits the advantages of dual quaternion algebra to model and control the robot coupled translation and rotation kinematics, following the steps and continuing the history introduced in Adorno's work [1]. The use of unit dual quaternions in robotics can be traced back to the works of [8–11], but only in Adorno's work a complete framework for robot kinematic modeling by means of unit dual quaternion is properly formalized. A careful analysis on the contributions stemming from [1] shed some light on its paradigm shift characteristics for rigid body representation in robotics. In this context, and deviating from the challenges inherent from the *Towards Robust Robotic Manufacturing* project, this work also aims at setting foundations for advanced control theory within unit dual quaternions by solving problems intrinsic to the algebra of dual quaternions and to the kinematic structure of robot manipulators, and providing tools that enable complex and sophisticated tasks to be performed robustly and efficiently.

## 1.1 CONTRIBUTIONS

This thesis presents solutions to a number of relevant and hard problems that arise in the field of kinematic control of robot manipulators using unit dual quaternion formalism. Particularly in this thesis, we are interested in addressing the aforementioned challenges that play an important role towards robust robotic manufacturing and the advancement of service robots. Moreover, theoretical and practical aspects of the dual quaternion algebra have been considered and studied in depth. Hence, this thesis also yields results towards a systematization of control techniques within dual quaternion algebra.

First, the following chapter provides for the reader a prelude prior to the contributions that introduces the reader to basic concepts and to the theoretical mathematical background regarding rigid body transformations, quaternion and dual quaternion algebras, robot arm kinematics, and basic control theory. This chapter presents the background needed to understand the concepts proposed in the thesis and sheds a light on the importance of a proper mathematical representation and the advantages that stems from using unit dual quaternions.

Apart from this introduction chapter and the following prelude chapter, this thesis organization and main contributions are outlined as follows:

**Dual quaternion based  $H_\infty$  control design** - In the light of practical robotics applications, Chapter 3 addresses the robot manipulator liability to modeling errors and uncertainties, exogenous disturbances and, most importantly, herein, we focus on robust solutions based on the explicit description of the system requirements into  $H_\infty$  control design problems. The proposed dual quaternion kinematic controllers derived in this chapter explicitly address different sources of uncertainties and disturbances and their influence over the orientation and translation in the  $H_\infty$  sense, which has the advantage of casting aside requirements regarding the distribution description—that are significantly hard to characterize within the group of rigid body transformations. Using the dual quaternion algebra, we adapt classic  $H_\infty$  techniques—suitable solely for additive noises—to derive easy-to-implement closed form  $H_\infty$  setpoint control and tracking strategies that also incorporate robustness requirements, disturbance attenuation, and performance properties, while minimizing the required control effort. The dual quaternion  $H_\infty$  criteria provide an intuitive and elegant connection between control effort and the performance effects over the end-effector trajectory and different sources of uncertainties and disturbances. The efficiency of the proposed controllers are evaluated in simulated scenarios both in Matlab and in the Virtual Robot Experimentation Platform (V-REP) from Coppelia Robotics GmbH.

**Dual quaternion based optimal tracking control** - To address the challenge of increasing the manipulation accuracy in the context of compliant robots and reduced velocity profiles, Chapter 4 addresses the robot manipulator task-space design control problem using unit dual quaternion in the context of optimal control theory. Novel task-space control criteria are proposed in order to find an optimal trajectory for the end-effector in dual quaternion space, providing a tool to balance more conveniently the end-effector error and its task-space velocity. The optimization-based controller extends the results from dual quaternion based controllers—sharing the inherent representation advantages—and provides the designer with a more intuitive set of performance indexes and enlarges the range of applications of the dual quaternion formalism in robotics. In contrast to standard optimal control techniques for manipulators, this chapter focuses in optimizing task-space variables which greatly simplifies the control implementation. As a consequence, we aim at obtaining an optimal result for the end-effector velocity at task-space. The analysis is particularly relevant in advanced manipulation tasks—for instance, manipulation in hazardous or unstructured environments, and multi-arm manipulation—that require precise and safe interaction in contrast to convergence speed. For instance, in the view of human-robot interaction, the speed of the end-effector largely influences the human acceptance of the contact and reduces the



stress and discomfort that arises from the interaction. A controlled speed at task-space also prevents drifts and overshoots caused by large accelerations requirements at the low level controllers. Lastly, to illustrate the efficiency and the reliability from the proposed dual quaternion optimal criteria, we present a set of numerical examples and simulations in different scenarios and evaluate the controllers experimentally in a Meka A2 compliant manipulator.

**Dual quaternion based  $H_\infty$  kinematic singularity avoidance** - In order to ensure proper manipulation capabilities throughout the whole end-effector task-space, Chapter 5 addresses the problem of singularity avoidance for robot manipulators. Singularities play a significant role in design and control of rigid body motion, particularly in the context of robot manipulators. The unit dual quaternion framework—similarly to unit quaternions for pure rotations—provides a escape for utterly describing the coupled kinematics without representation singularities. Still, regardless the rigid motion representation, manipulator tasks are liable to kinematic singularities where specific joint configurations render the differential forward kinematics to be ill-posed which implies in losing one or more degree-of-freedom. To study and avoid kinematic singularities of a manipulator is of great importance since at the neighborhood of these configurations several problems arise due to the Jacobian rank loss. Since most of the singularity avoidance solutions in the literature assume Euclidean task-space representation, this chapter provides tools to address kinematic singularities within dual quaternion space. For redundant manipulators, we prove that existing techniques based on the self-motion (i.e., motions projected on the Jacobian nullspace) can be extended when using the dual quaternion Jacobian and, for non-redundant manipulators, we propose a new singularity avoidance strategy based on the  $H_\infty$  dual quaternion controller derived in Chapter 3, suitable for the non-Euclidean task-space manifold, that explicitly regulates the trade-off between exactness of the solution and avoidance effort for inescapable singularities and non-redundant arms based on the  $H_\infty$  theory.

**Dual quaternion based hybrid robust kinematic control for global stability** - The approaches discussed above all rely on unit dual quaternion framework for utterly describing the manipulator coupled translation and rotation kinematics without representation singularities. Nonetheless, any proper rigid body representation presents a topological obstruction to global stabilization by means of a continuous feedback. Unit dual quaternion representation is no exception. In fact, every rigid body real pose is represented by a pair of antipodal dual quaternion elements which causes the unwinding phenomenon. In this context, using dual quaternion formalism, Chapter 6 addresses the problem of globally stabilizing a rigid body pose. An hybrid strategy is used to design a switching control law with hysteresis in such a way that the global asymptotic stability of the closed-loop system is guaranteed and such that the controller is robust against arbitrary small perturbations. The resulting controller is written in terms of the rigid body twist within unit dual quaternion formalism. Moreover, we adapt the proposed hybrid criterion to global stability in the context of robot manipulators and using the proposed controllers discussed above. Last, using numerical simulations, we illustrate the problems that arise from neglecting the double cover—as unwinding and chattering—and verify the effectiveness of the proposed controller to solve the robust global pose stability problem.

**Dual quaternion flexible task-execution applied to two-arm manipulation** - While the general kinematic task-space control problem has been addressed optimally and robustly concerning uncertainties, disturbances, kinematic singularities and even topological obstruction inherent to any rigid body representation, more dynamic scenarios require additional level of reactivity from the manipulator. In modern control tasks, we are also interested in satisfying secondary constraints such as avoiding joint limits, obstacles and different undesired poses—seldom known a priori. In this sense, self-motion is paramount to unfold the desired task flexibility to unforeseen scenarios by enabling motions of the links without disturbing the end-effector configuration. Still, even seemingly simple problems may demand all available DOFs leaving no room for self-motion.

In this context, Chapter 7 focuses on a novel strategy for enlarging the self-motion by relaxing control specifications according to end-effector's pose pertinence to regions of interest where fewer degrees of freedom are needed. To illustrate the effectiveness of enlarging the nullspace to allow further self-motion operations, the criterion is introduced in the context a two-arm manipulation which better illustrates both the need for further DOF and the advantages of the proposed technique.

The contributions of this thesis exceeds the sum of its individual parts through a portfolio of methods that as a whole pushes the state-of-the-art in control of robot manipulators and unfolds the tools required for sophisticated task execution in the context of robust robotic manufacturing and service robots. In this context, Chapter 8 presents the concluding remarks and perspectives for future works.

# 2

## FUNDAMENTALS FOR KINEMATIC MODELING AND CONTROL OF ROBOT MANIPULATORS

*Every morning on coming downstairs to breakfast, his eldest son would ask him, "Well, Papa, can you multiply triplets?" And each time he had to confess ruefully, "No, I can only add and subtract them.", Hamilton eldest son, [12]*

### 2.1 COMPLEX NUMBERS IN GEOMETRY

The introduction of complex numbers into algebra is connected with the solution of particular quadratic (and irreducible cubic) equations, for instance,  $x^2 + a = 0$ ,  $a > 0$ , [12–14]. The ingenious idea of expressing complex values of the radicals in terms of the square root of minus one ( $\sqrt{-a} = \sqrt{a}\sqrt{-1}$ ) originates from the manuscript *Algebra* (1572) from Rafael Bombelli. The use of the *special number*  $\sqrt{-1}$ —henceforth, to be known as imaginary unit—as to extend the idea of real numbers was only fully understood by William Rowan Hamilton (1805–1865) [15], who expressed such numbers in terms of couples—ordered pairs of real numbers—in almost the same way it is done in modern texts [12]. To ease the description of complex numbers, herein, we denote the imaginary unit as  $i$ , such that,  $i = \sqrt{-1}$  and  $i^2 = -1$ . In this sense, a complex number is composed of two real numbers combined with the imaginary unit.

**Definition 2.1** (Complex Numbers). Let  $\mathbb{C} \triangleq \{x + yi \mid x, y \in \mathbb{R}, i^2 = -1\}$  be the set of complex numbers. A set of elements  $x_\ell + y_\ell i$  are said to be ordinary complex numbers if the operations—addition/subtraction and multiplication—and equality on  $\mathbb{C}$  are defined as follows:

(a) The addition/subtraction operation  $\mathbb{C} \times \mathbb{C} \mapsto \mathbb{C}$  is defined as

$$(x_1 + y_1 i) \pm (x_2 + y_2 i) = (x_1 \pm x_2) + (y_1 \pm y_2) i.$$

(b) The multiplication operation  $\mathbb{C} \times \mathbb{C} \mapsto \mathbb{C}$  is defined as

$$(x_1 + y_1 i)(x_2 + y_2 i) = (x_2 + y_2 i)(x_1 + y_1 i) = x_1 x_2 - y_1 y_2 + (x_1 y_2 + y_1 x_2) i. \quad (2.1)$$

(c) For  $z_1, z_2 \in \mathbb{C}$ , with  $z_1 = x_1 + y_1 i$  and  $z_2 = x_2 + y_2 i$ , the equality  $z_1 = z_2$  on the set  $\mathbb{C}$  is satisfied if and only if  $x_1 = x_2$  and  $y_1 = y_2$ .

In the sense of Definition 2.1, it is clear that real numbers are a particular case of complex numbers, that is, the complex number  $x + yi$  is a real number if  $y = 0$ , that is,  $x + 0i = x \in \mathbb{R}$ . On the other hand, complex numbers  $0 + yi = yi \in \mathbb{C}$  are said to be **pure complex** numbers. To find the result from a division operation between two complex numbers  $z_1, z_2 \in \mathbb{C}$ , we introduce other complex number  $z_2^*$  such that  $z_2 z_2^*$  yields a real number. In this sense, we have

$$\frac{z_1}{z_2} = \frac{z_1}{z_2} \left( \frac{z_2^*}{z_2^*} \right) = \frac{z_1 z_2^*}{z_2 z_2^*}, \quad (2.2)$$

which is basically a complex number multiplication followed by a division by a real number.<sup>1</sup> According to the Definition 2.1, a convenient choice for  $z_2^*$  is simply the complex number  $(x - yi)$ —called **conjugate** of the complex number  $z_2$ —which yields a positive real number after complex number multiplications, that is,  $z_2 z_2^* = z_2^* z_2 = (x^2 + y^2) \in \mathbb{R}$ . The square root of the product, that is,  $\sqrt{x^2 + y^2}$ , is called the **modulus** of  $z_2$ , and the difference between  $z_2$  and its conjugate yields a pure complex number, that is,  $(2y)i$ .

From (2.2), the set of complex numbers can be said to be a division algebra. Hence, according to the Definition 2.1, the set of complex numbers can also be said to be a field over  $\mathbb{R}$ —although a non-ordered field, since the inequality  $z_1 < z_2$  cannot be defined for every element  $z_1, z_2 \in \mathbb{C}$ . The identity element is defined by  $1 + 0i = 1 \in \mathbb{R}$ , whereas the zero element is given by  $0 + 0i = 0 \in \mathbb{R}$ . Thus, for all complex numbers  $z \in \mathbb{C}$ , the following holds  $\frac{z}{z} = 1$  and  $z - z = 0$ .

**Definition 2.2.** Consider an ordinary complex number  $z \in \mathbb{C}$  composed of the real numbers  $x$  and  $y$ , that is,  $z = x + yi$ . The real number  $x$  is said to be the **real part** of  $z$  whereas the real number  $y$  is said to be the **imaginary part** of  $z$ . The values of the real and imaginary parts can be directly extracted from the complex number  $z$  through the respective functions<sup>a</sup>

$$\operatorname{Re}(z) \triangleq x,$$

$$\operatorname{Im}(z) \triangleq yi.$$

In the same way, the complex number  $z$  can be described by  $z = \operatorname{Re}(z) + \operatorname{Im}(z)$ .

<sup>a</sup>In contrast to Definition 2.2, for historic reasons some texts also refer to the imaginary part of  $z$  as  $\operatorname{Im}(z) = y$ .

The absence of a full understanding and a skeptical attitude toward these numbers led to different designation such as “impossible”, “nonexistent”, and—finally—“imaginary” numbers from Descartes’ *Géométrie* in the XVII century [12]—although the notation  $i = \sqrt{-1}$  stems from Euler in the eighteenth century. Indeed, despite different attempts for a proper—and physical—interpretation, such imaginary numbers were only geometrically understood three centuries later by Caspar Wessel—curiously (and understandable), a non-professional mathematician but a surveyor working with maps [14]—although the idea became widely known only after the works of K. F. Gauss and A. Cauchy.

The work of Wessel enlightened the close connection between the theory of complex numbers and the geometrical interpretation of complex numbers as points of a plane [13]. The rectangular Cartesian coordinates  $x, y \in \mathbb{R}$  from one point of a plane—as well as the polar representation with coordinates  $r = \sqrt{x^2 + y^2}$  and  $\varphi = \tan^{-1} \frac{y}{x}$ —corresponds to the complex number  $z \in \mathbb{C}$ ,

$$z = x + yi = r(\cos \varphi + i \sin \varphi),$$

and the algebra involving imaginary numbers is closely related to geometrical transformations on the plane. For example, translation, rotation, dilatation could be obtained with addition, subtraction, and multiplication among imaginary numbers.

<sup>1</sup>It is important to highlight that, similarly to  $\mathbb{R}$ , the division for the zero element 0 is unfeasible and undefined.

## 2.1.1 Most general complex numbers

The employment of imaginary numbers in geometry, and a better understanding of their behavior, influenced eminent mathematicians to study different generalizations of this special set of numbers and its applications to geometry [13]. A general complex number could therefore be expressed by any linear combination of

$$z = x + yE,$$

where  $x, y \in \mathbb{R}$  and addition/subtraction and equality operations are defined as ordinary complex numbers—stressed in Definition 2.1, but with a more general multiplication law, that is, for general complex numbers  $z_1, z_2$ ,

$$z_1 z_2 = z_2 z_1 = (x_1 + y_1 E)(x_2 + y_2 E) = x_1 x_2 + (x_1 y_2 + y_1 x_2)E + y_1 y_2 E^2,$$

where  $E^2$  is also a complex number. In this sense, the general complex number forms an algebraic commutative ring. Nonetheless, applications to geometry would often require a feasible solution for the division operation as in (2.2). Hence, the solution requires a new complex number  $z^*$  such that  $zz^*$  yields a real number. From the multiplication operation, it is clear that feasible solutions must lie within the set  $z^* = \alpha(x - yE)$ , where  $\alpha \in \mathbb{R}$ , and

$$zz^* = \alpha(x^2 - y^2 E^2).$$

For simplicity, let us regard  $\alpha = 1$ . In this case, there exists only three possible solutions for the value of  $E^2$  that yields a real valued number for the general expression, that is, for  $zz^* \in \mathbb{R}$ . The first solution,  $E^2 < 0$ , exploited in (2.1) yields ordinary imaginary numbers, whereas the others are  $E^2 = 0$  and  $E^2 > 0$ . Moreover, any resulting value for the general expression given  $E^2$  can be described by a by a simple linear combination with the set  $\{-1, 0, 1\}$ .

**Definition 2.3.** Given a commutative ring and a conjugate definition, all systems of the most general complex numbers can be reduced to the following three different systems [13]<sup>a</sup>:

$$\begin{cases} \text{Ordinary complex numbers} & E = i, \quad i^2 = -1, \\ \text{Dual numbers} & E = \varepsilon, \quad \varepsilon^2 = 0, \\ \text{Double numbers} & E = e, \quad e^2 = 1. \end{cases}$$

<sup>a</sup>More precisely, all feasible most general complex numbers are isomorphic to ordinary complex, dual, or double numbers when  $E^2 < 0$ ,  $E^2 = 0$ , or  $E^2 > 0$ , respectively.

It is important to emphasize that dual and double numbers differ from the ordinary complex set in the sense of not being a division algebra, since there exist non-null elements that are not invertible.

## 2.1.2 Dual numbers

Dual and double numbers—introduced in the nineteenth century by geometers E. Study and W. Clifford<sup>2</sup> [16]—have no connection to the theory of quadratic equations with real coefficients as the ordinary complex numbers, and their main application usually lies in geometry [13]. Double numbers is usually concerned with

<sup>2</sup>Clifford [16] who was concerned with the use of these numbers in mechanics called them *motors* [13, 16]

the non-Euclidean geometry of Lobachevskii or with pseudo-Euclidean geometry—closely related to the theory of relativity—which is out of the scope of the manuscript. Hence, in this Subsection we will focus our attention to the representation of dual numbers.

Dual numbers are two-dimensional commutative and associative algebra over the real numbers. Similarly to ordinary complex numbers (Definition 2.1), they can be described by the composition of two real numbers with a complex special unit,  $\varepsilon$  for dual numbers. Hence, a dual number can be described by  $\underline{z} = x + y\varepsilon$  for  $x, y \in \mathbb{R}$ .

**Definition 2.4** (Dual Numbers). Let  $\mathbb{D} \triangleq \{x + y\varepsilon \mid x, y \in \mathbb{R}, \varepsilon^2 = 0\}$ <sup>a</sup> be the set of dual numbers. Elements of the form  $\underline{z}_i = x_i + y_i\varepsilon$  composed of the real numbers  $x_i$  and  $y_i$  are said to be dual numbers if the operations—addition/subtraction and multiplication—and equality on  $\mathbb{D}$ , are defined as follows:

(a) The addition/subtraction operation  $\mathbb{D} \times \mathbb{D} \mapsto \mathbb{D}$  is defined as

$$\underline{z}_1 \pm \underline{z}_2 = (x_1 + y_1\varepsilon) \pm (x_2 + y_2\varepsilon) = x_1 \pm x_2 + (y_1 \pm y_2)\varepsilon$$

(b) The multiplication operation  $\mathbb{D} \times \mathbb{D} \mapsto \mathbb{D}$  is defined as

$$\underline{z}_1 \underline{z}_2 = \underline{z}_2 \underline{z}_1 = (x_1 + y_1\varepsilon)(x_2 + y_2\varepsilon) = x_1x_2 + (x_1y_2 + y_1x_2)\varepsilon.$$

(c) The equality on the set  $\mathbb{D}$ , that is  $\underline{z}_1 = \underline{z}_2$ , is satisfied if and only if  $x_1 = x_2$  and  $y_1 = y_2$ .

<sup>a</sup>The element  $\varepsilon$ —called dual unit—extends real numbers to the algebra of dual numbers. It is a nilpotent element (also called nilpotent Clifford unit) defined by  $\varepsilon \neq 0$  and  $\varepsilon^2 = 0$ .

**Definition 2.5.** (From [1]) Let  $\underline{z}$  be a dual number composed of the real numbers  $x$  and  $y$ , that is,  $\underline{z} = x + y\varepsilon$ . The real number  $x$  and  $y$  are said to be the **primary part**  $\mathcal{P}(\underline{z})$  and **dual part**<sup>a</sup>  $\mathcal{D}(\underline{z})$  of  $\underline{z}$ , respectively. Hence, the dual number  $\underline{z}$  can be described by  $\underline{z} = \mathcal{P}(\underline{z}) + \mathcal{D}(\underline{z})\varepsilon$ .

<sup>a</sup>Not to be confused with the real and imaginary parts of an ordinary number defined in Definition 2.2

As stressed, the algebra of dual numbers is a ring with addition/subtraction and multiplication operations as shown in Definition 2.4. Now, similarly to the ordinary complex numbers (2.2), we can derive the division operation based on the element  $\underline{z}^\dagger = \mathcal{P}(\underline{z}) - \mathcal{D}(\underline{z})\varepsilon$ .

*Remark 2.1.* The algebra of dual numbers is a commutative and associative ring. The algebra is not a division algebra—consequently, not a field—since purely complex elements, that is,  $\underline{z} = \mathcal{D}(\underline{z})$  are not invertible. Indeed, according to Definition 2.6 the division operation exists only if  $\mathcal{P}(\underline{z}) \neq 0$ .

Dual numbers, similarly to ordinary complex numbers, have a close connection to geometry theory. The dual numbers representation and algebra can be used to describe and perform linear transformations of oriented lines of a plane, see [13, Section 9] for a detailed description.

**Definition 2.6.** Let  $\underline{a}$  and  $\underline{b}$  be dual numbers with  $\mathcal{P}(\underline{b}) \neq 0$ , the division operation between them is defined by

$$\frac{\underline{a}}{\underline{b}} = \frac{\underline{a}\underline{b}^\dagger}{\underline{b}\underline{b}^\dagger} = \frac{\mathcal{P}(\underline{a})\mathcal{P}(\underline{b})}{\mathcal{P}(\underline{b})^2} + \frac{\mathcal{P}(\underline{b})\mathcal{D}(\underline{a}) - \mathcal{P}(\underline{a})\mathcal{D}(\underline{b})}{\mathcal{P}(\underline{b})^2}\varepsilon;$$

Hence, the inverse of the dual number  $\underline{b}$  is given by

$$\underline{b}^{-1} = \frac{\underline{b}^\dagger}{\underline{b}\underline{b}^\dagger} = \frac{1}{\mathcal{P}(\underline{b})^2} [\mathcal{P}(\underline{b}) - \mathcal{D}(\underline{b})\varepsilon].$$

## 2.2 QUATERNIONS

The study of quaternions can be traced back to the work by William Rowan Hamilton (1805–1865) [15]. Hamilton presents one of the earliest efforts to list systematically the properties of the real number system. In his studies, he excludes complex numbers from ordinary algebra, and defines complex numbers in terms of couples. The excel result led the search for the "Theory of Triplets", which he sought to relate hypercomplex numbers with three-dimensional space just as usual complex numbers are related to two-dimensional space [12], but such possibility has been latter disproved by Ferdinand Georg Frobenius (1849–1917):

**Proposition 2.1.** *There exists no three-dimensional algebra over the field of real numbers that extends the complex numbers. [17, p.3-4]*

*proof.*

Suppose the contrary and let  $(1, \hat{i}, \hat{j})$  be a basis of such algebra, such that  $\hat{i}^2 = -1$  and  $\hat{j}^2 = -1$ . Given the closed property of multiplication in an algebra,  $\hat{i}\hat{j}$  must be given by  $\hat{i}\hat{j} = \alpha_0 + \beta_0\hat{i} + \gamma_0\hat{j}$ , with  $\alpha_0, \beta_0, \gamma_0 \in \mathbb{R}$ . Hence, by multiplying the left side by  $\hat{i}$ , the following must hold

$$\begin{aligned} 0 &= -\hat{i}^2\hat{j} + \hat{i}(\alpha_0 + \beta_0\hat{i} + \gamma_0\hat{j}) = -\hat{i}^2\hat{j} + (\alpha_0\hat{i} - \beta_0 + \gamma_0\hat{i}\hat{j}) \\ &= +\hat{j} + (\alpha_0\hat{i} - \beta_0 + \gamma_0(\alpha_0 + \beta_0\hat{i} + \gamma_0\hat{j})) \\ &= (\alpha_0\gamma_0 - \beta_0) + (\alpha_0 + \beta_0\gamma_0)\hat{i} + (\gamma_0^2 + 1)\hat{j}, \end{aligned}$$

which in turn implies that  $\gamma_0^2 + 1 = 0$ , contradicting that  $\gamma_0 \in \mathbb{R}$ . □

Frustrated by his repeated failure to multiple triplets in a way that would preserve the properties of ordinary complex numbers [12], Hamilton fulfilled his idea with the derivation of quaternion through the ingenious idea of including a new term such that  $\hat{i}\hat{j} = -\hat{j}\hat{i} = \hat{k}$ .

The quaternion algebra, introduced in [18], is composed of the set

$$\mathbb{H} \triangleq \left\{ \mathbf{q} = \eta + \hat{i}\mu_1 + \hat{j}\mu_2 + \hat{k}\mu_3 \mid \eta, \mu_1, \mu_2, \mu_3 \in \mathbb{R}, \hat{i}^2 = \hat{j}^2 = \hat{k}^2 = \hat{i}\hat{j}\hat{k} = -1 \right\}.$$

The algebra is a four dimensional algebra over  $\mathbb{R}$  generated by the quadruple  $(\eta, \mu_1, \mu_2, \mu_3)$  with quaternionic

units  $\hat{i}, \hat{j}, \hat{k}$ , satisfying

$$\begin{aligned}\hat{i}\hat{j} &= -\hat{j}\hat{i} = \hat{k}, \\ \hat{j}\hat{k} &= -\hat{k}\hat{j} = \hat{i}, \\ \hat{k}\hat{i} &= -\hat{i}\hat{k} = \hat{j},\end{aligned}\tag{2.3}$$

being with  $\{1\}$  the basis of this algebra.<sup>3</sup> For the purpose of brevity, quaternion elements may also be denoted by

$$\mathbf{q} = \eta + \boldsymbol{\mu},$$

where  $\boldsymbol{\mu} = \hat{i}\mu_1 + \hat{j}\mu_2 + \hat{k}\mu_3$ .

**Definition 2.7** (Quaternions). Let

$$\mathbb{H} \triangleq \left\{ \eta + \hat{i}\mu_1 + \hat{j}\mu_2 + \hat{k}\mu_3 \mid \eta, \mu_1, \mu_2, \mu_3 \in \mathbb{R}, \hat{i}^2 = \hat{j}^2 = \hat{k}^2 = \hat{i}\hat{j}\hat{k} = -1 \right\}$$

be the set of quaternions, a four dimensional vector space over the real numbers, and let  $\mathbf{q}, \mathbf{q}' \in \mathbb{H}$  belong to this set such that  $\mathbf{q} = \eta + \boldsymbol{\mu}$  and  $\mathbf{q}' = \eta' + \boldsymbol{\mu}'$ . The algebra of quaternions is defined over the binary operations—addition/subtraction, scalar multiplication and multiplication—and equality on  $\mathbb{H}$

(a) The addition/subtraction operation  $\mathbb{H} \times \mathbb{H} \mapsto \mathbb{H}$  is defined as

$$\begin{aligned}\mathbf{q} \pm \mathbf{q}' &= \eta \pm \eta' + \boldsymbol{\mu} \pm \boldsymbol{\mu}' \\ &= (\eta \pm \eta') + \hat{i}(\mu_1 \pm \mu'_1) + \hat{j}(\mu_2 \pm \mu'_2) + \hat{k}(\mu_3 \pm \mu'_3).\end{aligned}$$

(b) The quaternion multiplication operation<sup>a</sup>  $\mathbb{H} \times \mathbb{H} \mapsto \mathbb{H}$  is defined as

$$\begin{aligned}\mathbf{q}\mathbf{q}' &= \left( \eta + \hat{i}\mu_1 + \hat{j}\mu_2 + \hat{k}\mu_3 \right) \left( \eta' + \hat{i}\mu'_1 + \hat{j}\mu'_2 + \hat{k}\mu'_3 \right) \\ &= (\eta\eta' - \mu_1\mu'_1 - \mu_2\mu'_2 - \mu_3\mu'_3) + \hat{i}(\eta\mu'_1 + \mu_1\eta' + \mu_2\mu'_3 - \mu_3\mu'_2) \\ &\quad + \hat{j}(\eta\mu'_2 + \mu_2\eta' + \mu_3\mu'_1 - \mu_1\mu'_3) + \hat{k}(\eta\mu'_3 + \mu_3\eta' + \mu_1\mu'_2 - \mu_2\mu'_1).\end{aligned}$$

(c) For  $\alpha \in \mathbb{R}$ , the scalar multiplication operation  $\mathbb{R} \times \mathbb{H} \mapsto \mathbb{H}$  is a special case of (b) that yields  $\alpha\mathbf{q} = \alpha\eta + \alpha\boldsymbol{\mu}$ .

(d) The equality on the set  $\mathbb{H}$ , that is  $\mathbf{q} = \mathbf{q}'$ , is satisfied if and only if  $\eta_1 = \eta_2$  and  $\mu_1 = \mu'_1$ ,  $\mu_2 = \mu'_2$  and  $\mu_3 = \mu'_3$ .

The zero and the identity elements of the algebra are respectively 0 and 1.

<sup>a</sup>Note that the quaternion multiplication is not commutative, that is,  $\mathbf{q}\mathbf{q}' \neq \mathbf{q}'\mathbf{q}$ .

<sup>3</sup>The quaternion algebra can also be directly derived from the even Clifford algebra  $C^+(\mathbb{R}^3)$  where the quaternionic units  $\hat{i}, \hat{j}, \hat{k}$  are associated with the basis bivectors  $\hat{i} = \mathbf{e}_2\mathbf{e}_3$ ,  $\hat{j} = \mathbf{e}_3\mathbf{e}_1$  and  $\hat{k} = \mathbf{e}_1\mathbf{e}_2$  (see [19, Chapter 4] for further details). In Clifford algebra, the orthonormal basis vectors  $\mathbf{e}_i$  are combined under product operation as follows:  $\mathbf{e}_i\mathbf{e}_j = -\mathbf{e}_j\mathbf{e}_i$ , for  $i \neq j$ , and  $\mathbf{e}_i\mathbf{e}_j = -1$  for  $i = j$ . Therefore, the quaternionic properties described in (2.3) can be obtained directly from Clifford algebra over  $\mathbb{R}$ .



**Definition 2.8.** (From [1]) Let  $q$  be a quaternion element belonging to the set  $\mathbb{H}$  composed of  $(\eta + \mu)$ . The **real component** and the **imaginary component** of  $q$  are defined by the operations

$$\begin{aligned}\operatorname{Re}(q) &\triangleq \eta, \\ \operatorname{Im}(q) &\triangleq \mu,\end{aligned}$$

such that the quaternion  $q$  can also be represented by  $q = \operatorname{Re}(q) + \operatorname{Im}(q)$ .

In the sense of Definition 2.8, quaternion elements with real part equal to zero, that is,  $x = \operatorname{Im}(x)$ , belong to the set of pure quaternions  $\mathbb{H}_0$  and are very convenient to represent vectors of  $\mathbb{R}^3$  within the quaternion formalism by means of a trivial isomorphism.

**Definition 2.9** (Pure quaternions). Let  $\mathbb{H}_0 \triangleq \{q_a \in \mathbb{H} \mid \operatorname{Re}(q_a) = 0\}$  be the set of pure quaternions (a subset of the quaternion set with real part equal to zero). The set can be used to represent vectors of  $\mathbb{R}^3$  within the quaternion formalism by means of a trivial isomorphism, that is,  $\{\mathbb{H}_0, +\} \cong \{\mathbb{R}^3, +\}$ . We define the isomorphism mapping between  $\mathbb{H}_0$  and  $\mathbb{R}^3$  by

$$\operatorname{vec}_3 : \mathbb{H}_0 \mapsto \mathbb{R}^3, \quad (2.4)$$

such that  $q_a = (q_{a1}\hat{i} + q_{a2}\hat{j} + q_{a3}\hat{k})$  yields  $\operatorname{vec}_3 q_a = [q_{a1} \ q_{a2} \ q_{a3}]^T$  from (2.4). The inverse mapping is defined by  $\underline{\operatorname{vec}}_3 : \mathbb{R}^3 \rightarrow \mathbb{H}_0$ .

Both cross product and dot product are defined for elements of  $\mathbb{H}_0$  and they are analogous to their counterparts in  $\mathbb{R}^3$ . More specifically, given  $u, v \in \mathbb{H}_0$ , the inner product  $\langle \cdot, \cdot \rangle$  and the cross product  $\times$  are respectively defined as [1]

$$\langle u, v \rangle \triangleq -\frac{uv + vu}{2} \quad \text{and} \quad u \times v \triangleq \frac{uv - vu}{2}. \quad (2.5)$$

An additional algebraic operation is the conjugate element. The conjugate of a quaternion  $q = \eta + \hat{i}\mu_1 + \hat{j}\mu_2 + \hat{k}\mu_3$  is given by the unique element

$$\begin{aligned}q^* &= \eta - \hat{i}\mu_1 - \hat{j}\mu_2 - \hat{k}\mu_3, \\ &= \eta - \mu,\end{aligned} \quad (2.6)$$

which may define a quaternion involution [20], and satisfies the following properties

$$\begin{cases} \alpha \in \mathbb{R}, q \in \mathbb{H}, & \implies (\alpha q)^* = \alpha q^*, \\ q^* q = 0, q \in \mathbb{H}, & \implies q = 0, \\ q_1, q_2 \in \mathbb{H}, & \implies (q_1 q_2)^* = q_2^* q_1^*. \end{cases}$$

Similar to the algebra of complex numbers (see Subsection 2.1), a consequence—and the objective—of the conjugate definition (2.6) is to yield the square norm  $\|q\|^2 \in \mathbb{R}$  of any arbitrary quaternion  $q \in \mathbb{H}$ ,

$$\begin{aligned}\|q\|^2 &= qq^* = q^*q \\ &= \eta^2 + \mu_1^2 + \mu_2^2 + \mu_3^2.\end{aligned}$$

Hence, the quaternion norm  $\|\mathbf{q}\| \triangleq \sqrt{\eta^2 + \mu_1^2 + \mu_2^2 + \mu_3^2} \in \mathbb{R}$  coincides with the Euclidean norm of a vector  $\begin{bmatrix} \eta & \mu_1 & \mu_2 & \mu_3 \end{bmatrix}^T \in \mathbb{R}^4$ . From the quaternion norm information, we can derive the inverse operation,

$$\mathbf{q}^{-1} = \frac{\mathbf{q}^*}{\|\mathbf{q}\|^2}. \quad (2.7)$$

The algebra of quaternion is therefore a four dimensional associative division algebra<sup>4</sup> over  $\mathbb{R}$  as it can easily be observed from Definition 2.7 and (2.7).

An additional consequence of the conjugate definition is the inner product between two quaternion elements  $\mathbf{h}_1, \mathbf{h}_2 \in \mathbb{H}$ , that is, the mapping  $\mathbb{H} \times \mathbb{H} \rightarrow \mathbb{R}$  of the form

$$\langle \mathbf{h}_1, \mathbf{h}_2 \rangle \triangleq \frac{\mathbf{h}_1 \mathbf{h}_2^* + \mathbf{h}_2 \mathbf{h}_1^*}{2}. \quad (2.8)$$

The algebraic representation of the inner product also implies that  $\langle \mathbf{h}_1, \mathbf{h}_1 \rangle = \|\mathbf{h}_1\|^2$ .

According to Frobenius' Theorem [17, p.21-24], "The only associative and division algebras over the real numbers are (up to isomorphism) the field of real numbers, the field of complex numbers, and the algebra of the quaternions".

## 2.2.1 Vector isomorphism and Hamilton operators for quaternions

As stressed in Definition 2.7, the quaternion multiplication is not commutative. Indeed, from Frobenius' Theorem [17, p.21-24], the algebra of the quaternions can be shown to be the only finite dimensional, associative and division algebra over real numbers which is not commutative. Nonetheless, we may exploit the matrix form of the algebra product (as for any Clifford algebra) to commute terms when performing quaternions multiplications.

First, taking that every  $n$ -dimensional real algebra is vector space isomorphic<sup>5</sup> to  $\mathbb{R}^n$ , we define a isomorphic mapping to  $\mathbb{R}^4$ , that is,

$$\text{vec}_4 : \mathbb{H} \longmapsto \mathbb{R}^4, \quad (2.9)$$

such that for any quaternion  $\mathbf{x}$ , defined as  $\mathbf{x} = x_1 + \hat{i}x_2 + \hat{j}x_3 + \hat{k}x_4$ , the vector space isomorphic mapping (2.9) yields an  $\mathbb{R}^4$  vector defined by  $\text{vec } \mathbf{x} = [x_1 \ x_2 \ x_3 \ x_4]^T$ .

When quaternions are mapped into  $\mathbb{R}^4$ , Hamilton operators (matrix form of the algebra product) can be used to commute terms when performing quaternions multiplications. For the quaternion  $\mathbf{z} = \mathbf{x}\mathbf{y}$ , the Hamilton operators are matrices that satisfy [1, 19, p.21-24]

$$\text{vec}_4 \mathbf{z} = \overset{+}{\mathbf{H}}_4(\mathbf{x}) \text{vec}_4 \mathbf{y} = \overset{-}{\mathbf{H}}_4(\mathbf{y}) \text{vec}_4 \mathbf{x},$$

where

$$\overset{+}{\mathbf{H}}_4(\mathbf{h}) \triangleq \begin{bmatrix} h_1 & -h_2 & -h_3 & -h_4 \\ h_2 & h_1 & -h_4 & h_3 \\ h_3 & h_4 & h_1 & -h_2 \\ h_4 & -h_3 & h_2 & h_1 \end{bmatrix} \quad \text{and} \quad \overset{-}{\mathbf{H}}_4(\mathbf{h}) \triangleq \begin{bmatrix} h_1 & -h_2 & -h_3 & -h_4 \\ h_2 & h_1 & h_4 & -h_3 \\ h_3 & -h_4 & h_1 & h_2 \\ h_4 & h_3 & -h_2 & h_1 \end{bmatrix}. \quad (2.10)$$

<sup>4</sup>Compared to complex numbers, the algebra of quaternions lacks the commutative law property but retains the associative law [12].

<sup>5</sup>See [21, Chapter 8] for further details

In addition, using the definition of conjugate of quaternions, it is easy to show that  $\text{vec}_4 \mathbf{x}^* = \mathbf{C}_4 \text{vec } \mathbf{x}$ , where  $\mathbf{C}_4 = \text{diag}(1, -1, -1, -1)$ .

*Alternative representation:*

It is interesting to highlight that an arbitrary quaternion can also be represented by the vector isomorphism as

$$\text{vec}_4 \mathbf{q} = \begin{bmatrix} \eta \\ \boldsymbol{\mu} \end{bmatrix},$$

where  $\eta \in \mathbb{R}$  denotes the scalar part and  $\boldsymbol{\mu} = [\mu_1 \ \mu_2 \ \mu_3]^T \in \mathbb{R}^3$  its vector part. In this sense, the zero and the identity elements of the quaternion algebra are respectively denoted by  $\text{vec}_4 0 = \begin{bmatrix} 0 & \mathbf{0} \end{bmatrix}^T$  and  $\text{vec}_4 1 = \begin{bmatrix} 1 & \mathbf{0} \end{bmatrix}^T$ . The conjugate element is denoted by  $\text{vec}_4 \mathbf{q}^* = \begin{bmatrix} \eta & -\boldsymbol{\mu}^T \end{bmatrix}^T$ . The quaternion multiplication (group operation) between two elements  $\text{vec}_4 \mathbf{q}_i = \begin{bmatrix} \eta_i & \boldsymbol{\mu}_i^T \end{bmatrix}^T$ ,  $i \in \{1, 2\}$ , is defined as

$$\text{vec}_4 (\mathbf{q}_1 \mathbf{q}_2) = \begin{bmatrix} \eta_1 \eta_2 - \boldsymbol{\mu}_1^T \boldsymbol{\mu}_2 \\ \eta_1 \boldsymbol{\mu}_2 + \eta_2 \boldsymbol{\mu}_1 + \boldsymbol{\mu}_1 \times \boldsymbol{\mu}_2 \end{bmatrix}. \quad (2.11)$$

## 2.3 DUAL QUATERNIONS

The origin of the dual quaternion algebra can be traced back to the work of W. K. Clifford [16] who first derived a broad generalization of real, complex, hypercomplex and quaternion numbers to a new algebra—Clifford algebra. Clifford called the extensions of quaternions as biquaternions. E. Study [22] studied (no pun intended) and redefined this new algebra in the context of rigid body displacements as an extension of quaternions [23], which became to be known as Study biquaternions and latter dual quaternion.<sup>6</sup>

The algebra of dual quaternions is an algebra over  $\mathbb{R}^8$  composed of the set

$$\mathbb{H} \otimes \mathbb{D} = \left\{ \left( \eta + \mu_1 \hat{i} + \mu_2 \hat{j} + \mu_3 \hat{k} \right) + \left( \eta' + \mu'_1 \hat{i} + \mu'_2 \hat{j} + \mu'_3 \hat{k} \right) \varepsilon \mid \eta, \mu_1, \mu_2, \mu_3, \eta', \mu'_1, \mu'_2, \mu'_3 \in \mathbb{R} \right\}$$

where the dual number  $\varepsilon$  is the nilpotent commutative Clifford unit introduced in Definition 2.4. We can also regard the real vector space  $\mathbb{H} \otimes \mathbb{D}$  as a linear combination of the canonical basis vectors from quaternion even Clifford algebra in  $\mathbb{R}^4$  with coefficients in the commutative ring  $\mathbb{D}$  (basically, dual numbers) [24], that is,

$$\underline{\mathbf{q}} = \mathbf{q} + \mathbf{q}' \varepsilon.$$

for  $\underline{\mathbf{q}} \in \mathbb{H} \otimes \mathbb{D}$ . Hence, we can basically extend the basis  $\{1, \hat{i}, \hat{j}, \hat{k}\}$  for  $\mathbb{R}^4$  to the basis  $\{1, 1\varepsilon, \hat{i}, \hat{i}\varepsilon, \hat{j}, \hat{j}\varepsilon, \hat{k}, \hat{k}\varepsilon\}$  for  $\mathbb{R}^8$  using the modulo relation  $\varepsilon^2 = 0$  and the commutative characteristic from  $\varepsilon$ , that is,  $\hat{i}\varepsilon = \varepsilon\hat{i}$ ,  $\hat{j}\varepsilon = \varepsilon\hat{j}$ ,  $\hat{k}\varepsilon = \varepsilon\hat{k}$ . The dual quaternion elements can also be regarded as pairs of elements in  $\mathbb{R}^4$ , and consequently, an element of  $\mathbb{R}^8$  [25].

<sup>6</sup>Since both Eduard Study and William Kingdon Clifford used and wrote about dual quaternions, at times authors refer to dual quaternions as "Study biquaternions" or "Clifford biquaternions". Since the claims of Clifford and Study are in contention, it is convenient to use the current designation dual quaternion to avoid conflict.

**Definition 2.10** (Dual Quaternions). Let  $\mathbb{H} \otimes \mathbb{D} = \{\mathbf{q} + \mathbf{q}'\varepsilon \mid \mathbf{q}, \mathbf{q}' \in \mathbb{H}\}$ , be the set of dual quaternions, a eight dimensional vector space over the real numbers, and let  $\underline{\mathbf{q}}_1 = \mathbf{q}_1 + \mathbf{q}'_1\varepsilon$  and  $\underline{\mathbf{q}}'_2 = \mathbf{q}_2 + \mathbf{q}'_2\varepsilon$  belong to this set. The algebra of dual quaternions is defined over the the binary operations—addition/subtraction, scalar multiplication and multiplication—and equality defined as

(a) The addition/subtraction operation  $\mathbb{H} \otimes \mathbb{D} \times \mathbb{H} \otimes \mathbb{D} \mapsto \mathbb{H} \otimes \mathbb{D}$  is defined as

$$\underline{\mathbf{q}}_1 \pm \underline{\mathbf{q}}_2 = (\mathbf{q}_1 \pm \mathbf{q}_2) + (\mathbf{q}'_1 \pm \mathbf{q}'_2)\varepsilon$$

(b) The dual quaternion multiplication operation<sup>a</sup>  $\mathbb{H} \otimes \mathbb{D} \times \mathbb{H} \otimes \mathbb{D} \mapsto \mathbb{H} \otimes \mathbb{D}$  is defined as

$$\underline{\mathbf{q}}_1 \underline{\mathbf{q}}_2 = \mathbf{q}_1 \mathbf{q}_2 + (\mathbf{q}_1 \mathbf{q}'_2 + \mathbf{q}'_1 \mathbf{q}_2)\varepsilon.$$

(b) For  $\alpha \in \mathbb{R}$ , the scalar multiplication operation  $\mathbb{R} \times \mathbb{H} \mapsto \mathbb{H}$  is a special case of (b) that yields  $\alpha \underline{\mathbf{q}}_1 = \alpha \mathbf{q}_1 + \alpha \mathbf{q}'_1\varepsilon$ .

(d) The equality on the set  $\mathbb{H} \otimes \mathbb{D}$  is satisfied if and only if  $\mathbf{q}_1 = \mathbf{q}_2$  and  $\mathbf{q}'_1 = \mathbf{q}'_2$ .

The zero and the identity elements of the dual quaternion algebra are respectively 0 and 1.

<sup>a</sup>Note that the dual quaternion multiplication is not commutative, that is,  $\underline{\mathbf{q}}_1 \underline{\mathbf{q}}_2 \neq \underline{\mathbf{q}}_2 \underline{\mathbf{q}}_1$ .

**Definition 2.11.** (From [1]) Referring the dual quaternions as pairs of elements in  $\mathbb{R}^4$ , we can define (similarly to Definition 2.2) the **primary part**  $\mathcal{P}(\underline{\mathbf{q}})$  and the **dual part**  $\mathcal{D}(\underline{\mathbf{q}})$  for any given dual quaternion  $\underline{\mathbf{q}} = \mathbf{q} + \mathbf{q}'\varepsilon$  belonging to the set  $\mathbb{H} \otimes \mathbb{D}$ , that is,

$$\begin{aligned} \mathcal{P}(\underline{\mathbf{q}}) &\triangleq \mathbf{q}, \\ \mathcal{D}(\underline{\mathbf{q}}) &\triangleq \mathbf{q}'. \end{aligned}$$

Hence, a dual quaternion element can also be described by  $\underline{\mathbf{q}} = \mathcal{P}(\underline{\mathbf{q}}) + \mathcal{D}(\underline{\mathbf{q}})\varepsilon$ .

In a different manner, we can also decompose  $\mathbb{H} \otimes \mathbb{D}$  into a direct sum of the form  $\mathbb{D} \oplus \mathbb{H}_0 \otimes \mathbb{D}$ , where  $\mathbb{D}$  is the two dimensional real algebra of dual numbers and  $\mathbb{H}_0 \otimes \mathbb{D}$  is a six dimensional real algebra subspace of dual quaternions, also known as pure dual quaternions. To maintain a similar notation from quaternions, the result from this decomposition will be defined as the **real component**<sup>a</sup> and the **imaginary component** of  $\underline{\mathbf{q}}$  and stems from the operations

$$\begin{aligned} \text{Re}(\underline{\mathbf{q}}) &\triangleq \text{Re}(\mathbf{q}) + \text{Re}(\mathbf{q}')\varepsilon = \eta + \eta'\varepsilon, \\ \text{Im}(\underline{\mathbf{q}}) &\triangleq \text{Im}(\mathbf{q}) + \text{Im}(\mathbf{q}')\varepsilon = \boldsymbol{\mu} + \boldsymbol{\mu}'\varepsilon, \end{aligned}$$

such that the dual quaternion can also be represented by  $\underline{\mathbf{q}} = \text{Re}(\underline{\mathbf{q}}) + \text{Im}(\underline{\mathbf{q}})$ .

<sup>a</sup>Note that the operator  $\text{Re}(\cdot)$  yields a dual number and not a real number as Definition 2.2. Still, we will keep the notation to ease the overall manuscript description.

The addition/subtraction and multiplication operations can be described using the primary and dual parts

from the dual quaternion, that is

$$\underline{\mathbf{q}}_1 \pm \underline{\mathbf{q}}_2 = \left[ \mathcal{P}(\underline{\mathbf{q}}_1) \pm \mathcal{P}(\underline{\mathbf{q}}_2) \right] + \left[ \mathcal{D}(\underline{\mathbf{q}}_1) \pm \mathcal{D}(\underline{\mathbf{q}}_2) \right] \varepsilon$$

and

$$\underline{\mathbf{q}}_1 \underline{\mathbf{q}}_2 = \left[ \mathcal{P}(\underline{\mathbf{q}}_1) \mathcal{P}(\underline{\mathbf{q}}_2) \right] + \left[ \mathcal{P}(\underline{\mathbf{q}}_1) \mathcal{D}(\underline{\mathbf{q}}_2) + \mathcal{D}(\underline{\mathbf{q}}_1) \mathcal{P}(\underline{\mathbf{q}}_2) \right] \varepsilon.$$

From Definition 2.11, dual quaternion elements with real part equal to zero, that is,  $\mathbf{x} = \text{Im}(\mathbf{x})$ , belong to the set of pure dual quaternions  $\mathbb{H}_0 \otimes \mathbb{D}$  (also, known as dual vectors). Similar to the relationship between pure quaternions and  $\mathbb{R}^3$ , pure dual quaternions are very convenient to represent vectors of  $\mathbb{R}^6$  within the dual quaternion formalism by means of a trivial isomorphism.

**Definition 2.12** (Pure dual quaternions). Let  $\mathbb{H}_0 \otimes \mathbb{D}$  be the set of pure dual quaternions

$$\mathbb{H}_0 \otimes \mathbb{D} \triangleq \{ \boldsymbol{\mu} + \boldsymbol{\mu}' \varepsilon \mid \boldsymbol{\mu}, \boldsymbol{\mu}' \in \mathbb{H}_0 \}.$$

The algebra of pure dual quaternion (also known as dual vectors) is a six real dimensional subspace of dual quaternions with real part equal to zero, that is  $\{ \underline{\mathbf{q}}_a \in \mathbb{H} \otimes \mathbb{D} \mid \text{Re}(\underline{\mathbf{q}}_a) = 0 \}$ , and can be used to represent vectors of  $\mathbb{R}^6$  within the dual quaternion (or dual vector) formalism by means of a vector space isomorphism between  $\mathbb{H}_0 \otimes \mathbb{D}$  and  $\mathbb{R}^6$  defined by the map

$$\text{vec}_6 : \mathbb{H}_0 \otimes \mathbb{D} \longmapsto \mathbb{R}^6, \quad (2.12)$$

such that pure dual quaternions  $\underline{\mathbf{q}}_a = (\mu_1 \hat{i} + \mu_2 \hat{j} + \mu_3 \hat{k}) + (\mu'_1 \hat{i} + \mu'_2 \hat{j} + \mu'_3 \hat{k}) \varepsilon$  yield six dimensional real vectors  $\text{vec}_6 \underline{\mathbf{q}}_a = [\mu_1 \ \mu_2 \ \mu_3 \ \mu_4 \ \mu_5 \ \mu_6]^T$ . The inverse mapping is defined by  $\text{vec}_6 : \mathbb{R}^6 \rightarrow \mathbb{H}_0 \otimes \mathbb{D}$ . Both cross and dot products are defined for elements of  $\mathbb{H}_0 \otimes \mathbb{D}$ , but differently from the  $\text{vec}_3$  mapping, they are not analogous to their counterparts in  $\mathbb{R}^6$ .

An additional algebraic operation is the conjugate element. The conjugate of a dual quaternion  $\underline{\mathbf{q}} = \mathcal{P}(\underline{\mathbf{q}}) + \mathcal{D}(\underline{\mathbf{q}}) \varepsilon$  is given by the conjugate of the primary and dual quaternion elements

$$\underline{\mathbf{q}}^* = \mathcal{P}(\underline{\mathbf{q}})^* + \mathcal{D}(\underline{\mathbf{q}})^* \varepsilon.$$

The conjugate satisfies the following properties

$$\begin{cases} \alpha \in \mathbb{R}, \underline{\mathbf{q}} \in \mathbb{H} \otimes \mathbb{D}, & \implies (\alpha \underline{\mathbf{q}})^* = \alpha \underline{\mathbf{q}}^*, \\ \underline{\mathbf{q}}^* \underline{\mathbf{q}} = 0, \underline{\mathbf{q}} \in \mathbb{H} \otimes \mathbb{D}, & \implies \mathcal{P}(\underline{\mathbf{q}}) = \mathbf{0}, \\ \underline{\mathbf{q}}_1, \underline{\mathbf{q}}_2 \in \mathbb{H} \otimes \mathbb{D}, & \implies (\underline{\mathbf{q}}_1 \underline{\mathbf{q}}_2)^* = \underline{\mathbf{q}}_2^* \underline{\mathbf{q}}_1^*. \end{cases} \quad (2.13)$$

Analogously to the algebras of complex numbers, dual numbers, and quaternions, the norm operation must be defined using the conjugate multiplication. Nonetheless, according to (2.13), for a nonzero dual quaternion element  $\underline{\mathbf{q}}$  defined with primary part equal to zero—that is,  $\underline{\mathbf{q}} = \mathcal{D}(\underline{\mathbf{q}}) \varepsilon$ —we have  $\underline{\mathbf{q}}^* \underline{\mathbf{q}}$  equal to zero even if for nonzero  $\underline{\mathbf{q}}$ . Hence, similar to quaternions, the algebra of dual quaternions is a eight dimensional associative, but not commutative algebra over  $\mathbb{R}^8$ —although is not a division algebra, as seen in Definition 2.10.<sup>7</sup>

<sup>7</sup>Compared to quaternions, the algebra of dual quaternions is a non-division algebra since it has divisors of zero. In this sense, dual quaternions should not be confused with octonions which defines a division algebra over  $\mathbb{R}^8$ .

Another consequence is that we cannot state a proper norm—which must be strictly positive for non-zero elements—for the dual quaternion algebra. Instead, we define a seminorm—that allows zero values for non-zero dual quaternion elements (in addition to the zero element).

**Definition 2.13.** Let  $\underline{q}$  be a dual quaternion belonging to the set  $\mathbb{H} \otimes \mathbb{D}$ , the seminorm  $\underline{q}$  is given by

$$\begin{aligned}
\|\underline{q}\| &= \sqrt{\underline{q}^* \underline{q}} \\
&= \sqrt{[\mathcal{P}(\underline{q})^* \mathcal{P}(\underline{q})] + [\mathcal{P}(\underline{q})^* \mathcal{D}(\underline{q}) + \mathcal{D}(\underline{q})^* \mathcal{P}(\underline{q})] \varepsilon} \\
&= \sqrt{\|\mathcal{P}(\underline{q})\|^2 + [\mathcal{P}(\underline{q})^* \mathcal{D}(\underline{q}) + (\mathcal{P}(\underline{q})^* \mathcal{D}(\underline{q}))^*] \varepsilon} \\
&= \sqrt{\|\mathcal{P}(\underline{q})\|^2 + 2\langle \mathcal{P}(\underline{q}), \mathcal{D}(\underline{q}) \rangle \varepsilon} \\
&= \sqrt{\left( \|\mathcal{P}(\underline{q})\| + \frac{1}{\|\mathcal{P}(\underline{q})\|} \langle \mathcal{P}(\underline{q}), \mathcal{D}(\underline{q}) \rangle \varepsilon \right)^2} \\
&= \|\mathcal{P}(\underline{q})\| + \frac{\langle \mathcal{P}(\underline{q}), \mathcal{D}(\underline{q}) \rangle}{\|\mathcal{P}(\underline{q})\|} \varepsilon.
\end{aligned}$$

The dual quaternion  $\underline{q}$  has a zero seminorm if and only if  $\|\mathcal{P}(\underline{q})\| = 0$ , while it has unit length if and only if  $\|\mathcal{P}(\underline{q})\|$  is a unit quaternion and  $\mathcal{P}(\underline{q}) \mathcal{D}(\underline{q}) = 0$ .

Note that, as opposed to real quaternions where the quaternion norm coincides with the Euclidean norm, the seminorm of the dual quaternions yields a dual number. Stemming from Definition 2.13, we can also derive the inverse operation.

**Definition 2.14.** Let  $\underline{q}$  be a dual quaternion, the inverse of  $\underline{q}$  is defined by

$$\underline{q}^{-1} = \frac{\underline{q}^*}{\underline{q}^* \underline{q}} = \frac{\underline{q}^*}{\|\underline{q}\|^2},$$

and exists if and only if  $\|\mathcal{P}(\underline{q})\| \neq 0$ . That is, the dual quaternion algebra is not a division algebra as previously stressed.

### 2.3.1 Vector isomorphism and Hamilton operators for dual quaternions

Similar to quaternion algebra, we have that dual quaternion algebra is a non commutative algebra. Hence, dual quaternion multiplication is not commutative, that is, given two dual quaternions  $\underline{x}$  and  $\underline{y}$ , then  $\underline{x}\underline{y} \neq \underline{y}\underline{x}$ . Nonetheless, we may exploit the matrix form of the algebra product (as for any Clifford algebra) to commute terms when performing dual quaternions multiplications.

First, taking that every  $n$ -dimensional real algebra is vector space isomorphic<sup>8</sup> to  $\mathbb{R}^n$ , we define a isomor-

<sup>8</sup>See [21, Chapter 8] for further details

phic mapping to  $\mathbb{R}^8$ , that is,

$$\text{vec}_8 : \mathbb{H} \otimes \mathbb{D} \rightarrow \mathbb{R}^8, \quad (2.14)$$

such that for any dual quaternion  $\underline{x}$ , defined as  $\underline{x} = x_1 + \hat{i}x_2 + \hat{j}x_3 + \hat{k}x_4 + \varepsilon(x_5 + \hat{i}x_6 + \hat{j}x_7 + \hat{k}x_8)$ , the vector space isomorphic mapping (2.14) yields an  $\mathbb{R}^8$  vector defined by  $\text{vec}_8 \underline{x} = [x_1 \ x_2 \ x_3 \ x_4 \ x_5 \ x_6 \ x_7 \ x_8]^T$ .

When dual quaternions are mapped into  $\mathbb{R}^8$  manifold, Hamilton operators (matrix form of the algebra product) can be used to commute terms when performing dual quaternions multiplications. For the dual quaternion  $\underline{z} = \underline{x}\underline{y}$ , the Hamilton operators<sup>9</sup> are matrices that satisfy [1, 19]

$$\text{vec}_8 \underline{z} = \overset{+}{\mathbf{H}}(\underline{x}) \text{vec}_8 \underline{y} = \bar{\mathbf{H}}(\underline{y}) \text{vec}_8 \underline{x},$$

where

$$\overset{+}{\mathbf{H}}(\underline{x}) \triangleq \begin{bmatrix} \overset{+}{\mathbf{H}}_4(\mathcal{P}(\underline{x})) & \mathbf{0}_4 \\ \overset{+}{\mathbf{H}}_4(\mathcal{D}(\underline{x})) & \overset{+}{\mathbf{H}}_4(\mathcal{P}(\underline{x})) \end{bmatrix}, \quad \bar{\mathbf{H}}(\underline{y}) \triangleq \begin{bmatrix} \bar{\mathbf{H}}_4(\mathcal{P}(\underline{y})) & \mathbf{0}_4 \\ \bar{\mathbf{H}}_4(\mathcal{D}(\underline{y})) & \bar{\mathbf{H}}_4(\mathcal{P}(\underline{y})) \end{bmatrix}, \quad (2.15)$$

and the Hamilton operators for an arbitrary quaternion  $\underline{x}$ , that is,  $\overset{+}{\mathbf{H}}_4(\underline{x})$  and  $\bar{\mathbf{H}}_4(\underline{x})$ , are defined in (2.9).

In addition, using the definition of conjugate of dual quaternions it is easy to show that  $\text{vec}_8 \underline{x}^* = \mathbf{C}_8 \text{vec}_8 \underline{x}$ , where  $\mathbf{C}_8 = \text{diag}(1, -1, -1, -1, 1, -1, -1, -1)$ .

*Alternative representation:*

It is interesting to highlight that an arbitrary dual quaternion can also be represented by the vector isomorphism as  $\underline{q} = \underline{q} + \underline{q}'\varepsilon$ , where  $\underline{q} = \begin{bmatrix} \eta & \boldsymbol{\mu}^T \end{bmatrix}^T \in \mathbb{H}$  and  $\underline{q}' = \begin{bmatrix} \eta' & \boldsymbol{\mu}'^T \end{bmatrix}^T \in \mathbb{H}$ ,

$$\text{vec}_8 \underline{q} = \begin{bmatrix} \eta + \boldsymbol{\mu}\varepsilon \\ \eta' + \boldsymbol{\mu}'\varepsilon \end{bmatrix} = \begin{bmatrix} \eta \\ \boldsymbol{\mu} \\ \eta' \\ \boldsymbol{\mu}' \end{bmatrix},$$

where  $\eta, \eta' \in \mathbb{R}$  are respectively the real components of the primary and dual parts, and  $\boldsymbol{\mu}, \boldsymbol{\mu}' \in \mathbb{R}^3$  are the imaginary components of the primary and dual parts, respectively.

In this context, the zero and the identity elements of the dual quaternion algebra are respectively denoted by  $\begin{bmatrix} 0 & \mathbf{0} & 0 & \mathbf{0} \end{bmatrix}^T$  and  $\begin{bmatrix} 1 & \mathbf{0} & 0 & \mathbf{0} \end{bmatrix}^T$ . The conjugate element is thus given by  $\text{vec}_8 \underline{q}^* = \begin{bmatrix} \eta - \boldsymbol{\mu}\varepsilon \\ \eta' - \boldsymbol{\mu}'\varepsilon \end{bmatrix}$ . Within this representation, the dual quaternion multiplication (group operation) between two dual quaternion elements  $\underline{q}_1$  and  $\underline{q}_2$  is defined as

$$\text{vec}_8(\underline{q}_1 \underline{q}_2) = \begin{bmatrix} \eta_1 \eta_2 - \boldsymbol{\mu}_1^T \boldsymbol{\mu}_2 \\ \eta_1 \boldsymbol{\mu}_2 + \eta_2 \boldsymbol{\mu}_1 + \boldsymbol{\mu}_1 \times \boldsymbol{\mu}_2 \\ \eta_1 \eta'_2 + \eta'_1 \eta_2 - \boldsymbol{\mu}_1^T \boldsymbol{\mu}'_2 - (\boldsymbol{\mu}'_1)^T \boldsymbol{\mu}_2 \\ \eta_1 \boldsymbol{\mu}'_2 + \eta'_1 \boldsymbol{\mu}_2 + \eta'_2 \boldsymbol{\mu}_1 + \eta_2 \boldsymbol{\mu}'_1 + \boldsymbol{\mu}_1 \times \boldsymbol{\mu}'_2 + \boldsymbol{\mu}'_1 \times \boldsymbol{\mu}_2 \end{bmatrix}.$$

<sup>9</sup>It is important to highlight that in this manuscript, we are using Hamilton operators with the  $\text{vec}_8$  mapping to the  $\mathbb{R}^8$  manifold, as derived in [1]. In this sense, the Hamilton operators in this manuscript should not be confused with the Hamilton operators defined in [26] which defines the dual matrix form of the algebra product combined with a dual quaternion mapping to  $\mathbb{D} \otimes \mathbb{R}^4$ .

## 2.4 RIGID BODY ATTITUDE

The geometric representation of attitude, that is, the orientation, of a rigid body with respect to another—a reference base—is connected to transformations of coordinate frames theory, that is, it relies on the relationship between coordinates frames rigidly attached to each body [27]. The linear transformation must preserve the distance between each pair of material points in the body and the handedness of the coordinate frames [28–30].

These frames can be defined by three dimensional orthogonal unit vectors ordered according to particular hand rule. Hence, the linear transformation is represented by a  $3 \times 3$  matrix that transforms a vector resolved in the body frame into its representation in the reference frame, that is, the three orthogonal unit basis vectors of the body-fixed frame resolved in the reference frame are represented by the three columns vectors of the representation matrix [30]. In the same manner, the three rows represent the three orthogonal unit basis vectors of the reference frame resolved in the body-fixed frame. In this sense, attitude transformation can be defined by the set of three dimensional orthogonal matrices, which in turn defines a Lie group over matrix multiplication (group operation), the orthogonal group— $O(3)$ .

### 2.4.1 Rotation group $SO(3)$

The algebraic orthogonal group<sup>10</sup>  $O(n, \mathbb{F})$  under matrix multiplication is a  $n \times n$  subgroup of the matrix Lie group  $GL(n, \mathbb{F})$ —general linear group—where the generic set  $\mathbb{F}$  is constrained to orthogonal matrices,

$$O(n, \mathbb{F}) = \left\{ \mathbf{A} \in GL(n, \mathbb{F}) \mid \mathbf{A}^T \mathbf{A} = \mathbf{I} \right\}.$$

Every group element has an inverse defined by its transpose—property inherent to orthogonal matrices [31]—that yields the unique identity element  $\mathbf{I}$ .

To simplify notation, over the field  $\mathbb{R}$  of real numbers, the orthogonal group  $O(n, \mathbb{R})$ —as well as the general linear group  $GL(n, \mathbb{R})$  and its subgroups  $E(n, \mathbb{R})$ ,  $SE(n, \mathbb{R})$ , and  $SO(n, \mathbb{R})$ —will be throughout the manuscript simply denoted by  $O(n)$ —and analogously  $GL(n)$ ,  $E(n)$ ,  $SE(n)$ , and  $SO(n)$ .

The engaging feature—in geometry theory—endowed by the orthogonal group is its relationship to isometries, where an isometry of  $\mathbb{R}^n$  is a distance preserving bijection  $f : \mathbb{R}^n \mapsto \mathbb{R}^n$ , i.e.,  $|f(x) - f(y)| = |x - y|$ ,  $x, y \in \mathbb{R}^n$ . For  $\mathbf{A} \in O(n)$  and vectors  $\mathbf{u}, \mathbf{v}$  in a  $n$ -dimensional real Euclidean space with regard to a fixed point, the isometry condition  $\mathbf{A}\mathbf{u} \cdot \mathbf{A}\mathbf{v} = \mathbf{u} \cdot \mathbf{v}$  is preserved [32, 33]. Hence,  $O(n)$  is the group of distance-preserving transformations of a  $n$ -dimensional Euclidean space, and that is particular interesting given that a rotation about an origin can be defined by a linear transformation that preserves the length of all vectors, i.e., isometry, and orientation, i.e., handedness of the space [34].

Nonetheless, one must note that the determinant of an orthogonal matrix can be either 1 or  $-1$ . In the case of negative determinant, we would have each unit vector reflected through the origin which would yield a reflection operation—roughly speaking a linear transformation that resolves a 180-degree rotation of the orthogonal unit basis vectors of the body frame with regard to the reference frame.

Therefore, the three-dimensional rotation<sup>11</sup> operation must be defined in a subgroup of  $O(3)$  with determinant restricted to 1—this group,  $SO(3)$ , is called the special orthogonal group or rotation group of  $\mathbb{R}^3$ .

<sup>10</sup>See further details about group definition in Appendix E.1.

<sup>11</sup>Note that a rotation can be obtained through two consecutive reflections.



**Definition 2.15** (Rotation group). Consider the set of  $3 \times 3$  real matrices, and let  $GL(3)$  be its subset containing only non-singular matrices. The group of rotations in  $\mathbb{R}^3$ , denoted by  $SO(3)$ , is the Lie group under matrix multiplication of special orthogonal transformations in  $\mathbb{R}^3$

$$SO(3) = \left\{ \mathbf{R} \in GL(3) \mid \mathbf{R}^T \mathbf{R} = \mathbf{I} \text{ and } \det \mathbf{R} = 1 \right\},$$

where  $\mathbf{I}$  is the identity transformation in  $\mathbb{R}^3$  and the inverse operation is defined by the transpose element. The corresponding Lie algebra, denoted,  $\mathfrak{so}(3)$ , is the space of skew-symmetric matrices

$$\mathfrak{so}(3) = \left\{ \mathbf{A} \in \mathfrak{gl}(3, \mathbb{R}) \mid \mathbf{A}^T = -\mathbf{A} \text{ and } \text{tr}(\mathbf{A}) = 0 \right\},$$

where  $\mathfrak{gl}(3, \mathbb{R})$  is the Lie algebra corresponding to Lie group  $GL(3)$  and describes the space of linear transformations in  $\mathbb{R}^3$ .

**Definition 2.16** (Rotation group as a rigid transformation). A rotation  $\mathbf{R} \in SO(3)$  is a rigid body transformation in the sense that preserves the length of all vectors and orientation—ensuring that particles in a rigid body can rotate but not translate with respect to each other [35]. In this sense, a rotation  $\mathbf{R}$  maintains the distance and orientation between any two elements of a rigid body,  $p$  and  $q$ , that is,

- Preserves Distance:  $\|\mathbf{R}q - \mathbf{R}p\| = \|q - p\|, \forall q, p \in \mathbb{R}^3,$
- Preserves Orientation:  $\mathbf{R}(q \times p) = \mathbf{R}q \times \mathbf{R}p, \forall q, p \in \mathbb{R}^3.$

Every configuration of a rigid body that is free to rotate relative to the fixed base frame can be identified with a unique rotation matrix  $\mathbf{R} \in SO(3)$ , which can also define a transformation taking coordinates from a point to one frame to another [35].

## 2.4.2 Unit quaternions

In the turn of the nineteenth century, there was a dispute between matrix-vector and quaternion based notations for modern geometry [23]. The quaternion-Clifford algebra lost and quaternion based applications and results were neglected till recently. Particularly, in the last thirty to forty years, unit quaternion based representation has gained considerably attention due to its compactness, efficiency and elegant representation for finite rotations in three-dimensional space [15].

Stemming from the set  $\mathbb{H}$  of quaternions, unit quaternions are elements whose norm is unit, that is, the ones that lies in the subset of unit sphere of three dimensions in  $\mathbb{R}^4$ ,

$$\mathcal{S}^3 \triangleq \{q \in \mathbb{H} \mid \|q\| = 1\},$$

which forms a group under the operation (2.11).

**Definition 2.17** (Unit Quaternions). Let  $\mathcal{S}^3 = \{\mathbf{q} \in \mathbb{H} \mid \|\mathbf{q}\| = 1\}$  be the set of unit quaternions, a subset of the quaternion set  $\mathbb{H}$  constrained to be within the unit sphere of three dimensions in  $\mathbb{R}^4$ . The group of unit quaternions  $\text{Spin}(3)$  is defined under quaternion multiplication operation (see Definition 2.7) with identity element defined by  $\mathbf{1} \triangleq 1$  and inverse element defined by its conjugate (see (2.6)) as to satisfy the following axioms

- (a) Associative: For all  $\mathbf{q}_1, \mathbf{q}_2, \mathbf{q}_3 \in \text{Spin}(3)$ , we have  $(\mathbf{q}_1 \mathbf{q}_2) \mathbf{q}_3 = \mathbf{q}_1 (\mathbf{q}_2 \mathbf{q}_3)$ ;
- (b) Identity: For all unit quaternion element  $\mathbf{q} \in \text{Spin}(3)$ , we have  $\mathbf{q}\mathbf{1} = \mathbf{1}\mathbf{q} = \mathbf{q}$ ;
- (c) Inverse: For all unit quaternion element  $\mathbf{q} \in \text{Spin}(3)$ , there exists an inverse element in  $\text{Spin}(3)$  denoted by  $\mathbf{q}^{-1}$ —which is also defined by the conjugate of  $\mathbf{q}$ , that is,  $\mathbf{q}^*$ —such that

$$\mathbf{q}\mathbf{q}^{-1} = \mathbf{q}\mathbf{q}^* = \mathbf{q}^*\mathbf{q} = \mathbf{1};$$

- (d) Closure: The product from any unit quaternion elements  $\mathbf{q}_1, \mathbf{q}_2 \in \text{Spin}(3)$  yields an unit quaternion element, that is,  $\mathbf{q}_1 \mathbf{q}_2 \in \text{Spin}(3)$ .

The unit quaternion group forms a Lie group whose Lie algebra is given by the quaternions with real components equal to zero—pure quaternions [36] (see Definition 2.9).

Analogously to the way that complex numbers are used to represent rotations in the plane, unit quaternions encapsulates the group of three-dimensional rotations  $SO(3)$  in the sphere. This way, an arbitrary three-dimensional rotation of  $\phi$  (rotation angle) around the orthogonal rotation axis  $\mathbf{n} = n_x \hat{i} + n_y \hat{j} + n_z \hat{k}$  can be represented by the unit quaternion [37]

$$\mathbf{r} = \cos(\phi/2) + \sin(\phi/2)\mathbf{n}.$$

Within unit quaternions, the conjugate element  $\mathbf{r}^* = \cos(\phi/2) - \sin(\phi/2)\mathbf{n}$  also defines the inverse operation; that is,  $\mathbf{r}\mathbf{r}^* = 1$ . Furthermore, the unit quaternion group double covers the rotation group  $SO(3)$ . Therefore, the unit quaternion  $-\mathbf{r}$  also represents the same rotation of  $\mathbf{r}$  [23].

Unit quaternions are very useful either to describe a point by the coordinates of two frames different from each other only by a rotation and to represent a point resulting of a rotation applied to another point of the same frame. First, it is important to highlight that points and translations can be represent by pure quaternions, that is, quaternions with real part equal to zero. This property follows straight from the Definition 2.9 and from the natural isomorphism with  $\mathbb{R}^3$ .

To represent a point  $\mathbf{p}$  in a different frame, consider the pure quaternions  $\mathbf{p}^0$  and  $\mathbf{p}^1$  to be the representation of the point  $\mathbf{p}$  with respect to the frames  $\mathcal{F}_0$  and  $\mathcal{F}_1$ , respectively. If the frame  $\mathcal{F}_1$  is obtained by rotating the former frame by a quaternion  $\mathbf{r}_1^0$ , then the representation of the point in the frame  $\mathcal{F}_1$ , that is,  $\mathbf{p}^1$  is given by the transformation [37]

$$\mathbf{p}^1 = \mathbf{r}_1^{0*} \mathbf{p}^0 \mathbf{r}_1^0. \quad (2.16)$$

This transformation is called frame rotation.

In the same sense, but with a different perspective, let  $\mathbf{p}_0^0$  be a point with respect to a coordinate frame  $\mathcal{F}_0$ . The transformation that corresponds to a rotation within the same coordinate frame yielding to a new point is called a point rotation [37],

$$\mathbf{p}_1^0 = \mathbf{r}_1^0 \mathbf{p}_0^0 \mathbf{r}_1^{0*}. \quad (2.17)$$

The difference between frame rotation and point rotation is a matter of perspective. In the former, observers located at the point will be stationary while the frame moves. Conversely, in point rotation, observers located at the frame will be stationary while the point moves [1].

*Rotation Matrix from Unit Quaternion Elements, and Unit Quaternion Double Cover*

The Lie group of unit quaternions  $\text{Spin}(3)$  can be used to parametrize the group of rotations through the isomorphic mapping defined in (2.9) and (2.4). In this sense, consider the matrix form of the quaternion transformation (2.17) obtained using the mapping to  $\mathbb{R}^n$ ,

$$\text{vec}_4 \mathbf{p}_1^0 = \overset{+}{\mathbf{H}}_4(\mathbf{r}) \overset{-}{\mathbf{H}}_4(\mathbf{r}^*) \text{vec}_4 \mathbf{p}_0^0.$$

Note that the matrix representation from the quaternion rotation  $\mathbf{r} = \mathbf{r}_1^0 = \cos(\phi/2) + \sin(\phi/2)\mathbf{n}$  can be rewritten as

$$\begin{aligned} \overset{+}{\mathbf{H}}_4(\mathbf{r}) &= \begin{bmatrix} \cos(\frac{\phi}{2}) & -\sin(\frac{\phi}{2}) \text{vec}_3^T \boldsymbol{\mu} \\ \sin(\frac{\phi}{2}) \text{vec}_3 \boldsymbol{\mu} & \cos(\frac{\phi}{2}) \mathbf{I} + \sin(\frac{\phi}{2}) \mathbf{S} \end{bmatrix}, \\ \overset{-}{\mathbf{H}}_4(\mathbf{r}^*) &= \begin{bmatrix} \cos(\frac{\phi}{2}) & +\sin(\frac{\phi}{2}) \text{vec}_3^T \boldsymbol{\mu} \\ -\sin(\frac{\phi}{2}) \text{vec}_3 \boldsymbol{\mu} & \cos(\frac{\phi}{2}) \mathbf{I} + \sin(\frac{\phi}{2}) \mathbf{S} \end{bmatrix}. \end{aligned}$$

where  $\mathbf{S} = \{\text{vec}_3 \mathbf{n}\}^\times$  is the skew symmetric matrix from the unit vector  $\text{vec}_3 \mathbf{n}$ . Hence,  $\overset{+}{\mathbf{H}}_4(\mathbf{r}) \overset{-}{\mathbf{H}}_4(\mathbf{r}^*)$  is given by

$$\begin{bmatrix} \cos^2(\frac{\phi}{2}) + \sin^2(\frac{\phi}{2}) \text{vec}_3^T \boldsymbol{\mu} \text{vec}_3 \boldsymbol{\mu} & -\sin^2(\frac{\phi}{2}) \text{vec}_3^T \boldsymbol{\mu} \mathbf{S} \\ -\sin^2(\frac{\phi}{2}) \mathbf{S} \text{vec}_3 \boldsymbol{\mu} & \begin{pmatrix} \sin^2(\frac{\phi}{2}) \text{vec}_3 \boldsymbol{\mu} \text{vec}_3^T \boldsymbol{\mu} + \cos^2(\frac{\phi}{2}) \mathbf{I} \\ +2 \cos(\frac{\phi}{2}) \sin(\frac{\phi}{2}) \mathbf{S} + \sin^2(\frac{\phi}{2}) \mathbf{S}^2 \end{pmatrix} \end{bmatrix}.$$

Note that the expression can be considerably simplified if we consider the identities

$$\begin{aligned} \cos^2(\frac{\phi}{2}) + \sin^2(\frac{\phi}{2}) \text{vec}_3^T \boldsymbol{\mu} \text{vec}_3 \boldsymbol{\mu} &= \|\mathbf{r}\| = 1, \\ \mathbf{S} \text{vec}_3(\boldsymbol{\mu}) &= \text{vec}_3^T(\boldsymbol{\mu}) \mathbf{S} = 0, \\ \text{vec}_3 \boldsymbol{\mu} \text{vec}_3^T \boldsymbol{\mu} &= \mathbf{I} + \{\text{vec}_3 \boldsymbol{\mu}\}^\times{}^2. \end{aligned}$$

Hence,

$$\begin{aligned} \overset{+}{\mathbf{H}}_4(\mathbf{r}) \overset{-}{\mathbf{H}}_4(\mathbf{r}^*) &= \begin{bmatrix} 1 & \mathbf{0}^T \\ \mathbf{0} & \sin^2(\frac{\phi}{2}) (\mathbf{I} + \mathbf{S}^2) + \cos^2(\frac{\phi}{2}) \mathbf{I} + 2 \cos(\frac{\phi}{2}) \sin(\frac{\phi}{2}) \mathbf{S} + \sin^2(\frac{\phi}{2}) \mathbf{S}^2 \end{bmatrix} \\ &= \begin{bmatrix} 1 & \mathbf{0}^T \\ \mathbf{0} & (\cos(\frac{\phi}{2}) \mathbf{I} + \sin(\frac{\phi}{2}) \mathbf{S})^2 + \sin^2(\frac{\phi}{2}) (\mathbf{I} + \mathbf{S}^2) \end{bmatrix}, \end{aligned} \quad (2.18)$$

where  $\mathbf{0}$  is a three dimensional zero vector.

We can find that the  $3 \times 3$  submatrix from (2.18) yields exactly the orthogonal matrix  $\mathbf{R}$  such that  $\text{vec}_3 \mathbf{p}_1^0 = \mathbf{R} \text{vec}_3 \mathbf{p}_0^0$ .

It is however interesting to highlight that the rotation matrix

$$\mathbf{R} = (\cos(\frac{\phi}{2}) \mathbf{I} + \sin(\frac{\phi}{2}) \mathbf{S})^2 + \sin^2(\frac{\phi}{2}) (\mathbf{I} + \mathbf{S}^2)$$

is a quadratic function of the quaternion components. Therefore, the quaternion  $\mathbf{r}$  and  $-\mathbf{r}$  represents the same rotation. The result is a two-to-one covering map from the rotation group.

## Attitude Representation

As the group of rotations is not an Euclidean space, but rather a differentiable manifold [38], attitude control is typically studied using various attitude representations [28–30, 39–41]. Rigid body attitude is often represented using three or four components, and the representation can be defined in an Euclidean space, as in the case of Euler angles, which lie in  $\mathbb{R}^3$ , or non-Euclidean spaces, as in the case of quaternions, which lie in the non-Euclidean three-sphere  $\mathcal{S}^3$ . Nonetheless, due to topological properties of the rotation group  $SO(3)$ , all existing representations fail to represent the set of attitudes both globally and uniquely [29, 30, 42].

Three-parameter representations of attitude include the Euler angles as well as parameters derived from the unit quaternions as in the case of the Rodrigues parameters and the modified Rodrigues parameters. These three-parameter sets can be viewed as embedded subsets of  $\mathbb{R}^3$ , thus allowing methods of analysis that are suited to the Euclidean space  $\mathbb{R}^3$ . Nonetheless, these Euclidean representations will inherently present singularities. For instance, Euler angles can represent every attitude, however this representation is not unique at kinematic singular points—described by a gimbal lock [30]—and yields an unfeasible representation for the time-derivative of the angles; that is, the transformation from their time rates of change to the angular velocity vector is not globally defined. The Rodrigues parameters and modified Rodrigues parameters are geometrically singular since they are not defined for  $180^\circ$  of rotation. Therefore, continuous control laws using these three-parameter representations cannot be globally defined, and, as such, these representations are limited to local attitude maneuvers.

On the other hand, the non-Euclidean space of unit quaternions provides a convenient and efficient mathematical notation for representing orientations and rotations in three dimensional space. Indeed, unit quaternions can represent all possible attitudes, rotations, and angular velocities transformations, that is, they are global in their representation of attitude. Still, the map from the space of unit quaternions to the space of  $SO(3)$  is not unique. Indeed, it is a two-fold covering map, where each physical attitude  $\mathbf{R} \in SO(3)$  is represented by a pair of antipodal unit quaternions  $\pm \mathbf{q} \in \mathcal{S}^3$  [30]. In this sense, continuous control laws using unit quaternions four dimensional space representation can be used to globally define the rotation group without singularities, however cannot ensure global stability yielding the undesirable phenomenon of unwinding [30, 42, 43].

Indeed, regardless of the choice of parameterization, there exist no controller defined in a continuous vector field that can globally stabilizes the compact group of rotations  $SO(3)$ .

### Theorem 2.1 Theoretical limitations for global stability (from [42])

Let  $\mathcal{M}$  be a manifold of dimension  $m$  and consider a continuous vector field on  $\mathcal{M}$ . Suppose  $\pi : \mathcal{M} \mapsto \mathcal{L}$  is a vector bundle over  $\mathcal{L}$ , where  $\mathcal{L}$  is a compact,  $r$ -dimensional manifold with  $r \leq m$ . Then there exists no equilibrium point of  $f$  that is globally asymptotically stable.

## Advantages of unit quaternions

The main advantage of using unit quaternions four parameters representation for describing finite rotations in space is their global representation of attitude. Unit quaternions is the universal covering map—that is, it covers all connected covers of  $SO(3)$ —for the set of rotation matrices  $SO(3)$ , and provides a globally nonsingular parametrization of  $SO(3)$  [42], that is, they can represent all possible attitudes, rotate coordinate frames, and transform angular velocities continuously without singularities [30, 44].

Unit quaternions parametrization of  $SO(3)$  is based on the set of quaternions that lie on the sphere manifold  $\mathcal{S}^3$ , which is easily parametrized in terms of four parameters subject to one constraint, while a rotation matrix

contains nine parameters satisfying six constraints [42]. Hence, quaternion elements are as efficient, more compact, and more elegant than their matrix counterparts [45]. Moreover, unit quaternions seem to offer a more intuitive framework for using and understanding the effects of three-dimensional rotations because the axis and angle of rotation appear explicitly in their definition [45].

In the context of computational applications, the finite precision arithmetic will inherently introduce errors. If the rotation is represented as an orthogonal matrix, then the errors will mean the result is probably not orthogonal. To recover an orthogonal matrix requires a time consuming Gramm Schmidt process. By contrast, if the rotation is represented by a unit quaternion, all that is needed is to divide by the sum of the squares of the components [23].

Furthermore, for  $n \geq 3$ , the group  $\text{Spin}(n)$  is simply connected (a fact that it not so easy to prove without some machinery) whereas  $SO(n)$  is not simply connected. Hence,  $\text{Spin}(3)$  is topologically simpler than the group  $SO(3)$  which, intuitively speaking, is more twisted than  $\text{Spin}(3)$  [46]. This is an important advantage when dealing with robotics, particularly in the case of defining the configuration space for robots and for motion planning. Being simply connected, it is easier to define harmonic functions for navigation through unit quaternions (see, [47, chapters 3 and 8]).

In this context, the efficiency, compactness, and elegance of the quaternion algebra makes the unit quaternion formalism a rewarding alternative in research and pedagogical environments for representing finite rotations in space [15, 45].

Still, as previously stressed, there is no continuous control laws that can globally stabilize the rotation group, regardless of the parametrization. The map from the  $\mathcal{S}^3$  of unit quaternions to the space of  $SO(3)$  is a two-fold covering map, where a pair of antipodal unit quaternions  $\pm \mathbf{q} \in \mathcal{S}^3$  defines the same physical attitude in  $SO(3)$ . This constraint will be further detailed and investigated in Chapter 6.

## 2.5 RIGID BODY POSE REPRESENTATION

### 2.5.1 Unit dual quaternions

Since the first studies from E. Study (no pun intended), dual quaternion algebra has been used as a tool to describe rigid body displacements through Clifford algebra. Similarly to the matrix-vector notation, that is, the use of homogeneous transformation matrices, dual quaternions provide a powerful representation to describe both positions and orientations simultaneously [1, 9, 48]—that is, within a single mathematical element. Moreover, dual quaternions completely describe the rigid motion using only eight parameters, in contrast to twelve parameters from homogeneous transformation matrices, being probably the neatest and most useful way of picturing the rigid body motion group manifold [23].

Stemming from the set  $\mathbb{H} \otimes \mathbb{D}$ , unit dual quaternions are elements whose seminorm is unit, that is,  $\|\mathcal{P}(\underline{\mathbf{q}})\|$  is a unit quaternion and  $\mathcal{P}(\underline{\mathbf{q}})\mathcal{D}(\underline{\mathbf{q}}) = 0$ . Under the dual quaternion multiplication (see Definition 2.10), the unit dual quaternions set

$$\mathcal{S} = \{ \underline{\mathbf{q}} \in \mathbb{H} \otimes \mathbb{D} \mid \|\mathcal{P}(\underline{\mathbf{q}})\| = 1 \text{ and } \mathcal{P}(\underline{\mathbf{q}})\mathcal{D}(\underline{\mathbf{q}}) = 0 \}, \quad (2.19)$$

forms the Lie group of unit dual quaternions [49]— $\text{Spin}(3) \times \mathbb{R}^3$ .

**Definition 2.18** (Unit Dual Quaternions). Let

$$\underline{\mathcal{S}} = \{ \underline{\mathbf{q}} \in \mathbb{H} \otimes \mathbb{D} \mid \|\mathcal{P}(\underline{\mathbf{q}})\| = 1 \text{ and } \mathcal{P}(\underline{\mathbf{q}}) \mathcal{D}(\underline{\mathbf{q}}) = 0 \}$$

be the set of unit dual quaternions, a subset of the dual quaternion set  $\mathbb{H} \otimes \mathbb{D}$ . The group of unit dual quaternions  $\text{Spin}(3) \times \mathbb{R}^3$  is defined under quaternion multiplication operation (see Definition 2.7) with identity element 1 and inverse element defined by its conjugate (see (2.13)) as to satisfy the following axioms

(a) Associative: For all  $\underline{\mathbf{q}}_1, \underline{\mathbf{q}}_2, \underline{\mathbf{q}}_3 \in \text{Spin}(3) \times \mathbb{R}^3$ , we have

$$\left( \underline{\mathbf{q}}_1 \underline{\mathbf{q}}_2 \right) \underline{\mathbf{q}}_3 = \underline{\mathbf{q}}_1 \left( \underline{\mathbf{q}}_2 \underline{\mathbf{q}}_3 \right);$$

(b) Identity: For all unit dual quaternion elements  $\underline{\mathbf{q}} \in \text{Spin}(3) \times \mathbb{R}^3$ , we have

$$\underline{\mathbf{q}} 1 = 1 \underline{\mathbf{q}} = \underline{\mathbf{q}};$$

(c) Inverse: For all elements  $\underline{\mathbf{q}} \in \text{Spin}(3) \times \mathbb{R}^3$ , there exists an inverse element in  $\text{Spin}(3) \times \mathbb{R}^3$  denoted by  $\underline{\mathbf{q}}^{-1}$ —which is also defined by the conjugate of  $\underline{\mathbf{q}}$ , that is,  $\underline{\mathbf{q}}^*$ —such that

$$\underline{\mathbf{q}} \underline{\mathbf{q}}^{-1} = \underline{\mathbf{q}} \underline{\mathbf{q}}^* = \underline{\mathbf{q}}^* \underline{\mathbf{q}} = 1;$$

(d) Closure: The product from any elements  $\underline{\mathbf{q}}_1, \underline{\mathbf{q}}_2 \in \text{Spin}(3) \times \mathbb{R}^3$  yields an unit dual quaternion element, that is,  $\underline{\mathbf{q}}_1 \underline{\mathbf{q}}_2 \in \text{Spin}(3) \times \mathbb{R}^3$ .

The unit dual quaternion group forms a Lie group whose Lie algebra is given by the dual quaternions with real components equal to zero—pure dual quaternions (see Definition 2.12).

In this sense, and analogously to the way unit quaternions cover the rotation group  $SO(3)$ , the unit quaternion group encapsulates  $SE(3)$  with a double cover. Hence, the complete rigid body motion, coupled with translation and rotation operations, can be described using unit dual quaternion algebra [23].

An arbitrary rigid body displacement defined by a translation  $\mathbf{p}$  followed by a rotation  $\mathbf{r}$  is represented by the unit dual quaternion element<sup>12</sup>

$$\underline{\mathbf{x}} = \mathbf{r} + \varepsilon(1/2)\mathbf{p}\mathbf{r}, \quad (2.20)$$

where  $\mathbf{r} = \cos(\phi/2) + \sin(\phi/2)\mathbf{n}$ , is a unit quaternion from  $\text{Spin}(3)$  that represents the rotation and  $\mathbf{p} = (p_x \hat{i} + p_y \hat{j} + p_z \hat{k}) \in \mathbb{H}_0$  represent the translation operator in the form of a pure quaternion (i.e., a quaternion with real part equal to zero that is isomorphic to  $\mathbb{R}^3$ ). The translation can also be easily retrieved from (2.20):

$$\mathbf{p} = 2\mathcal{D}(\underline{\mathbf{x}})\mathcal{P}(\underline{\mathbf{x}})^*,$$

where the operations  $\mathcal{P}()$  and  $\mathcal{D}()$  are described in Definition (2.11).

Within unit dual quaternions, the conjugate element  $\underline{\mathbf{x}}^* = \mathbf{r}^* + \varepsilon(1/2)\mathbf{r}^*\mathbf{p}^* = \mathbf{r}^* - \varepsilon(1/2)\mathbf{r}^*\mathbf{p}$  also defines the inverse operation; that is,  $\underline{\mathbf{x}}\underline{\mathbf{x}}^* = \underline{\mathbf{x}}^*\underline{\mathbf{x}} = 1$ . Furthermore, the unit dual quaternion group double covers the rigid body motion group  $SE(3)$ , in an analogous manner to unit quaternions double covering the  $SO(3)$  group. Therefore, the unit dual quaternion  $-\underline{\mathbf{x}}$  also represents the same rigid body transformation of  $\underline{\mathbf{x}}$ .

<sup>12</sup>Similarly, the rigid motion could also be represented by a rotation  $\mathbf{r}$  followed by a translation  $\hat{\mathbf{p}}$  [50], that is,  $\underline{\mathbf{x}} = \mathbf{r} + \varepsilon(1/2)\mathbf{r}\hat{\mathbf{p}}$ . We can also relate both transformation by taking  $\hat{\mathbf{p}}$  to be defined as  $\hat{\mathbf{p}} = \mathbf{r}^*\mathbf{p}\mathbf{r}$ .

A sequence of rigid motions can be represented by a sequence of unit dual quaternion multiplications; for instance, given that  $\underline{\mathbf{x}}_1^0$  represents frame  $\mathcal{F}_1$  with respect to  $\mathcal{F}_0$  and  $\underline{\mathbf{x}}_2^1$  represents frame  $\mathcal{F}_2$  with respect to  $\mathcal{F}_1$ , then the transformation from  $\mathcal{F}_0$  to  $\mathcal{F}_2$  is  $\underline{\mathbf{x}}_2^0 = \underline{\mathbf{x}}_1^0 \underline{\mathbf{x}}_2^1$ . Alternatively, the transformation  $\underline{\mathbf{x}}_2^0$  can be regarded as a coordinate change from the coordinate system  $\mathcal{F}_0$  to the coordinate system  $\mathcal{F}_2$ .

As the unit dual quaternion group is a Lie group, we can derive the corresponding maps from and to its Lie algebra.

**Proposition 2.2.** [51, 52] Let  $\underline{\mathbf{x}} = \mathbf{r} + \varepsilon(1/2)\mathbf{p}\mathbf{r}$ , be a unit dual quaternion with rotation operator defined by the quaternion  $\mathbf{r} = \cos(\phi/2) + \sin(\phi/2)\mathbf{n}$ , where  $\mathbf{n} = n_x\hat{i} + n_y\hat{j} + n_z\hat{k}$  and  $\mathbf{p} = p_x\hat{i} + p_y\hat{j} + p_z\hat{k}$  is the pure quaternion that defines the translational operator, then the logarithm of  $\underline{\mathbf{x}}$  is

$$\log \underline{\mathbf{x}} = \frac{1}{2} (\phi \mathbf{n} + \mathbf{p}).$$

**Proposition 2.3.** [1, 53] Let  $\underline{\mathbf{x}} = \mathcal{P}(\underline{\mathbf{x}}) + \mathcal{D}(\underline{\mathbf{x}})\varepsilon$  be a dual quaternion with real numbers equal to zero, that is, formed by pure quaternions  $\mathcal{P}(\underline{\mathbf{x}}) = (a_1\hat{i} + a_2\hat{j} + a_3\hat{k})$  and  $\mathcal{D}(\underline{\mathbf{x}}) = (b_1\hat{i} + b_2\hat{j} + b_3\hat{k})$ . The exponential of  $\underline{\mathbf{x}}$  is

$$\underline{\mathbf{y}} = \exp \underline{\mathbf{x}} = \mathcal{P}(\exp \underline{\mathbf{x}}) + \mathcal{D}(\underline{\mathbf{x}}) \mathcal{P}(\exp \underline{\mathbf{x}}) \varepsilon,$$

where

$$\mathcal{P}(\exp \underline{\mathbf{x}}) = \begin{cases} \cos \|\mathcal{P}(\underline{\mathbf{x}})\| + \frac{\sin \|\mathcal{P}(\underline{\mathbf{x}})\|}{\|\mathcal{P}(\underline{\mathbf{x}})\|} \mathcal{P}(\underline{\mathbf{x}}), & \text{if } \|\mathcal{P}(\underline{\mathbf{x}})\| \neq 0, \\ 1, & \text{otherwise.} \end{cases}$$

**Definition 2.19.** (From [1]) Given the aforementioned Propositions 2.2 and 2.3, the dual quaternion  $\underline{\mathbf{x}}$  raised to the  $u$ -th power is given by

$$\underline{\mathbf{x}}^u \triangleq \exp(u \log \underline{\mathbf{x}}).$$

#### Homogeneous Transformation Matrix from Unit Dual Quaternions, and Unit Dual Quaternion Double Cover

The Lie group of unit dual quaternions  $\text{Spin}(3) \times \mathbb{R}^3$  can be used to parametrize the group of rigid motion through the isomorphic mapping defined in (2.9) and (2.4), similarly to quaternions parametrization for  $SO(3)$  in (2.18).

In this sense, an element of  $SE(3)$  given in its homogeneous representation [35]

$$\begin{bmatrix} \mathbf{R} & \mathbf{p} \\ 0 & 1 \end{bmatrix},$$

where  $\mathbf{R}$  is a rotation matrix (obtained in (2.18)) and  $\mathbf{p}$  is the translation vector, can be related to a unit dual quaternion  $\underline{\mathbf{x}} = (\eta + \boldsymbol{\mu}) + (\eta' + \boldsymbol{\mu}')\varepsilon$  through the mapping

$$\begin{bmatrix} (\eta I + \|\text{vec}_3 \boldsymbol{\mu}\|^2 \mathbf{S})^2 + 2(\{\boldsymbol{\mu}\}^\times)^2 & 2(\eta \boldsymbol{\mu}' - \eta' \boldsymbol{\mu} - \boldsymbol{\mu} \times \boldsymbol{\mu}') \\ \mathbf{0}^T & 1 \end{bmatrix}. \quad (2.21)$$

with  $\mathbf{S} = \{\text{vec}_3 \boldsymbol{\mu}\}^\times$  being the skew symmetric matrix from  $\text{vec}_3 \boldsymbol{\mu}$  and  $\mathbf{0}$  being a three dimensional zero vector.

We can find that the  $3 \times 3$  submatrix from (2.21) yields exactly the orthogonal matrix  $\mathbf{R}$  and the expression  $2(\eta\boldsymbol{\mu}' - \eta'\boldsymbol{\mu} - \boldsymbol{\mu} \times \boldsymbol{\mu}')$  yields the translation  $\mathbf{p}$ .

It is interesting to highlight that similar to (2.18) the rotation matrix is a quadratic function of the dual quaternion elements and the translational is a combination from elements from the primary and dual parts from  $\underline{\mathbf{x}}$ . In this sense,  $\mathbf{p}$  yields exactly the same value if we were to take negative elements from  $\underline{\mathbf{x}}$ , that is,  $\mathbf{p} = 2(\eta\boldsymbol{\mu}' - \eta'\boldsymbol{\mu} - \boldsymbol{\mu} \times \boldsymbol{\mu}') = 2((-\eta)(-\boldsymbol{\mu}') - (-\eta')(-\boldsymbol{\mu}) - (-\boldsymbol{\mu}) \times (-\boldsymbol{\mu}'))$ .

Therefore, the unit dual quaternion  $\underline{\mathbf{x}}$  and  $-\underline{\mathbf{x}}$  represents the same rigid body transformaton. The result is a two-to-one covering map from the  $SE(3)$ .

### Advantages of unit dual quaternions

In the study of rigid body kinematics problems, a suitable representation is fundamental for effective description and solution of the control problems. Several rigid motion representations detach and individually address attitude and translational dynamics. Nonetheless, detached approaches neglects the coupling between the full rigid motion dynamics—that is, the orientation and position coupling—which often yield into an improper description of the rigid body motion. In this sense, it is fundamental that a suitable framework should stem from a proper parametrization of the elements of the special Euclidean group  $SE(3)$ .

Among unified frameworks, homogeneous transformation matrices (HTM) are one of the most widely employed representations. Still, it requires additional calculations in order to extract control parameters from the matrices. Furthermore, to maintain stability properties, trajectory generation should be performed as to ensure small rotational errors due to the approximate nature of the extracted rotational parameters [54].

Although it is usual to describe the rigid motion using matrices to represent the elements of Lie groups (see, for example, [41, 55]), unit dual quaternion group has shown to be an elegant and effective framework for unified  $SE(3)$  representation without singularities. Moreover, unit dual quaternions completely and globally describes the rigid motion in a more compact way—only eight coordinates against twelve from HTM.

Analogously to the unit quaternion group for  $SO(3)$ , the  $\text{Spin}(3) \times \mathbb{R}^3$  has computational advantages compared to its matricial counterpart [23, 51], elements multiplication are less expensive [1, p. 42], and it is straightforward to extract geometric parameters [1, 51] (translation, axis of rotation, angle of rotation). Indeed, just as real quaternions give a computationally-efficient algorithm for dealing with rigid-body rotations in real time, dual quaternions give a computationally-efficient algorithm for dealing with rigid-body motions that also include translations, such as the motion of joints in manipulators [23].

In this sense, and motivated by the advantageous properties, unit dual quaternions representation for rigid body transformation has emerged as a topic of significant interest to the research community (for examples, see [1, 4, 8, 26, 36, 49–52, 56–64]). The efficiency, compactness, and elegance of the dual quaternion algebra makes the unit dual quaternion formalism a rewarding alternative in research environments for representing finite rigid body transformations in space.

### 2.5.2 Theoretical limitations for global stability

The unit dual quaternion framework provides a concise way to utterly represent the coupled rigid body kinematics with no singularities. Still, as it is the case for any parametrization of the  $SE(3)$  group, the  $\text{Spin}(3) \times \mathbb{R}^3$  presents an obstruction for the global stability of a continuous vector. The theorem that follows states this particular obstruction for the global asymptotic stability of a continuous vector field on its underlying manifold.



**Theorem 2.2** Theoretical limitations for global stability within unit dual quaternions

Let  $f$  be a continuous vector field defined on the underlying manifold  $\underline{\mathcal{S}}$  of the Lie group of unit dual quaternions. Then there exists no equilibrium point of  $f$  that is globally asymptotically stable.

*proof.*

For an arbitrary unit dual quaternion element  $\underline{q} = \mathbf{q} + \varepsilon \mathbf{q}' = \eta + \boldsymbol{\mu} + \varepsilon (\eta' + \boldsymbol{\mu}')$  belonging to the  $\underline{\mathcal{S}}$ , as described in Definition 2.18, it is possible to verify by direct calculation that the constraint  $\mathbf{q}\mathbf{q}^{f*} + \mathbf{q}'\mathbf{q}'^* = 0$  implies

$$\eta\eta' + \boldsymbol{\mu} \cdot \boldsymbol{\mu}' = 0. \quad (2.22)$$

Furthermore, due to the unit quaternion constraint  $\|\mathbf{q}\| = 1$ , then  $\mathbf{q}$  lies in  $\mathcal{S}^3$ . In addition,  $\mathbb{H}$  is isomorphic to  $\mathbb{R}^4$  as a vector space, which implies that  $\mathbf{q}' \in \mathbb{H}$  lies in a three-dimensional hyperplane, with  $\mathbf{q}$  being its normal vector, due to constraint (2.22). In this sense,  $\underline{\mathcal{S}}$  can be regarded as the product manifold  $\mathcal{S}^3 \times \mathbb{R}^3$  [19].

The projection map from the product  $\mathcal{S}^3 \times \mathbb{R}^3$  onto  $\mathcal{S}^3$ , that is,  $\mathcal{S}^3 \times \mathbb{R}^3 \mapsto \mathcal{S}^3$ , yields a vector bundle  $\mathcal{S}^3 \times \mathbb{R}^3$  over the compact manifold  $\mathcal{S}^3$ , namely the trivial bundle [65]. Since  $\mathcal{S}^3$  is compact, it follows from Theorem 2.1 that there is no equilibrium point of any continuous vector field  $f$  that is globally asymptotically stable.  $\square$

Theorem 2.2 extends to any rigid transformation with some rotational degrees of freedom, as it is still possible to write the state space as a vector bundle over the compact rotational manifold [42].

## 2.6 RIGID BODY KINEMATICS

### 2.6.1 Rigid body attitude kinematics using unit quaternions

The unit quaternion  $\mathbf{q}$  can describe the attitude of a rigid body in  $SO(3)$ —as previously seen in Section 2.4—and, thus, represent a rotation of a coordinate expressed in the body frame to a coordinate expressed in the inertial frame. In this sense, the kinematic equation of the attitude of rigid body in  $SO(3)$  can be defined by a transformation of the velocity expressed in the body frame to the inertial frame, that is,

$$\dot{\mathbf{q}} = \frac{1}{2} \mathbf{q} \boldsymbol{\omega}, \quad (2.23)$$

where  $\boldsymbol{\omega}$  is a pure quaternion isomorphic to the group of 3–real vectors representing the angular velocity given in the body frame. This differential equation is well-posed since  $\boldsymbol{\omega}$  is in the Lie algebra corresponding to  $\text{Spin}(3)$ .

The quaternion kinematics expressed in (2.23) can also be derived if we consider the derivative of a point rotation described in (2.17). Let  $\mathbf{p}_0 \in \mathbb{H}_0$  be a pure quaternion representing a point with respect to frame  $\mathcal{F}_0$  and let  $\mathbf{p}_1 \in \mathbb{H}_0$  be the pure quaternion representing the point resulting from the rotation of  $\mathbf{p}_0$  by the unit quaternion  $\mathbf{r} \in \text{Spin}(3)$ . In this sense, we have  $\mathbf{p}_1 = \mathbf{r} \mathbf{p}_0 \mathbf{r}^*$  and, consequently,  $\mathbf{p}_0 = \mathbf{r}^* \mathbf{p}_1 \mathbf{r}$ . Differentiating

$\mathbf{p}_0$  yields

$$\dot{\mathbf{p}}_0 = \dot{\mathbf{r}}^* \mathbf{p}_1 \mathbf{r} + \mathbf{r}^* \dot{\mathbf{p}}_1 \mathbf{r} + \mathbf{r}^* \mathbf{p}_1 \dot{\mathbf{r}},$$

which in turn can be rewritten as

$$\begin{aligned} \dot{\mathbf{p}}_0 &= \dot{\mathbf{r}}^* (\mathbf{r} \mathbf{p}_0 \mathbf{r}^*) \mathbf{r} + \mathbf{r}^* \dot{\mathbf{p}}_1 \mathbf{r} + \mathbf{r}^* (\mathbf{r} \mathbf{p}_0 \mathbf{r}^*) \dot{\mathbf{r}} \\ &= \dot{\mathbf{r}}^* \mathbf{r} \mathbf{p}_0 (\mathbf{r}^* \mathbf{r}) + \mathbf{r}^* \dot{\mathbf{p}}_1 \mathbf{r} + (\mathbf{r}^* \mathbf{r}) \mathbf{p}_0 \mathbf{r}^* \dot{\mathbf{r}} \\ &= \dot{\mathbf{r}}^* \mathbf{r} \mathbf{p}_0 + \mathbf{r}^* \dot{\mathbf{p}}_1 \mathbf{r} + \mathbf{p}_0 \mathbf{r}^* \dot{\mathbf{r}}. \end{aligned} \quad (2.24)$$

Since  $\mathbf{r}$  is an unit quaternion, the following identity

$$\dot{\mathbf{r}} \mathbf{r}^* + \mathbf{r} \dot{\mathbf{r}}^* = \dot{\mathbf{r}}^* \mathbf{r} + \mathbf{r}^* \dot{\mathbf{r}} = 0,$$

that stems from the differentiation of the  $\mathbf{r} \mathbf{r}^* = \mathbf{r}^* \mathbf{r} = 1$ , implies that  $\beta = \mathbf{r}^* \dot{\mathbf{r}} = -\dot{\mathbf{r}}^* \mathbf{r}$ . Moreover, since  $\beta^* = -\beta$ , we can also conclude that  $\beta$  must be a pure quaternion, that is,  $\beta \in \mathbb{H}_0$ . Replacing  $\beta$  back in (2.24) and considering that  $\beta$  and  $\mathbf{r}_0$  are pure vector quaternions, we have that

$$\begin{aligned} \dot{\mathbf{p}}_0 &= -\beta \mathbf{p}_0 + \mathbf{r}^* \dot{\mathbf{p}}_1 \mathbf{r} + \mathbf{p}_0 \beta, \\ &= \mathbf{r}^* \dot{\mathbf{p}}_1 \mathbf{r} + 2\mathbf{p}_0 \beta, \end{aligned}$$

which can be written in matrix vectorial form using the fact that  $\beta$  and  $\mathbf{r}_0$  are pure vector quaternions, that is,

$$\dot{\mathbf{p}}_0 = 2\mathbf{p}_0 \times \beta + \underline{\text{vec}}_4 \left( \overset{+}{\mathbf{H}}(\mathbf{r}^*) \bar{\mathbf{H}}(\mathbf{r}) \underline{\text{vec}}_4 \dot{\mathbf{p}}_1 \right). \quad (2.25)$$

Exploiting the group isomorphism from pure quaternions and the group of three-dimensional real vectors under cross product operation, we can represent the same rotation,  $\mathbf{p}_0 = \mathbf{r}^* \mathbf{p}_1 \mathbf{r}$ , in matrix vectorial form by  $\rho_0 = \mathbf{R} \rho_1$  where  $\mathbf{R} = \overset{+}{\mathbf{H}}(\mathbf{r}^*) \bar{\mathbf{H}}(\mathbf{r})$  and  $\rho_0, \rho_1$  stems from  $\mathbf{p}_0, \mathbf{p}_1 \in \mathbb{H}_0$  using the group isomorphism. The first order differentiation (considering the attitude kinematics coming straight from Poisson's kinematical equation [66]) of the same rotation thus yields

$$\begin{aligned} \dot{\rho}_0 &= \frac{d\mathbf{R}}{dt} \rho_1 + \mathbf{R} \dot{\rho}_1 \\ &= -\boldsymbol{\Omega}_R \mathbf{R} \rho_1 = -\boldsymbol{\omega}_R \times \rho_0 + \mathbf{R} \dot{\rho}_1 \\ &= \rho_0 \times \boldsymbol{\omega}_R + \mathbf{R} \dot{\rho}_1, \end{aligned}$$

where  $\boldsymbol{\Omega}_R = \{\boldsymbol{\omega}_R\}^\times$  is the angular velocity matrix described by the skew symmetric matrix corresponding to the angular velocity vector  $\boldsymbol{\omega}_R$ . Comparing the first order differentiation with (2.25) and considering the group isomorphism that maps  $\rho_0, \rho_1$  to  $\mathbf{p}_0, \mathbf{p}_1$ , we recognize that  $2\beta$  is in fact the angular velocity  $\boldsymbol{\omega}$  in the three-dimensional space [15]. Therefore,

$$\boldsymbol{\omega} = 2\beta = 2\mathbf{r}^* \dot{\mathbf{r}}.$$

The angular velocity described in quaternions thus yields the differential equation

$$\dot{\mathbf{r}} = \frac{1}{2} \mathbf{r} \boldsymbol{\omega}$$

with  $\boldsymbol{\omega}$  identified with angular kinematic velocity described by a pure quaternion.

## 2.6.2 Rigid body kinematics using unit dual quaternions

Similarly, the unit dual quaternion  $\underline{q}$  can describe the coupled attitude and position, and the kinematic equation of a rigid body motion is given by

$$\dot{\underline{q}} = \frac{1}{2} \underline{\omega} \underline{q}, \quad (2.26)$$

where  $\underline{\omega}$  is the generalized twist expressed in inertial frame,

$$\underline{\omega} = \omega + \varepsilon (\dot{\mathbf{p}} + \mathbf{p} \times \omega), \quad (2.27)$$

with  $\omega$  and  $\dot{\mathbf{p}}$  being the angular and linear velocities of the task frame relative to the inertial expressed in the inertial frame.<sup>13</sup>

The remarkable similarity between (2.23) and (2.26) is due to the principle of transference, whose various forms as stated in [67] can be summarized in modern terms as [23, Sec 7.6]: “All representations of the group  $SO(3)$  become representations of  $SE(3)$  when tensored with the dual numbers”. This means that several properties and algebraic identities of  $SO(3)$  and the quaternions can be carried to  $SE(3)$  and the dual quaternions algebra, respectively.

The principle of transference may mislead one to think that every theorem in quaternions can be transformed in another theorem in dual quaternions by a transference process. However this is not the case, as shown by simple counterexamples in [67].

## 2.7 ROBOTIC MANIPULATOR KINEMATICS

In this section, we provide for the reader basic concepts on how to relate the pose of the end-effector of manipulator with the robot joint configuration by means of the forward kinematic modeling (FKM) and the robot Jacobian that maps the differential kinematics. We also describe how to obtain the FKM and the Jacobian for the manipulator using D-H notation (both standard and modified).

It is important to highlight that tasks specifications and control requirements in the context of robot manipulators are defined at the end-effector task-space—the non-Euclidean manifold of position and orientation herein described using unit dual quaternions—which, in turn, renders a discrepancy with regard to the joint configuration space—the space (usually, Euclidean) where actuation indeed takes places. Hence, the importance of the FKM and differential FKM maps.

The inverse kinematics (IK) provides a escape from this discrepancy by mapping a task specification to a set of matching joint configurations. Hence, when the robot inverse kinematics is known, trajectory planning can be used in conjunction to suitable controllers to ensure that the current vector of joint positions converge to a desired value. Solutions for the inverse kinematics, however, are generally not easily derived and, in some cases, the IK may even result in impossible or in an infinite number of solutions [27].

On the other hand, as modern manipulators are often equipped with low level controllers at joint level, a control law can be applied straightly at the end-effector task-space, making direct use of the available low level

<sup>13</sup>If we consider an unit dual quaternion composed of a rotation  $\mathbf{r}$  followed by a translation  $\hat{\mathbf{p}}$  (instead of a translation  $\mathbf{p}$  followed by a rotation  $\mathbf{r}$ ), then we can use the same first order kinematic equation (2.26) with  $\mathbf{p} = \mathbf{r}^* \hat{\mathbf{p}} \mathbf{r}$  or we can redefine the (2.26) as  $\dot{\underline{q}} = \frac{1}{2} \underline{q} \hat{\underline{\omega}}$  where  $\hat{\underline{\omega}}$  is the twist in body frame described by  $\hat{\underline{\omega}} = \hat{\omega} + \varepsilon (\hat{\mathbf{p}} + \hat{\omega} \times \hat{\mathbf{p}})$  with  $\hat{\omega}$  and  $\hat{\mathbf{p}}$  being the angular and linear velocities of the task frame relative to the inertial frame expressed in the task-frame.

controllers instead of redesigning them. In this sense, a convenient approach, firstly introduced by Whitney for non-redundant manipulators [68], is to define control laws directly at the end-effector and then invert the differential forward kinematics model as to provide suitable references for the low level controllers.

This thesis is henceforth concerned to design high level controllers with suitable references for the low level joint-space controllers. In this sense, the results herein concerning robotic manipulator kinematics provide the mathematical background—including some novel concepts—needed to understand the ideas and results that follows throughout the thesis.

## 2.7.1 Dual quaternion forward kinematic model (DQ-FKM)

The forward kinematic model provides a mapping from the joint configuration of a  $n$ -joint serial robot to its end-effector pose. If the combined position and orientation of the end-effector is described as an unit dual quaternion element, then we have the mapping  $\underline{f}_{\text{FKM}} : \mathbb{R}^n \rightarrow \text{Spin}(3) \times \mathbb{R}^3$  described by [1]

$$\underline{x}_E = \underline{f}_{\text{FKM}}(\boldsymbol{\theta}) \quad (2.28)$$

where  $\underline{x}_E$  is the unit dual quaternion representing the end-effector pose and  $\boldsymbol{\theta}$  is the joint configuration vector, that is, the vector of joint positions.

If we consider intermediate links from the robot, we can exploit the serial chain to describe the transformation between the base to the end-effector pose. The description of the end-effector pose of a  $n$ -joint serial robot, where joints are attached to the beginning of links, therefore stems from a series of dual quaternion multiplications.

Let the rigid transformation between the extremities of any links  $i+1$  and  $i$  to be defined by the unit dual quaternion  $\underline{x}_{i+1}^i$ . Note that the transformation  $\underline{x}_{i+1}^i$  sole depends on the position of the  $i$ -th joint angle  $\theta_i$ . If we consider a serial chain of links, then from the base to the second link, we would have the transformation given by  $\underline{x}_2^0 = \underline{x}_1^0 \underline{x}_2^1$ . In this sense, the serial transformation from the base to the end-effector pose can be described by [1]

$$\underline{x}_E \triangleq \underline{x}_1^0 \underline{x}_2^1 \dots \underline{x}_n^{n-1}. \quad (2.29)$$

Because  $\underline{x}_{i+1}^i$  is a function of the  $i$ -th robot joint position angle  $\theta_i$  described by  $\underline{x}_{i+1}^i = \underline{f}_{\text{FKM},i}(\theta_i)$ , where  $\underline{f}_{\text{FKM},i}$  is the mapping from the position angle to the unit dual quaternion that describes the transformation, that is,  $\underline{f}_{\text{FKM},i} : \mathbb{R} \mapsto \text{Spin}(3) \times \mathbb{R}^3$ ; then the forward kinematics is a function of all joints, i.e.,  $\underline{x}_E = \underline{f}_{\text{FKM}}(\theta_0, \dots, \theta_{n-1})$  as described in (2.28).

### 2.7.1.1 D-H convention to dual quaternion FKM

The description of the end-effector transformation to the base in a serial robot can be described by a series of dual quaternion multiplications from each intermediate link transformation. Hence, it is important to define a convention to describe the pose of each link with respect to the previous one in the kinematic serial chain. Typically in robotics, the link transformation is described using the Denavit-Hartenberg (D-H) convention [27, 69]—a four parameter based convention.

The D-H convention can be described in a standard form and using modified parameters. In the case of the former, the parametrization is given by [1, 27]: first a rotation  $\theta$  is performed around the  $z$ -axis from the base

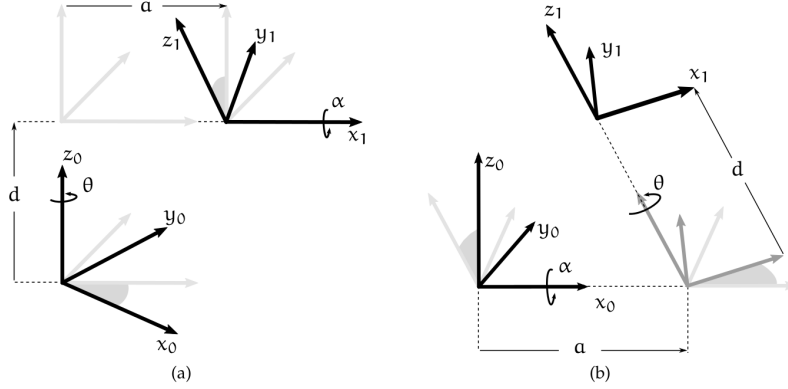


Figure 2.1: Denavit-Hartenberg parameters: (a) standard and (b) modified conventions (figure extracted from [1]).

link; then we consider a translation  $d$  along the  $z$ -axis followed by another translation  $a$  along the resulting  $x$ -axis; finally, we consider a rotation  $\alpha$  around the  $x$ -axis. The convention is shown in Figure 2.1(a).

The dual quaternion space representation for the D-H convention transformation basically consists in four dual quaternion multiplications, one for each transformation. Hence, the link transformation can be described by [1]:

$$\underline{\mathbf{x}}_{DH} = \mathbf{r}_{z,\theta} \underline{\mathbf{p}}_{z,d} \underline{\mathbf{p}}_{x,a} \mathbf{r}_{x,\alpha}, \quad (2.30)$$

where

$$\begin{cases} \mathbf{r}_{z,\theta} = \cos \frac{\theta}{2} + \sin \frac{\theta}{2} \hat{k} & \text{denotes the quaternion rotation of } \theta \text{ along the } z\text{-axis;} \\ \mathbf{r}_{x,\alpha} = \cos \frac{\alpha}{2} + \sin \frac{\alpha}{2} \hat{i} & \text{denotes the quaternion rotation of } \alpha \text{ along the } x\text{-axis;} \\ \underline{\mathbf{p}}_{z,d} = 1 + (\frac{1}{2}d)\hat{k}\varepsilon & \text{denotes the pure translation of } d \text{ along the } z\text{-axis;} \\ \underline{\mathbf{p}}_{x,a} = 1 + (\frac{1}{2}a)\hat{i}\varepsilon & \text{denotes the pure translation of } a \text{ along the } x\text{-axis.} \end{cases} \quad (2.31)$$

Expanding the multiplication in (2.30), the unit dual quaternion representing the transformation in terms of the D-H parameters is given by

$$\underline{\mathbf{x}}_{DH} = \mathcal{P}(\underline{\mathbf{x}}_{DH}) + \mathcal{D}(\underline{\mathbf{x}}_{DH})\varepsilon, \quad (2.32)$$

where

$$\begin{aligned} \mathcal{P}(\underline{\mathbf{x}}_{DH}) &= h_{DH,\eta} + h_{DH,\mu1}\hat{i} + h_{DH,\mu2}\hat{j} + h_{DH,\mu3}\hat{k}, \\ \mathcal{D}(\underline{\mathbf{x}}_{DH}) &= -\frac{1}{2}(d \cdot h_{DH,\mu3} + a \cdot h_{DH,\mu1}) + \frac{1}{2}(-d \cdot h_{DH,\mu2} + a \cdot h_{DH,\eta})\hat{i} \\ &\quad + \frac{1}{2}(d \cdot h_{DH,\mu1} + a \cdot h_{DH,\mu3})\hat{j} + \frac{1}{2}(d \cdot h_{DH,\eta} - a \cdot h_{DH,\mu2})\hat{k}, \end{aligned}$$

with  $h_{DH,\eta} = \cos \frac{\theta}{2} \cos \frac{\alpha}{2}$ ,  $h_{DH,\mu1} = \cos \frac{\theta}{2} \sin \frac{\alpha}{2}$ ,  $h_{DH,\mu2} = \sin \frac{\theta}{2} \sin \frac{\alpha}{2}$ , and  $h_{DH,\mu3} = \sin \frac{\theta}{2} \cos \frac{\alpha}{2}$ .

### 2.7.1.2 Differential forward kinematics using D-H convention

The D-H convention provides a map from the  $i$ -th joint position to the transformation between connected links, that is, the extremity of link  $i+1$  with link  $i$ . To understand how changes in the joint value influences the transformation between links, we take the first derivative of the transformation  $\underline{\mathbf{x}}_{i+1}^i$  described in (2.32) as

illustrated in [1]:

$$\begin{aligned}\dot{\mathbf{x}}_{i+1} &= \frac{d}{dt} \mathbf{x}_{i+1} \\ &= \frac{\partial \mathbf{x}_{i+1}}{\partial \theta_i} \frac{d\theta_i}{dt},\end{aligned}$$

where

$$\begin{aligned}\mathcal{P} \left( \frac{\partial \mathbf{x}_{i+1}}{\partial \theta_i} \right) &= \frac{\partial}{\partial \theta_i} h_{\text{DH},\eta} + \frac{\partial}{\partial \theta_i} h_{\text{DH},\mu 1} \hat{i} + \frac{\partial}{\partial \theta_i} h_{\text{DH},\mu 2} \hat{j} + \frac{\partial}{\partial \theta_i} h_{\text{DH},\mu 3} \hat{k}, \\ \mathcal{D} \left( \frac{\partial \mathbf{x}_{i+1}}{\partial \theta_i} \right) &= -\frac{1}{2} \left( d \cdot \frac{\partial}{\partial \theta_i} h_{\text{DH},\mu 3} + a \cdot \frac{\partial}{\partial \theta_i} h_{\text{DH},\mu 1} \right) + \frac{1}{2} \left( -d \cdot \frac{\partial}{\partial \theta_i} h_{\text{DH},\mu 2} + a \cdot \frac{\partial}{\partial \theta_i} h_{\text{DH},\eta} \right) \hat{i} \\ &\quad + \frac{1}{2} \left( d \cdot \frac{\partial}{\partial \theta_i} h_{\text{DH},\mu 1} + a \cdot \frac{\partial}{\partial \theta_i} h_{\text{DH},\mu 3} \right) \hat{j} + \frac{1}{2} \left( d \cdot \frac{\partial}{\partial \theta_i} h_{\text{DH},\eta} - a \cdot \frac{\partial}{\partial \theta_i} h_{\text{DH},\mu 2} \right) \hat{k}\end{aligned}$$

Calculating the derivative of (2.32) with respect to  $\theta_i$  yields the following identities

$$\begin{aligned}\frac{\partial}{\partial \theta_i} h_{\text{DH},\eta} &= -\frac{1}{2} \sin \frac{\theta_i}{2} \cos \frac{\alpha}{2} = -\frac{1}{2} h_{\text{DH},\mu 3}, & \frac{\partial}{\partial \theta_i} h_{\text{DH},\mu 1} &= -\frac{1}{2} \sin \frac{\theta_i}{2} \sin \frac{\alpha}{2} = -\frac{1}{2} h_{\text{DH},\mu 2}, \\ \frac{\partial}{\partial \theta_i} h_{\text{DH},\mu 2} &= +\frac{1}{2} \cos \frac{\theta_i}{2} \sin \frac{\alpha}{2} = +\frac{1}{2} h_{\text{DH},\mu 1}, & \frac{\partial}{\partial \theta_i} h_{\text{DH},\mu 3} &= +\cos \frac{\theta_i}{2} \cos \frac{\alpha}{2} = +\frac{1}{2} h_{\text{DH},\eta}.\end{aligned}$$

Hence,

$$\begin{aligned}\mathcal{P} \left( \frac{\partial \mathbf{x}_{i+1}}{\partial \theta_i} \right) &= \frac{1}{2} \left[ -h_{\text{DH},\mu 3} - h_{\text{DH},\mu 2} \hat{i} + h_{\text{DH},\mu 1} \hat{j} + h_{\text{DH},\eta} \hat{k} \right], \\ \mathcal{D} \left( \frac{\partial \mathbf{x}_{i+1}}{\partial \theta_i} \right) &= -\frac{1}{4} (d \cdot h_{\text{DH},\eta} - a \cdot h_{\text{DH},\mu 2}) + \frac{1}{4} (-d \cdot h_{\text{DH},\mu 1} - a \cdot h_{\text{DH},\mu 3}) \hat{i} \\ &\quad + \frac{1}{4} (-d \cdot h_{\text{DH},\mu 2} + a \cdot h_{\text{DH},\eta}) \hat{j} + \frac{1}{4} (-d \cdot h_{\text{DH},\mu 3} - a \cdot h_{\text{DH},\mu 1}) \hat{k}.\end{aligned}\tag{2.33}$$

Using the rigid body kinematics description in (2.26), we can also relate the velocity within the  $i$ -th joint with the rigid body twist between related links, that is,

$$\dot{\mathbf{x}}_{i+1} = \frac{1}{2} \underline{\omega}_{i+1} \mathbf{x}_{i+1} = \frac{\partial \mathbf{x}_{i+1}}{\partial \theta_i} \frac{d\theta_i}{dt}.$$

Therefore, the twist  $\underline{\omega}_{i+1}$  between links is given by

$$\underline{\omega}_{i+1} = 2 \frac{\partial \mathbf{x}_{i+1}}{\partial \theta_i} \frac{\partial \theta_i}{\partial t} (\mathbf{x}_{i+1})^* = 2 \left[ \frac{\partial \mathbf{x}_{i+1}}{\partial \theta_i} (\mathbf{x}_{i+1})^* \right] \frac{d\theta_i}{dt}.$$

Replacing (2.32) and (2.33), we have

$$\underline{\omega}_{i+1} = 2 \frac{\partial \mathbf{x}_{i+1}}{\partial \theta_i} (\mathbf{x}_{i+1})^* = \underline{\omega}_{i+1} \hat{\theta}_i,\tag{2.34}$$

where

$$\underline{\omega}_{i+1} \triangleq \hat{k}.$$

### 2.7.1.3 Modified D-H convention to dual quaternion FKM

The modified D-H parameters differs from the conventional standard as shown in Figure 2.1(b). In this case, the resulting parameters stems from the following procedure [1, 70]: first a rotation  $\alpha$  is performed along

the  $x$ -axis followed by translation  $\alpha$  along the  $x$ -axis; then we consider a rotation  $\theta$  along the resulting  $z$ -axis followed by a translation  $d$  along the same  $z$ -axis.

The dual quaternion space representation for the D-H convention transformation basically consists in four dual quaternion multiplications, one for each transformation. Hence, the link transformation can be described by [1]:

$$\underline{\mathbf{x}}_{DH} = \mathbf{r}_{x,\alpha} \underline{\mathbf{p}}_{x,a} \mathbf{r}_{z,\theta} \underline{\mathbf{p}}_{z,d}, \quad (2.35)$$

where  $\mathbf{r}_{z,\theta}$ ,  $\mathbf{r}_{x,\alpha}$ ,  $\underline{\mathbf{p}}_{z,d}$ , and  $\underline{\mathbf{p}}_{x,a}$  are described in (2.31).

Expanding the multiplication in (2.35), the unit dual quaternion representing the transformation in terms of the D-H parameters is given by  $\underline{\mathbf{x}}_{DH} = \mathcal{P}(\underline{\mathbf{x}}_{DH}) + \mathcal{D}(\underline{\mathbf{x}}_{DH}) \varepsilon$ , where

$$\begin{aligned} \mathcal{P}(\underline{\mathbf{x}}_{DH}) &= h_{DH,\eta} + h_{DH,\mu1} \hat{i} - h_{DH,\mu2} \hat{j} + h_{DH,\mu3} \hat{k}, \\ \mathcal{D}(\underline{\mathbf{x}}_{DH}) &= -\frac{1}{2} (d \cdot h_{DH,\mu3} + a \cdot h_{DH,\mu1}) + \frac{1}{2} (-d \cdot h_{DH,\mu2} + a \cdot h_{DH,\eta}) \hat{i} \\ &\quad - \frac{1}{2} (d \cdot h_{DH,\mu1} + a \cdot h_{DH,\mu3}) \hat{j} + \frac{1}{2} (d \cdot h_{DH,\eta} - a \cdot h_{DH,\mu2}) \hat{k}, \end{aligned}$$

with  $h_{DH,\eta} = \cos \frac{\theta}{2} \cos \frac{\alpha}{2}$ ,  $h_{DH,\mu1} = \cos \frac{\theta}{2} \sin \frac{\alpha}{2}$ ,  $h_{DH,\mu2} = \sin \frac{\theta}{2} \sin \frac{\alpha}{2}$ , and  $h_{DH,\mu3} = \sin \frac{\theta}{2} \cos \frac{\alpha}{2}$ .

#### 2.7.1.4 Differential forward kinematics using modified D-H convention

Similarly to the kinematic description using standard D-H convention, we take the first derivative of (2.35) to understand how joint velocities influences the transformation between links. The result follows from [1]:

$$\begin{aligned} \dot{\underline{\mathbf{x}}}_{i+1} &= \frac{d}{dt} \underline{\mathbf{x}}_{i+1} \\ &= \frac{\partial \underline{\mathbf{x}}_{i+1}}{\partial \theta_i} \frac{d\theta_i}{dt}, \end{aligned}$$

where

$$\begin{aligned} \mathcal{P} \left( \frac{\partial \underline{\mathbf{x}}_{i+1}}{\partial \theta_i} \right) &= \frac{1}{2} \left[ -h_{DH,\mu3} - h_{DH,\mu2} \hat{i} - h_{DH,\mu1} \hat{j} + h_{DH,\eta} \hat{k} \right], \\ \mathcal{D} \left( \frac{\partial \underline{\mathbf{x}}_{i+1}}{\partial \theta_i} \right) &= -\frac{1}{4} (d \cdot h_{DH,\eta} - a \cdot h_{DH,\mu2}) + \frac{1}{4} (-d \cdot h_{DH,\mu1} - a \cdot h_{DH,\mu3}) \hat{i} \\ &\quad - \frac{1}{4} (-d \cdot h_{DH,\mu2} + a \cdot h_{DH,\eta}) \hat{j} + \frac{1}{4} (-d \cdot h_{DH,\mu3} - a \cdot h_{DH,\mu1}) \hat{k}. \end{aligned} \quad (2.36)$$

Using the rigid body kinematics description in (2.26), we can also relate the joint velocity with the rigid body twist between links, that is,

$$\underline{\boldsymbol{\omega}}_{i+1} = 2 \frac{\partial \underline{\mathbf{x}}_{i+1}}{\partial \theta_i} \frac{\partial \theta_i}{\partial t} (\underline{\mathbf{x}}_{i+1})^* = 2 \left[ \frac{\partial \underline{\mathbf{x}}_{i+1}}{\partial \theta_i} (\underline{\mathbf{x}}_{i+1})^* \right] \frac{d\theta_i}{dt}.$$

Replacing (2.35) and (2.36), we have

$$\underline{\boldsymbol{\omega}}_{i+1} = 2 \frac{\partial \underline{\mathbf{x}}_{i+1}}{\partial \theta_i} (\underline{\mathbf{x}}_{i+1})^* = \underline{\boldsymbol{\omega}}_{i+1}^i \dot{\theta}_i, \quad (2.37)$$

where

$$\underline{\boldsymbol{\omega}}_{i+1}^i \triangleq \left[ \left( -\sin \alpha_i \hat{j} + \cos \alpha_i \hat{k} \right) - a_i (\cos \alpha_i \hat{j} + \sin \alpha_i) \varepsilon \right] \dot{\theta}_i.$$

## 2.7.2 Dual quaternion based end-effector pose Jacobian ( $J_{\text{vec}}$ )

The end-effector pose Jacobian from a manipulator provides a map between the joint velocity vector to the end-effector velocity at task-space. It defines a mapping from the  $n$ -dimensional joint-vector to an  $m$ -dimensional representation for the task-space, usually a linear Euclidean mapping of the form  $\mathbb{R}^n \mapsto \mathbb{R}^m$ . If the vector space mapping from (2.14) is used, then the differential kinematics of the robotic manipulator yields a transformation satisfying [1]

$$\text{vec}_8 \dot{\mathbf{x}}_E = \mathbf{J}_{\text{vec}} \dot{\boldsymbol{\theta}}, \quad (2.38)$$

where  $\boldsymbol{\theta} = [\theta_0 \dots \theta_{n-1}]^T$  is the measured vector of joint variables and  $\mathbf{J}_{\text{vec}}$  is the matrix representation for the derivative  $\partial \mathbf{x}_E / \partial \boldsymbol{\theta}$  representing the analytical Jacobian that characterizes the transformation  $\mathbb{R}^n \mapsto \mathbb{R}^8$ . To find the dual quaternion based Jacobian, consider the forward kinematics as serial of dual quaternion transformations between links. Taking the first derivative of (2.29) yields [1]

$$\begin{aligned} \dot{\mathbf{x}}_E &= \mathbf{x}_1^0 \dot{\mathbf{x}}_1^0 \mathbf{x}_2^1 \dots \mathbf{x}_n^{n-1} + \mathbf{x}_1^0 \mathbf{x}_2^1 \dot{\mathbf{x}}_2^1 \dots \mathbf{x}_n^{n-1} + \dots \\ &= + \mathbf{x}_1^0 \mathbf{x}_2^1 \dots \dot{\mathbf{x}}_{n-1}^{n-2} \mathbf{x}_n^{n-1} + \mathbf{x}_1^0 \mathbf{x}_2^1 \dots \mathbf{x}_{n-1}^{n-1} \dot{\mathbf{x}}_n^{n-1} \\ &= \sum_{i=0}^{n-1} \mathbf{x}_i^0 \dot{\mathbf{x}}_{i+1}^i \mathbf{x}_n^{i+1}. \end{aligned} \quad (2.39)$$

From the rigid body kinematics description in (2.26) and considering each transformation between links, that is,  $\dot{\mathbf{x}}_{i+1}^i = \frac{1}{2} \boldsymbol{\omega}_{i+1}^i \mathbf{x}_{i+1}^i$ , we have

$$\dot{\mathbf{x}}_E = \sum_{i=0}^{n-1} \mathbf{x}_i^0 \left( \frac{1}{2} \boldsymbol{\omega}_{i+1}^i \mathbf{x}_{i+1}^i \right) \mathbf{x}_n^{i+1}.$$

Replacing the twist between links  $\boldsymbol{\omega}_{i+1}^i$  calculated in (2.34) for the standard D-H convention and in (2.37) for modified D-H parameters, yields

$$\begin{aligned} \dot{\mathbf{x}}_E &= \sum_{i=0}^{n-1} \mathbf{x}_i^0 \left( \frac{1}{2} \boldsymbol{\varpi}_{i+1}^i \theta_i \right) \mathbf{x}_n^{i+1} \\ &= \frac{1}{2} \sum_{i=0}^{n-1} \mathbf{x}_i^0 \left( \boldsymbol{\varpi}_{i+1}^i \theta_i \right) [\mathbf{x}_i^0]^* [\mathbf{x}_i^0] \mathbf{x}_n^{i+1} \\ &= \frac{1}{2} \sum_{i=0}^{n-1} \left( \mathbf{x}_i^0 \boldsymbol{\varpi}_{i+1}^i \mathbf{x}_i^{0*} \right) \mathbf{x}_E \theta_i. \end{aligned} \quad (2.40)$$

Note that the end-effector velocity description stems from a linear combination from dual quaternion elements weighted by individual joint velocities. Using the mapping (2.14) and comparing the desired form for the end-effector Jacobian (2.38) with (2.40), it turns out that  $\mathbf{J}_{\text{vec}}$  can be represented by

$$\mathbf{J}_{\text{vec}} = \begin{bmatrix} \mathbf{j}_0 & \dots & \mathbf{j}_{n-1} \end{bmatrix}, \quad (2.41)$$

where

$$\mathbf{j}_i = \frac{1}{2} \text{vec}_8 \left\{ \left( \mathbf{x}_i^0 \boldsymbol{\varpi}_{i+1}^i \mathbf{x}_i^{0*} \right) \mathbf{x}_E \right\}, \quad i=0, \dots, n-1.$$

The general procedure to calculate the dual quaternion based end-effector Jacobian is summarized in Algorithm 2.1. The calculations for  $\mathbf{x}_i^0$ ,  $\boldsymbol{\varpi}_{i+1}^i$  are found in (2.30),(2.34) for the standard D-H convention and in (2.35),(2.37) for modified D-H parameters, and  $\mathbf{x}_E$  is the unit dual quaternion representation for the end-effector pose found in (2.29).



---

**Algorithm 2.1** Calculations of the dual quaternion based end-effector Jacobian (from [1])

---

- 1: Calculate  $\underline{\mathbf{x}}_E$
  - 2: Set  $\underline{\mathbf{x}}$  to 1, that is,  $\underline{\mathbf{x}} \leftarrow 1$
  - 3: **for**  $i = 0$  to  $n - 1$  **do**
  - 4:     Calculate  $\underline{\mathbf{j}}_i \leftarrow \frac{1}{2} \text{vec}_8 \{ (\underline{\mathbf{x}} \underline{\boldsymbol{\omega}}_{i+1}^* \underline{\mathbf{x}}^*) \underline{\mathbf{x}}_E \}$
  - 5:     Update  $\underline{\mathbf{x}}$  with link transformation, that is,  $\underline{\mathbf{x}} \leftarrow \underline{\mathbf{x}} \underline{\mathbf{x}}_{i+1}^i$
  - 6: **end for**
  - 7:  $\underline{\mathbf{J}}_{\text{vec}} \leftarrow \begin{bmatrix} \underline{\mathbf{j}}_0 & \dots & \underline{\mathbf{j}}_{n-1} \end{bmatrix}$
- 

### 2.7.3 Dual quaternion Jacobian ( $\underline{\mathbf{J}}_{\underline{\boldsymbol{\omega}}}$ )

The differential FKM mapping from the joint velocity vector to the end-effector velocity can be seen as a transformation that maps the influence of changes in the  $n$ -joint serial configuration to the end-effector configuration. In the Euclidean space, task-space changes are characterized as in (2.38) since the derivative is well defined in the same Euclidean manifold. However, task-space transformations—considering translation and rotation—describe rigid body transformations in the non-Euclidean manifold  $SE(3)$ . As seen in Subsection 2.5.1, the group of unit dual quaternions can globally represent  $SE(3)$  without singularities. Still, as a non-Euclidean manifold, changes in this space are not described as in (2.38). Instead, for the dual quaternion differential FKM to be well-posed, we need to consider the dual quaternion kinematics as in (2.26), that is,

$$\dot{\underline{\mathbf{x}}}_E = \frac{1}{2} \underline{\boldsymbol{\omega}}_E \underline{\mathbf{x}}_E. \quad (2.42)$$

In this case, end-effector changes are described by the twist  $\underline{\boldsymbol{\omega}}_E = \boldsymbol{\omega}_E + \varepsilon (\dot{\mathbf{p}}_E + \mathbf{p}_E \times \boldsymbol{\omega}_E)$ , where  $\boldsymbol{\omega}_E$  and  $\dot{\mathbf{p}}_E$  denote the pure quaternions describing the end-effector rotational and translational velocities, respectively. Since  $\underline{\boldsymbol{\omega}}_E$  is not an unit dual quaternion but rather an element of the Lie algebra of  $\text{Spin}(3) \times \mathbb{R}^3$ , it lies in the pure dual quaternion space ( $\mathbb{H}_0 \otimes \mathbb{D}$ ) which is isomorphic to  $\mathbb{R}^6$  as shown in Definition 2.12.

In this sense, we can exploit this natural isomorphism to define a new dual quaternion Jacobian that maps changes in the  $n$ -joint configuration to end-effector twist  $\underline{\boldsymbol{\omega}}_E$ . In other words, a mapping of the form  $\mathbb{R}^n \mapsto \mathbb{H}_0 \otimes \mathbb{D}$  from the  $n$ -joint configuration velocities to the end-effector twist given by

$$\underline{\boldsymbol{\omega}}_E = \underline{\mathbf{J}}_{\underline{\boldsymbol{\omega}}} \boldsymbol{\theta}, \quad (2.43)$$

where  $\boldsymbol{\theta} = [\theta_0 \dots \theta_{n-1}]^T$  is the measured vector of joint variables and  $\underline{\mathbf{J}}_{\underline{\boldsymbol{\omega}}}$  is the pure dual quaternion that describes the Jacobian transformation.

To find the value for dual quaternion Jacobian  $\underline{\mathbf{J}}_{\underline{\boldsymbol{\omega}}}$ , recall the first derivative (2.39) of the serial of dual quaternion transformations between links describing the end-effector. Considering the rigid body kinematics description in (2.26) for each transformation between links and replacing the resulting twists for the values calculated in in (2.34) for the standard D-H convention and in (2.37) for modified D-H parameters, we have

$$\begin{aligned} \dot{\underline{\mathbf{x}}}_E &= \sum_{i=0}^{n-1} \underline{\mathbf{x}}_i^0 \dot{\underline{\mathbf{x}}}_{i+1}^i \underline{\mathbf{x}}_n^{i+1} \\ &= \sum_{i=0}^{n-1} \underline{\mathbf{x}}_i^0 \left( \frac{1}{2} \underline{\boldsymbol{\omega}}_{i+1}^i \underline{\mathbf{x}}_{i+1}^i \right) \underline{\mathbf{x}}_n^{i+1} \\ &= \frac{1}{2} \sum_{i=0}^{n-1} (\underline{\mathbf{x}}_i^0 \underline{\boldsymbol{\omega}}_{i+1}^i \underline{\mathbf{x}}_i^{0*}) \dot{\theta}_i \underline{\mathbf{x}}_E. \end{aligned} \quad (2.44)$$

The result in (2.44) follows a similar step to the one derived in (2.40) and in [1]. Nonetheless, instead of using the  $\text{vec}_8$  mapping to  $\mathbb{R}^8$  for each combined element  $(\underline{x}_i^0 \underline{\varpi}_{i+1}^i \underline{x}_i^{0*}) \underline{x}_E$ , we define the dual quaternion Jacobian  $\underline{J}_\omega \in \mathbb{H}_0 \otimes \mathbb{D}$  that describes the dual quaternion differential forward kinematics mapping (2.42)-(2.43) by

$$\underline{J}_\omega = \sum_{i=0}^{n-1} \underline{j}_i, \quad (2.45)$$

where  $\underline{j}_i$  are dual quaternion elements defined as

$$\underline{j}_i \triangleq \underline{x}_i^0 \underline{\varpi}_{i+1}^i \underline{x}_i^{0*}. \quad (2.46)$$

Inspecting (2.46), it turns out that  $\underline{j}_i$  are pure dual quaternion elements, that is, pure dual vectors belonging to the set  $\mathbb{H}_0 \otimes \mathbb{D}$ . Hence, the dual quaternion Jacobian in (2.45) is indeed a pure dual quaternion element. Using the natural isomorphism between  $\mathbb{H}_0 \otimes \mathbb{D}$  and  $\mathbb{R}^6$  provided by the mapping  $\text{vec}_6$ , and the inverse mapping  $\underline{\text{vec}}_6$ , we can also extract a matrix form for the dual quaternion Jacobian (2.45), that is,

$$\underline{J}_\omega \triangleq \left[ \text{vec}_6 \underline{j}_0 \quad \dots \quad \text{vec}_6 \underline{j}_{n-1} \right] \quad (2.47)$$

such that the dual quaternion differential FKM can be described by

$$\begin{aligned} \dot{\underline{x}}_E &= \frac{1}{2} \sum_{i=0}^{n-1} \underline{j}_i \dot{\theta}_i \underline{x}_E \\ &= \frac{1}{2} \underline{\text{vec}}_6 \left( \underline{J}_\omega \dot{\theta} \right) \underline{x}_E, \end{aligned} \quad (2.48)$$

where  $\underline{\text{vec}}_6 \left( \underline{J}_\omega \dot{\theta} \right)$  describes the end-effector twist in dual quaternion space.

---

**Algorithm 2.2** Calculations of the dual quaternion Jacobian

---

- 1: Calculate  $\underline{x}_E$
  - 2: Set  $\underline{x}$  to 1, that is,  $\underline{x} \leftarrow 1$
  - 3: **for**  $i = 0$  to  $n - 1$  **do**
  - 4:     Calculate the dual quaternion  $\underline{j}_i \leftarrow \underline{x}_i^0 \underline{\varpi}_{i+1}^i \underline{x}_i^{0*}$
  - 5:     Update  $\underline{x}$  with link transformation, that is,  $\underline{x} \leftarrow \underline{x} \underline{\varpi}_{i+1}^i$
  - 6: **end for**
  - 7:  $\underline{J}_\omega \leftarrow \left[ \text{vec}_6 \underline{j}_0 \quad \dots \quad \text{vec}_6 \underline{j}_{n-1} \right]$
- 

## 2.7.4 Jacobian matrices comparison and kinematic singularities

It is important to highlight that at specific joint configurations, the Jacobian matrix may lose rank—regardless the choice of Jacobian. At these singular configurations, the desired differential kinematics within unit dual quaternion is ill-posed and unfolds outside the Jacobian range space—in other words, the manipulator temporarily loses one or more degrees-of-freedom (DOFs) at task-space.

The end-effector pose Jacobian  $\underline{J}_{\text{vec}}$  is particularly liable to kinematic singularities due to its construction since it maps the  $n$ -joint velocity vector to an  $\mathbb{R}^8$  manifold whereas describing a six degrees-of-freedom space. In other words, the obtained Jacobian  $\underline{J}_{\text{vec}}$  is rank deficient in the sense that it maps the differential joint input vector to an  $\mathbb{R}^8$  manifold which only has six degrees of freedom. In this sense, control strategies based on

a least square optimization from the differential dual quaternion kinematics requires a robust pseudoinverse technique, but least square solutions may still lie in the Jacobian range space due to the two linear constraints from unit dual quaternions. Despite this drawback, being fully construct in vector space eases the derivation of different solutions using the end-effector pose Jacobian  $J_{\text{vec}}$  which is entailed with less topological constraints.

On the other hand, the dual quaternion Jacobian  $\underline{J}_w$  has the advantage of being derived in dual quaternion space which enhances its geometric significance and, at the same time, describes a linear transformation between the joint velocity inputs where actuation takes place and the rigid body twist. In this sense, the dual quaternion Jacobian combines the geometric significance of the Lie algebra of  $\text{Spin}(3) \times \mathbb{R}^3$  with the practicality of being a linear transformation between the corresponding vector space to the joint velocity vector. As a consequence, the Jacobian is fully redundant for a six joint serial manipulator.

Nonetheless, regardless the pose representation or the choice of Jacobian, the kinematic structure of the manipulator is liable to move towards such undesired singular configurations. In this context, singularity avoidance techniques based on dual quaternion algebra are presented in Chapter 5.

## 2.8 THEORETICAL BACKGROUND ON CONTROL

### 2.8.1 Stability analysis

The dynamic systems stability theory plays a key role in the theory and analysis of control systems. It is the first—and probably the most important—feature we seek to obtain in a control system [71]. To better understand the concept of stability, it is interesting to first introduce the concept of equilibrium points.

#### 2.8.1.1 Equilibrium points

Equilibrium points are fundamental to the analysis of dynamic systems, because they define the states in which the operating conditions of a dynamic system remains constant, that is, in situations where the system dynamics is in a steady condition [2]. In other words, given an initial condition  $x(0)$  such that the trajectory  $x(t)$  remains constant—that is, equal to  $x(0)$ —, we say that that  $x(0)$  is an **equilibrium point** [3]. A dynamic system can have none, one, multiples, or infinity equilibria.

Consider a dynamic system given by

$$\frac{dx}{dt} = F(x), \quad (2.49)$$

then  $x_e$  is said to be an equilibrium point of (2.49) if  $F(x_e) = 0$ , that is, if at a given moment  $t_e > 0$ , the trajectory of  $x(t)$  led to  $x(t_e) = x_e$ , then

$$x_e \text{ is an equilibrium point} \quad \Leftrightarrow \quad \forall t \geq t_e, x(t) \equiv x_e.$$

To ease the analysis, every equilibrium point that is different from zero, that is,  $x_e \neq 0$  will be transformed by a simple variable change, such that,

$$\begin{cases} z = x - x_e, \\ \dot{z} = F(z + x_e), \end{cases}$$

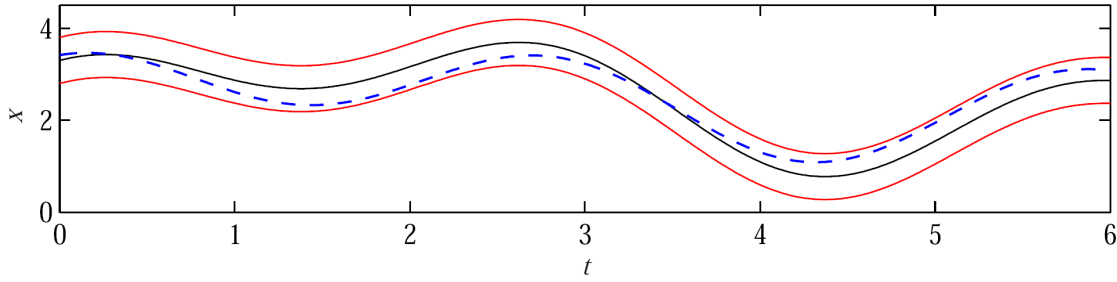


Figure 2.2: Trajectory of the state  $x$  over time (dashed line) for an stable equilibrium point (solid green line) [2].

and  $z_e = 0$  is the new equilibrium instead of  $x = x_e$ .

Intuitively, an equilibrium point is a desired point of operation for the dynamic system. However, the initial condition of the dynamic system is most often in a point different from the equilibrium. Hence, it is interesting to study the behavior of the system, that is, to investigate if the system trajectory will get closer or further away from the equilibrium. In this sense, we can roughly say that an equilibrium is stable if all solutions starting at a neighborhood from the equilibrium point are maintained within this neighborhood, otherwise, that is, if the trajectory tends to take the system away from the neighborhood, we say that the equilibrium is unstable. [2, 72].

**Definition 2.20.** [3, 72] An equilibrium point  $x_e = 0$  is **stable** if for any  $R > 0$ , there exists a  $r > 0$ —that depends and is smaller than the value of  $R$ , that is,  $0 < r(R) < R$ —, such that  $\|x(t_0)\| < r$ , where  $x(t_0)$  is the initial state, then  $\|x(t)\| < R$ , for all  $t \geq t_0$ .  
The aforementioned Definition 2.20 implies that a trajectory that starts near the equilibrium point, particularly within a ball  $r$  around the equilibrium point, will never escape a ball  $R$  around the equilibrium [3]. This notion is illustrated in the Figure 2.2, where the solution represented by the solid line is stable if we can guarantee that all solutions remain within a tube of diameter  $R$  by choosing initial conditions sufficiently close the solution.

This notion of stability is known as stability in the sense of Lyapunov,<sup>14</sup> the mathematician who first introduced this concept. Lyapunov proposed the first theoretical work on the stability of nonlinear dynamic systems which was published in 1892 in his doctoral thesis (*The General Problem of Motion Stability*) [73]. In his works, Lyapunov proposed two methods to investigate the stability of a dynamic system around the equilibrium point. The first method is based on the analysis and investigation of the stability of nonlinear systems through its linearized model [74]. The second method, known as direct method of Lyapunov, investigates the behavior of dynamic systems around a balance with the aid of a scalar function called Lyapunov function [3].

The Lyapunov function  $V : \mathbb{R}^n \mapsto \mathbb{R}$  is similar to an energy function that can be used to determine the stability of a dynamic system [2]. The concept of energy relates to the real world where whether mechanical, electrical or other, or amplifying system usually has a dissipation of energy. Hence, whenever the dissipation exceeds the amplification, the energy decay of the system and the system variables (oscillation amplitudes, velocities, voltages, currents, etc.) tend to evolve to zero (equilibrium point). Studying the energy associated to the system, or other convenient magnitude becomes possible to analyze its behavior, in particular its stability [3]. In this context, we are ready to characterize the stability conditions for an equilibrium point  $x_e = 0$  for a

<sup>14</sup>For further information regarding Aleksandr Lyapunov, please refer [73]

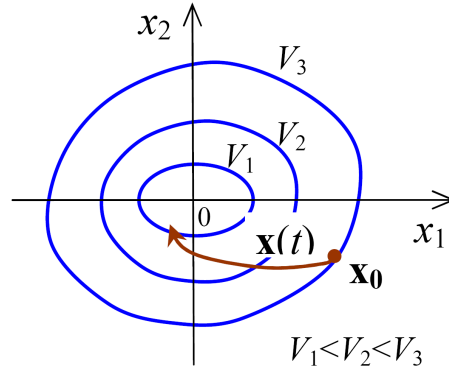


Figure 2.3: Geometric representation of the level curves of a Lyapunov function [3].

generic system (2.49).

**Theorem 2.3** Lyapunov Stability Theory (from [72, chapter 3])

Given an equilibrium point  $x_e = 0$ , if there is a ball  $B_R$  with diameter given by  $R > 0$  around an equilibrium point, for which there exists a continuous positive definite function  $V : \mathbb{R}^n \mapsto \mathbb{R}$  with time-derivate over the trajectory of the dynamic system (2.49),

$$\dot{V} = \frac{\partial V}{\partial x} \frac{dx}{dt} = \frac{\partial V}{\partial x} F(x),$$

negative semidefinite for all  $x \in B_R$ , then the equilibrium is locally stable in the sense of Lyapunov. If the statement is valid for all  $R > 0$ , then the equilibrium point is globally stable in the sense of Lyapunov. Moreover, if  $\dot{V}$  is negative definite, then the equilibrium point is asymptotically stable in the sense of Lyapunov.

All functions that satisfies the conditions from the Theorem 2.3 are called **Lyapunov functions**. Figure 2.3 illustrates a geometrical representation of this result for two dimensional system. Note that the level curves for a positive defined Lyapunov function are represented by  $0 < V_1 < V_2 < V_3$ . Hence, the condition  $\dot{V}(x) \leq 0$  implies that the trajectory of the system tend to the origin passing through different level curves that corresponds to smaller Lyapunov functions—as it approaches the equilibrium. Moreover, if the Lyapunov time derivative  $\dot{V}(x)$  is negative definite, then  $x(t) \rightarrow 0$  as  $t \rightarrow \infty$ .

The Theorem 2.3 also refers to concepts of stability and asymptotic stability of the equilibrium points. The former concept—also called neutrally stable in the Lyapunov sense—implies that for a given ball  $B_R$  with diameter  $R > 0$  around the equilibrium, if the initial state is within the ball  $B_R$ , that is,  $\|x(t_0)\| < R$ , where  $x(t_0)$  is the initial state, then  $\|x(t)\| < R$ , for all  $t \geq t_0$ . This concept is illustrate in Figure 2.4. Note that the system norm  $\|x(t)\|$  does not converges to the equilibrium, but remains limited within  $R$  throughout  $t > 0$ . On the other hand, if the equilibrium point is asymptotically stable then the system is neutrally stable in the Lyapunov sense and the the trajectory of the system also converges to the equilibrium, that is,  $\lim_{t \rightarrow \infty} x(t) \rightarrow x_e$ . Figure 2.5 illustrates the asymptotic stability definition.

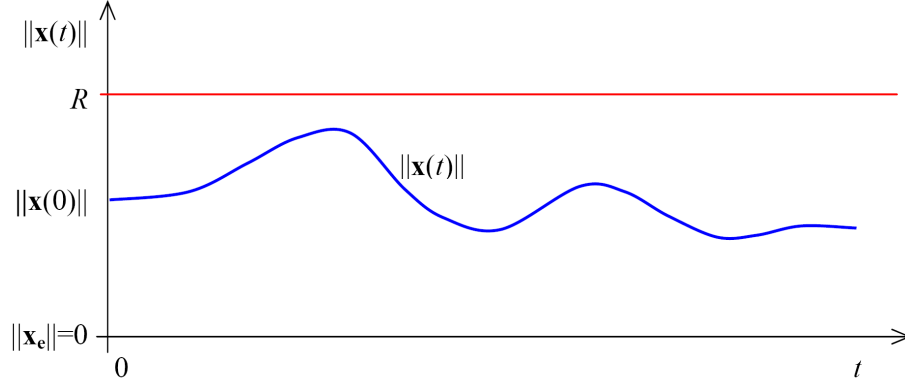


Figure 2.4: System with stable equilibrium point  $x_e = 0$  in the Lyapunov sense [3].

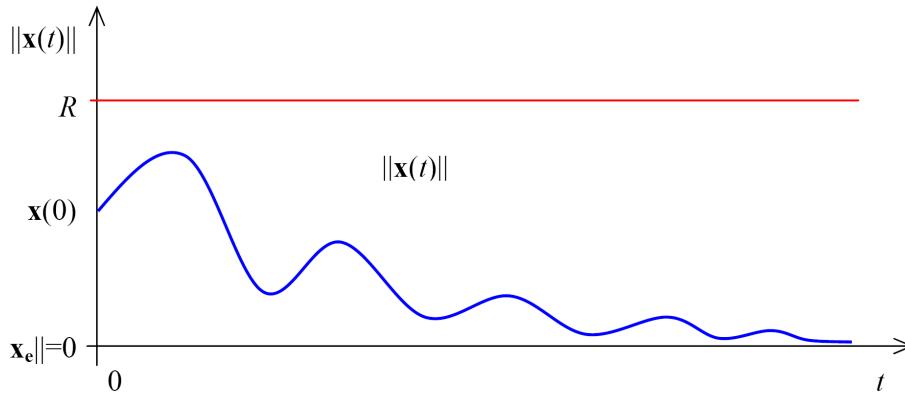


Figure 2.5: System with asymptotically stable equilibrium point  $x_e = 0$  in the Lyapunov sense [3].

## 2.9 LITERATURE REVIEW ON DUAL QUATERNION BASED KINEMATIC CONTROLLERS

Kinematic model of rigid bodies has been extensively studied in the last forty years, e.g., [27, 48, 75], and it is fundamental for practical aspects such as control, design, motion planning, singularity and workspace analysis [76]. Kinematic control is particularly regarded as an essential topic in the literature, which is reflected by its coverage on most textbooks in robotics (for example, see [27, 75]). It is suitable when the robot dynamics can be neglected, as in the case of stiff robots with harmonic drives operating at relatively low velocities.

In the study of kinematics, it is important to define a suitable representation for the rigid body displacement. Minimal representations such as Euler angles plus Cartesian coordinates lead to representation singularities (i.e., ambiguities that make the inverse problem ill-posed), whereas non-singular representations usually cannot be used directly as control variables.

Homogeneous transformation matrices (HTM) are a very popular choice for representing the coupled kinematics, but the control parameters must be extracted from the matrix, which requires additional calculations. Moreover, as stressed in this Chapter, the unit dual quaternions representation,  $\text{Spin}(3) \times \mathbb{R}^3$ , is more efficient and compact (eight elements against twelve), being less computationally demanding [1, 51, 56, 77]. In addition, control laws are defined directly over a vector field, eliminating the need to extract additional parameters or to

design matrix-based controllers (i.e., controllers based on the matrix structure of  $SE(3)$ ).

In the light of those advantages, there has been an increasing interest in the study of kinematic control in dual quaternion space. Those work comprise rigid body motion stabilization and tracking [36, 49, 52, 58–61], rigid body multi-agent coordination [62], and kinematic control of manipulators with single and multiple arms and human-robot interaction [4, 63, 78].

The aforementioned works can also be divided in two sets: the ones concerning general rigid body motion and the ones designed for robot manipulators.

Results designed for rigid body motion control are all based on a logarithmic mapping approximation and its relation to Lie algebra, which provides a geometric significance for the controller [36, 49, 52, 58–62]. The approach and results are thoroughly investigated in [49], where the authors provide the conditions for the logarithmic mapping approximation, its relation to Lie algebra, and a geometric viewpoint for the stability analysis. The technique has been extended to a leader-to-formation stability analysis in [62], and to application with dynamic controllers with a error function invariant to changes in the body coordinate frame in [36, 52].

Nonetheless, aforementioned results solely regard the general rigid body kinematics; that is, none deals with the specificities of manipulators. This is specially important because manipulator tasks are better described at the end-effector, but the control is performed at the joint level, which imposes an additional mapping between the dual quaternion representing the end-effector pose/velocity and the vector corresponding to the joint positions/velocities. Since this second mapping arises from the manipulator kinematics, it is crucial to satisfy its constraints in order to design feasible controllers for this class of robots.

On the other hand, results designed for manipulator control (see, [4, 63, 78]) explicitly regard the robotic arm kinematics in order to perform dual quaternion control, which produces a more intuitive manner to define the robot objective. The authors therein propose a control strategy based on the dual quaternion error mapping to the eight-dimensional real manifold, which has the advantage of being considerably more straightforward and attractive from the control point of view. Although it is not invariant to changes in the reference coordinate system and lacks an explicit geometric significance for the designer due to the error mapping.

### **2.9.1 In the control point of view: differences between quaternions and dual quaternions**

The literature of attitude modeling and control using quaternions is extensive with excel theoretical and practical results. These results are unfortunately not reflected within dual quaternions literature. The challenge lies in the fact that albeit some algebraic identities in quaternion algebra can be carried over to the dual quaternion algebra by the principle of transference [23, 67], most generalization does not follow by the principle of transference. In fact, counterexamples shown in [67] illustrate the failure of the transfer principle outside the algebraic realm.

Whereas unit quaternions are used to model only attitude and is a double cover for the Lie group  $SO(3)$ , unit dual quaternions model the coupled attitude and position and is a double cover for the Lie group  $SE(3)$ . The necessity of different procedures for quaternion and dual quaternion stems from their different topologies and group structures. For example, the unit quaternion group is a compact manifold, while the unit dual quaternion group is not a compact manifold. This reflects in the use of distinct approaches to controller design (see for instance, the control differences between  $SO(3)$  and  $SE(3)$  which is detailed described in [55]). Moreover, due to  $SO(3)$  being compact, it has a natural bi-invariant metric. The same is valid for the group of

unit quaternions. Nonetheless, the same can not be said from  $SE(3)$ , nor from  $\text{Spin}(3) \times \mathbb{R}^3$ —both of which do not possess any bi-invariant metric.

It is also interesting to highlight that The unit dual quaternion group is not a subgroup from  $\text{Spin}(3)$ —it is indeed the other way around—and boundedness, geodesic distance, norm properties, and other manifold features that are valid on  $\mathcal{S}^3$  cannot be directly carried to  $\text{Spin}(3) \times \mathbb{R}^3$ .

In this sense, the extension of control results to  $\text{Spin}(3) \times \mathbb{R}^3$  is not trivial, which is reflected by the gap between quaternion based results and dual quaternion based controllers. To overcome this gap of representation and control is one of the main motivations of the present manuscript.



# 3

## DUAL QUATERNION BASED ROBUST $H_\infty$ KINEMATIC CONTROL OF MANIPULATOR ROBOTS

---

*Noise, like most things in life, is beneficial in moderate amounts. We also see this in human psychological responses to noise. Too much noise will drive humans insane, but too little noise might also result in loss of sanity. Noise is especially beneficial for control engineers, who would not only lose their sanity, but would also lose their research funding if not for noise – Yaakov Bar-Shalom*

Rigid body motion have been extensively studied within the robotics community in the last forty years and its description is closely related to specificities of a prescribed control task. In the context of robotic arms, several tasks can be accomplished by stiff manipulators at relatively low velocities and accelerations, justifying the use of kinematic description and control strategies (see, e.g., [27, 48, 75]). Simplifications that arise from such description allows designing controllers that do not require inertial parameter specifications of the manipulator. Still, in practical applications, the control problem for manipulators is liable to modeling errors and uncertainties, exogenous disturbances, kinematic singularities and, depending on the topological framework, even representation singularities. In the present chapter, we take interest at studying kinematic uncertainties and designing more efficient controllers in the sense of noise sensitivity, performance and control effort.

The problem of kinematic representing the rigid motion of manipulators has been extensively studied in the last forty years and is one of the classic topics covered by most of robotics textbooks (for example, see [27, 75]). The study of manipulator control and task specifications is inherently connected to the research on efficient representations for rigid body transformation since, task specifications are usually defined at a non-Euclidean manifold, the group of rigid body motions,  $SE(3)$ . In the light of the unit dual quaternion advantages for describing rigid body motions (see Chapter 2), there has been an increasing interest in the study and representation of kinematics using unit dual quaternions.

Nonetheless, among existing results concerning kinematic control in dual quaternion space, either for rigid body stabilization or for kinematic control of manipulators—and, despite their contributions—there is no result in dual quaternion literature that studies the geometric influence of uncertainties and disturbances, nor solutions and analysis on robustness and performance, energy efficiency, nor suitable controllers to overcome their detrimental influence.

Indeed, we have introduced in [64] an initial discussion on disturbances and robust control for rigid motion, but it is the only result in the literature. Still, only twist disturbances are considered, the trajectory as well as the external disturbances are defined in an  $\mathbb{R}^8$  manifold, and there is no relation nor discussion regarding the actual physical meaning—which, as a consequence, reduces its applicability.

In this context and motivated by the problem of optimizing the system performance, this chapter first introduces a detailed discussion and analysis on the influence of exogenous disturbances and uncertainties over the kinematic modeling for manipulators—which in turn yields a new a new kinematic description. Moreover, an invariant error function that describes the spatial difference between the desired and current end-effector

configuration is introduced.

Thereafter, this chapter is concerned to explicitly describe the system requirements into an  $H_\infty$  control design. The  $H_\infty$  control theory, originated as a technique to reduce the feedback system sensitivity [79], allows the designer to incorporate robustness requirements, disturbance attenuation, and performance properties<sup>1</sup> into one stabilization problem [81]. The proposed dual quaternion kinematic controllers derived in this chapter explicitly address different sources of uncertainties and disturbances and their influence over the orientation and translation in the  $H_\infty$  sense, which has the advantage of casting aside requirements regarding the distribution description—that are significantly hard to characterize within  $SE(3)$  or within  $\text{Spin}(3) \times \mathbb{R}^3$ . Using the dual quaternion algebra, we adapt classic  $H_\infty$  techniques—suitable solely for additive noises—to derive easy-to-implement closed form  $H_\infty$  control and tracking strategies that also incorporate robustness requirements, disturbance attenuation, and performance properties, while minimizing the required control effort.

Based on the two results for the task-space differential kinematics of the robotic manipulator described in (2.38) and in (2.42), we also derive two different  $H_\infty$  control strategies.

The first technique is based on the dual quaternion mapping to an Euclidean manifold. The resulting closed-loop system is described in the  $\mathbb{R}^8$  manifold which lacks an explicitly geometric influence for the end-effector transformations but, on the other hand, let us derive a discrete-time implementation which in turn enlarges the universe of practical applications for the contributions.

The second criterion—based on the differential kinematic description (2.42)-(2.43)—proposes a new framework for kinematic control of robot manipulators by deriving a control law in dual quaternion tangent space. Using the dual quaternion Jacobian  $\underline{J}_w$  mapping between the Lie algebra of unit dual quaternions and the joint velocity vector, this is the first result to combine the geometric significance of the Lie algebra of  $\text{Spin}(3) \times \mathbb{R}^3$  with the practicability of being linearly directly mapped to the joint velocity inputs. The method provides an intuitive and elegant connection between control effort and the performance effects over the end-effector trajectory and different sources of uncertainties and disturbances.

The last section of the chapter is dedicated to simulations with different scenarios and conditions using Matlab and the Virtual Robot Experimentation Platform (V-REP) from Coppelia Robotics GmbH.

### 3.1 MODELING WITH UNCERTAINTIES AND ERROR DEFINITION

This section address the description and the influence of different sources of exogenous disturbances and uncertainties which affect the accuracy of the system representation and, as a direct consequence, the control performance. Hence, the description of an  $n$ -joint serial manipulator using unit dual quaternion framework is extended in order to explicitly incorporate their influence. Moreover, an invariant error function that describes the spatial difference between the desired and current end-effector configuration is introduced.

---

<sup>1</sup>Other properties and design problems, such as reducing the model uncertainty “ball”, may be expressed within the  $H_\infty$  norm, see [80, 81] for further discussion on problem formulations in terms of the  $H_\infty$  norm.

### 3.1.1 Manipulator kinematic model with uncertainties and exogenous disturbances

According to the  $n$ -joint serial manipulator description stressed in Section 2.7, the forward kinematics relates the configuration of all joints to the configuration  $\underline{\boldsymbol{x}}_E$  of the end-effector; that is,  $\underline{\boldsymbol{x}}_E = \underline{\boldsymbol{x}}_1^0 \underline{\boldsymbol{x}}_2^1 \dots \underline{\boldsymbol{x}}_n^{n-1}$ , and the differential forward kinematics is hence given by  $\dot{\underline{\boldsymbol{x}}}_E = \sum_{i=0}^{n-1} \underline{\boldsymbol{x}}_i^0 \dot{\underline{\boldsymbol{x}}}_{i+1}^i \underline{\boldsymbol{x}}_n^{i+1}$ . Because  $\underline{\boldsymbol{x}}_{i+1}^i$  is a function of  $\theta_i$ , i.e.,  $\underline{\boldsymbol{x}}_{i+1}^i = \underline{\boldsymbol{f}}_i(\theta_i)$ , where  $\underline{\boldsymbol{f}}_i : \mathbb{R} \rightarrow \text{Spin}(3) \times \mathbb{R}^3$ , we have that  $\dot{\underline{\boldsymbol{x}}}_{i+1}^i = \underline{\boldsymbol{f}}_i'(\theta_i) = \underline{\boldsymbol{w}}_i \dot{\theta}_i \underline{\boldsymbol{f}}_i(\theta_i)$  with  $\underline{\boldsymbol{w}}_i \in \mathbb{H}_0 \otimes \mathbb{D}$ . Explicitly considering the dual quaternion differential FKM to be well defined within the unit dual quaternion group, we have a differential FKM described as in (2.42)-(2.48), that is,

$$\begin{aligned} \dot{\underline{\boldsymbol{x}}}_E &= \frac{1}{2} \sum_{i=0}^{n-1} \underline{\boldsymbol{j}}_i \dot{\theta}_i \underline{\boldsymbol{x}}_E \\ &= \frac{1}{2} \text{vec}_6 \left( \underline{\boldsymbol{J}}_{\underline{\boldsymbol{w}}} \dot{\boldsymbol{\theta}} \right) \underline{\boldsymbol{x}}_E, \end{aligned} \quad (3.1)$$

where  $\text{vec}_6 \left( \underline{\boldsymbol{J}}_{\underline{\boldsymbol{w}}} \dot{\boldsymbol{\theta}} \right)$  describes the end-effector twist in dual quaternion space,  $\boldsymbol{\theta} = [\theta_0 \dots \theta_{n-1}]^T$  is the measured vector of joint variables and  $\underline{\boldsymbol{J}}_{\underline{\boldsymbol{w}}}$  is the Jacobian, which can be found by using Algorithm 2.2.

Nonetheless, in more realistic scenarios, there exists several influences acting upon the system, such that the description of (3.1) is not perfect, and it is interesting to consider the effects of different disturbances over the system. Indeed, in practical applications, the trajectory of the system is often influenced by different sources of exogenous disturbances, arm parameters may not be exactly accurate, and the forward kinematics liable to unknown uncertainties, such as unmodeled viscosities, friction, etc. To improve the kinematics accuracy and the control performance, the influence of these uncertainties and disturbances over the system must be explicitly regarded, as neglecting their influence would most likely lead to poor performance. In this sense, different sources of disturbances acting on a serial manipulator, classified as twist and pose configuration uncertainties, are investigated which leads to a more complete and accurate kinematics description, although being more challenging.

Twist uncertainties  $\underline{\boldsymbol{v}}_w$  represent unmodeled twists describing multiple sources of exogenous disturbances, unmodeled time-varying uncertainties, and forces acting directly at the pose of the end-effector (e.g., gravity or interaction with the environment) or at different links from the serial manipulator, such that

$$\dot{\underline{\boldsymbol{x}}}_E = \frac{1}{2} \sum_{i=0}^{n-1} \underline{\boldsymbol{j}}_i \dot{\theta}_i \underline{\boldsymbol{x}}_E + \frac{1}{2} \underline{\boldsymbol{v}}_w \underline{\boldsymbol{x}}_E. \quad (3.2)$$

The differential equation is well-posed as  $\underline{\boldsymbol{v}}_w \triangleq \underline{\boldsymbol{v}}_w + \varepsilon \underline{\boldsymbol{v}}_w'$ , with  $\underline{\boldsymbol{v}}_w, \underline{\boldsymbol{v}}_w' \in \mathbb{H}_0$ , is in the Lie algebra of  $\text{Spin}(3) \times \mathbb{R}^3$ .

The influence of uncertainties over the pose configuration often arises from unforeseen inaccuracies within model parameters and time-varying uncertainties and disturbances on the coordinate base of the manipulator or at the reference frame. It may be described as an unknown transformation in the forward kinematics model and, therefore, mapped to (3.1)-(3.2) as

$$\underline{\boldsymbol{x}} = \underline{\boldsymbol{x}}_E \underline{\boldsymbol{c}}, \quad (3.3)$$

where  $\underline{\boldsymbol{c}} \in \text{Spin}(3) \times \mathbb{R}^3$  and  $\underline{\boldsymbol{x}}$  denotes the real configuration of the disturbed end-effector. In this sense and with regard to the kinematics of the unknown pose disturbance,  $\dot{\underline{\boldsymbol{c}}} = \frac{1}{2} \underline{\boldsymbol{c}} \underline{\boldsymbol{v}}_c'$ , the overall differential kinematics

yields

$$\begin{aligned}
\dot{\underline{\boldsymbol{x}}} &= \dot{\underline{\boldsymbol{x}}_E} \underline{\boldsymbol{c}} + \underline{\boldsymbol{x}}_E \dot{\underline{\boldsymbol{c}}} \\
&= \frac{1}{2} \sum_{i=0}^{n-1} \underline{\boldsymbol{j}}_i \dot{\theta}_i \underline{\boldsymbol{x}}_E \underline{\boldsymbol{c}} + \frac{1}{2} \underline{\boldsymbol{v}}_w \underline{\boldsymbol{x}}_E \underline{\boldsymbol{c}} + \frac{1}{2} \underline{\boldsymbol{x}}_E \underline{\boldsymbol{c}} \tilde{\underline{\boldsymbol{v}}}_c \\
&= \frac{1}{2} \left( \sum_{i=0}^{n-1} \underline{\boldsymbol{j}}_i \dot{\theta}_i \underline{\boldsymbol{x}} + \underline{\boldsymbol{v}}_w \underline{\boldsymbol{x}} + \underline{\boldsymbol{x}} \tilde{\underline{\boldsymbol{v}}}_c \right).
\end{aligned}$$

where  $\tilde{\underline{\boldsymbol{v}}}_c \in \mathbb{H}_0 \otimes \mathbb{D}$ . To improve the readability, we redefine  $\tilde{\underline{\boldsymbol{v}}}_c$  using the adjoint transformation,  $\tilde{\underline{\boldsymbol{v}}}_c \triangleq \underline{\boldsymbol{x}}^* \underline{\boldsymbol{v}}_c \underline{\boldsymbol{x}}$ , which does not affect the induced norm,  $\|\underline{\boldsymbol{v}}_c\| = \|\tilde{\underline{\boldsymbol{v}}}_c\|$ , such that,

$$\dot{\underline{\boldsymbol{x}}} = \frac{1}{2} \left( \sum_{i=0}^{n-1} \underline{\boldsymbol{j}}_i \dot{\theta}_i \underline{\boldsymbol{x}} + \underline{\boldsymbol{v}}_w \underline{\boldsymbol{x}} + \underline{\boldsymbol{v}}_c \underline{\boldsymbol{x}} \right). \quad (3.4)$$

*Remark 3.1.* It is important to highlight that specific joint configurations may render the differential FKM to be ill-posed—that is, the joint-dependent Jacobian matrix which maps the joint-vector velocity to task-space end-effector velocity loses rank. At these singularities, the desired differential kinematics within unit dual quaternion unfolds outside the Jacobian range space—in other words, the manipulator temporarily loses one or more degrees-of-freedom (DOFs) at task-space. Regardless the pose representation or the choice of Jacobian, the kinematic structure of the manipulator is liable to move towards such undesired configurations. Herein, to better illustrate the advantages of the proposed criteria and to maintain conciseness and simplicity, Jacobian matrix is assumed to be well-posed. Still, avoidance techniques in the context of dual quaternion algebra are presented in Chapter 5.

### 3.1.2 Error definition and problem statement

In this chapter, we are particularly interested in stabilizing the end-effector to a desired configuration and to reduce the influence of uncertainties and disturbances upon the controlled pose. In other words, given a desired output, we seek to reduce the noise-to-output influence while maintaining the system internal stability.

To this aim, given a desired fixed end-effector configuration  $\underline{\boldsymbol{x}}_d$ , we define the spatial difference in  $\text{Spin}(3) \times \mathbb{R}^3$  as

$$\underline{\boldsymbol{x}}_e = \underline{\boldsymbol{x}} \underline{\boldsymbol{x}}_d^* = \underline{\boldsymbol{r}}_e + \varepsilon \frac{1}{2} \underline{\boldsymbol{p}}_e \underline{\boldsymbol{r}}_e, \quad (3.5)$$

where  $\underline{\boldsymbol{r}}_e$  denote the orientation error in  $\text{Spin}(3)$  and  $\underline{\boldsymbol{p}}_e$  the position error in  $\mathbb{H}_0$ . Hence, the spatial differential kinematics for  $\underline{\boldsymbol{x}}_e$  yields

$$\begin{aligned}
\dot{\underline{\boldsymbol{x}}}_e &= \frac{1}{2} \left( \sum_{i=0}^{n-1} \underline{\boldsymbol{j}}_i \dot{\theta}_i \underline{\boldsymbol{x}} + \underline{\boldsymbol{v}}_w \underline{\boldsymbol{x}} + \underline{\boldsymbol{v}}_c \underline{\boldsymbol{x}} \right) \underline{\boldsymbol{x}}_d^* \\
&= \frac{1}{2} \left( \sum_{i=0}^{n-1} \underline{\boldsymbol{j}}_i \dot{\theta}_i + \underline{\boldsymbol{v}}_w + \underline{\boldsymbol{v}}_c \right) \underline{\boldsymbol{x}}_e.
\end{aligned} \quad (3.6)$$

From the spatial difference, we also define an invariant dual quaternion error function of the form  $\underline{\boldsymbol{e}} : \text{Spin}(3) \times \mathbb{R}^3 \mapsto \mathbb{H} \otimes \mathbb{D}$ , given by

$$\underline{\boldsymbol{e}} = 1 - \underline{\boldsymbol{x}}_e = \underline{\boldsymbol{e}} + \varepsilon \underline{\boldsymbol{e}}' \quad (3.7)$$

with dynamics described by  $\dot{\underline{\boldsymbol{e}}} = -\dot{\underline{\boldsymbol{x}}}_e$ . In this sense, when  $\underline{\boldsymbol{x}}$  converges to  $\underline{\boldsymbol{x}}_d$ , the spatial difference  $\underline{\boldsymbol{x}}_e$  tends to 1 and, consequently, the dual quaternion error function  $\underline{\boldsymbol{e}} \rightarrow 0$ . Analogously, to stabilize  $\underline{\boldsymbol{e}}$  to 0 yields the end-effector convergence to the desired pose.

It is interesting to highlight that the convergence properties from  $\underline{x}$  to  $\underline{x}_d$  are utterly related to the definition of the dual quaternion error function,  $\underline{e}$ , which is invariant with respect to coordinate changes with regard to arbitrary right shifts.<sup>2</sup> For instance, let us assume that both end-effector frame and desired set point have been transformed by a coordinate change represented by the unit dual quaternion  $\underline{y}$ ; that is,

$$\begin{aligned}\underline{x}' &= \underline{x}\underline{y} \\ \underline{x}'_d &= \underline{x}_d\underline{y}.\end{aligned}$$

Since  $\underline{e} = 1 - \underline{x}_e$ , the error in the new coordinate system is given by

$$\begin{aligned}\underline{e}' &= 1 - \underline{x}'_e = 1 - \underline{x}'\underline{x}'_d^* \\ &= 1 - \underline{x}\underline{y}\underline{y}^*\underline{x}_d^* \\ &= \underline{e},\end{aligned}$$

which is independent of  $\underline{y}$ . Similar properties are described for matrix representations in the excel work of Bullo and Murray, [55]. In this context, to asymptotically stabilize the system (3.7) is to assume  $\underline{x} \rightarrow \underline{x}_d$  as  $t \rightarrow \infty$ , independently from the choice of the robot base coordinate system and from coordinate changes.

To address the detrimental influence of the uncertainties and disturbances in the  $H_\infty$  sense, we assume that  $\mathbf{v}_w, \mathbf{v}'_w, \mathbf{v}_c, \mathbf{v}'_c \in L_2[0, \infty)$ .<sup>3</sup> The gain that defines the  $H_\infty$  norm arises from the induced norm of the map  $\mathbf{v} \rightarrow \mathbf{z}$ , where  $\mathbf{z} \in L_2[0, \infty)$  is the desired output state [81], and represents the supremum of the noise amplification upon the system output

$$\sup \left\{ \frac{\|\mathbf{z}\|_2}{\|\mathbf{v}\|_2}, \mathbf{v} \in L_2 \setminus \{0\} \right\}, \quad (3.8)$$

that is, the worst-case influence of the noise over the controlled output. The main advantage of the  $H_\infty$  norm is the needlessness for assumptions regarding the statistics of the uncertainties and noises—although this information, if available, can improve analysis [83]. This is particular sensible for the space of rigid body transformations as probability density functions are in general not well defined for such non-Euclidean spaces.

Since a direct minimization from (3.8) may not be tractable, we introduce a variable  $\gamma$  that upper bounds the induced norm

$$\|\mathbf{z}\|_2 \leq \gamma \|\mathbf{v}\|_2.$$

The smaller is the value of the noise-to-output upper bound  $\gamma$ , the smaller is the influence of  $\mathbf{v}$  over  $\mathbf{z}$ . Hence, the reduction of the index  $\gamma$  provides a way of reducing the disturbance influence from the output,  $\mathbf{z}$ . Therefore, the goal of the  $H_\infty$  control is to reduce the noise-to-output upper bound  $\gamma$ , while maintaining the system internal stability.

## 3.2 DUAL QUATERNION BASED $H_\infty$ CONTROLLER IN $\mathbb{R}^8$ MANIFOLD

As discussed in the preceding section, the impact of different sources of uncertainties and disturbances over the system kinematics must be explicitly regarded, and the controller must be designed in accordance to

<sup>2</sup>Moreover, the error function (3.7) is also right invariant with regard to its norm at the Lie group tangent space. In this sense, due to the topological constraint inherent from  $SE(3)$ , there exists no continuous metric function for rigid motion that are invariant under arbitrary left and right shifts. Still, the proposed right invariant error also ensures bi-invariance under pure rotations [82].

<sup>3</sup> $L_2$  is the Hilbert space of all square-integrable functions.

their influence, as neglecting their effects jeopardizes the overall stability. Since classic  $H_\infty$  theory is based on additive noises, instead of multiplicative disturbances as in (3.6), this section presents a new control strategies that ensures  $H_\infty$  performance for the control requirements based on the dual quaternion mapping to an  $\mathbb{R}^8$  manifold where the problem is redefined and solutions to the  $H_\infty$  control derived. The first part of the section presents solutions for the continuous-time  $H_\infty$  control problem, whereas the second part extends the analysis to the discrete-time domain which also includes discretization based uncertainties.

### 3.2.1 Continuous-time dual quaternion based $H_\infty$ controller in $\mathbb{R}^8$ manifold

In this subsection, we address different control design strategies for the continuous-time kinematic model based on the dual quaternion space mapping to an  $\mathbb{R}^8$  manifold.

To this aim, we first redesign the differential FKM subject to uncertainties and exogenous disturbances described in (3.4) using the vector space mapping from (2.14). Hence, the differential kinematics of the robotic manipulator considering the effects of different disturbances over the system is given by

$$\text{vec}_8 \dot{\underline{\boldsymbol{x}}} = \sum_{i=0}^{n-1} \text{vec}_8 \left\{ \frac{1}{2} \underline{\boldsymbol{j}}_i \underline{\boldsymbol{x}} \right\} \dot{\theta}_i + \frac{1}{2} \bar{\boldsymbol{H}}(\underline{\boldsymbol{x}}) \text{vec}_8 (\underline{\boldsymbol{v}}_w + \underline{\boldsymbol{v}}_c), \quad (3.9)$$

where  $\bar{\boldsymbol{H}}(\underline{\boldsymbol{x}})$  is the matrix representation for dual quaternion multiplication as described in (2.15). Moreover, inspecting the first element in the right side of the equation, it turns out that the term yields the dual quaternion based Jacobian  $\boldsymbol{J}_{\text{vec}}$  described in (2.38)-(2.41). Hence, considering  $\underline{\boldsymbol{v}} \triangleq \underline{\boldsymbol{v}}_w + \underline{\boldsymbol{v}}_c$ , we can redefine (3.9) as

$$\text{vec}_8 \dot{\underline{\boldsymbol{x}}} = \boldsymbol{J}_{\text{vec}} \dot{\boldsymbol{\theta}} + \boldsymbol{B} \text{vec}_8 \underline{\boldsymbol{v}} \quad (3.10)$$

where  $\boldsymbol{\theta} = [\theta_0 \dots \theta_{n-1}]^T$  is the measured vector of joint variables,  $\boldsymbol{J}_{\text{vec}}$  is the analytical dual quaternion based Jacobian, which can be found by using Algorithm 2.1,  $\boldsymbol{B}$  is a known matrix concerning  $\underline{\boldsymbol{x}}$  and  $\underline{\boldsymbol{v}}$  is the dual quaternion denoting the exogenous disturbances, whose influence we want to minimize. Note that  $\underline{\boldsymbol{v}}$  actually belongs to the set of pure dual quaternions  $\mathbb{H}_0 \otimes \mathbb{D}$  which in turn is isomorphic to  $\mathbb{R}^6$ .

The differential forward kinematics (3.10) has a direct influence on the error function dynamics which must also be described in the same manifold. Hence, rewriting (3.5)(3.7) as  $\underline{\boldsymbol{e}} = (\underline{\boldsymbol{x}}_d - \underline{\boldsymbol{x}}) \underline{\boldsymbol{x}}_d^*$ , the error function can be mapped into the  $\mathbb{R}^8$  manifold, using (2.14)-(2.15), as

$$\text{vec}_8 \underline{\boldsymbol{e}} = \bar{\boldsymbol{H}}(\underline{\boldsymbol{x}}_d^*) \text{vec}_8 (\underline{\boldsymbol{x}}_d - \underline{\boldsymbol{x}}). \quad (3.11)$$

For  $\underline{\boldsymbol{x}}_d$  constant, the first derivative of (3.11) yields

$$\text{vec}_8 \dot{\underline{\boldsymbol{e}}} = -\bar{\boldsymbol{H}}(\underline{\boldsymbol{x}}_d^*) \text{vec}_8 \dot{\underline{\boldsymbol{x}}}.$$

Since the differential kinematics for the end-effector is given by (3.10), then the error dynamics can be described by

$$\begin{aligned} \text{vec}_8 \dot{\underline{\boldsymbol{e}}} &= -\bar{\boldsymbol{H}}(\underline{\boldsymbol{x}}_d^*) \boldsymbol{J}_{\text{vec}} \dot{\boldsymbol{\theta}} - \bar{\boldsymbol{H}}(\underline{\boldsymbol{x}}_d^*) \boldsymbol{B} \text{vec}_8 \underline{\boldsymbol{v}} \\ &\quad - \boldsymbol{N} \dot{\boldsymbol{\theta}} - \boldsymbol{B}_v \boldsymbol{v}, \end{aligned} \quad (3.12)$$

where  $\boldsymbol{N} = \bar{\boldsymbol{H}}(\underline{\boldsymbol{x}}_d^*) \boldsymbol{J}_{\text{vec}}$  and  $\boldsymbol{B}_v = \bar{\boldsymbol{H}}(\underline{\boldsymbol{x}}_d^*) \boldsymbol{B}$ . Moreover, note that  $\underline{\boldsymbol{v}}$  belongs to the pure dual quaternion set. Hence, from the natural isomorphism from  $\mathbb{H}_0 \otimes \mathbb{D}$  and  $\mathbb{R}^6$ , it turns out that  $\text{vec}_8 \underline{\boldsymbol{v}}$  yields an  $\mathbb{R}^8$  vector with

first and fourth elements being zero. This particular eight dimensional vector will be denoted  $\underline{v}$ , and its norm is given by  $\|\text{vec}_6 \underline{v}\|$ .

For the  $H_\infty$  control, we seek a control law that makes the dual quaternion configuration  $\underline{x}$  asymptotically converges to  $\underline{x}_d$ , whereas ensuring disturbances attenuation properties, i.e., attenuating the influence of any exogenous signal  $\underline{v} \in L_2[0, \infty)$ . In this context and based on [81], the following definition describes the robust performance in the  $H_\infty$  sense for the closed-loop system described by a dual quaternion mapping to  $\mathbb{R}^8$ .

**Definition 3.1.** (Based on [81]) For a prescribed scalar  $\gamma > 0$ , the robust control performance is achieved with an  $H_\infty$  norm bound  $\gamma$ , if the following hold

- (1) The error dynamics (3.12) is asymptotically stable for  $\underline{v} \equiv 0$ ;
- (2) Under the assumption of zero initial conditions, the disturbance influence on the error,  $\text{vec}_8 \underline{e}$ , is attenuated below a desired level  $\gamma$ ,  $\|\text{vec}_8 \underline{e}\|_2 \leq \gamma \|\underline{v}\|_2$  for all nonzero  $\underline{v} \in L_2[0, \infty)$ .

Considering the system description and Definition 3.1, we state a solution for the  $H_\infty$  control problem in the following criterion.<sup>4</sup>

**Theorem 3.1** Dual quaternion and LMI based  $H_\infty$  controller

For a prescribed  $\gamma > 0$ , there exist a task-space controller such that (3.12) achieves robust stability with  $H_\infty$  performance  $\gamma$ , in the sense of Definition 3.1, if there exist matrices  $\mathbf{P} = \mathbf{P}^T > 0$  and  $\mathbf{G} = \mathbf{G}^T > 0$ , such that

$$\begin{bmatrix} (-2\mathbf{G} + \mathbf{I}) & -\mathbf{P}\mathbf{B}_v \\ -\mathbf{B}_v^T \mathbf{P} & -\gamma^2 \mathbf{I} \end{bmatrix} < 0. \quad (3.13)$$

Moreover, if the above conditions are satisfied, a stabilizing joint velocity vector control is given by  $\dot{\boldsymbol{\theta}} = \mathbf{N}^+ (\mathbf{P}^{-1} \mathbf{G}) \text{vec}_8 \underline{e}$ , where  $\mathbf{N}^+$  is the pseudoinverse of  $\mathbf{N}$ .

*proof.*

Let us choose as Lyapunov function candidate the positive definite quadratic function:

$$V = \text{vec}_8 \underline{e}^T \mathbf{P} \text{vec}_8 \underline{e}. \quad (3.14)$$

Taking the time-derivative of (3.14) with respect to  $t$  along the trajectory (3.12) and by setting the task-space controller as  $\dot{\boldsymbol{\theta}} \triangleq \mathbf{N}^+ \mathbf{K} \mathbf{P} \text{vec}_8 \underline{e}$ , yields

$$\begin{aligned} \dot{V} &= \text{vec}_8 \underline{\dot{e}}^T \mathbf{P} \text{vec}_8 \underline{e} + \text{vec}_8 \underline{e}^T \mathbf{P} \text{vec}_8 \underline{\dot{e}} = 2 \text{vec}_8 \underline{e}^T \mathbf{P} \text{vec}_8 \underline{\dot{e}} \\ &= -2 \text{vec}_8 \underline{e}^T \mathbf{P} (\mathbf{N} \dot{\boldsymbol{\theta}} + \mathbf{B}_v \underline{v}) \\ &= -2 \text{vec}_8 \underline{e}^T \mathbf{P} (\mathbf{K} \mathbf{P} \text{vec}_8 \underline{e} + \mathbf{B}_v \underline{v}). \end{aligned}$$

<sup>4</sup>Avoidance techniques for kinematic singularities are considered in Chapter 5. Herein, the Jacobian matrix  $\mathbf{N}$  is assumed to be well-posed.

For any  $\mathbf{K} > 0$ , it is easy to see that  $\dot{V} < 0$  holds for  $\mathbf{v} \equiv 0$ , which in turn implies  $V \rightarrow 0$  as  $t \rightarrow \infty$ . Hence,  $\text{vec}_8 \underline{\mathbf{e}}$  converges to zero, and the first condition in Definition 3.1 is satisfied. Now, let us define  $\dot{V}_{H_\infty} \triangleq \dot{V} + \text{vec}_8 \underline{\mathbf{e}}^T \text{vec}_8 \underline{\mathbf{e}} - \gamma^2 \mathbf{v}^T \mathbf{v}$ , such that

$$\dot{V}_{H_\infty} = -\text{vec}_8 \underline{\mathbf{e}}^T (2\mathbf{PKP} - \mathbf{I}) \text{vec}_8 \underline{\mathbf{e}} - 2 \text{vec}_8 \underline{\mathbf{e}}^T \mathbf{PB}_v \mathbf{v} - \gamma^2 \mathbf{v}^T \mathbf{v},$$

which can also be written as

$$\dot{V}_{H_\infty} = \begin{bmatrix} \text{vec}_8 \underline{\mathbf{e}} \\ \mathbf{v} \end{bmatrix}^T \begin{bmatrix} (-2\mathbf{G} + \mathbf{I}) & -\mathbf{PB}_v \\ -\mathbf{B}_v^T \mathbf{P} & -\gamma^2 \mathbf{I} \end{bmatrix} \begin{bmatrix} \text{vec}_8 \underline{\mathbf{e}} \\ \mathbf{v} \end{bmatrix},$$

for  $\mathbf{G} = \mathbf{PKP}$ . Note that the condition (3.13) holds if and only if the term  $\dot{V}_{H_\infty}$  is negative definite. Thus, we must have  $\dot{V} + \text{vec}_8 \underline{\mathbf{e}}^T \text{vec}_8 \underline{\mathbf{e}} - \gamma^2 \mathbf{v}^T \mathbf{v} < 0$ . Integrating the inequality from 0 to  $t$ , yields

$$\int_0^t \left[ \dot{V} + \text{vec}_8 \underline{\mathbf{e}}^T \text{vec}_8 \underline{\mathbf{e}} - \gamma^2 \mathbf{v}^T \mathbf{v} \right] dt - V(0) + \int_0^t \left[ \text{vec}_8 \underline{\mathbf{e}}^T \text{vec}_8 \underline{\mathbf{e}} - \gamma^2 \mathbf{v}^T \mathbf{v} \right] dt < 0.$$

Now, under zero initial conditions and given the Lyapunov function positiveness properties, we have  $\int_0^t \text{vec}_8 \underline{\mathbf{e}}^T \text{vec}_8 \underline{\mathbf{e}} dt - \int_0^t \gamma^2 \mathbf{v}^T \mathbf{v} dt < 0$ , for all  $t > 0$ . Note that  $\mathbf{v} \in L_2[0, \infty)$ , thus  $\text{vec}_8 \underline{\mathbf{e}}$  is also  $L_2$  and the inequality converges, which in turn is equivalent to  $\|\text{vec}_8 \underline{\mathbf{e}}\|_2 < \gamma \|\mathbf{v}\|_2$ . Hence, the conditions in Definition 3.1 are satisfied, and the proof is completed.  $\square$

Theorem 3.1 provides a feasible solution for the  $H_\infty$  problem that ensures the asymptotic stability of the dual quaternion error dynamics by mapping the error to an  $\mathbb{R}^8$  manifold, while attenuating all exogenous disturbances. The resulting control scheme is obtained through the solution of an LMI.<sup>5</sup> Alternatively, we can state a new control procedure based on the solution of an algebraic Riccati equation,

$$\mathbf{A}_{ARE}^T \mathbf{P} + \mathbf{P} \mathbf{A}_{ARE} - \mathbf{P} \mathbf{M} \mathbf{P} + \mathbf{C}_{ARE} = 0. \quad (3.15)$$

### Theorem 3.2 Dual quaternion and algebraic Riccati equation-based $H_\infty$ controller

For a given scalar  $\alpha > 1$  and a prescribed  $\gamma > 0$ , a task-space  $H_\infty$  controller that stabilizes the error dynamics, whereas ensuring disturbance attenuation properties in the sense of Definition 3.1, is given by

$$\dot{\boldsymbol{\theta}} = \mathbf{N}^+ \overline{\mathbf{K}} \text{vec}_8 \underline{\mathbf{e}},$$

where  $\mathbf{N}^+$  is the pseudoinverse of  $\mathbf{N}$  and  $\overline{\mathbf{K}} = \frac{1}{2} \left( \frac{1}{\gamma^2} \mathbf{B}_v \mathbf{B}_v^T + \mathbf{M} \right) \mathbf{P}$ , for any positive definite matrix  $\mathbf{M}$ , and with the matrix  $\mathbf{P}$  given as the solution of the ARE (3.15), for  $\mathbf{A}_{ARE} = \mathbf{0}$ , and  $\mathbf{C}_{ARE} = \alpha \mathbf{I}$ .

**proof.**

From the Schur complement of the LMI condition in Theorem 3.1, we have that (3.13) holds if and only if

$$\mathbf{I} - 2\mathbf{PKP} + \mathbf{PB}_v \frac{1}{\gamma^2} \mathbf{B}_v^T \mathbf{P} = \mathbf{P} \left( \frac{1}{\gamma^2} \mathbf{B}_v \mathbf{B}_v^T - 2\mathbf{K} \right) \mathbf{P} + \mathbf{I} < 0,$$

<sup>5</sup>Interior point based algorithms, as the LMI Control Toolbox from Matlab, can solve this convex problem in polynomial time.



where  $PKP = G$ . Then, choosing

$$\mathbf{K} \triangleq \frac{1}{2} \left( \frac{1}{\gamma^2} \mathbf{B}_v \mathbf{B}_v^T + \mathbf{M} \right), \quad (3.16)$$

we obtain the inequality

$$-\mathbf{PMP} + \mathbf{I} < \mathbf{0}, \quad (3.17)$$

which is satisfied by the Riccati equation in (3.15), if  $\mathbf{C}_{ARE}$  is chosen such that  $\mathbf{C}_{ARE} > \mathbf{I}$ .  $\square$

To further simplify the choice of a feasible gain  $\mathbf{M} > \mathbf{0}$ , we may consider  $\mathbf{M} = \sigma \mathbf{I}$ , where  $\sigma$  is a positive scalar. In this particular case, the following theorem presents an optimal choice of  $\sigma$  in the sense of minimizing the norm of the control gain  $\bar{\mathbf{K}}$  in Theorem 3.2.

### Theorem 3.3 Dual quaternion based $H_\infty$ controller—closed-form solution

For a prescribed  $\gamma > 0$ , a task-space  $H_\infty$  controller that stabilizes the error dynamics  $\text{vec}_8 \dot{\underline{e}} = -\mathbf{N}\dot{\underline{\theta}} - \mathbf{B}_v \mathbf{v}$ , whereas ensuring disturbance attenuation properties in the sense of Definition 3.1, is given by  $\dot{\underline{\theta}} = \mathbf{N}^+ \bar{\mathbf{K}} \text{vec}_8 \underline{e}$ , where  $\mathbf{N}^+$  is the pseudoinverse of  $\mathbf{N}$  and

$$\bar{\mathbf{K}} = \frac{1}{\gamma} \left( \mathbf{B}_v \mathbf{B}_v^T + \left[ \frac{\sqrt{2}}{4} \mathbf{B}_v^T \mathbf{B}_v \right] \mathbf{I} \right) \frac{\alpha}{\sqrt{\mathbf{B}_v^T \mathbf{B}_v \sqrt{2}}}, \quad (3.18)$$

for any scalar  $\alpha > 1$ .

Moreover, the norm of  $\bar{\mathbf{K}}$  is given by  $\|\bar{\mathbf{K}}\|_2 = \frac{1}{\gamma} \alpha \sqrt{\frac{1}{2}(1+\sqrt{8}) \mathbf{B}_v^T \mathbf{B}_v}$ .

*proof.*

From (3.17) and taking the positive matrix  $\mathbf{M}$  to be  $\mathbf{M} = \sigma \mathbf{I}$ , where  $\sigma$  is a positive scalar, we have  $-\sigma \mathbf{P} \mathbf{P} + \mathbf{I} < \mathbf{0}$ , which is satisfied if

$$-\sigma \mathbf{P} \mathbf{P} + \alpha^2 \mathbf{I} = \mathbf{0}$$

holds for  $\alpha > 1$ . A trivial solution for the above equation is  $\mathbf{P} = \frac{\alpha}{\sqrt{\sigma}} \mathbf{I}$ . Then, substituting this feasible  $\mathbf{P}$  in  $\bar{\mathbf{K}}$  yields

$$\bar{\mathbf{K}} = \frac{1}{2} \frac{\alpha}{\sqrt{\sigma}} \left( \frac{1}{\gamma^2} \mathbf{B}_v \mathbf{B}_v^T + \sigma \mathbf{I} \right). \quad (3.19)$$

The Frobenius norm of  $\bar{\mathbf{K}}$  is given by  $\|\bar{\mathbf{K}}\|_F = \frac{1}{2} \frac{\alpha}{\sqrt{\sigma}} \left\| \frac{1}{\gamma^2} \mathbf{B}_v \mathbf{B}_v^T + \sigma \mathbf{I} \right\|_F$ , which in turn yields

$$\|\bar{\mathbf{K}}\|_F = \frac{1}{2} \frac{\alpha}{\sqrt{\sigma}} \sqrt{\text{tr} \left( \frac{\mathbf{B}_v \mathbf{B}_v^T \mathbf{B}_v \mathbf{B}_v^T}{\gamma^4} + \frac{2\sigma}{\gamma^2} \mathbf{B}_v \mathbf{B}_v^T + \sigma^2 \mathbf{I} \right)}.$$

Using trace properties, we are looking for the  $\sigma$  that minimizes  $\|\overline{\mathbf{K}}\|_F$ , i.e.,  $\hat{\sigma} = \arg \min_{\sigma} \|\overline{\mathbf{K}}\|_F$ ,

$$\begin{aligned}\hat{\sigma} &= \arg \min_{\sigma} \left\{ \frac{\alpha}{2} \sqrt{\frac{1}{\sigma} \left( \frac{[\mathbf{B}_v^T \mathbf{B}_v]^2}{\gamma^4} + \frac{2[\mathbf{B}_v^T \mathbf{B}_v]}{\gamma^2} \sigma + 8\sigma^2 \right)} \right\} \\ &= \arg \min_{\sigma} \left\{ \frac{1}{\sigma} \left( \frac{[\mathbf{B}_v^T \mathbf{B}_v]^2}{\gamma^4} + \frac{2[\mathbf{B}_v^T \mathbf{B}_v]}{\gamma^2} \sigma + 8\sigma^2 \right) \right\}.\end{aligned}$$

After some manipulation, we find the optimum value for  $\hat{\sigma}$  to be given by  $\hat{\sigma} = \frac{\sqrt{2}}{4\gamma^2} \mathbf{B}_v^T \mathbf{B}_v$  and, in turn, the minimum norm given by  $\|\overline{\mathbf{K}}\|_2 = \frac{1}{\gamma} \alpha \sqrt{\frac{1}{2}(1 + \sqrt{8}) \mathbf{B}_v^T \mathbf{B}_v}$ . Thus, replacing  $\sigma$  in (3.19) yields the control gain given in (3.18).  $\square$

Theorem 3.3 provides a straightforward solution for the  $H_{\infty}$  control problem. The resulting task-space control law yielding joint velocity inputs is easier to implement than the one of Theorem 3.1, as the control gain  $\overline{\mathbf{K}}$  in (3.18) is a closed-form expression. Also, the solution is based on the optimal value for  $M = \sigma \mathbf{I}$ , in the sense of reducing the gain norm, which in turn reduces the control effort required to maintain the  $H_{\infty}$  performance.

*Remark 3.2.* Both position and orientation configurations are regarded in an unified framework, which allows more efficient control techniques compared to conventional decoupled-based control. This is thanks to the fact that in our unified framework the error is invariant with respect to the choice of coordinate system, whereas in the decoupled-based approach the error in position will always be dependent on the choice of coordinate system; that is, given the error

$$\mathbf{e}_p = \mathbf{p}_d - \mathbf{p}_m \quad (3.20)$$

between the desired and measured positions, a coordinate change given by a rotation  $\mathbf{r}$  will result in  $\mathbf{e}_p = \mathbf{r}(\mathbf{p}_d - \mathbf{p}_m)\mathbf{r}^*$ , which is clearly different from the original position error (3.20). This way, using unit dual quaternions with an invariant error definition, all the proposed control strategies ensure the asymptotically convergence of the error to zero, while satisfying the attenuation properties described in Definition 3.1, and with a behavior that is independent of the choice of coordinate system.

The results from Theorem 3.1, which can be shown to be equivalent to Theorem 2, are more general and less conservative than Theorem 3.3. However, the proposed conditions yield any feasible result, without regard to the control effort. In this context, Theorem 3.3, although being slightly more conservative, provides an easy to implement closed-form gain expression that also represents the minimum norm solution for (3.16) with  $M = \sigma \mathbf{I}$ .

### 3.2.2 Discrete-time dual quaternion based $H_{\infty}$ controller in $\mathbb{R}^8$ manifold

Despite the theoretical soundness of the continuous-time differential forward kinematics model (3.4), in practical applications it is rather common to regard discrete measurements for the joint variables and for the end-effector configuration. Nonetheless, all results in dual quaternion literature are exclusively designed for continuous-time domain. Indeed, the continuous-time analysis is more straightforward, and adapting these methods to discrete-time is not trivial. Still, neglecting the discrete analysis restricts the universe of practical

applications and degrades digital implementation performance.

From the dual quaternion space mapping to an  $\mathbb{R}^8$  provided in the Subsection 3.2.1, Euler based and classic discretization based techniques can be exploited. In this sense, the discretization of (3.10) leads to

$$\Delta \text{vec}_8 \underline{\boldsymbol{x}}[k] = \mathbf{J}_{\text{vec}} (\boldsymbol{\theta}[k+1] - \boldsymbol{\theta}[k]) + \mathbf{B}\mathbf{v}[k] + \mathbf{v}_d[k], \quad (3.21)$$

where  $\Delta \text{vec}_8 \underline{\boldsymbol{x}}[k] = \text{vec}_8 \underline{\boldsymbol{x}}[k+1] - \text{vec}_8 \underline{\boldsymbol{x}}[k]$  and the vector  $\mathbf{v}_d[k] \in \mathbb{R}^8$  describes unknown uncertainties arising from the discretization procedure that takes  $\text{vec}_8 \underline{\boldsymbol{x}}[k+1]$ , that is, the  $\text{vec}_8$  mapping of the end-effector pose in instant  $t+1$ , out of the unit dual quaternion group.

This accurate description of the end-effector transformation that explicitly considers different sources of uncertainties and disturbances with the inherent discretization error yields a more complete description for the end effector pose at instant  $k + 1$ . From this description, we can define a discrete error function based on the  $\text{vec}_8$  mapping of dual quaternion error (3.5)-(3.7) to an  $\mathbb{R}^8$  manifold, as in (3.11), that is

$$\text{vec}_8 \underline{\boldsymbol{e}}[k] = \bar{\mathbf{H}}(\underline{\boldsymbol{x}}_d^*[k]) \text{vec}_8(\underline{\boldsymbol{x}}_d[k] - \underline{\boldsymbol{x}}[k]). \quad (3.22)$$

From the dual quaternion based differential kinematics mapped to  $\mathbb{R}^8$ , the error dynamics can be described by

$$\begin{aligned} \text{vec}_8 \underline{\boldsymbol{e}}[k+1] &= \bar{\mathbf{H}}(\underline{\boldsymbol{x}}_d^*) \text{vec}_8(\underline{\boldsymbol{x}}_d - \underline{\boldsymbol{x}}[k+1]) \\ &= \bar{\mathbf{H}}(\underline{\boldsymbol{x}}_d^*) (\text{vec}_8(\underline{\boldsymbol{x}}_d) - \text{vec}_8(\underline{\boldsymbol{x}}[k]) - \mathbf{J}_{\text{vec}}(\boldsymbol{\theta}[k+1] - \boldsymbol{\theta}[k]) - \mathbf{B}\mathbf{v}[k] - \mathbf{v}_d[k]) \end{aligned}$$

where  $\underline{\boldsymbol{x}}_d$  is a desired constant configuration. Moreover, since the discretization error is inherently connected to the value of  $\underline{\boldsymbol{x}}[k]$ , similarly to  $\mathbf{B}$ , we can construct a combined disturbance vector  $\mathbf{w}[k]$  to address both disturbances and discretization error. In this sense,

$$\begin{aligned} \text{vec}_8 \underline{\boldsymbol{e}}[k+1] &= \text{vec}_8 \underline{\boldsymbol{e}}[k] - \bar{\mathbf{H}}(\underline{\boldsymbol{x}}_d^*) (\mathbf{J}_{\text{vec}}(\boldsymbol{\theta}[k+1] - \boldsymbol{\theta}[k]) + \mathbf{B}\mathbf{w}[k]) \\ &= \text{vec}_8 \underline{\boldsymbol{e}}[k] - \mathbf{N}(\boldsymbol{\theta}[k+1] - \boldsymbol{\theta}[k]) + \mathbf{B}_v \mathbf{w}[k], \end{aligned} \quad (3.23)$$

where  $\mathbf{N} = \bar{\mathbf{H}}(\underline{\boldsymbol{x}}_d^*) \mathbf{J}_{\text{vec}}$  and  $\mathbf{B}_v = \bar{\mathbf{H}}(\underline{\boldsymbol{x}}_d^*) \mathbf{B}$ .

In practical scenarios, it is also interesting to consider a variable trajectory for the end-effector which, in turn, yields a tracking problem—a problem more general than stabilization [84, 85]. Given a varying pose configuration, the error dynamics from (3.22)-(3.23) can be rewritten as

$$\begin{aligned} \text{vec}_8 \underline{\boldsymbol{e}}[k+1] &= \bar{\mathbf{H}}(\underline{\boldsymbol{x}}_d^*[k+1]) \text{vec}_8(\underline{\boldsymbol{x}}_d[k+1] - \underline{\boldsymbol{x}}[k+1]) \\ &= \bar{\mathbf{H}}(\underline{\boldsymbol{x}}_d^*[k+1]) \text{vec}_8(\underline{\boldsymbol{x}}_d[k+1] - \underline{\boldsymbol{x}}[k] - \mathbf{J}_{\text{vec}}(\boldsymbol{\theta}[k+1] - \boldsymbol{\theta}[k]) + \mathbf{B}\mathbf{w}[k]). \end{aligned} \quad (3.24)$$

To ease the analysis, let us recall that

$$\bar{\mathbf{H}}(\underline{\boldsymbol{x}}_d^*[k+1]) \text{vec}_8 \underline{\boldsymbol{x}}_d[k+1] = \bar{\mathbf{H}}(\underline{\boldsymbol{x}}_d^*[k]) \text{vec}_8 \underline{\boldsymbol{x}}_d[k] = \mathbf{I}.$$

In this sense, by adding the null expression  $\bar{\mathbf{H}}(\underline{\boldsymbol{x}}_d^*[k]) \text{vec}_8(\underline{\boldsymbol{x}}[k] - \underline{\boldsymbol{x}}[k]) = 0$  to (3.24), yields

$$\begin{aligned} \text{vec}_8 \underline{\boldsymbol{e}}[k+1] &= \bar{\mathbf{H}}(\underline{\boldsymbol{x}}_d^*[k]) (\text{vec}_8 \underline{\boldsymbol{x}}_d[k] - \text{vec}_8 \underline{\boldsymbol{x}}[k]) - \bar{\mathbf{H}}(\underline{\boldsymbol{x}}_d^*[k+1] - \underline{\boldsymbol{x}}_d^*[k]) \text{vec}_8 \underline{\boldsymbol{x}}[k] \\ &\quad - \bar{\mathbf{H}}(\underline{\boldsymbol{x}}_d^*[k+1]) (\mathbf{J}_{\text{vec}}(\boldsymbol{\theta}[k+1] - \boldsymbol{\theta}[k]) - \mathbf{B}\mathbf{w}[k]), \end{aligned}$$

which can be written as

$$\text{vec}_8 \underline{e}[k+1] = \text{vec}_8 \underline{e}[k] - \mathbf{N} (\boldsymbol{\theta}[k+1] - \boldsymbol{\theta}[k]) + \mathbf{B}_v \mathbf{w}[k] - \text{vec}_8 \underline{\mathbf{x}}_{trk}[k], \quad (3.25)$$

where  $\mathbf{N} = \bar{\mathbf{H}} (\underline{\mathbf{x}}_d^*[k+1]) \mathbf{J}_{\text{vec}}$ ,  $\mathbf{B}_v = \bar{\mathbf{H}} (\underline{\mathbf{x}}_d^*[k+1]) \mathbf{B}$ , and  $\text{vec}_8 \underline{\mathbf{x}}_{trk}[k] = \bar{\mathbf{H}} (\underline{\mathbf{x}}_d^*[k+1] - \underline{\mathbf{x}}_d^*[k]) \text{vec}_8 \underline{\mathbf{x}}[k]$ .

It is interesting to highlight that the convergence properties from  $\underline{\mathbf{x}}$  to  $\underline{\mathbf{x}}_d$  are utterly related to the definition of the error function as described in Section 3.1. In this context, to asymptotically stabilize the system (3.23) is to assume  $\underline{\mathbf{x}}[k] \rightarrow \underline{\mathbf{x}}_d[k]$  as  $k \rightarrow \infty$ , independently from the choice of the robot base coordinate systems and from coordinate changes.

For the  $H_\infty$  control, we seek a control law that makes the dual quaternion configuration  $\underline{\mathbf{x}}[k]$  asymptotically converges to  $\underline{\mathbf{x}}_d[k]$ , whereas ensuring disturbances attenuation properties, i.e., attenuating the influence of the disturbances  $\mathbf{w}[k] \in \ell_2[0, \infty)$ <sup>6</sup> regardless of their distribution characteristics over the coupled kinematics. In this context, the following definition based on [81] describes the robust performance in the  $H_\infty$  sense.

**Definition 3.2.** (Based on [81]) For a prescribed scalar  $\gamma > 0$ , the robust control performance is achieved with an  $H_\infty$  norm bound  $\gamma$ , if the following hold

- (1) The discrete-time error dynamics (3.23) is asymptotically stable for  $\mathbf{w}[k] \equiv \mathbf{0}$ ;
- (2) Under the assumption of zero initial conditions, the disturbance influence on the error,  $\text{vec}_8 \underline{e}[k]$ , is attenuated below a desired level  $\gamma$ , that is,  $\|\text{vec}_8 \underline{e}\|_2 \leq \gamma \|\mathbf{w}\|_2$  for all nonzero  $\mathbf{w} \in \ell_2[0, \infty)$ .

Considering the system description and Definition 3.2, we first state a solution for the  $H_\infty$  setpoint control problem in the following criterion.

**Theorem 3.4** Discrete dual quaternion and LMI based  $H_\infty$  setpoint controller

For a prescribed  $\gamma > 0$ , there exist a controller given by  $\boldsymbol{\theta}[k+1] = \boldsymbol{\theta}[k] + \mathbf{N}^+ \mathbf{K} \text{vec}_8 \underline{e}[k]$ , such that (3.23) achieves robust stability with  $H_\infty$  performance  $\gamma$ , in the sense of Definition 3.2, if there exist matrices  $\mathbf{P} = \mathbf{P}^T > \mathbf{I}$  and  $\mathbf{G} = \mathbf{G}^T > 0$ , such that

$$\begin{bmatrix} \mathbf{P} - \mathbf{G} & \mathbf{P} \mathbf{B}_v \\ \mathbf{B}_v^T \mathbf{P} & \mathbf{B}_v^T \mathbf{P} \mathbf{B}_v - \gamma^2 \mathbf{I} \end{bmatrix} < 0, \quad (3.26)$$

where  $\mathbf{N}^+$  is the pseudoinverse of  $\mathbf{N}$ . Moreover, if the above conditions are satisfied, a stabilizing control gain  $\mathbf{K}$  is given by<sup>a</sup>

$$\mathbf{K} = \mathbf{I} - \sqrt{\mathbf{G}^{-1} \sqrt{\mathbf{P} - \mathbf{I}}}. \quad (3.27)$$

<sup>a</sup>In general, a matrix can have several representations for its square root. Nevertheless, a positive-definite matrix has precisely one positive-definite representation. This unique positive square root, defined as the principal square root, is the representation used throughout this thesis.

*proof.*

<sup>6</sup> $\ell_2$  is the Hilbert space of all square-summable sequences.

Let us choose as discrete Lyapunov candidate the positive definite quadratic function:

$$V[k] = \text{vec}_8^T \underline{e}[k] \mathbf{P} \text{vec}_8 \underline{e}[k], \quad (3.28)$$

where  $\mathbf{P}$  is a positive definite matrix. The criterion presented in Theorem 3.4 stems mostly from the first difference of the Lyapunov candidate along the trajectory (3.23),

$$\begin{aligned} \Delta V &= V[k+1] - V[k] \\ &= \text{vec}_8^T \underline{e}[k+1] \mathbf{P} \text{vec}_8 \underline{e}[k+1] - \text{vec}_8^T \underline{e}[k] \mathbf{P} \text{vec}_8 \underline{e}[k]. \end{aligned}$$

Regarding a feedback linearization control scheme,

$$\boldsymbol{\theta}[k+1] = \boldsymbol{\theta}[k] + \mathbf{N}^+ \mathbf{K} \text{vec}_8 \underline{e}[k], \quad (3.29)$$

the first difference of (3.28) may be rewritten as

$$\begin{aligned} \Delta V &= ((\mathbf{I} - \mathbf{K}) \text{vec}_8 \underline{e}[k] + \mathbf{B}_v \mathbf{w}[k])^T \mathbf{P} ((\mathbf{I} - \mathbf{K}) \text{vec}_8 \underline{e}[k] + \mathbf{B}_v \mathbf{w}[k]) - \text{vec}_8^T \underline{e}[k] \mathbf{P} \text{vec}_8 \underline{e}[k] \\ &= (\overline{\mathbf{K}} \text{vec}_8 \underline{e}[k] + \mathbf{B}_v \mathbf{w}[k])^T \mathbf{P} (\overline{\mathbf{K}} \text{vec}_8 \underline{e}[k] + \mathbf{B}_v \mathbf{w}[k]) - \text{vec}_8^T \underline{e}[k] \mathbf{P} \text{vec}_8 \underline{e}[k] \\ &= 2 \text{vec}_8^T \underline{e}[k] \overline{\mathbf{K}}^T \mathbf{P} \mathbf{B}_v \mathbf{w}[k] + \mathbf{w}^T[k] \mathbf{B}_v^T \mathbf{P} \mathbf{B}_v \mathbf{w}[k] + \text{vec}_8^T \underline{e}[k] (\overline{\mathbf{K}}^T \mathbf{P} \overline{\mathbf{K}} - \mathbf{P}) \text{vec}_8 \underline{e}[k], \end{aligned} \quad (3.30)$$

where  $\overline{\mathbf{K}} = \mathbf{I} - \mathbf{K}$ .

For every  $\mathbf{K}$ , it is easy to see that the inequality  $\overline{\mathbf{K}}^T \mathbf{P} \overline{\mathbf{K}} - \mathbf{P} < 0$  deems  $\Delta V$  to be negative semidefinite for  $\mathbf{w} \equiv 0$ , which from Barbalat's Lemma [86,87] implies that  $\text{vec} \underline{e}[k]$  converges to zero as  $k \rightarrow \infty$ . Hence, the first condition in Definition 3.2 is satisfied.

Now, to investigate the the  $H_\infty$  performance, let us define

$$\Delta V_{H_\infty} \triangleq \Delta V + \text{vec}_8^T \underline{e}[k] \text{vec}_8 \underline{e}[k] - \gamma^2 \mathbf{w}^T[k] \mathbf{w}[k], \quad (3.31)$$

such that

$$\Delta V_{H_\infty} = \text{vec}_8^T \underline{e}[k] (\overline{\mathbf{K}}^T \mathbf{P} \overline{\mathbf{K}} - \mathbf{P} + \mathbf{I}) \text{vec}_8 \underline{e}[k] + 2 \text{vec}_8^T \underline{e}[k] (\overline{\mathbf{K}}^T \mathbf{P} \mathbf{B}_v) \mathbf{w}[k]$$

which can also be written as  $\Delta V_{H_\infty} = \zeta^T[k] \boldsymbol{\Omega} \zeta[k]$ , where  $\zeta[k] = \begin{bmatrix} \text{vec}_8^T \underline{e}[k] & \mathbf{w}^T[k] \end{bmatrix}^T$  and

$$\boldsymbol{\Omega} = \begin{bmatrix} \overline{\mathbf{K}}^T \mathbf{P} \overline{\mathbf{K}} - \mathbf{P} + \mathbf{I} & \overline{\mathbf{K}}^T \mathbf{P} \mathbf{B}_v \\ \mathbf{B}_v^T \mathbf{P} \overline{\mathbf{K}} & \mathbf{B}_v^T \mathbf{P} \mathbf{B}_v - \gamma^2 \mathbf{I} \end{bmatrix}.$$

If we regard a nonsingular block diagonal matrix,  $\text{diag} \left\{ \overline{\mathbf{K}} \quad \mathbf{I} \right\}$ , to prove  $\boldsymbol{\Omega} < 0$  is the same of proving  $\text{diag}^T \left\{ \overline{\mathbf{K}}^{-1} \quad \mathbf{I} \right\} \boldsymbol{\Omega} \text{diag} \left\{ \overline{\mathbf{K}}^{-1} \quad \mathbf{I} \right\} < 0$ . Moreover, given the inequality  $\mathbf{P} - \mathbf{I} > 0$ , defining

$$\mathbf{G} \triangleq \left( \overline{\mathbf{K}} (\mathbf{P} - \mathbf{I})^{-1} \overline{\mathbf{K}}^T \right)^{-1}, \quad (3.32)$$

yields exactly the same condition presented in (3.26). Therefore, Theorem 3.4, if satisfied, yields  $\Delta V_{H_\infty} < 0$ , and consequently

$$\Delta V + \text{vec}_8^T \underline{e}[k] \text{vec}_8 \underline{e}[k] - \gamma^2 \mathbf{w}^T[k] \mathbf{w}[k] < 0. \quad (3.33)$$

Furthermore, if  $\Delta V_{H_\infty}$  is definite negative, then it is straightforward that  $\overline{\mathbf{K}}^T \mathbf{P} \overline{\mathbf{K}} - \mathbf{P} < 0$ , and the first condition in Definition 3.2 is satisfied. Now, taking (3.33) and summing (3.31), from 0 to  $k$ , yields

$$\begin{aligned} & \sum_{i=0}^k (V[i+1] - V[i] + \text{vec}_8^T \underline{\mathbf{e}}[i] \text{vec}_8 \underline{\mathbf{e}}[i] - \gamma^2 \mathbf{w}^T[i] \mathbf{w}[i]) = \\ & V[k+1] - V(0) + \sum_{i=0}^k (\text{vec}_8^T \underline{\mathbf{e}}[i] \text{vec}_8 \underline{\mathbf{e}}[i] - \gamma^2 \mathbf{w}^T[i] \mathbf{w}[i]) < 0. \end{aligned}$$

Under zero initial conditions and given the Lyapunov function positiveness properties, we must have

$$\sum_{i=0}^k \text{vec}_8^T \underline{\mathbf{e}}[i] \text{vec}_8 \underline{\mathbf{e}}[i] - \sum_{i=0}^k \gamma^2 \mathbf{w}^T[i] \mathbf{w}[i] < 0,$$

for all  $k \geq 0$ . Note that  $\mathbf{w} \in \ell_2[0, \infty)$ , thus  $\text{vec}_8 \underline{\mathbf{e}}$  is also  $\ell_2[0, \infty)$  and both terms converge. The inequality is therefore equivalent to  $\|\text{vec}_8 \underline{\mathbf{e}}\|_2 \leq \gamma \|\mathbf{w}\|_2$ . Hence, the conditions in Definition 3.2 are satisfied, and the proof is completed.

To retrieve a control gain  $\mathbf{K} = \mathbf{I} - \overline{\mathbf{K}}$  from the resulting matrices,  $\mathbf{G}$  and  $\mathbf{P}$ , we suppose that  $\overline{\mathbf{K}}$  is defined as  $\overline{\mathbf{K}} \triangleq M \sqrt{\mathbf{P} - \mathbf{I}}$  with  $M > 0$ . In this sense, stemming from (3.32), it follows that

$$\begin{aligned} \mathbf{G}^{-1} &= \overline{\mathbf{K}} (\mathbf{P} - \mathbf{I})^{-1} \overline{\mathbf{K}}^T \\ &= \left[ M \sqrt{\mathbf{P} - \mathbf{I}} \right] (\mathbf{P} - \mathbf{I})^{-1} \left[ \sqrt{\mathbf{P} - \mathbf{I}} M \right] \\ &= \mathbf{M} \mathbf{M}, \end{aligned} \tag{3.34}$$

such that  $M = \sqrt{\mathbf{G}^{-1}}$ , and consequently  $\overline{\mathbf{K}} = \sqrt{\mathbf{G}^{-1}} \sqrt{\mathbf{P} - \mathbf{I}}$ . After some manipulation, we find the control gain, obtained from the resulting matrices,  $\mathbf{G}$  and  $\mathbf{P}$ , given by  $\mathbf{K} = \mathbf{I} - \sqrt{\mathbf{G}^{-1}} \sqrt{\mathbf{P} - \mathbf{I}}$ . □

Theorem 3.4 provides a feasible solution for the  $H_\infty$  control problem ensuring the asymptotic stability of the error dynamics (3.23), while attenuating all exogenous disturbances and discretization errors. The resulting control scheme is obtained through the solution of an LMI,<sup>7</sup> which provides a static value for the gain  $\mathbf{K}$ . Regarding the matrix gain as a constant term, ease the implementation and the analysis. Nevertheless, if we regard changes in the coordinate base or a time-varying reference configuration  $\underline{\mathbf{x}}_d$ , e.g., a tracking system, a new control gain must be calculated, which requires new feasibility tests for the LMI (3.26). Due to time constraints related to the solution of an LMI problem, Theorem 3.4 becomes unsuitable for practical implementations. Motivated by this problem, we state a solution for the  $H_\infty$  tracking control problem as follows.

<sup>7</sup>Interior point based algorithms, as the LMI Control Toolbox from Matlab, can solve this convex problem in polynomial time.

**Theorem 3.5** Discrete dual quaternion based  $H_\infty$  tracking controller

For a prescribed performance parameter  $\gamma > 0$ , and given a positive scalar  $\alpha < 1$  and matrix  $\mathbf{P}$ , satisfying  $\mathbf{P} > \mathbf{I}$  and  $\mathbf{P} < \gamma^2 [\mathbf{B}_v \mathbf{B}_v^T]^{-1}$ , a control strategy that ensures  $H_\infty$  tracking performance  $\gamma$  for the system (3.25) with exogenous disturbances and errors in the sense of Definition 3.2 is given by

$$\boldsymbol{\theta}[k+1] = \boldsymbol{\theta}[k] + \mathbf{N}^+ ((\mathbf{I} - \bar{\mathbf{K}}) \text{vec}_8 \underline{\mathbf{e}}[k] + \text{vec}_8 \underline{\mathbf{x}}_{trk}[k]), \quad (3.35)$$

where  $\mathbf{N}^+$  is the pseudoinverse of  $\mathbf{N} = \bar{\mathbf{H}}(\underline{\mathbf{x}}_d^*[k+1]) \mathbf{J}_{\text{vec}}$  with  $\mathbf{B}_v = \bar{\mathbf{H}}(\underline{\mathbf{x}}_d^*[k+1]) \mathbf{B}$ , the control gain is given by

$$\bar{\mathbf{K}} = \alpha \sqrt{\mathbf{P}^{-1} - \gamma^{-2} \mathbf{B}_v \mathbf{B}_v^T} \sqrt{\mathbf{P} - \mathbf{I}}, \quad (3.36)$$

and the feedforward term by

$$\text{vec}_8 \underline{\mathbf{x}}_{trk}[k] = \bar{\mathbf{H}}(\underline{\mathbf{x}}_d^*[k+1] - \underline{\mathbf{x}}_d^*[k]) \text{vec}_8 \underline{\mathbf{x}}[k]. \quad (3.37)$$

*proof.*

From the Lyapunov function candidate described in (3.28), we have

$$\Delta V = \text{vec}_8^T \underline{\mathbf{e}}[k+1] \mathbf{P} \text{vec}_8 \underline{\mathbf{e}}[k+1] - \text{vec}_8^T \underline{\mathbf{e}} \mathbf{P} \text{vec}_8 \underline{\mathbf{e}}[k].$$

Now, by using the tracking controller defined in (3.35), the error dynamics (3.25) can be rewritten as

$$\begin{aligned} \text{vec}_8 \underline{\mathbf{e}}[k+1] &= \text{vec}_8 \underline{\mathbf{e}}[k] - \text{vec}_8 \underline{\mathbf{x}}_{trk}[k] - \mathbf{N}(\boldsymbol{\theta}[k+1] - \boldsymbol{\theta}[k]) + \mathbf{B}_v \mathbf{w}[k] \\ &= \bar{\mathbf{K}} \text{vec}_8 \underline{\mathbf{e}}[k] + \mathbf{B}_v \mathbf{w}[k]. \end{aligned}$$

The first difference of Lyapunov function can thus be rewritten as

$$\Delta V = 2 \text{vec}_8^T \underline{\mathbf{e}}[k] \bar{\mathbf{K}}^T \mathbf{P} \mathbf{B}_v \mathbf{w}[k] + \mathbf{w}^T[k] \mathbf{B}_v^T \mathbf{P} \mathbf{B}_v \mathbf{w}[k] + \text{vec}_8^T \underline{\mathbf{e}}[k] (\bar{\mathbf{K}}^T \mathbf{P} \bar{\mathbf{K}} - \mathbf{P}) \text{vec}_8 \underline{\mathbf{e}}[k].$$

It is easily noticed that the first difference in this case is the same of the Lyapunov difference obtained in (3.30). Consequently, following exactly the same steps from Theorem 3.4, the  $H_\infty$  tracking performance of the closed-loop system is ensured in accordance to Definition 3.2.

Nonetheless, investigating the LMI condition (3.26) in Theorem 3.4, and using the Schur Lemma, the condition (3.26) holds if and only if  $\mathbf{P} - \mathbf{G} < 0$ , and

$$\begin{aligned} \mathbf{B}_v^T \mathbf{P} \mathbf{B}_v - \gamma^2 \mathbf{I} - \mathbf{B}_v^T \mathbf{P} (\mathbf{P} - \mathbf{G})^{-1} \mathbf{P} \mathbf{B}_v &< 0 \\ -\gamma^2 \mathbf{I} + \mathbf{B}_v^T [\mathbf{P} - \mathbf{P} (\mathbf{P} - \mathbf{G})^{-1} \mathbf{P}] \mathbf{B}_v &< 0. \end{aligned}$$

Using Sherman–Morrison–Woodbury matrix identity, we have

$$-\gamma^2 \mathbf{I} + \mathbf{B}_v^T (\mathbf{P}^{-1} - \mathbf{G}^{-1})^{-1} \mathbf{B}_v < 0,$$

which in turn implies  $P^{-1} - G^{-1} > \gamma^{-2} B_v B_v^T$ , and

$$G^{-1} < P^{-1} - \gamma^{-2} B_v B_v^T. \quad (3.38)$$

Stemming from the definition in (3.32), the inequality (3.38) deems

$$\bar{K} (P - I)^{-1} \bar{K}^T < P^{-1} - \gamma^{-2} B_v B_v^T.$$

Similarly to the analysis performed in (3.34), we set  $\bar{K} = \alpha \sqrt{P^{-1} - \gamma^{-2} B_v B_v^T} \sqrt{P - I}$  with a scalar  $\alpha < 1$ . Thus (3.38) is satisfied, and we find that the control gain which ensures  $H_\infty$  performance to (3.23) is given by  $K = I - \bar{K}$ , where  $\bar{K}$  satisfies (3.36),  $P > I$ , and  $P < \gamma^2 (B_v B_v^T)^{-1}$ .

□

Theorem 3.5 provides an easy way to update the control signal in accordance to theoretical results from Theorem 3.4 and considering a time-varying task-space desired configuration. Still, there may exist an infinity number of solutions for the matrix  $P$  that satisfies the conditions in Theorem 3.5. To further simplify and improve the choice of a feasible solution, we seek a closed-form solution for the positive matrix  $P_{opt}$  that optimizes a given criterion. In this particular case, we seek  $P_{opt}$  that minimizes the norm of the control gain  $K$  in Theorem 3.5.

### Theorem 3.6 Discrete dual quaternion based $H_\infty$ tracking controller—closed form solution

For a prescribed performance parameter  $\gamma > 0$ , a control strategy with minimum norm for the control gain that ensures  $H_\infty$  tracking performance  $\gamma$  for the system (3.25) with exogenous disturbances and errors in the sense of Definition 3.2 is given by

$$\theta[k+1] = \theta[k] + N^+ ((I - \bar{K}) \text{vec}_8 \underline{e}[k] + \text{vec}_8 \underline{x}_{trk}[k]), \quad (3.39)$$

where  $N^+$  is the pseudoinverse of  $N = \bar{H}(\underline{x}_d^*[k+1]) J_{\text{vec}}$  with  $B_v = \bar{H}(\underline{x}_d^*[k+1]) B$ , the feedforward term is given by  $\text{vec}_8 \underline{x}_{trk}[k] = \bar{H}(\underline{x}_d^*[k+1] - \underline{x}_d^*[k]) \text{vec}_8 \underline{x}[k]$ , and the minimum control gain by

$$\bar{K} = \alpha \sqrt{P^{-1} - \gamma^{-2} B_v B_v^T} \sqrt{P - I}, \quad (3.40)$$

with

$$P = \gamma \sqrt{B_v B_v^T}^{-1}. \quad (3.41)$$

**proof.**

First, recall that the proposed tracking controller (3.39) ensures  $H_\infty$  tracking performance  $\gamma$  for the system (3.25) with exogenous disturbances and errors as described in Theorem 3.5. Investigating the proposed controller, it is easily noted that feedforward term as described in (3.37) compensates for the desired end-effector velocities and does not depend on the control gain. Indeed, the stabilizing control gain  $(I - \bar{K})$  defines the controller performance in the sense of Definition 3.2 with  $\bar{K}$  satisfying (3.36)—which ensures the  $H_\infty$  performance  $\gamma$ . Therefore, the gain  $\bar{K}$  is the only variable in the proposed tracking controller (3.39) and can be chosen according to some optimal criterion.



To reduce the norm of the gain  $\mathbf{K}$ , we first seek to prove that  $\overline{\mathbf{K}}$  has only positive eigenvalues which are upper bounded by 1, i.e.,  $0 < \lambda_i(\overline{\mathbf{K}}) < 1$ . The positiveness assumption is easily proved, since  $\overline{\mathbf{K}}$  arises from the product of two positive terms which yields positive eigenvalues, although not necessarily a positive matrix. The latter assumption is only proved to be true if the following holds:

$$\overline{\mathbf{K}}^T \overline{\mathbf{K}} = \alpha^2 \sqrt{\mathbf{P}-\mathbf{I}} \left( \mathbf{P}^{-1} - \gamma^{-2} \mathbf{B}_v \mathbf{B}_v^T \right) \sqrt{\mathbf{P}-\mathbf{I}} < \mathbf{I}. \quad (3.42)$$

Pre- and post-multiplying both sides of the inequality by the positive term  $\sqrt{\mathbf{P}-\mathbf{I}}$  yields

$$\begin{aligned} (\mathbf{P}-\mathbf{I}) \left( \mathbf{P}^{-1} - \gamma^{-2} \mathbf{B}_v \mathbf{B}_v^T \right) (\mathbf{P}-\mathbf{I}) &< (\mathbf{P}-\mathbf{I}) \\ \left( \mathbf{I}-\mathbf{P}^{-1} - (\mathbf{P}-\mathbf{I}) \gamma^{-2} \mathbf{B}_v \mathbf{B}_v^T \right) (\mathbf{P}-\mathbf{I}) &< (\mathbf{P}-\mathbf{I}) \\ \mathbf{P}-\mathbf{I}-\mathbf{I}+\mathbf{P}^{-1} - (\mathbf{P}-\mathbf{I}) \gamma^{-2} \mathbf{B}_v \mathbf{B}_v^T (\mathbf{P}-\mathbf{I}) &< (\mathbf{P}-\mathbf{I}) \\ -\mathbf{I}+\mathbf{P}^{-1} - (\mathbf{P}-\mathbf{I}) \gamma^{-2} \mathbf{B}_v \mathbf{B}_v^T (\mathbf{P}-\mathbf{I}) &< 0. \end{aligned}$$

From the conditions of Theorem 3.5, we have  $\mathbf{P} \geq \mathbf{I}$ , which in turn implies  $\mathbf{P}^{-1} \leq \mathbf{I}$ , and since  $\gamma^{-2} \mathbf{B}_v \mathbf{B}_v^T$  is positive definite, we have that (3.42) always holds. Given the norm properties, we then have  $\|\overline{\mathbf{K}}\|_2^2 = \lambda_{max}^2(\overline{\mathbf{K}}) < 1$ , which implies  $\lambda_i(\overline{\mathbf{K}}) < 1$ .

Let us now address the Frobenius norm of gain matrix,  $\mathbf{K} = \mathbf{I} - \overline{\mathbf{K}}$ , that is

$$\begin{aligned} \|\mathbf{K}\|_F &= \sqrt{\text{tr} \left\{ \mathbf{K}^T \mathbf{K} \right\}} = \sqrt{\text{tr} \left\{ \mathbf{I} - \overline{\mathbf{K}}^T - \overline{\mathbf{K}} + \overline{\mathbf{K}}^T \overline{\mathbf{K}} \right\}} \\ &= \sqrt{\text{tr} \left\{ \mathbf{I} \right\} - 2\text{tr} \left\{ \overline{\mathbf{K}} \right\} + \text{tr} \left\{ \overline{\mathbf{K}}^T \overline{\mathbf{K}} \right\}}. \end{aligned}$$

As the trace of  $\mathbf{K}$  stems from the sum of eigenvalues, that is,  $\text{tr} \left\{ \overline{\mathbf{K}} \right\} = \sum_{i=1}^8 \lambda_i(\overline{\mathbf{K}})$ , the trace of  $\overline{\mathbf{K}}^T \overline{\mathbf{K}}$  is defined by  $\sum_{i=1}^8 \lambda_i^2(\overline{\mathbf{K}})$ . Due to the previously demonstrated properties of  $\lambda_i(\overline{\mathbf{K}})$ , that is,  $0 < \lambda_i(\overline{\mathbf{K}}) < 1$ , we have that the inequality  $\text{tr} \left\{ \overline{\mathbf{K}} \right\} > \text{tr} \left\{ \overline{\mathbf{K}}^T \overline{\mathbf{K}} \right\}$  always holds. Moreover, given the eigenvalues constraints, the function  $f(\overline{\mathbf{K}}) = 2\text{tr} \left\{ \overline{\mathbf{K}} \right\} - \text{tr} \left\{ \overline{\mathbf{K}}^T \overline{\mathbf{K}} \right\}$  is monotonically increasing. In this context, to minimize the Frobenius norm of gain matrix,  $\min \|\mathbf{K}\|_F$ , is the same of maximizing the gain  $\overline{\mathbf{K}}$ . In other words, we are now seeking for a positive matrix  $\mathbf{P}_{opt}$  that satisfies

$$\mathbf{P}_{opt} \triangleq \arg \max_{\mathbf{P}} \|\overline{\mathbf{K}}\|_F.$$

The Frobenius norm of  $\overline{\mathbf{K}}$  is given by

$$\|\overline{\mathbf{K}}\|_F = \sqrt{\text{tr} \left\{ \overline{\mathbf{K}} \overline{\mathbf{K}} \right\}} = \sqrt{\text{tr} \left\{ \sqrt{\mathbf{P}-\mathbf{I}} \left( \mathbf{P}^{-1} - \gamma^{-2} \mathbf{B}_v \mathbf{B}_v^T \right) \sqrt{\mathbf{P}-\mathbf{I}} \right\}}.$$

Using the cyclic properties of the trace, we have

$$\begin{aligned} \|\overline{\mathbf{K}}\|_F &= \sqrt{\text{tr} \left\{ \left( \mathbf{P}^{-1} - \gamma^{-2} \mathbf{B}_v \mathbf{B}_v^T \right) \sqrt{\mathbf{P}-\mathbf{I}} \sqrt{\mathbf{P}-\mathbf{I}} \right\}} = \sqrt{\text{tr} \left\{ \left( \mathbf{P}^{-1} - \gamma^{-2} \mathbf{B}_v \mathbf{B}_v^T \right) (\mathbf{P}-\mathbf{I}) \right\}} \\ &= \sqrt{\text{tr} \left\{ \mathbf{I} - \mathbf{P}^{-1} - \gamma^{-2} \mathbf{B}_v \mathbf{B}_v^T \mathbf{P} + \gamma^{-2} \mathbf{B}_v \mathbf{B}_v^T \right\}}. \end{aligned}$$

Since square root is a monotonically increasing function, to maximize  $\|\overline{\mathbf{K}}\|_{\mathbb{F}}$  is to find  $\mathbf{P}_{opt}$  that satisfies

$$\mathbf{P}_{opt} = \arg \max_{\mathbf{P}} -\text{tr} \{ \mathbf{P}^{-1} \} - \text{tr} \{ \gamma^{-2} \mathbf{B}_v \mathbf{B}_v^T \mathbf{P} \}.$$

To find  $\mathbf{P}_{opt}$ , let us take the first derivative of these trace functions [88],  $\mathbf{P}^{-2} - \gamma^{-2} \mathbf{B}_v \mathbf{B}_v^T = 0$ , which in turn yields

$$\mathbf{P}_{opt} = \gamma \sqrt{\mathbf{B}_v \mathbf{B}_v^T}^{-1}. \quad (3.43)$$

□

The control scheme provided by Theorem 3.6 is a straightforward solution for the  $H_{\infty}$  control of manipulators using dual quaternion representation. Indeed, the controller is easier to implement than the results from Theorems 3.4 and 3.5, as the control gain in Theorem 3.6 is given by a closed-form expression and solely depends on the given scalars  $\gamma$ ,  $\alpha$ , on the known matrix  $\mathbf{B}_v$ , and the the known feedforward term. Furthermore, the resulting control scheme deems the gain value to be optimal in the sense of reducing its norm, which in turn reduces the control effort required to asymptotically stabilize the end effector while maintaining the  $H_{\infty}$  performance. To the best of the authors knowledge, given the dual quaternion framework, this is the first work to exploit any of the aforementioned characteristics in the control design, and the first to explicitly regard several sources of uncertainties and disturbances acting on the discretized model.

### 3.3 $H_{\infty}$ CONTROLLER IN DUAL QUATERNION SPACE

This section proposes a new framework for kinematic setpoint control and tracking of robot manipulators by deriving a control law explicitly in unit dual quaternion Lie algebra. Since the underlying vector space from the Lie algebra is in fact the tangent space of the  $\text{Spin}(3) \times \mathbb{R}^3$ , we can exploit a linear transformation from this space to the joint velocity vector where actuation takes place in task-space context. To the best of the authors knowledge, this is the first result to combine the geometric significance of the Lie algebra of  $\text{Spin}(3) \times \mathbb{R}^3$  with the practicability of being defined in the range space of the dual quaternion error with a linear mapping to the joint velocity inputs.

In this context, the new method provides an intuitive and elegant connection between control effort in task-space and the performance effects over the end-effector trajectory and different sources of uncertainties and disturbances. Using the dual quaternion algebra and the dual quaternion Jacobian  $\underline{\mathbf{J}}_w$  mapping between the vector space stemming from the associated Lie algebra for  $\text{Spin}(3) \times \mathbb{R}^3$  and the joint velocity vector, we adapt classic  $H_{\infty}$  techniques—suitable solely for additive noises—to the dual quaternion space (without mapping the error dynamics to  $\mathbb{R}^8$  manifold). In this sense, we derive easy-to-implement closed form  $H_{\infty}$  control and tracking strategies in dual quaternion space that also incorporate robustness requirements, disturbance attenuation, and performance properties, while minimizing the required control effort.

To address the detrimental influence of the uncertainties and disturbances in the  $H_{\infty}$  sense, we assume that  $\mathbf{v}_w, \mathbf{v}'_w, \mathbf{v}_c, \mathbf{v}'_c \in L_2[0, \infty)$  and introduce a variable  $\gamma$  that upper bounds the induced  $H_{\infty}$  norm, that is, upper bounds the noise-to-error attenuation from (3.6). At this juncture, it is interesting to remind for the reader the error function definition from (3.5)-(3.7), that is,  $\underline{\mathbf{e}} : \text{Spin}(3) \times \mathbb{R}^3 \mapsto \mathbb{H} \otimes \mathbb{D}$ , given by

$$\underline{\mathbf{e}} = 1 - \underline{\mathbf{x}}_e = \mathbf{e} + \varepsilon \mathbf{e}' \quad (3.44)$$

where  $\underline{\boldsymbol{x}}_e = \underline{\boldsymbol{x}}\underline{\boldsymbol{x}}_d^* = \boldsymbol{r}_e + \varepsilon \frac{1}{2} \boldsymbol{p}_e \boldsymbol{r}_e$  is the spatial difference in  $\text{Spin}(3) \times \mathbb{R}^3$ , and  $\boldsymbol{r}_e$  denote the orientation error in  $\text{Spin}(3)$  and  $\boldsymbol{p}_e$  the position error in  $\mathbb{H}_0$ .

In this sense, we address as variable of interest the orientation and translational errors from (3.44) defined respectively as

$$\begin{aligned}\mathcal{O}(\underline{\boldsymbol{e}}) &\triangleq 1 - \boldsymbol{r}_e, \\ \mathcal{T}(\underline{\boldsymbol{e}}) &\triangleq \boldsymbol{p}_e.\end{aligned}$$

*Remark 3.3.* Both orientation and translational errors can be easily extracted from  $\underline{\boldsymbol{e}}$ . The former is basically the invariant quaternion error for orientation obtained from the primary quaternion from (3.44), that is,  $\mathcal{O}(\underline{\boldsymbol{e}}) = \boldsymbol{e}$ . The second denotes the Cartesian error between the current and desired position and it is extracted from (3.44) using  $\mathcal{T}(\underline{\boldsymbol{e}}) = -2\boldsymbol{e}'(1-\boldsymbol{e}^*)$ .

In this context, the following definition based on [81] describes the robust performance in the  $H_\infty$  sense, in terms of the dual quaternion error (3.44) and the orientation and translational errors.

**Definition 3.3.** (Based on [81]) For prescribed positive scalars  $\gamma_{\mathcal{O}1}, \gamma_{\mathcal{O}2}, \gamma_{\mathcal{T}1}, \gamma_{\mathcal{T}2}$ , the robust control performance is achieved in the  $H_\infty$  sense, if the following hold

- (1) The error (3.44) is exponentially stable for  $\underline{\boldsymbol{v}}_w \equiv \underline{\boldsymbol{v}}_c \equiv \mathbf{0}$ ;
- (2) Under the assumption of zero initial conditions, the disturbances influence upon the orientation and translational errors is attenuated below a desired level

$$\begin{aligned}\|\mathcal{O}(\underline{\boldsymbol{e}})\|_2 &\leq \gamma_{\mathcal{O}1} \|\boldsymbol{v}_w\|_2 + \gamma_{\mathcal{O}2} \|\boldsymbol{v}_c\|_2 \quad \forall \boldsymbol{v}_w, \boldsymbol{v}_c \in L_2[0, \infty) \setminus \{0\}; \\ \|\mathcal{T}(\underline{\boldsymbol{e}})\|_2 &\leq \gamma_{\mathcal{T}1} \|\boldsymbol{v}'_w\|_2 + \gamma_{\mathcal{T}2} \|\boldsymbol{v}'_c\|_2 \quad \forall \boldsymbol{v}'_w, \boldsymbol{v}'_c \in L_2[0, \infty) \setminus \{0\}.\end{aligned}\tag{3.45}$$

### 3.3.1 Dual quaternion $H_\infty$ controller

The impact of different sources of uncertainties and disturbances over the system kinematics must be explicitly regarded, and the controller must be designed in accordance to their influence, as neglecting their effects jeopardizes the overall stability.

This section presents a new control strategy that ensures  $H_\infty$  performance for both control and tracking problems without decoupling the rotational and translational dynamics. Since traditional  $H_\infty$  theory is unable to deal with multiplicative noises as in (3.6), the proposed analysis exploits the dual quaternion algebra properties to redefine the problem in order to solve the  $H_\infty$  problem. First, we exploit the isomorphism mapping from (2.12) such that the differential forward kinematics (3.6) yields

$$\begin{aligned}\dot{\underline{\boldsymbol{x}}}_e &= \frac{1}{2} \left( \sum_{i=0}^{n-1} \underline{\boldsymbol{j}}_i \dot{\theta}_i + \underline{\boldsymbol{v}}_w + \underline{\boldsymbol{v}}_c \right) \underline{\boldsymbol{x}}_e \\ &= \frac{1}{2} \left( \underline{\text{vec}} \left( \underline{\boldsymbol{J}}_w \dot{\boldsymbol{\theta}} \right) + \underline{\boldsymbol{v}}_w + \underline{\boldsymbol{v}}_c \right) \underline{\boldsymbol{x}}_e.\end{aligned}\tag{3.46}$$

where  $\boldsymbol{\theta} = [\theta_0 \dots \theta_{n-1}]^T$  is the measured vector of joint variables and  $\underline{\boldsymbol{J}}_w = [\underline{\text{vec}} \underline{\boldsymbol{j}}_0 \dots \underline{\text{vec}} \underline{\boldsymbol{j}}_{n-1}]$  is an analytical Jacobian, which can be extracted directly from Algorithm (2.2). In this sense, from the isomorphism mapping (2.12), we can find solutions in the real space for  $\dot{\boldsymbol{\theta}}$  such that differential equation (3.46) is well-posed [89, Prop. 2.1] as  $\underline{\text{vec}} \left( \underline{\boldsymbol{J}}_w \dot{\boldsymbol{\theta}} \right) \in \mathbb{H}_0 \otimes \mathbb{D}$  lies in the Lie algebra of  $\text{Spin}(3) \times \mathbb{R}^3$ .

To solve the problem of robust exponential stabilization of the dual quaternion error function (3.44), we propose a task-space controller that yields the following joint velocity inputs<sup>8</sup>

$$\dot{\theta} = \underline{\mathbf{J}}_{\omega}^+ \left[ \mathbf{K}_{\mathcal{O}} \text{vec}_3^T (\text{Im}(\mathcal{O}(\underline{\mathbf{e}}))) \quad -\mathbf{K}_{\mathcal{T}} \text{vec}_3^T (\mathcal{T}(\underline{\mathbf{e}})) \right]^T \quad (3.47)$$

where  $\underline{\mathbf{e}} \in \mathbb{H} \otimes \mathbb{D}$  is defined in (3.5)-(3.7) and redefined in (3.44),  $\mathbf{K}_{\mathcal{O}}, \mathbf{K}_{\mathcal{T}} \in \mathbb{R}^{3 \times 3}$  are respectively the orientation and translation gain matrices,  $\underline{\mathbf{J}}_{\omega}^+$  is the pseudoinverse of  $\underline{\mathbf{J}}_{\omega}$ , and the transformation  $\text{vec}_3 : \mathbb{H}_0 \rightarrow \mathbb{R}^3$  uses the isomorphism from  $\mathbb{H}_0$  and  $\mathbb{R}^3$  to map elements from  $\text{Spin}(3)$  to the Euclidean vector space as described in (2.4).<sup>9</sup>

### Theorem 3.7 Dual quaternion $H_{\infty}$ controller

For prescribed positive scalars  $\gamma_{\mathcal{O}1}, \gamma_{\mathcal{O}2}, \gamma_{\mathcal{T}1}, \gamma_{\mathcal{T}2}$ , the closed-loop system (3.46) with task-space controller that yields joint velocity inputs as defined in (3.47) with

$$\mathbf{K}_{\mathcal{O}} \geq \sqrt{2} \sqrt{\gamma_{\mathcal{O}1}^{-2} + \gamma_{\mathcal{O}2}^{-2}} \mathbf{I} \quad \text{and} \quad \mathbf{K}_{\mathcal{T}} \geq \sqrt{\gamma_{\mathcal{T}1}^{-2} + \gamma_{\mathcal{T}2}^{-2}} \mathbf{I}$$

achieves exponential stability with  $H_{\infty}$  disturbance rejection in the sense of Definition 3.3 with minimum control effort.

*proof.*

To study the stability of closed loop system, let us regard the following Lyapunov candidate function

$$V(t, \underline{\mathbf{e}}) = \|\underline{\mathbf{e}}(t)\| = \alpha_1 \|e(t)\|_2^2 + \alpha_2 \|e'(t)\|_2^2, \quad (3.48)$$

with given positive scalars  $\alpha_1$  and  $\alpha_2$ . Taking the time-derivative along the trajectory (3.46) (see Appendix C.1) in the absence of disturbances, that is,  $\underline{\mathbf{v}}_w \equiv \underline{\mathbf{v}}_c \equiv \mathbf{0}$ , we have

$$\begin{aligned} \dot{V}(t, \underline{\mathbf{e}}) &\leq -\frac{\alpha_1 \sigma_m\{\mathbf{K}_{\mathcal{O}}\}}{2} \|e(t)\|_2^2 - 2\alpha_2 \sigma_m\{\mathbf{K}_{\mathcal{T}}\} \|e'(t)\|_2^2 \\ &\leq -\min \left\{ \frac{\sigma_m\{\mathbf{K}_{\mathcal{O}}\}}{2}, 2\sigma_m\{\mathbf{K}_{\mathcal{T}}\} \right\} V(t, \underline{\mathbf{e}}) \leq 0. \end{aligned} \quad (3.49)$$

where  $\sigma_m\{\mathbf{K}_{\mathcal{O}}\}$  and  $\sigma_m\{\mathbf{K}_{\mathcal{T}}\}$  denote the minimum singular value from  $\mathbf{K}_{\mathcal{O}}, \mathbf{K}_{\mathcal{T}}$ , respectively. Hence, by the Comparison Lemma [72, pg. 85], we have that the closed-loop system (3.46) with (3.47) is exponentially stable in the absence of disturbances, that is,

$$\begin{aligned} \|e(t)\|_2^2 &\leq \|e(t_0)\|_2^2 e^{-\frac{1}{2}\sigma_m\{\mathbf{K}_{\mathcal{O}}\}(t-t_0)}, \\ \text{and } \|e'(t)\|_2^2 &\leq \|e'(t_0)\|_2^2 e^{-2\sigma_m\{\mathbf{K}_{\mathcal{T}}\}(t-t_0)}. \end{aligned}$$

Hence, the Condition (1) in Definition 3.3 is satisfied for  $\mathbf{K}_{\mathcal{O}} > 0$  and  $\mathbf{K}_{\mathcal{T}} > 0$ .

Now, explicitly addressing the influence of uncertainties and disturbances over the closed-loop system,

<sup>8</sup>In terms of the spatial difference  $\underline{\mathbf{x}}_e = \underline{\mathbf{x}}\underline{\mathbf{x}}_d^* = \mathbf{r}_e + \varepsilon \frac{1}{2} \mathbf{p}_e \mathbf{r}_e$ , the dual quaternion controller (3.47) can be rewritten as  $\dot{\theta} = \underline{\mathbf{J}}_{\omega}^+ \left[ -\mathbf{K}_{\mathcal{O}} \text{vec}_3^T (\text{Im}(\mathbf{r}_e)) \quad -\mathbf{K}_{\mathcal{T}} \text{vec}_3^T (\mathbf{p}_e) \right]^T$  where  $\text{Im}(\mathbf{r}_e)$  and  $\mathbf{p}_e$  can be directly extracted from the dual quaternion components of  $\underline{\mathbf{x}}_e = \eta + \boldsymbol{\mu} + \varepsilon(\eta' + \boldsymbol{\mu}')$  as  $\text{Im}(\mathbf{r}_e) = \boldsymbol{\mu}$  and  $\mathbf{p}_e = \eta\boldsymbol{\mu}' - \eta'\boldsymbol{\mu} + \boldsymbol{\mu} \times \boldsymbol{\mu}'$ .

<sup>9</sup>Avoidance techniques for kinematic singularities are considered in Chapter 5. Herein, the Jacobian  $\underline{\mathbf{J}}_{\omega}$  is assumed to be well-posed.

the Lyapunov derivative (see Appendix C.2) yields

$$\begin{aligned} \dot{V}(t, \underline{e}) = & -\alpha_1 \text{vec}_3^T \text{Im}(\mathcal{O}(\underline{e})) (\mathbf{K}_\circ \text{vec}_3 \text{Im}(\mathcal{O}(\underline{e})) + \text{vec}_3(\mathbf{v}_w + \mathbf{v}_c)) \\ & - \frac{\alpha_2}{2} \text{vec}_3^T \mathcal{T}(\underline{e}) (\mathbf{K}_\tau \text{vec}_3 \mathcal{T}(\underline{e}) - \text{vec}_3(\mathbf{v}'_w + \mathbf{v}'_c)). \end{aligned} \quad (3.50)$$

To investigate the  $H_\infty$  performance, let us define  $V_{\gamma_\circ} \triangleq \|\mathcal{O}(\underline{e})\|_2^2 - \gamma_{\circ 1}^2 \|\mathbf{v}_w\|_2^2 - \gamma_{\circ 2}^2 \|\mathbf{v}_c\|_2^2$  and  $V_{\gamma_\tau} \triangleq \|\mathcal{T}(\underline{e})\|_2^2 - \gamma_{\tau 1}^2 \|\mathbf{v}'_w\|_2^2 - \gamma_{\tau 2}^2 \|\mathbf{v}'_c\|_2^2$ , such that

$$V_{H_\infty} = \dot{V}(t, \underline{e}) + V_{\gamma_\circ} + V_{\gamma_\tau}.$$

Note that  $\|\mathcal{O}(\underline{e})\|_2^2 \leq 2 \|\text{vec}_3 \text{Im}(\mathcal{O}(\underline{e}))\|_2^2$  for  $\eta \in [0, 1]$ . Hence,

$$\begin{aligned} V_{H_\infty} \leq & -\text{vec}_3^T(\text{Im}(\mathcal{O}(\underline{e}))) (\alpha_1 \mathbf{K}_\circ - 2\mathbf{I}) \text{vec}_3(\text{Im}(\mathcal{O}(\underline{e}))) - \text{vec}_3^T(\mathcal{T}(\underline{e})) \left(\frac{\alpha_2}{2} \mathbf{K}_\tau - \mathbf{I}\right) \text{vec}_3(\mathcal{T}(\underline{e})) \\ & + \alpha_1 \text{vec}_3^T(\text{Im}(\mathcal{O}(\underline{e}))) \text{vec}_3(\mathbf{v}_w + \mathbf{v}_c) - \gamma_{\circ 1}^2 \|\mathbf{v}_w\|_2^2 - \gamma_{\circ 2}^2 \|\mathbf{v}_c\|_2^2 \\ & + \frac{\alpha_2}{2} \text{vec}_3^T(\mathcal{T}(\underline{e})) \text{vec}_3(\mathbf{v}'_w + \mathbf{v}'_c) - \gamma_{\tau 1}^2 \|\mathbf{v}'_w\|_2^2 - \gamma_{\tau 2}^2 \|\mathbf{v}'_c\|_2^2. \end{aligned}$$

Using Schur complement, we have that  $V_{H_\infty} \leq 0$  if and only if

$$\begin{aligned} \mathbf{K}_\circ & \geq \frac{2}{\alpha_1} \mathbf{I} + \frac{\alpha_1}{4} (\gamma_{\circ 1}^{-2} + \gamma_{\circ 2}^{-2}) \mathbf{I}, \\ \text{and } \mathbf{K}_\tau & \geq \frac{2}{\alpha_2} \mathbf{I} + \frac{\alpha_2}{8} (\gamma_{\tau 1}^{-2} + \gamma_{\tau 2}^{-2}) \mathbf{I}. \end{aligned} \quad (3.51)$$

In this context, if the inequalities are satisfied for both  $\mathbf{K}_\circ$  and  $\mathbf{K}_\tau$ , then  $\dot{V}(t, \underline{e}) + V_{\gamma_\circ} \leq 0$  and  $\dot{V}(t, \underline{e}) + V_{\gamma_\tau} \leq 0$  also holds. Now, under zero initial conditions and given the Lyapunov function positiveness properties, the integration from 0 to  $\infty$  yields  $\int_0^\infty \|\mathcal{O}(\underline{e})\|_2^2 - \gamma_{\circ 1}^2 \|\mathbf{v}_w\|_2^2 - \gamma_{\circ 2}^2 \|\mathbf{v}_c\|_2^2 \leq 0$  and  $\int_0^\infty \|\mathcal{T}(\underline{e})\|_2^2 - \gamma_{\tau 1}^2 \|\mathbf{v}'_w\|_2^2 - \gamma_{\tau 2}^2 \|\mathbf{v}'_c\|_2^2 \leq 0$ , which is equivalent to the conditions presented in (3.45). Hence, the conditions in Definition 3.3 are satisfied.

Still, there exist an infinity number of solutions for  $\alpha_1$  and  $\alpha_2$  that satisfies (3.51). To further simplify and improve the choice of a feasible solution, we seek a closed-form control solution that optimizes a prescribed criterion. In this particular case, we seek  $\alpha_{1opt}$  and  $\alpha_{2opt}$  that minimizes the norm of the control gains  $\mathbf{K}_\circ$  and  $\mathbf{K}_\tau$ . After some manipulation, taking the minimum of (3.51) with regard to  $\alpha_1$  and  $\alpha_2$ , we have  $\alpha_{1opt} = 2\sqrt{2} \sqrt{\frac{\gamma_{\circ 1}^2 \gamma_{\circ 2}^2}{\gamma_{\circ 1}^2 + \gamma_{\circ 2}^2}}$  and  $\alpha_{2opt} = 4 \sqrt{\frac{\gamma_{\tau 1}^2 \gamma_{\tau 2}^2}{\gamma_{\tau 1}^2 + \gamma_{\tau 2}^2}}$ . Therefore, control gains  $\mathbf{K}_\circ$  and  $\mathbf{K}_\tau$  with minimum norm that satisfies (3.51) are  $\mathbf{K}_\circ \geq \sqrt{2} \sqrt{\gamma_{\circ 1}^{-2} + \gamma_{\circ 2}^{-2}} \mathbf{I}$  and  $\mathbf{K}_\tau \geq \sqrt{\gamma_{\tau 1}^{-2} + \gamma_{\tau 2}^{-2}} \mathbf{I}$ .  $\square$

*Remark 3.4.* Note that there is no unique natural metric for  $\text{Spin}(3) \times \mathbb{R}^3$ , similarly to the case for  $SE(3)$ . Hence, there is more freedom left for the control design [55]. The proposed bilinear form defined in (3.48) exploits the natural metric for  $\mathbb{H}$  which yields control actions along the geodesic directions for both orientation and translational errors.

The control scheme provided by Theorem 3.7 is a straightforward solution for the  $H_\infty$  control of manipulators using dual quaternion representation. Indeed, the resulting controller gain is given by a closed-form expression and solely depends on the prescribed scalars  $\gamma_{\circ 1}, \gamma_{\circ 2}, \gamma_{\tau 1}, \gamma_{\tau 2}$ . Furthermore, the resulting control scheme renders the gain value to be optimal in the sense of reducing its norm, which in turn reduces the control effort required to exponentially stabilize the end effector while maintaining the  $H_\infty$  performance. To the best of the authors knowledge, given the dual quaternion framework, this is the first work to explicitly regard several

sources of uncertainties and disturbances acting on the manipulator and exploit the dual quaternion properties to ensure a satisfying control performance in the  $H_\infty$  sense.

### 3.3.2 Dual quaternion $H_\infty$ tracking controller

For practical applications, it is interesting to consider a more general scenario with time-varying reference trajectories, that is, a tracking system. At this juncture, the desired end-effector trajectory over time is described by the first order differential kinematic equation of a rigid body (2.26),

$$\dot{\underline{\mathbf{x}}}_d = \frac{1}{2}\underline{\boldsymbol{\omega}}_d \underline{\mathbf{x}}_d, \quad (3.52)$$

where  $\underline{\boldsymbol{\omega}}_d$  is the twist for the desired pose in inertial frame. Hence, in the context of varying pose configurations, the error differential kinematics (3.5), (3.6), (3.46) can be rewritten as

$$\begin{aligned} \dot{\underline{\mathbf{x}}}_e &= \dot{\underline{\mathbf{x}}}_d^* + \underline{\mathbf{x}}_d^* \dot{\underline{\mathbf{x}}}_d \\ &= \frac{1}{2} \left( \text{vec}_6 \left( \underline{\mathbf{J}}_w \dot{\underline{\boldsymbol{\theta}}} \right) \underline{\mathbf{x}} + \underline{\mathbf{v}}_w \underline{\mathbf{x}} + \underline{\mathbf{v}}_c \underline{\mathbf{x}} \right) \underline{\mathbf{x}}_d^* + \frac{1}{2} \underline{\mathbf{x}}_d^* \underline{\boldsymbol{\omega}}_d^* \\ &= \frac{1}{2} \left( \text{vec}_6 \left( \underline{\mathbf{J}}_w \dot{\underline{\boldsymbol{\theta}}} \right) + \underline{\mathbf{v}}_w + \underline{\mathbf{v}}_c \right) \underline{\mathbf{x}}_e - \frac{1}{2} \underline{\mathbf{x}}_e \underline{\boldsymbol{\omega}}_d. \end{aligned} \quad (3.53)$$

From Definition 3.3 and Theorem 3.7, we state a solution for the  $H_\infty$  tracking control problem as follows

#### Theorem 3.8 Dual quaternion $H_\infty$ tracking controller

For prescribed positive performance scalar parameters  $\gamma_{o1}, \gamma_{o2}, \gamma_{\tau1}, \gamma_{\tau2}$ , the task-space controller yielding joint velocity inputs

$$\begin{aligned} \dot{\underline{\boldsymbol{\theta}}}_{tr} &= \underline{\mathbf{J}}_w^+ \left[ \mathbf{K}_o \text{vec}_3^T (\text{Im}(\mathcal{O}(\underline{\mathbf{e}}))) \quad -\mathbf{K}_\tau \text{vec}_3^T (\mathcal{T}(\underline{\mathbf{e}})) \right]^T \\ &\quad + \underline{\mathbf{J}}_w^+ (\text{vec}_6(\underline{\mathbf{x}}_e \underline{\boldsymbol{\omega}}_d \underline{\mathbf{x}}_e^*)) \end{aligned} \quad (3.54)$$

with feedforward term  $\text{vec}_6(\underline{\mathbf{x}}_e \underline{\boldsymbol{\omega}}_d \underline{\mathbf{x}}_e^*)$  based on the desired end-effector twist  $\underline{\boldsymbol{\omega}}_d$  described in (3.52), and control gains  $\mathbf{K}_o \geq \sqrt{2} \sqrt{\gamma_{o1}^{-2} + \gamma_{o2}^{-2}} \mathbf{I}$  and  $\mathbf{K}_\tau \geq \sqrt{\gamma_{\tau1}^{-2} + \gamma_{\tau2}^{-2}} \mathbf{I}$  ensures exponential  $H_\infty$  tracking performance with disturbance rejection in the sense of Definition 3.3 with minimum control effort for the closed-loop system (3.44), (3.53).

*proof.*

From the proposed tracking controller (3.54), the closed-loop system (3.53) yields

$$\begin{aligned} \dot{\underline{\mathbf{x}}}_e &= \frac{1}{2} \left( \text{vec}_6 \left( \underline{\mathbf{J}}_w \dot{\underline{\boldsymbol{\theta}}} \right) + \underline{\mathbf{v}}_w + \underline{\mathbf{v}}_c \right) \underline{\mathbf{x}}_e - \frac{1}{2} \underline{\mathbf{x}}_e \underline{\boldsymbol{\omega}}_d \\ &= \frac{1}{2} \left( \text{vec}_6 \left( \underline{\mathbf{J}}_w \tilde{\underline{\boldsymbol{\theta}}} \right) + \underline{\mathbf{v}}_w + \underline{\mathbf{v}}_c \right) \underline{\mathbf{x}}_e, \end{aligned}$$

where  $\tilde{\underline{\boldsymbol{\theta}}} = \underline{\mathbf{J}}_w^+ \left[ \mathbf{K}_o \text{vec}_3^T (\text{Im}(\mathcal{O}(\underline{\mathbf{e}}))) \quad -\mathbf{K}_\tau \text{vec}_3^T (\mathcal{T}(\underline{\mathbf{e}})) \right]^T$ . Note that this is the same closed-loop dynamics obtained in (3.44) with task-space controller defined as in (3.47). Consequently, the rest of the proof follows exactly the same steps from Theorem 3.7.  $\square$

From Theorems 3.7 and 3.8, it is also interesting to consider particular cases where either it is difficult to

decouple both sources of uncertainties or the designer explicitly sets the performance to be the same, that is,  $\gamma_{\tau} = \gamma_{\tau_1} = \gamma_{\tau_2}$  and  $\gamma_o = \gamma_{o_1} = \gamma_{o_2}$ .

**Corollary 3.1.** *For prescribed positive scalars  $\gamma_o, \gamma_{\tau}$ , the closed-loop system (3.44), (3.53), with task-space controller defined in (3.54) with  $\mathbf{K}_o \geq 2\gamma_o^{-1}\mathbf{I}$  and  $\mathbf{K}_{\tau} \geq \sqrt{2}\gamma_{\tau}^{-1}\mathbf{I}$  achieves exponential  $H_{\infty}$  tracking performance with disturbance rejection in the sense of Definition 3.3 with minimum control effort.*

### 3.4 NUMERICAL EXAMPLES AND SIMULATIONS

This section assesses the effectiveness and advantages of the proposed results within this chapter. To this aim, different scenarios and conditions were devised using a diverse set of platforms as to investigate the benefits from the proposed techniques and to compare with traditional controllers for robot manipulators.

In summary, this section presents three different numerical examples implemented in Open Robotics Automation Virtual Environment (OpenRAVE) without a physics engine to simulate rigid body dynamics, and two more realistic simulations devised and implemented in the Virtual Experimentation Platform (VREP) from Coppelia RObotics GmbH (see, [90]) using Bullet Physics Library<sup>10</sup> as the physics engine. For examples using OpenRAVE, all controllers were implemented using Matlab and the DQ\_Robotics toolbox<sup>11</sup>; whereas the VREP simulations were implemented using The Robot Operating System (ROS)<sup>12</sup> and the DQ\_Robotics toolbox with a sampling time of 5ms.

**Example 3.1** (Comau SMART SiX robot using OpenRAVE). This example investigates the effectiveness from dual-quaternion based controllers mapped to  $\mathbb{R}^8$  manifold, that is, the results from Subsection 3.2.1.

Consider a simple task of moving the manipulator end-effector from one pose to another in a scenario subjected to exogenous disturbances. For this task, we considered a Comau SMART SiX robot (a six-link robot manipulator) with initial configuration described by the joint configuration  $\theta_{\text{init}} = [-54 \quad 36 \quad -90 \quad 0 \quad 90 \quad 0]^T$ , which corresponds to the following unit dual quaternion pose

$$\mathbf{x}_{\text{init}} = -0.275 - 0.432\hat{i} + 0.847\hat{j} - 0.140\hat{k} - \left(0.184 + 0.387\hat{i} + 0.197\hat{j} - 0.362\hat{k}\right).$$

The desired end-effector position and orientation configuration is given by

$$\mathbf{x}_d = 0 + 0.707\hat{i} + 0.707\hat{j} + 0\hat{k} + \left(0.282 - 0.380\hat{i} + 0.380\hat{j} + 0.282\hat{k}\right).$$

In this scenario, we simulated the exogenous disturbance acting on the system. To ease the analysis, we set the exogenous disturbance to be described by  $v = 1.1 \cos(5t)$  and  $B = [1 \ 1 \ 1 \ 1 \ 1 \ 1 \ 1 \ 1]^T$ . In the  $H_{\infty}$  sense, the control requirement is to maintain the noise to error amplification less than the upper bound  $\gamma = 0.002$ .

The first result regards the time response of each component of the dual quaternion vector, shown in Figure 3.1. Besides the large disturbance, each component asymptotically converges to its desired reference. The end-effector position are shown in Figure 3.2, which also demonstrates the convergence efficiency of the control technique. Figure 3.3(a) regards the evolution of the convergence error, which is described by the evolution of its norm, i.e.,  $\|\text{vec } \underline{e}\|_2$ . It is clear that the  $H_{\infty}$  control technique succeeded in reducing the disturbance influence upon the closed-loop system, whereas maintaining the system stability. Indeed, under zero initial

<sup>10</sup><http://www.bulletphysics.org/>

<sup>11</sup><http://dqrobotics.sourceforge.net>

<sup>12</sup><http://www.ros.org/>

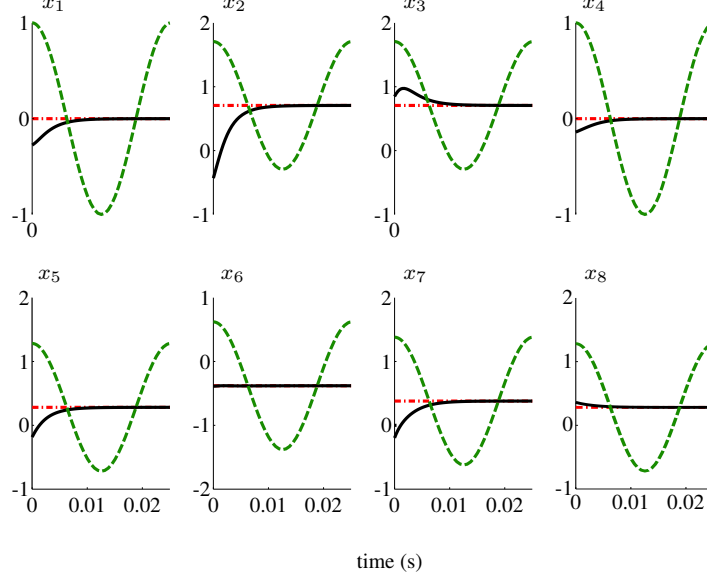


Figure 3.1: [Example 3.1] Exogeneous disturbance (green dashed curve), desired dual quaternion coefficient (red dash-dotted curve), and measured dual quaternion coefficient (black solid curve).

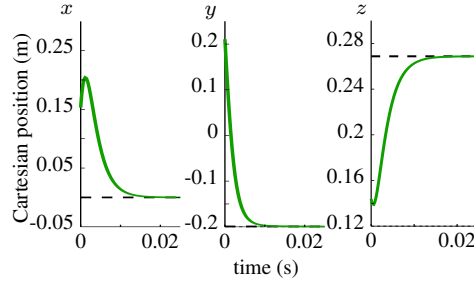


Figure 3.2: [Example 3.1] Three dimensional position: reference (black dashed curve) and measured value (solid green).

conditions and numerically computing the error and noise norms, the resulting noise to error amplification is  $\frac{\int_{t_0}^{t_1} \|\text{vec } \underline{e}\|_2}{\int_{t_0}^{t_1} \|\underline{v}\|_2} = 0.0013$ , which is less than the calculated upper bound  $\gamma = 0.002$ .

Moreover, in order to allow comparison with previous results, we have empirically chosen a controller, using the results from [63], with the same control performance obtained with Theorem 3.3, i.e., with a noise to error attenuation of 0.0013. The control effort of this brute-force manually chosen controller is shown in Figure 3.3(b) (light green). The resulting control is up to 5 times more expensive than the controller obtained with Theorem 3.3, which minimizes a given energy criterion. The result enlightens the importance of the proposed robust control techniques in comparison to previous results.

**Example 3.2** (Discrete-time control of a Baxter WAM arm using OpenRAVE). This example is particularly designed for discrete time controllers using the  $\text{vec}_8$  to an  $\mathbb{R}^8$  manifold. In this scenario, we are considering a WAM arm, a seven-link manipulator from Barrett Technology Inc., under simulated uncertainties and exogenous disturbances.

Similarly to the former example, in this scenario we seek to move the end-effector from an initial pose,  $\underline{x}_{\text{init}} = 0.27 - \hat{i}0.47 + \hat{j}0.76 + \hat{k}0.35 - \varepsilon(\hat{j}0.11 - \hat{k}0.24)$ , to a desired one,  $\underline{x}_d = 0.27 - \hat{i}0.47 + \hat{j}0.76 +$



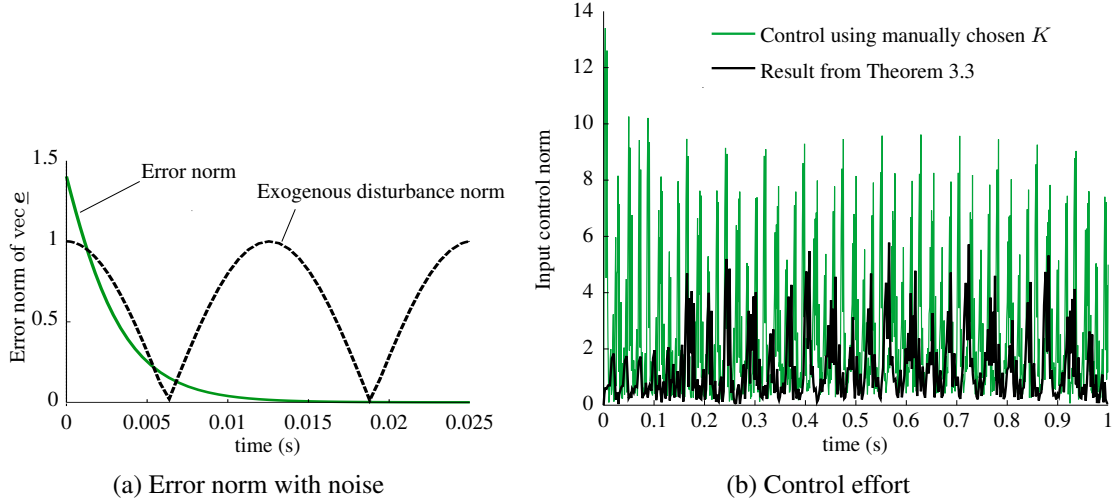


Figure 3.3: [Example 3.1] Plot (a) shows the error norm compared to the exogenous disturbances whereas in (b) it is shown the control effort from the controller compared to a random gain  $K$  with similar error norm.

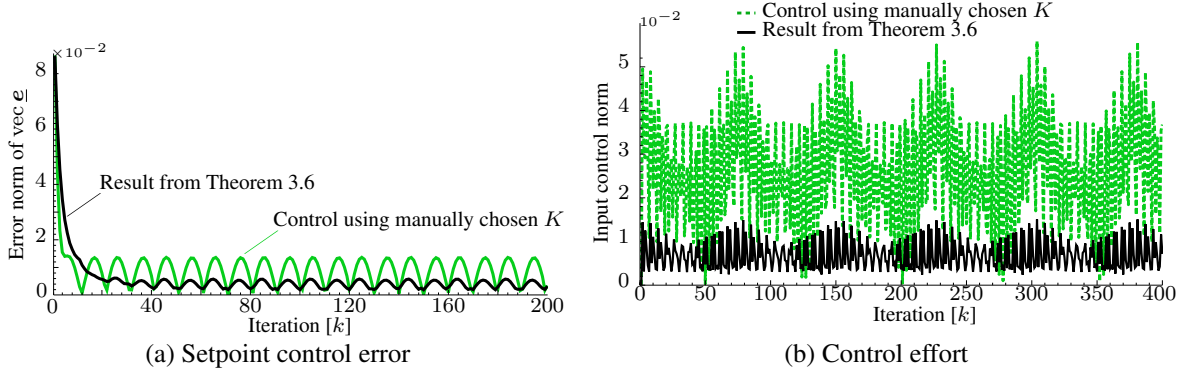


Figure 3.4: [Example 3.2] Setpoint error norm (a) and control effort (b).

$\hat{k}0.35 - \varepsilon(0.08 + \hat{i}0.03 + \hat{j}0.10 - \hat{k}0.24)$ . The task represents a single end-effector translation of 10 cm in each axis, whereas holding the original orientation. In addition to the discretization error, we enforce exogenous disturbances upon the twist and pose configuration of the end-effector. The control requirement is to maintain a noise to error amplification less than the upper bound  $\gamma = 0.05$ .

The evolution of the convergence error is compared against the discretized version of [63]. As a simple discretization could yield unstable results, and to allow fair comparison, a try-and-error strategy has been set to find a suitable controller with similar control effort compared to Theorem 3.6. In this sense, the gain for the manually chosen controller, based on [63], stemmed from a tedious brute-force search where different gains were generated and tested for feasibility and control effort. The results are shown in Figure 3.4(a), and illustrates the effectiveness of the discrete  $H_\infty$  controller, which succeeded in reducing the disturbance influence. Indeed, under zero initial conditions, the numerically computed noise to output attenuation for the results from Theorem 3.6 is 0.044, which is less than the prescribed upper bound  $\gamma = 0.05$ , whereas the results from the manually chosen controller is 0.097, up to 2.2 times worst. The end-effector position and orientation are shown in Figs. 3.5(a) and 3.5(b), respectively, and also demonstrates the advantages of the proposed technique.

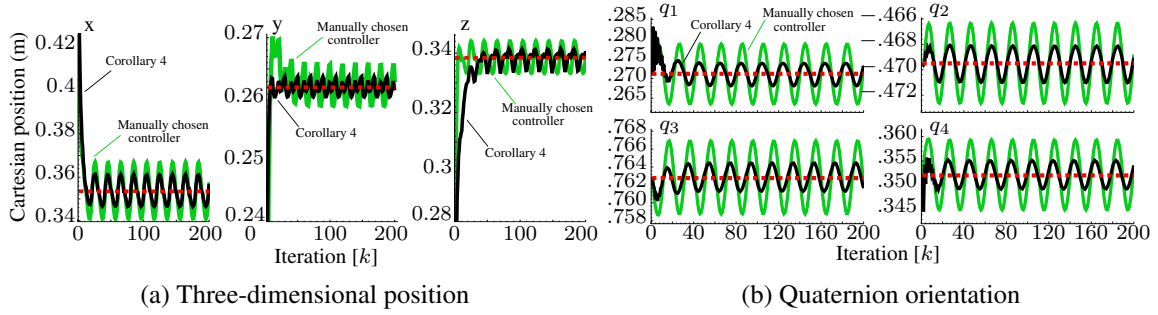


Figure 3.5: [Example 3.2] Three-dimensional position and quaternion orientation: reference (red dashed curve), measured values from manually chosen controller (green) and from Theorem 3.6 (black).

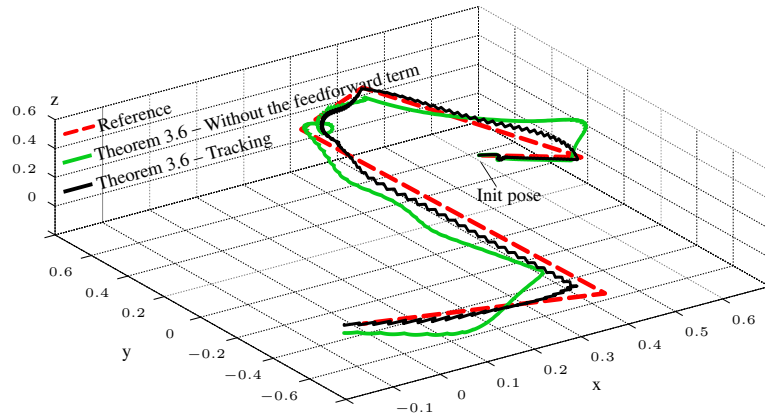


Figure 3.6: [Example 3.2] Cartesian position: tracking reference (red dashed curve) and measured positions from Theorem 3.6 without the feedforward term, i.e., setpoint control (green) and from Theorem 3.6 considering the feedforward term, that is, tracking controller (black).

Within the same scenario, in order to compare the control effort, we investigate the influence of the disturbances whereas holding a fixed pose. To allow a fair comparison, the gain for the discretized controller from [63] has been randomly selected using a brute force search as to obtain a similar performance obtained using Theorem 3.6, that is,  $\gamma=0.044$ . The control effort from both techniques are shown in Figure 3.4(b). The brute-force manually chosen controller is up to four times more expensive than the proposed controller, which highlights the efficiency of the minimization criterion from Theorem 3.6.

Moreover, in order to illustrate the effectiveness of the tracking strategy under high disturbance influence, the fixed desired pose was replaced for a task trajectory along task-space. The task trajectory is composed of five straight lines with the same orientation. Figure 3.6 illustrates the Cartesian displacement of the end-effector from the tracking controller using Theorem 3.6 compared to the stabilizing setpoint controller (Theorem 3.6 without the feedforward term). For this particular task trajectory, the mean numerically calculated error from the proposed tracking criterion is 0.016, whereas the mean error obtained using the setpoint controller (Theorem 3.6 without feedforward) and the manually chosen controller are 0.053 and 0.066, that is, over three and four times higher than Theorem 3.6, respectively. The results illustrates the importance of considering a tracking controller instead of a moving setpoint control strategy.

**Example 3.3** (Comparison between control strategies based on a simulation with KUKA LBRIV arm using V-REP). This example assesses the effectiveness and differences between the control frameworks proposed

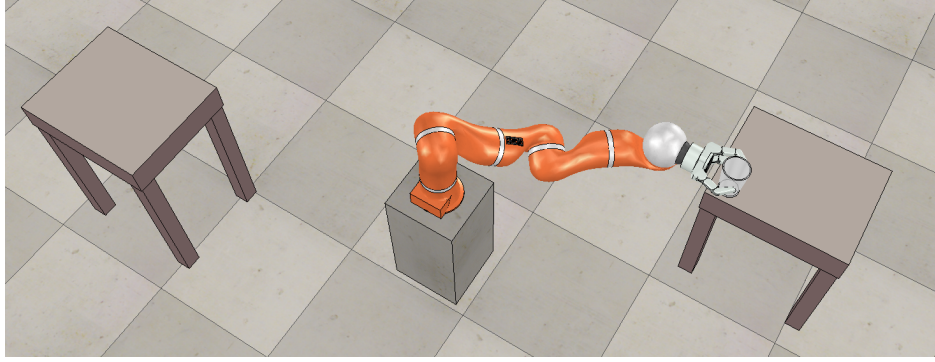


Figure 3.7: [Example 3.3] Screenshot from the simulated task (V-REP platform).

in this chapter, particularly, between the controllers based on the dual quaternion space mapping to an  $\mathbb{R}^8$  manifold (Section 3.2) and strictly dual quaternion controllers (Section 3.3).

To this aim, different simulation tasks were devised and implemented in the Virtual Robot Experimentation Platform (V-REP) from Coppelia Robotics GmbH—using Bullet Physics Library as the physics engine—with a KUKA LBR IV arm, a seven-link manipulator from Kuka Robotics, connected to a Barret Hand for grasping. All V-REP simulations were performed using a 5 ms sampling time and the proposed controller was implemented using the DQ\_robotics toolbox.

In the first scenario, the manipulator was set to an initial configuration,  $\underline{x}(0) = 0.46 - 0.60\hat{i} + 0.35\hat{j} + 0.55\hat{k} - \varepsilon(0.17 + 0.30\hat{i} + 0.72\hat{j} - 0.28\hat{k})$ , from where it was supposed to travel to an specific pose,  $\underline{x}_d = 0.707 + 0\hat{i} + 0.707\hat{j}\hat{k} + 0\hat{k}) + \varepsilon(0.13 + 0.32\hat{i} - 0.13\hat{j} + 0.78\hat{k})$ , and grasp the cup. The final pose of the task is illustrated in Figure 3.7. At this juncture, there is no disturbances except for the platform dynamic precision and modeling approximations.

The scenario was simulated using the controller from Theorem 3.7 and compared against the controllers from [4] and from Theorem 3.3—both of which are based on the dual quaternion error mapping to an  $\mathbb{R}^8$  manifold—and against a decoupled approach based on  $\text{Spin}(3)$  and  $\mathbb{R}^3$  which concerns independent orientation and translational task Jacobians. To allow a fair comparison, for this scenario, all controllers were set with the same constant control gain  $K = 0.005$ .

The evolution of the convergence error is illustrated in Figure 3.8 whereby it is easy to see the advantages that stems from deriving a control law with exponential convergence at the unit dual quaternion tangent space and, at the same time, with a linear map to the joint velocity vector. The end-effector orientation and translational trajectories shown in Figure 3.9 also demonstrates the advantages of the proposed criteria. Clearly, Theorem 3.7 is the only to achieve exponential convergence concerning both the orientation and translation errors which yields a combined error norm (orientation and translation) without spikes as shown in Figure 3.8.

Within the same scenario, we devised a task tracking trajectory to move the end-effector to an specific point at the second table and then release the cup. The suggested trajectory takes the arm to highly complex configurations in the sense of proximity to singularities and joint limits. At this point, it is important to emphasize that the errors—associated with the trajectory—are proportional to the tracking time that is set with the trajectory. The smaller the time, the larger the errors. This context is rather interesting as larger errors may lead the arm to singular and joint limits configurations<sup>13</sup> which in turn may disrupt the task. Indeed, after fifty trials per

<sup>13</sup>To maintain the fairness, singularity avoidance was not considered at this point for none of the controllers

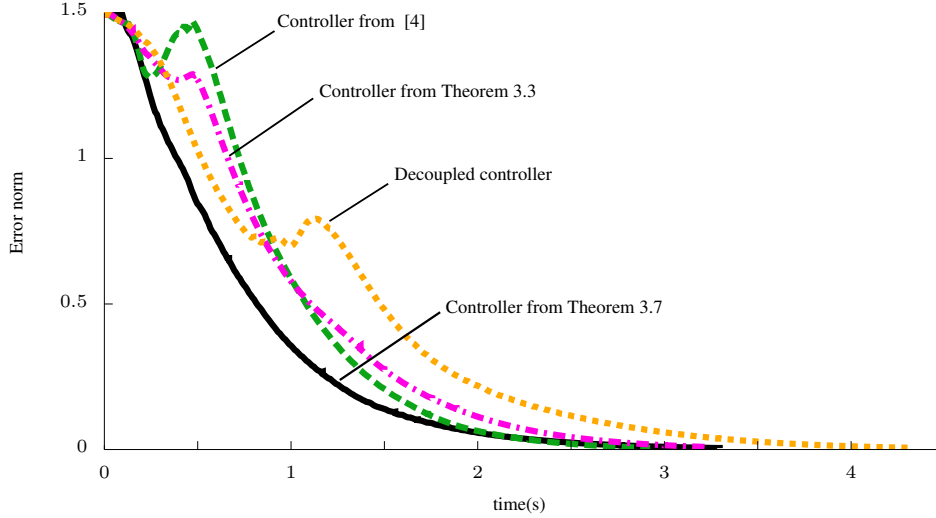


Figure 3.8: [Example 3.3] Setpoint control error.

Decoupled controller	Controller from [4]	Theorem 3.3	Theorem 3.7
0%	26%	48%	96%

Table 3.1: [Example 3.3] Percentage of successfully completed tracking task from fifty trials per controller

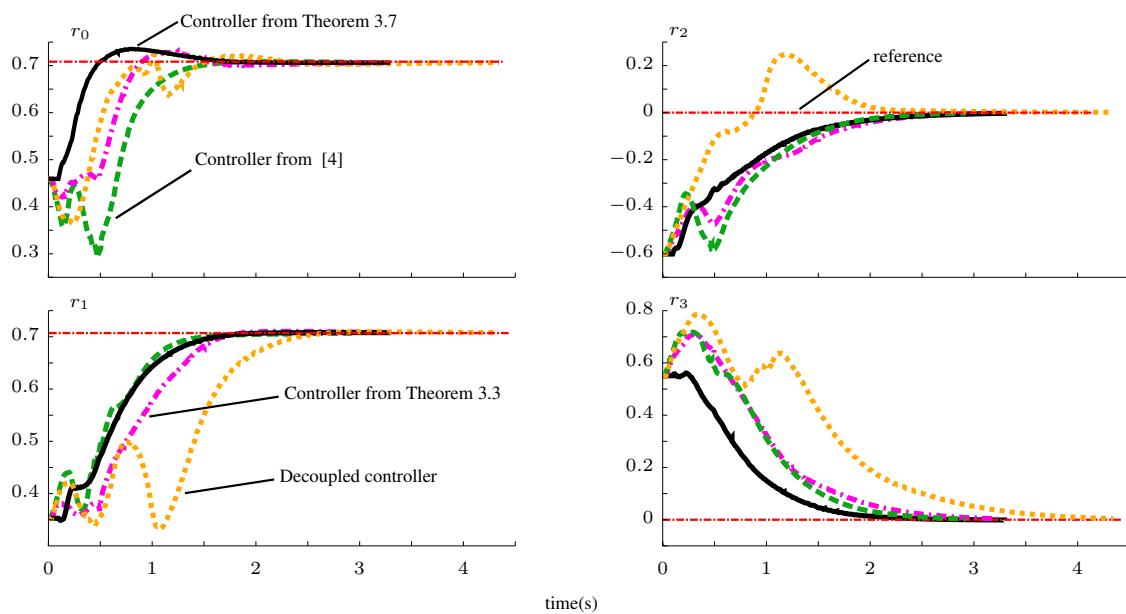
controller with a 5 ms sampling time, the decoupled technique was unable to cope with the complex trajectory, the controllers from [4] and Theorem 3.3 successfully completed 26% and 48% of the simulations, respectively, whereas the tracking controller from Theorem 3.7 was able to complete 96% of the simulations. The results are shown in Table 3.1.

Concerning only successful trials and despite having the same control gain, Theorem 3.8 provided superior results in the sense of tracking errors compared to [4] and Theorem 3.3 as shown in Figure 3.10. Furthermore, the controllers from [4] and Theorem 3.3 required higher joint velocities to cope with the task trajectory, as shown in Figure 3.11.

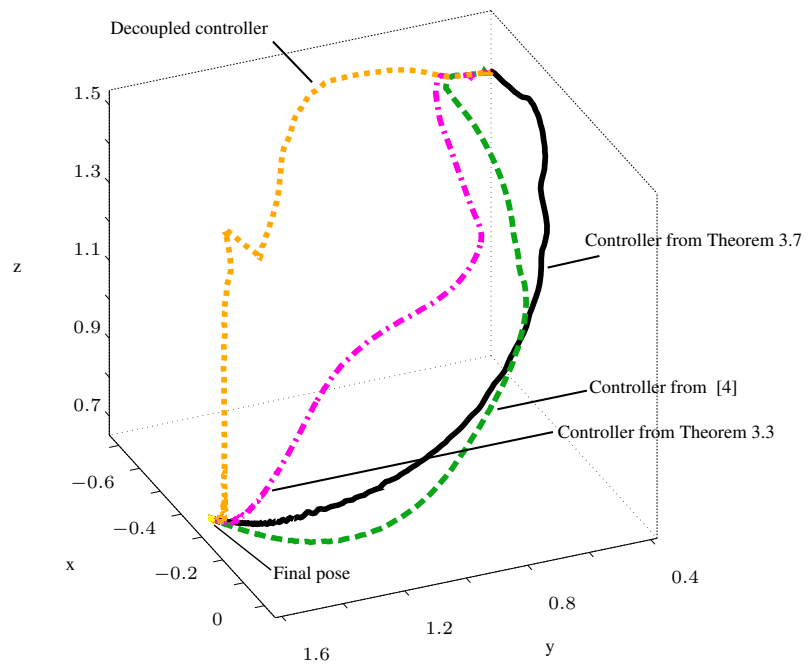
**Example 3.4** (Dual quaternion  $H_\infty$  Controller with a KUKA LBRIV arm using V-REP). This example assesses the effectiveness of the proposed dual quaternion based  $H_\infty$  controller under uncertainties and disturbances (Section 3.3). Similarly to the former example, the simulation was devised and implemented in the Virtual Robot Experimentation Platform (V-REP) from Coppelia Robotics GmbH—using Bullet Physics Library as the physics engine—with a KUKA LBRIV arm, a seven-link manipulator from Kuka Robotics, connected to a Barret Hand for grasping.

To illustrate the effectiveness of the proposed dual quaternion  $H_\infty$  controller under uncertainties and disturbances, we devised a more elaborated task assignment. The control task consists in maintaining the relative pose between the end effector and a non-fixed target, in this case, the cup which is connected to a mobile platform—a Pioneer P3-DX from Adept Mobile Robots LCC—as shown in Figure 3.12. The proposed context is similar to the case of a mobile manipulator with disturbances and uncertainties concerning the mobile pose. Within this scenario, the manipulator, in addition to modeling and numerical precision errors, was subjected to random induced disturbances as unmodeled twists and to disturbances on the reference frame—due to the unknown time-varying movement of the Pioneer robot.

The control task was simulated using Corollary 3.1 (considering  $\gamma_\tau = \gamma_{\tau_1} = \gamma_{\tau_2}$  and  $\gamma_o = \gamma_{o_1} = \gamma_{o_2}$ ) with



(a) Quaternion orientation ( $\mathbf{r} = r_0 + r_1\hat{i} + r_2\hat{j} + r_3\hat{k}$ )



(b) Cartesian three-dimensional position

Figure 3.9: [Example 3.3] End-effector translation and orientation for setpoint control: Theorem 3.7 (solid black line), decoupled controller (orange dotted-line), controller from [4] (green dashed line) and from Theorem 3.3 (magenta point-dashed line).

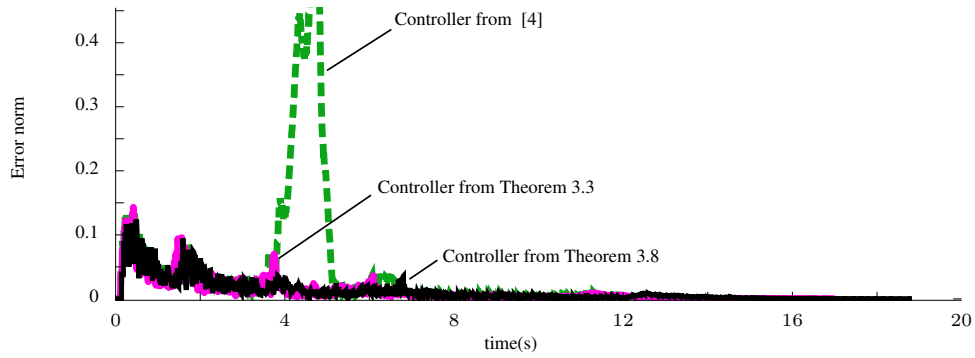


Figure 3.10: [Example 3.3] Tracking error along time: Theorem 3.8 (solid black line), controller from [4] (green dashed line) and from Theorem 3.3 (magenta point-dashed line).

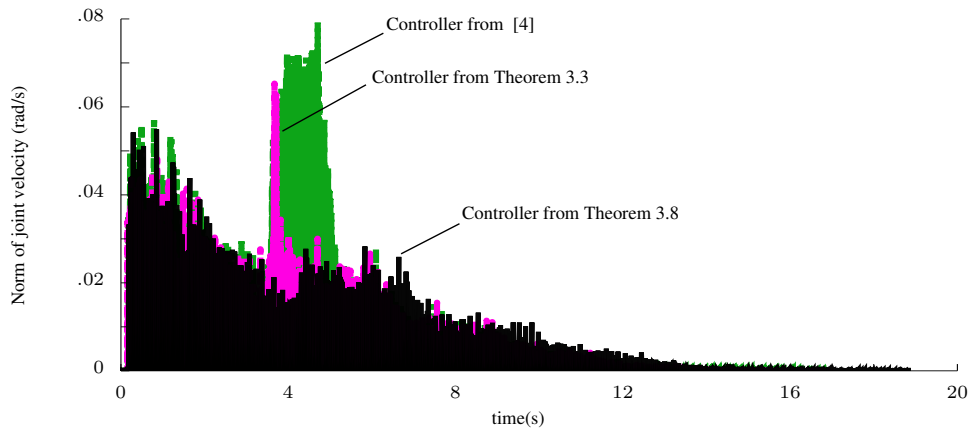


Figure 3.11: [Example 3.3] Joint velocity comparison.

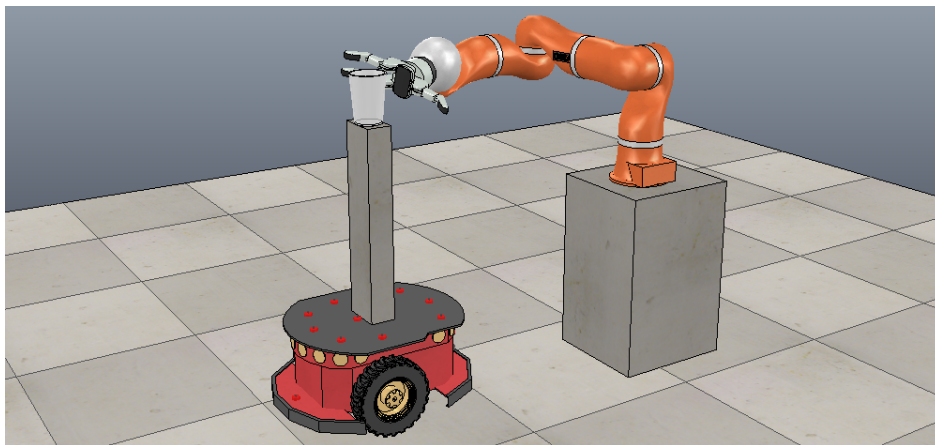


Figure 3.12: [Example 3.4] Screenshot from the simulated task (V-REP platform).

$\gamma_{\mathcal{T}}$	3.5	2.0	0.9	0.6	0.5	0.4	0.2
$\gamma_{\mathcal{T} sim}$	1.914	1.235	0.736	0.528	0.404	0.326	0.167
$\gamma_{\mathcal{O}}$	2	2	2	2	2	2	2
$\gamma_{\mathcal{O} sim}$	0.95	1.01	0.99	1.03	1.04	1.01	0.99

Table 3.2: [Example 3.4] Comparison between theoretical upper bound for the  $H_{\infty}$  performance  $(\gamma_{\mathcal{T}}, \gamma_{\mathcal{O}})$  with the numerically calculated noise-to-error attenuation from simulation  $(\gamma_{\mathcal{T} sim}, \gamma_{\mathcal{O} sim})$

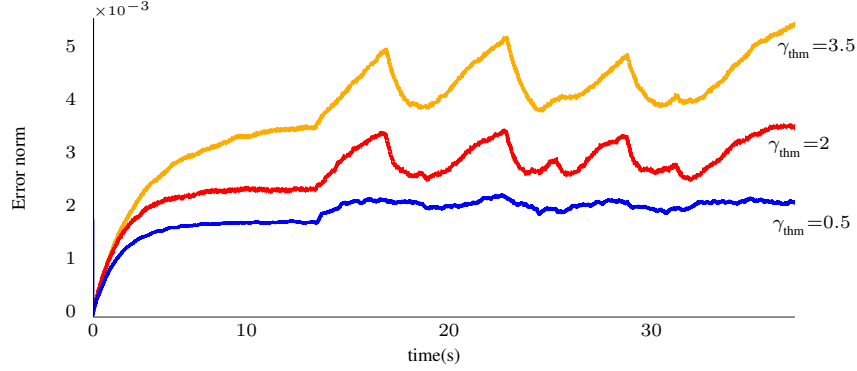


Figure 3.13: [Example 3.4] Control error from Theorem 3.7 for different values of the noise-to-error prescribed upper bound  $\gamma$ .

different values for  $\gamma_{\mathcal{T}}$  and  $\gamma_{\mathcal{O}} = 2$ . Table 3.2 summarizes the numerically computed noise to error attenuation  $(\gamma_{\mathcal{T} sim}$  and  $\gamma_{\mathcal{O} sim})$  compared to the theoretical values from Corollary 3.1  $(\gamma_{\mathcal{T}}$  and  $\gamma_{\mathcal{O}})$  which illustrates the effectiveness of the proposed strategy. It is also interesting to highlight that, due to their coupled behavior, the orientation performance varies slightly with changes in translational performance despite having the same theoretical upper bound value. The control results are also graphically depicted in Figure 3.13 that shows the relative pose error along time for  $\gamma_{\mathcal{T}} = \{0.5, 2, 3.5\}$  and  $\gamma_{\mathcal{O}} = 2$ . It is clear that, despite the uncertainties and disturbances, the proposed control criterion attenuates their influence and successfully holds the desired relative pose.

The proposed  $H_{\infty}$  dual quaternion based control strategy with (Corollary 3.1 with  $\gamma_{\mathcal{T}}=0.4$ ,  $\gamma_{\mathcal{O}}=1$ ) was also compared against the control results from [4] and Theorem 3.3. To maintain fairness, all controllers were set with similar control effort. Figure 3.14 illustrates the evolution of the error norm and highlights the advantages from the proposed criterion. The numerically calculated noise-to-error attenuation from the simulations were  $(\gamma_{\mathcal{T} sim}=0.61, \gamma_{\mathcal{O} sim}=0.87)$  and  $(\gamma_{\mathcal{T} sim}=0.63, \gamma_{\mathcal{O} sim}=0.86)$  for the controllers from [4] and Theorem 3.3 and  $(\gamma_{\mathcal{T} sim}=0.32, \gamma_{\mathcal{O} sim}=0.65)$  from Corollary 3.1.

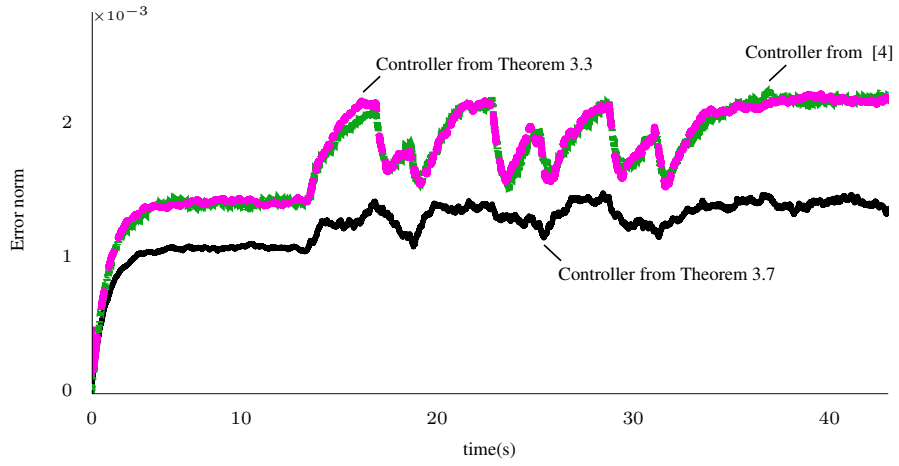


Figure 3.14: [Example 3.4] Pose error subjected to multiple disturbances.



# 4

## DUAL QUATERNION BASED OPTIMAL CONTROLLER FOR TRAJECTORY TRACKING OF ROBOT MANIPULATORS

---

*Bellman was a renowned mathematician with contributions in many, many areas. I learned two things from him. First, over the years I continue to marvel at the significance of the optimality principle in the form of the verification theorem, which I have used in many contexts. Second and more important, I learned that good theory is very practical – Pravin Varaiya*

The study of rigid body motion and kinematic control of robot manipulators is closely intertwined with the study of efficient representations for rigid body transformations. In preceding chapters, we have shown that unit dual quaternions presents itself as a suitable framework for simultaneously describing the attitude and position of the manipulator end-effector due to its efficiency, compactness, and lack of singularity. Motivated by dual quaternion algebra advantages for rigid body kinematics description, this chapter addresses the robot manipulator task-space design control problem using unit dual quaternion in the context of optimal control theory. Novel optimal task-space control criteria are proposed in order to find an optimal trajectory for the end-effector in dual quaternion space, providing a tool to balance more conveniently the end-effector error and its task-space velocity.

Applications of kinematic controllers branch from the stable proportional gain feedback to several sub-fields of study as, for instance, robustness to singularities and perturbations, workspace optimization, simultaneous execution of multiple tasks, and several forms of optimization [27, 75]. Particularly, in the light of dual quaternion algebra, there has been an increasing interest in works related to the design of kinematic controllers. Those works, summarized in Section 2.9, comprise rigid motion stabilization and tracking [52], multiple rigid body coordination [62], multiple arm manipulation [1], and human-robot interaction [78].

Nonetheless, results in dual quaternion literature aim mostly at stabilizing the trajectory of the rigid body, without much concern on control effort and optimality. For instance, although stable, the proportional gain controller [63] shows an intrinsic delay in the presence of time-varying trajectories. Adding a feedforward term with the proportional gain may eliminate the delay, but has the disadvantage of requiring a control effort that inevitably grows alongside the trajectory time derivative. In this context, optimal criteria allow the designer to choose a performance in an intermediate ground, with no phase shift and with optimal control effort.

Among optimal and robust control of robot manipulators, earlier works considered mostly the dynamic model of the robot, using a computed torque control, and optimization techniques to compensate for uncertainties in the system parameters. Particularly, considerable research effort has been dedicated to the robust control of robot manipulators [91]. For instance, [92] uses minimum variance control to find optimal controllers considering input constraints, with results applied to a two degree-of-freedom (DOF) planar manipulator. Similarly, [93] proposes an optimal solution based on linear quadratic regulator theory and computed torque to optimize the control performance under bounded uncertainties in the load and in the manipulator dynamics—therein, the uncertainties and nonlinearities are considered to be upper bounded and the solution tackles their previously known linear bounding information. The robust control of robot manipulators dynamics based on optimal control theory and computed torque is also studied in [91, 94]. A related work uses fuzzy

neural networks to approximately compute the optimal control [95] based on optimal control theory and using fuzzy controller to approximate and cancel the robot manipulator dynamics nonlinearities. Another approach uses a single network adaptive critic controller, resulting in a near optimal solution, which is tested using two DOF of a simulated WAM robotic manipulator [96]. The aforementioned fuzzy controllers are able to show approximate results even without much knowledge of the manipulator dynamics. On the other hand, fuzzy controllers have a large degree of arbitrariness in parameter selection. Furthermore, works using the computed torque technique optimize in the manipulator joint-space, usually, requiring an external tool to obtain the optimal inverse kinematics. The implementation complexity also reduces most examples to two DOF robots. Concerning trajectory generation, in [97], a linear-quadratic optimization is used to generate a trajectory that is followed using computed torque control. Using a different approach and with a different focus, the authors in [98] presented optimal results in the sense of convergence time based on the initial work from [99] on time-optimal control of manipulators. In this context, instead of optimizing the end-effector trajectory, the authors are interested in bringing the end-effector to a final location in minimum time with minimum control effort in joint-space based on the manipulator dynamics. The result is applied to a three degree planar manipulator. Similarly results can be found in the technical report [100]. Overall, existing results in robotics manipulators literature mostly concern in finding an efficient and practical trajectory smoothing algorithm with reduced control effort in joint-space, using the computed torque technique.

Nonetheless, when using optimal controllers, we generally seek to limit the manipulator trajectory velocities and accelerations which in turn justifies the use of kinematic controllers for stiff robotic manipulators. Moreover, as modern manipulator robots are often equipped with low level controllers at joint level, task-space techniques have the advantage of defining the control law directly at the end-effector workspace, making direct use of the available low level controllers instead of redesigning them or requiring an external IK planner.

In this context and motivated by the problem of optimizing the task-space control trajectory and velocity, herein, we take interest at optimization-based kinematic controllers at the task-space of general serial-link manipulator. The optimization-based controller extends the results from dual quaternion based controllers—sharing the inherent representation advantages—and provides the designer with a more intuitive set of performance indexes and extends the range of applications of the dual quaternion formalism in robotics. In contrast to standard optimal control techniques for manipulators, this chapter focuses in optimizing task-space variables which greatly simplifies the control implementation. As a consequence, instead of optimizing the joint-space velocity, we aim at obtaining an optimal result for the end-effector velocity at task-space. The analysis is particularly relevant in advanced manipulation tasks—for instance, manipulation in hazardous or unstructured environments, and multi-arm manipulation—that require precise and safe interaction in contrast to convergence speed. In the view of human-robot interaction, the speed of the end-effector largely influences the human acceptance of the contact [101]. Indeed, even if the robotic system is able to prevent undesired injuries, a human is likely to be in a state of constant stress and discomfort [102]. A controlled speed at task-space also prevents drifts and overshoots caused by large accelerations requirements at the low level controllers.

In this chapter, we derive two distinguish optimal control criteria based on unit dual quaternions representation and on the two results for the task-space differential kinematics of the robotic manipulator described in Section 2.7.

The first technique is based on the dual quaternion error mapping to an  $\mathbb{R}^8$  manifold. By defining the control law in the Euclidean manifold, the closed-loop system can be reduced to an affine time-varying system with respect to the dual quaternion transformation invariant error. This allows us to obtain a recursive expression for the optimal controller using linear quadratic regulator (LQR) theory. By modeling a continuous trajectory as

the perturbation of the error, the proposed dual quaternion LQR can be used as a trajectory tracking controller, while also considering other modeled error disturbances. On the other hand, the controller lacks an explicit geometric significance for the transformations at task-space which in turn renders an addition complexity for parameters and matrices gains selection.

In the second part of this chapter, we derive an optimal criterion based on the differential kinematics description in (2.42)-(2.48) and the dual quaternion Jacobian  $\underline{\mathbf{J}}_{\underline{\mathbf{q}}}$ . Using the linear transformation between inputs of joint velocities and the vector space isomorphic to the range space of the end-effector twist, we provide a tool to optimize the dual quaternion error exponential convergence rate at its tangent space with respect to the controlled twist upon the end-effector.

In contrast to the first optimal strategy, the criterion has a direct geometric significance which enlarges its applicability, improves parameters significance and, in turn, eases the process of parameter selection. On the hand, due to highly and complex nonlinearities within the differential coupled kinematics in dual quaternion space, there is a significant increase in analysis complexity.

Lastly, to illustrate the validity, the efficiency and the reliability from the proposed dual quaternion optimal criteria, we present a set of numerical examples and simulations in different scenarios and with different control specifications and conditions. Moreover, the proposed controllers are also evaluated using a real robot platform: an anthropomorphic Meka Robotics A2 Arm compliant manipulator.<sup>1</sup>

## 4.1 OPTIMAL DUAL QUATERNION BASED CONTROLLER IN $\mathbb{R}^8$ MANIFOLD

This section presents a novel control strategy based on the dual quaternion mapping to  $\mathbb{R}^8$  manifold in the context of optimal control theory. Reviewing the kinematics equations from Section 2.7 and using the vector space isomorphism mapping, we show that the differential kinematic closed-loop system with a time-varying reference from the point of view of error can be reduced to a linear time-varying system with an additive perturbation term. Hence, linear quadratic regulator theory can be exploited to derive a optimal solution to the control problem.

First, consider an arbitrary continuous desired trajectory  $\underline{\mathbf{x}}_d \triangleq \underline{\mathbf{x}}_d(t)$  in dual quaternion space and the current end-effector pose  $\underline{\mathbf{x}}$ . Similarly to Section 3.1, we define the spatial difference in  $\text{Spin}(3) \times \mathbb{R}^3$  between the current and desired end-effector configuration:

$$\underline{\mathbf{x}}_e = \underline{\mathbf{x}}^* \underline{\mathbf{x}}_d = \mathbf{r}_e + \varepsilon \frac{1}{2} \mathbf{p}_e \mathbf{r}_e, \quad (4.1)$$

where  $\mathbf{r}_e$  denote the orientation error in  $\text{Spin}(3)$  and  $\mathbf{p}_e$  the position error in  $\mathbb{H}_0$ . From the spatial difference, we also define an invariant dual quaternion error function of the form  $\underline{\mathbf{e}} : \text{Spin}(3) \times \mathbb{R}^3 \mapsto \mathbb{H} \otimes \mathbb{D}$ , given by

$$\underline{\mathbf{e}} = 1 - \underline{\mathbf{x}}_e = \mathbf{e} + \varepsilon \mathbf{e}'. \quad (4.2)$$

In this sense, when  $\underline{\mathbf{x}}$  converges to  $\underline{\mathbf{x}}_d$ , the dual quaternion error function  $\underline{\mathbf{e}} \rightarrow 0$ . Analogously, to stabilize  $\underline{\mathbf{e}}$  to 0 yields the end-effector convergence to the desired pose. It is interesting to highlight that the error

---

<sup>1</sup>It is important to underline that the work described in the first part of this chapter was developed in collaboration with Murilo Marques Marinho, a PhD student from the University of Tokyo.

definition is invariant with respect to coordinate changes with regard to arbitrary right shifts—further details on the invariance for unit dual quaternions are discussed in Section 3.1.

Since the optimization computation assumes future knowledge of the explicit variables, we need to remove any direct dependency on  $\underline{x}$ . Hence,

$$\underline{e} = 1 - \underline{x}^* \underline{x}_d \implies \underline{e} \underline{x}_d^* = \underline{x}_d^* - \underline{x}^* \implies \underline{x}^* = \underline{x}_d^* - \underline{e} \underline{x}_d^*.$$

With time-varying  $\underline{x}$  and  $\underline{x}_d$ , the derivative of (4.2) is given by  $\dot{\underline{e}} = -\dot{\underline{x}}^* \underline{x}_d - \underline{x}^* \dot{\underline{x}}_d$ . Therefore

$$\dot{\underline{e}} = -\dot{\underline{x}}^* \underline{x}_d - (\underline{x}_d^* - \underline{e} \underline{x}_d^*) \dot{\underline{x}}_d = -\dot{\underline{x}}^* \underline{x}_d + \underline{e} \underline{x}_d^* \dot{\underline{x}}_d - \underline{x}_d^* \dot{\underline{x}}_d.$$

Using the vector space mapping from (2.14),  $\text{vec}_8$ , on both sides and defining  $e \triangleq \text{vec}_8 \underline{e}$  yields

$$\dot{e} = -\bar{H}(\underline{x}_d) C_8 \text{vec}_8 \dot{\underline{x}} + \bar{H}(\underline{x}_d^* \dot{\underline{x}}_d) e - \text{vec}_8(\underline{x}_d^* \dot{\underline{x}}_d).$$

The dual quaternion differential kinematics of the end-effector mapped to the  $\mathbb{R}^8$  manifold,  $\text{vec}_8 \dot{\underline{x}}$ , can be derived as in Subsection 2.7.2 using the dual quaternion based Jacobian  $J_{\text{vec}}$  described in (2.38)-(2.41). Hence, the dual quaternion error mapped in  $\mathbb{R}^8$  can be rewritten as

$$\dot{e} = -\bar{H}(\underline{x}_d) C_8 J_{\text{vec}} \dot{\theta} + A e + c,$$

where  $\theta = [\theta_0 \dots \theta_{n-1}]^T$  is the measured vector of joint variables,  $A \triangleq \bar{H}(\underline{x}_d^* \dot{\underline{x}}_d)$ ,  $c \triangleq -\text{vec}_8(\underline{x}_d^* \dot{\underline{x}}_d)$ , and  $C_8 \triangleq \text{diag}(1, -1, -1, -1, 1, -1, -1, -1)$ . Finally, setting  $N \triangleq \bar{H}(\underline{x}_d) C_8 J_{\text{vec}}$ , we have

$$\dot{e} = A e - N \dot{\theta} + c. \quad (4.3)$$

Instead of considering  $\dot{\theta}$  as the input control signal for the system, we investigate and minimize the end effector velocity  $u$  using the mapping  $u = -N \dot{\theta}$ . This allows the optimization to be done in task-space variables. Hence, we focus on finding the optimal controller for the affine time-varying system

$$\dot{e}(t) = A(t)e(t) + u(t) + c(t). \quad (4.4)$$

Therefore, from the error point-of-view, we can solve the tracking problem for a continuous trajectory using a finite horizon LQR applied to a disturbed system, as the error disturbance caused by the time-varying trajectory is given by  $c(t)$ . Other modeled continuous disturbances can also be grouped into  $c(t)$  and used in the same solution.

To solve a given task trajectory described in time  $t \in [0, t_f]$  at the the manipulator reachable space, we aim at minimizing the following cost function

$$F = \frac{1}{2} e(t_f)^T S e(t_f) + \frac{1}{2} \int_{t_0}^{t_f} (e^T Q e + u^T R u) dt, \quad (4.5)$$

given the gain matrices  $S \geq 0$ ,  $Q(t) \geq 0$  and  $R(t) > 0$  with  $S, Q, R \in \mathbb{R}^{8 \times 8}$ .

The matrix  $S$  is the weight of the final error norm, while the time-varying matrices  $Q$  and  $R$  respectively weigh the error cost along the trajectory and the control effort in terms of end-effector velocity norm. The constrained optimization of (4.5) leads to an optimal feedback without excessive expenditure of control energy while keeping the error  $e(t)$  near zero [103].

For a continuously differentiable optimal trajectory  $\mathbf{x}_{opt}(t) = (\mathbf{e}_{opt}(t), \mathbf{u}_{opt}(t))$  along the constraint surface

$$G(t) = \mathbf{A}(t)\mathbf{e}(t) + \mathbf{u}(t) + \mathbf{c}(t) - \dot{\mathbf{e}}(t) = 0 \quad (4.6)$$

a necessary and sufficient condition for the global minimum is given by  $\partial F/\partial \mathbf{u} = 0$  and  $\partial F/\partial \mathbf{e} = 0$  as  $F$  is convex. From the optimal trajectory, we also find that the gradient of  $F$ , that is  $\nabla F$ , is perpendicular to constrained surface (4.6), that is, there must be no component of  $\nabla F$  parallel to  $G$  at an optimal point—otherwise, we could move away from  $\mathbf{x}_{opt}$  and down the gradient of  $F$  while remaining on (4.6), contrary to the assumption that  $\mathbf{x}_{opt}$  is a minimum [104, 105]. In this sense, to constrain the optimization to a feasible trajectory, we define the augmented cost function

$$H = F + \int_{t_0}^{t_f} \mathbf{p}^T (\mathbf{A}\mathbf{e} + \mathbf{u} + \mathbf{c} - \dot{\mathbf{e}}) dt, \quad (4.7)$$

where  $\mathbf{p}$  is the Lagrange multiplier for the state equations. Since  $\nabla G$  defines the normal vector to  $G$ , the constrained trajectory is satisfied if  $\nabla F$  is collinear to  $\nabla G$ , that is,  $\nabla F + \mathbf{p}^T \nabla G = 0$ , where  $\mathbf{p}$  defines the magnitude difference.

Hence, according to [105, 106], we have  $\partial H/\partial \mathbf{u} = 0$  and  $\partial H/\partial \mathbf{e} = 0$  as necessary and sufficient conditions for the optimal trajectory,

$$\frac{\partial H}{\partial \mathbf{u}} = 0 \implies \mathbf{u} = -\mathbf{R}^{-1} \mathbf{p}. \quad (4.8)$$

In addition, we use the Leibniz integral rule in (4.7), that is,

$$-\int_{t_0}^{t_f} \mathbf{p}^T \dot{\mathbf{e}} dt = \mathbf{p}^T(t_0)\mathbf{e}(t_0) - \mathbf{p}^T(t_f)\mathbf{e}(t_f) + \int_{t_0}^{t_f} \dot{\mathbf{p}}^T \mathbf{e} dt,$$

to find  $\frac{\partial H}{\partial \mathbf{e}} = 0$ , which in turn implies

$$\dot{\mathbf{p}} = -(\mathbf{Q}\mathbf{e} + \mathbf{A}^T \mathbf{p}). \quad (4.9)$$

Please note that  $\partial^2 H/\partial \mathbf{u}^2$  must be positive to minimize (4.7), which requires  $\mathbf{R} > 0$ . The system and proposed cost function allow the use of the costate function [106]

$$\mathbf{p}(t) = \mathbf{P}\mathbf{e} + \boldsymbol{\xi}, \quad (4.10)$$

where  $\mathbf{P}$  is a time-varying proportional gain and  $\boldsymbol{\xi}$  is a weighted feedforward term. The derivative of (4.10) yields

$$\dot{\mathbf{p}}(t) = \dot{\mathbf{P}}\mathbf{e} + \mathbf{P}\dot{\mathbf{e}} + \dot{\boldsymbol{\xi}}. \quad (4.11)$$

After using (4.10) in (4.8) and substituting the result in (4.4), and using (4.10) in (4.9), we replace the resulting equations in (4.11) to find

$$-\dot{\boldsymbol{\xi}} - \mathbf{A}^T \boldsymbol{\xi} + \mathbf{P}\mathbf{R}^{-1} \boldsymbol{\xi} - \mathbf{P}\mathbf{c} = (\dot{\mathbf{P}} + \mathbf{P}\mathbf{A} + \mathbf{A}^T \mathbf{P} - \mathbf{P}\mathbf{R}^{-1} \mathbf{P} + \mathbf{Q}) \mathbf{e}. \quad (4.12)$$

Considering that (4.12) must hold for any choice of initial state  $\mathbf{e}$  and that both  $\mathbf{P}$  and  $\boldsymbol{\xi}$  do not depend on the initial error, we need simultaneously

$$\begin{cases} \dot{\mathbf{P}} + \mathbf{P}\mathbf{A} + \mathbf{A}^T \mathbf{P} - \mathbf{P}\mathbf{R}^{-1} \mathbf{P} + \mathbf{Q} & = \mathbf{0} \\ \dot{\boldsymbol{\xi}} + \mathbf{A}^T \boldsymbol{\xi} - \mathbf{P}\mathbf{R}^{-1} \boldsymbol{\xi} + \mathbf{P}\mathbf{c} & = \mathbf{0}, \end{cases}$$

which means

$$\begin{cases} \dot{\mathbf{P}} &= -\mathbf{P}\mathbf{A} - \mathbf{A}^T\mathbf{P} + \mathbf{P}\mathbf{R}^{-1}\mathbf{P} - \mathbf{Q} \\ \dot{\boldsymbol{\xi}} &= -\mathbf{A}^T\boldsymbol{\xi} + \mathbf{P}\mathbf{R}^{-1}\boldsymbol{\xi} - \mathbf{P}\mathbf{c}. \end{cases} \quad (4.13)$$

The boundary conditions to solve (4.13) are obtained using the final time,  $t_f$ , of our trajectory. We set the feed-forward term to zero in the terminal time—that is,  $\boldsymbol{\xi}(t_f) = 0$ —to find the first boundary condition. From (4.10) with  $\boldsymbol{\xi}(t_f) = 0$ , we find that  $\partial H/\partial e(t_f) = 0$  yields  $\mathbf{P}(t_f) = \mathbf{S}$ .

Note that we know  $\mathbf{A}(t) = \bar{\mathbf{H}} \left( \underline{\mathbf{h}}_d^* \dot{\underline{\mathbf{h}}}_d \right)$  for all  $t$ , as it depends only on the desired trajectory. We can then numerically solve the differential Riccati equation  $\mathbf{P}(t)$  backwards in time. As  $\mathbf{c} = -\underline{\mathbf{h}}_d^* \dot{\underline{\mathbf{h}}}_d$  is also known for all  $t$  and, with the solution of  $\mathbf{P}(t)$ , we can find  $\boldsymbol{\xi}(t)$  by also solving it backwards in time.

Therefore, from (4.8) and (4.10) the optimal control is given by  $\mathbf{u}(t) = -\mathbf{R}^{-1}(\mathbf{P}\mathbf{e} + \boldsymbol{\xi})$ . Applying as joint velocities, we find  $\dot{\boldsymbol{\theta}} = \mathbf{N}^+\mathbf{R}^{-1}(\mathbf{P}\mathbf{e} + \boldsymbol{\xi})$ . Summarizing the control results, we can state the following dual quaternion based optimal control theorem.

**Theorem 4.1** Dual quaternion based optimal quadratic controller in  $\mathbb{R}^8$  manifold

For prescribed gain matrices  $\mathbf{S}, \mathbf{Q}, \mathbf{R}$  satisfying  $\mathbf{S} \geq 0$ ,  $\mathbf{Q}(t) \geq 0$  and  $\mathbf{R}(t) > 0$ , the closed loop system (4.3) with the differential kinematic controller

$$\dot{\boldsymbol{\theta}} = \mathbf{N}^+\mathbf{R}^{-1}(\mathbf{P}\mathbf{e} + \boldsymbol{\xi}), \quad (4.14)$$

where  $\mathbf{P}$  and  $\boldsymbol{\xi}$  are derived from (4.13), defines the dynamic system that minimizes the quadratic cost function (4.5). In other words, the optimal controller (4.14) defines the optimal trajectory along (4.3) for the cost function (4.5).

*Remark 4.1.* It is important to highlight that the substitution from  $\mathbf{u} = -\mathbf{N}\dot{\boldsymbol{\theta}}$  in (4.3) results in fact

$$\dot{e}(t) = \mathbf{A}(t)e(t) + \mathbf{N}\mathbf{N}^+\mathbf{u}(t) + \mathbf{c}(t).$$

To simplify the optimal control problem, and as a first solution to such problem, we supposed in this section that the resulting control signal  $\mathbf{u}(t)$  is always defined in the range space of the current transformation  $\mathbf{N}$ . Hence, using the pseudoinverse of  $\mathbf{N}$  yields (4.4) and the optimal controller follows as described.

Nonetheless, note that  $\mathbf{N}\mathbf{N}^+ \neq \mathbf{I} \forall \boldsymbol{\theta}, \underline{\mathbf{x}}_d$ . Hence, in more realistic scenarios, we cannot assume that  $\mathbf{u}(t)$  will always be defined in  $\mathbf{N}$ 's range space. In this sense, we can separate  $\mathbf{N}\mathbf{N}^+$  into its matched and unmatched components, which in turn results in

$$\dot{e}(t) = \mathbf{A}(t)e(t) + \mathbf{I}\mathbf{u}(t) + (\mathbf{N}\mathbf{N}^+ - \mathbf{I})\mathbf{u}(t) + \mathbf{c}(t). \quad (4.15)$$

Applying the dual quaternion optimal control procedures from Theorem 4.1 in the exact system defined by (4.15) would require future knowledge of  $\mathbf{N}\mathbf{N}^+$ , which violates causality. Therefore, we can assume the effects of  $(\mathbf{N}\mathbf{N}^+ - \mathbf{I})\mathbf{u}(t)$  as a disturbance upon the optimal trajectory. In this sense, explicitly considering the influence of  $(\mathbf{N}\mathbf{N}^+ - \mathbf{I})\mathbf{u}(t)$  reduces Theorem 4.1 to a suboptimal criterion. In practical applications, nevertheless, we suppose the effects of  $(\mathbf{N}\mathbf{N}^+ - \mathbf{I})\mathbf{u}(t)$  do not greatly disturb the system as illustrated in Sections 4.4 and 4.5. The effectiveness of the suboptimal controller motivates the study of the optimal control result explicitly defined in dual quaternion space derived in next section that is designed to escape such topology issue.

## 4.2 OPTIMAL QUADRATIC CONTROLLER IN DUAL QUATERNION SPACE

The solution proposed in the previous section relies on the dual quaternion error mapping to an  $\mathbb{R}^8$  manifold which in turn simplifies the problem to an affine time-varying system. The simplification that arises from the described error mapping renders a more practical approach for solving problems based on control algorithms belonging to optimal control family. Indeed, using linear quadratic regulator theory, Section 4.1 introduced a novel criterion that albeit being suboptimal—when  $\mathbf{u}(t)$  isn't defined in  $N$ 's range space—can successfully be used to real life problems as shown in Section 4.5. The control result, on the other hand, contrasts with the mathematical rigor from previous chapters where we focus on finding an adequate, accurate, and stable representation for the manipulator kinematics, for the controller and for the closed loop system in dual quaternion space.

In this sense and motivated by the effectiveness of the controller from Theorem 4.1—as shown in Sections 4.4 and 4.5—this section proposes a novel framework for robot manipulators kinematic control tracking by deriving an optimal control law explicitly in dual quaternion tangent space. The controller concept stems from the control structure proposed in Section 3.3 where the controller is defined in dual quaternion space, particularly, in the Lie algebra of  $\text{Spin}(3) \times \mathbb{R}^3$ . Hence, it yields an explicitly geometric significance for the controller at the same time that it provides a well-defined map between the range space of the dual quaternion error dynamics to the space where the actuation takes place. As stressed in Section 3.3, this framework provides an elegant and intuitive understanding on the performance influence over the end-effector trajectory. The formalism yields an optimal controller ease to implement and suitable for practical applications with a detailed and proper analysis on stability. The main challenge stems from the highly and complex nonlinearities within the differential coupled kinematics in the end-effector dual quaternion space.

Considering the spatial difference in  $\text{Spin}(3) \times \mathbb{R}^3$  between the current and desired end-effector pose to be defined as

$$\begin{aligned}\mathbf{x}_e &= \mathbf{x}\mathbf{x}_d^* \\ &= \mathbf{r}_e + \frac{1}{2}\varepsilon(\mathbf{p}_e\mathbf{r}_e),\end{aligned}$$

with a time-varying reference trajectory, that is, a tracking system, then the spatial difference kinematics is given by

$$\dot{\mathbf{x}}_e = \dot{\mathbf{x}}\mathbf{x}_d^* + \mathbf{x}\dot{\mathbf{x}}_d^*$$

where the end-effector differential kinematics is defined in (2.48) and the desired end-effector trajectory over time is described by the first order kinematic equation of a rigid body (2.26),

$$\dot{\mathbf{x}}_d = \frac{1}{2}\boldsymbol{\omega}_d\mathbf{x}_d, \quad (4.16)$$

with  $\boldsymbol{\omega}_d$  being the twist of the desired pose in inertial frame. Replacing (2.48) and (4.16) in the spatial difference kinematics yields

$$\dot{\mathbf{x}}_e = \frac{1}{2}\text{vec}_6(\mathbf{J}_{\underline{\boldsymbol{\omega}}}\dot{\boldsymbol{\theta}})\mathbf{x}_e - \frac{1}{2}\mathbf{x}_e\boldsymbol{\omega}_d, \quad (4.17)$$

where  $\boldsymbol{\theta} = [\theta_0 \dots \theta_{n-1}]^T$  is the measured vector of joint variables and  $\mathbf{J}_{\underline{\boldsymbol{\omega}}} = [\text{vec } \underline{\mathbf{j}}_0 \dots \text{vec } \underline{\mathbf{j}}_{n-1}]$  is an analytical Jacobian from Algorithm (2.2). From the isomorphism mapping (2.12), we can find solutions in the real space for  $\dot{\boldsymbol{\theta}}$  such that differential equation (4.17) is well-posed [89, Prop. 2.1] as  $\text{vec}(\mathbf{J}_{\underline{\boldsymbol{\omega}}}\dot{\boldsymbol{\theta}}) \in \mathbb{H}_0 \otimes \mathbb{D}$  lies in the Lie algebra of  $\text{Spin}(3) \times \mathbb{R}^3$ .

The complexity and nonlinearities inherent from (4.17) justifies the gap between existing stability results for unit dual quaternions and the optimal control theory. Indeed, there are no results for optimal control in the literature explicitly defined within the non-Euclidean space of unit dual quaternions. In fact, even for the case of pure rotations defined using unit quaternions, most results are based on a local linearization of the quaternion elements [107].

To address such nonlinearities, we exploit the exponentially stable controller derived in Section 3.3. Hence, to solve the optimal problem, let us first assume a dual quaternion based task-space controller with joint velocity vector inputs of the form

$$\dot{\theta} = \underline{J}_{\omega}^+ [\mathbf{u}_c + \text{vec}_6(\underline{\mathbf{x}}_e \underline{\boldsymbol{\omega}}_d \underline{\mathbf{x}}_e^*)], \quad (4.18)$$

where

$$\mathbf{u}_c = \left[ \mathbf{K}_O \text{vec}_3^T(\text{Im}(\mathbf{r}_e)) \quad \frac{1}{2} \mathbf{K}_{\tau} \text{vec}_3^T(\mathbf{p}_e) \right]^T, \quad (4.19)$$

and  $\underline{J}_{\omega}^+$  is the pseudoinverse of  $\underline{J}_{\omega}$ ,  $\mathbf{K}_O$  and  $\mathbf{K}_{\tau}$  are real valued  $3 \times 3$  matrices, and the transformation  $\text{vec}_3 : \mathbb{H}_0 \rightarrow \mathbb{R}^3$  defines the isomorphism mapping from  $\mathbb{H}_0$  and  $\mathbb{R}^3$  as described in (2.4). Also, note that if  $\underline{J}_{\omega}$  is well defined, then the solution is always in the range space of  $\underline{J}_{\omega}$ . Hence, from (4.18), the closed-loop spatial difference kinematics yields

$$\dot{\underline{\mathbf{x}}}_e = \frac{1}{2} \text{vec}_6(\mathbf{u}_c) \underline{\mathbf{x}}_e.$$

From the spatial difference, we also define an invariant dual quaternion error function of the form  $\underline{e} : \text{Spin}(3) \times \mathbb{R}^3 \mapsto \mathbb{H} \otimes \mathbb{D}$ , given by

$$\underline{e} = 1 - \underline{\mathbf{x}}_e = \mathbf{e} + \varepsilon \mathbf{e}'. \quad (4.20)$$

Hence,  $\underline{\mathbf{x}}$  converges to  $\underline{\mathbf{x}}_d$  if and only if the dual quaternion error function  $\underline{e} \rightarrow 0$ .

#### Theorem 4.2 Dual quaternion exponentially stable controller

The closed-loop system (4.17) with dual quaternion task-space controller (4.18)-(4.19) achieves exponential stability with negative definite matrices  $\mathbf{K}_O$  and  $\mathbf{K}_{\tau}$ . Moreover the convergence decay is defined by

$$\begin{aligned} \frac{d}{dt} \|\text{vec}_3 \{\text{Im}(\mathbf{r}_e)\}\|^2 &\leq \text{vec}_3^T \{\text{Im}(\mathbf{r}_e)\} \mathbf{K}_O \text{vec}_3 \{\text{Im}(\mathbf{r}_e)\}, \\ \frac{d}{dt} \|\text{vec}_3 \{\mathbf{p}_e\}\|^2 &\leq \text{vec}_3^T \{\mathbf{p}_e\} \mathbf{K}_{\tau} \text{vec}_3 \{\mathbf{p}_e\}. \end{aligned} \quad (4.21)$$

*proof.*

The end-effector spatial differential kinematics (4.17) with dual quaternion task-space controller (4.18)-(4.19) yields the closed-loop spatial difference kinematics:

$$\dot{\underline{\mathbf{x}}}_e = \frac{1}{2} \text{vec}_6(\underline{J}_{\omega} \tilde{\theta}) \underline{\mathbf{x}}_e,$$

where  $\tilde{\theta} = \underline{J}_{\omega}^+ \left[ \mathbf{K}_O \text{vec}_3^T(\text{Im}(\mathbf{r}_e)) \quad \frac{1}{2} \mathbf{K}_{\tau} \text{vec}_3^T(\mathbf{p}_e) \right]^T$ . To study the stability of closed loop system, let us regard the Lyapunov candidate function proposed in (3.48), with the error function defined in (4.20), that is,

$$V(t, \underline{e}) = \|\underline{e}(t)\| = \alpha_1 \|e(t)\|_2^2 + \alpha_2 \|e'(t)\|_2^2,$$

with given positive scalars  $\alpha_1$  and  $\alpha_2$ . Taking the time-derivative along the trajectory (4.17)-(4.20) as



described in Appendix C.1 for  $\mathcal{O}(\underline{e}) \triangleq 1 - \mathbf{r}_e$ , and  $\mathcal{T}(\underline{e}) \triangleq \mathbf{p}_e$ , it turns out that

$$\begin{aligned} \dot{V}(t, \underline{e}) &\leq \frac{\alpha_1 \sigma_m\{\mathbf{K}_\mathcal{O}\}}{2} \|\mathbf{e}(t)\|_2^2 + 2\alpha_2 \sigma_m\{\frac{1}{2}\mathbf{K}_\mathcal{T}\} \|\mathbf{e}'(t)\|_2^2 \\ &\leq \max\left\{\frac{\sigma_m\{\mathbf{K}_\mathcal{O}\}}{2}, \sigma_m\{\mathbf{K}_\mathcal{T}\}\right\} V(t, \underline{e}) \leq 0. \end{aligned} \quad (4.22)$$

where  $\sigma_m\{\mathbf{K}_\mathcal{O}\}$  and  $\sigma_m\{\mathbf{K}_\mathcal{T}\}$  denote the minimum singular value from  $\mathbf{K}_\mathcal{O}$ ,  $\mathbf{K}_\mathcal{T}$ , respectively. By the Comparison Lemma [72, pg. 85], and considering negative definite matrices  $\mathbf{K}_\mathcal{O}$  and  $\mathbf{K}_\mathcal{T}$ , the closed-loop system (4.17) with dual quaternion task-space controller (4.18)-(4.19) is exponentially stable. Moreover, after some manipulation, we find that

$$\begin{aligned} \frac{d}{dt} \|\text{vec}_3\{\text{Im}(\mathbf{r}_e)\}\|_2^2 &\leq \text{vec}_3^T\{\text{Im}(\mathbf{r}_e)\} \mathbf{K}_\mathcal{O} \text{vec}_3\{\text{Im}(\mathbf{r}_e)\}, \\ \frac{d}{dt} \|\text{vec}_3\{\mathbf{p}_e\}\|_2^2 &\leq \text{vec}_3^T\{\mathbf{p}_e\} \mathbf{K}_\mathcal{T} \text{vec}_3\{\mathbf{p}_e\}. \end{aligned}$$

□

*Remark 4.2.* Note that there is no unique natural metric for  $\text{Spin}(3) \times \mathbb{R}^3$ , similarly to the case for  $SE(3)$ . The proposed bilinear form defined in the Lyapunov function from Theorem 4.2 exploits the natural metric for  $\mathbb{H}$  which yields control actions along the geodesic directions for both orientation and translational errors.

In this sense, the proposed dual quaternion task-space controller (4.18)-(4.19) yields an exponential convergence within the Lie algebra of the group. For being a Lie group, the Lie algebra of  $\text{Spin}(3) \times \mathbb{R}^3$  also defines the tangent space of the unit dual quaternion manifold, which is a differentiable Riemannian manifold. Therefore, the obtained exponential convergence can be defined in the real vector space  $\mathbb{R}^6$  corresponding to the unit dual quaternion tangent space. The inner product of the dual quaternion error on the tangent space at each point that varies smoothly from point to point, and from (4.21), the dynamics of the smooth variation can be described in the real vector space  $\mathbb{R}^6$  as

$$\dot{\mathbf{e}} = \text{diag}(\mathbf{K}_\mathcal{O}, \mathbf{K}_\mathcal{T}) \mathbf{e}, \quad (4.23)$$

where  $\mathbf{e} = \left[ \text{vec}_3^T\{\text{Im}(\mathbf{r}_e)\} \quad \text{vec}_3^T\{\mathbf{p}_e\} \right]^T$ .

In this sense, instead of directly addressing the complex nonlinearities inherent from (4.17), we exploit the exponentially stable controller from Theorem 4.2 in order to optimize the exponential gains  $\mathbf{K}_\mathcal{O}$ ,  $\mathbf{K}_\mathcal{T}$  within the Lie algebra of unit dual quaternions. The optimization of the exponential gains is performed at the tangent space of the dual quaternion task-space, which in turn is mapped to the geodesic direction for rotation and translation—since the proposed bilinear form from the Lyapunov function of Theorem 4.2 exploits the natural metric for  $\mathbb{H}$  which yields control actions along the geodesic directions for both orientation and translational errors.<sup>2</sup>

The optimal control policy is therefore based on the aforementioned mapping and provides a tool to optimize the task trajectory error at the tangent space of the unit dual quaternion space and the controlled twist upon the end-effector. To explicit the control output vector that we seek to optimize, consider the error dynamics in the tangent space to be described as

$$\dot{\mathbf{e}} = \mathbf{u}, \quad (4.24)$$

<sup>2</sup>As previously stressed, there is no geodesic direction for  $SE(3)$  nor for any of its cover spaces

where  $\mathbf{u}$  must satisfy the following constraint

$$\mathbf{u} = \text{diag}(\mathbf{K}_\sigma, \mathbf{K}_\tau) \mathbf{e}. \quad (4.25)$$

Note that using the error dynamics in the unit dual quaternion tangent space, we are actually studying the convergence of a vector space which has the desired properties for optimal control analysis. The optimal exponential controller can therefore be extracted from the following cost function

$$F = \frac{1}{2} \mathbf{e}^T(t_f) \mathbf{S} \mathbf{e}(t_f) + \frac{1}{2} \int_{t_0}^{t_f} (\mathbf{e}^T(\tau) \mathbf{Q} \mathbf{e}(\tau) + \mathbf{u}^T(\tau) \mathbf{R} \mathbf{u}(\tau)) d\tau \quad (4.26)$$

where  $\mathbf{S}$ ,  $\mathbf{Q}$ ,  $\mathbf{R}$  are gain matrices defined in  $\mathbb{R}^{6 \times 6}$  satisfying  $\mathbf{S} \geq 0$ ,  $\mathbf{Q}(t) \geq 0$  and  $\mathbf{R}(t) > 0$ . The matrix  $\mathbf{S}$  is the weight of the final error norm, the time-varying matrix  $\mathbf{Q}$  weighs the error cost along the trajectory, and the time-varying matrix  $\mathbf{R}$  weighs the control effort in terms of end-effector velocity norm. As long as  $\underline{\mathbf{J}}_{\underline{\mathbf{u}}}$  is well conditioned, an increase in  $\mathbf{R}$  will lead to an overall decrease in joint velocities. The optimization of (4.26) leads to an optimal feedback in unit dual quaternion tangent space without excessive expenditure of control energy while optimizing the the exponential convergence of the dual quaternion error function.

To solve the optimization problem, we introduce the costate variable  $p$ , which acts as a Lagrange multiplier for the state equations. Hence, using the equality constraint defined in (4.24), the function (4.26) can be rewritten as

$$H = F + \int_{t_0}^{t_f} \mathbf{p}^T (\mathbf{u} - \dot{\mathbf{e}}) dt. \quad (4.27)$$

According to [106] and to distribution theory applied to optimality conditions, we have  $\partial H / \partial \mathbf{u} = 0$  and  $\partial H / \partial \mathbf{e} = 0$  as necessary conditions for the optimal trajectory. Hence,

$$\begin{aligned} \frac{\partial H}{\partial \mathbf{u}} = 0 &\implies \mathbf{R} \mathbf{u} + \mathbf{p} = 0 \\ &\implies \mathbf{u} = -\mathbf{R}^{-1} \mathbf{p}. \end{aligned} \quad (4.28)$$

In order to satisfy (4.25) as to obtain a error dynamics described in (4.23), we propose a costate function [106] of the form

$$\mathbf{p}(t) = \mathbf{P}(t) \mathbf{e}(t), \quad (4.29)$$

where  $\mathbf{P}$  is a time-varying proportional gain. To fully satisfy the constraint (4.25), we still need to consider  $\mathbf{R}$  and  $\mathbf{P}$  as block diagonal matrices, that is,

$$\mathbf{R} = \text{diag}(\mathbf{R}_1 \ \mathbf{R}_2) \quad \text{and} \quad \mathbf{P} = \text{diag}(\mathbf{P}_1 \ \mathbf{P}_2),$$

where  $\mathbf{R}_1, \mathbf{R}_2$ , are positive semidefinite  $3 \times 3$  matrices and  $\mathbf{P}_1, \mathbf{P}_2$  are positive definite matrices of the same size. The derivative of (4.29) yields

$$\begin{aligned} \dot{\mathbf{p}}(t) &= \dot{\mathbf{P}}(t) \mathbf{e}(t) + \mathbf{P}(t) \dot{\mathbf{e}}(t) \\ &= \dot{\mathbf{P}}(t) \mathbf{e}(t) - \mathbf{P}(t) \mathbf{R}^{-1} \mathbf{P}(t) \mathbf{e}(t). \end{aligned} \quad (4.30)$$

As a necessary conditions for the optimal trajectory, we still need to consider  $\partial H / \partial \mathbf{e} = 0$ . However, let us first use the Leibniz integral rule in (4.27) as to obtain

$$\begin{aligned} - \int_{t_0}^{t_f} \mathbf{p}^T \dot{\mathbf{e}} dt &= - \int_{t_0}^{t_f} \left( \frac{d}{dt} (\mathbf{p}^T \mathbf{e}) - \dot{\mathbf{p}}^T \mathbf{e} \right) dt \\ &= \mathbf{p}^T(t_0) \mathbf{e}(t_0) - \mathbf{p}^T(t_f) \mathbf{e}(t_f) + \int_{t_0}^{t_f} \dot{\mathbf{p}}^T \mathbf{e} dt. \end{aligned}$$

By replacing the left term of the equation in (4.27), we find

$$\frac{\partial H}{\partial \mathbf{e}} = 0 \implies \dot{\mathbf{p}} = -\mathbf{Q}\mathbf{e}. \quad (4.31)$$

Using (4.31), and considering that  $\mathbf{P}$  do not depend on the initial error, we compare the resulting equations in (4.30) to find

$$\dot{\mathbf{P}} = \mathbf{P}\mathbf{R}^{-1}\mathbf{P} - \mathbf{Q} \quad (4.32)$$

Since we are constraining  $\mathbf{P}$  and  $\mathbf{R}$  to be block diagonal, then it is needless to prove that  $\mathbf{Q}$  also needs to be block diagonal. The boundary conditions to solve (4.32) are obtained using the final time,  $t_f$ , of our trajectory. From (4.29), we find that  $\partial H/\partial \mathbf{e}(t_f) = 0$  yields  $\mathbf{P}(t_f) = \mathbf{S}$ . We can then numerically solve the differential Riccati equation  $\mathbf{P}(t)$  backwards in time.

Therefore, from (4.28) and (4.29) the optimal control is given by  $\mathbf{u}(t) = -\mathbf{R}^{-1}\mathbf{P}(t)\bar{\mathbf{e}}(t)$ . Comparing the result with (4.25), we find that the exponential gains for the dual quaternion end-effector convergence is given by the equality

$$\text{diag}(\mathbf{K}_\circ, \mathbf{K}_\tau) = -\mathbf{R}^{-1}\mathbf{P}(t),$$

where  $\mathbf{R}^{-1}\mathbf{P}(t)$  yields a block diagonal matrix. Using the resulting  $3 \times 3$  matrices  $\mathbf{K}_\circ$  and  $\mathbf{K}_\tau$ , we find a dual quaternion based task-space controller as described in (4.18), which has been shown to be exponentially stable, with

$$\mathbf{u}_c = -\mathbf{R}^{-1}\mathbf{P}(t)\mathbf{e}. \quad (4.33)$$

Combining (4.18) with (4.33), the dual quaternion based task-space controller can be simplified to the following joint velocity inputs

$$\dot{\boldsymbol{\theta}} = \underline{\mathbf{J}}_{\boldsymbol{\omega}}^+ [-\mathbf{R}^{-1}\mathbf{P}(t)\mathbf{e} + \text{vec}_6(\underline{\mathbf{x}}_c \underline{\boldsymbol{\omega}}_d \underline{\mathbf{x}}_c^*)] \quad (4.34)$$

#### Theorem 4.3 Optimal quadratic controller in dual quaternion space

The dual quaternion task-space controller (4.34) with gain matrices  $\mathbf{Q}$ ,  $\mathbf{S}$ ,  $\mathbf{R}$  satisfying  $\mathbf{S} \geq 0$ ,  $\mathbf{Q}(t) \geq 0$  and  $\mathbf{R}(t) > 0$ , defines an optimal quadratic controller for the closed loop system (4.17),(4.34) with positive definite matrix  $\mathbf{P}$  being derived from (4.32).

### 4.3 COMPUTATION AND PARAMETER SELECTION

Both controllers from Theorems 4.1 and 4.3 respectively depend on the solution of the system (4.13) and (4.32). Still the systems containing the Riccati equation are nonlinear, and the closed-form solution may not be found for all cases. As a consequence, finite differences approximations are normally used; that is,

$$\frac{d}{dt}\mathbf{P}(t) \approx \frac{\mathbf{P}(t+\tau) - \mathbf{P}(t)}{\tau}$$

for a small sampling time  $\tau$  that directly affects the approximation precision.

Replacing the Euler based discretization in (4.13) and (4.32), we use an algebraic Riccati equation solver to find  $\mathbf{P}(t_{f-1})$  using a known value for  $\mathbf{P}(t_f)$ . Using a backward algorithm, we can then apply the same solver to find the value of  $\mathbf{P}(t_i)$  using previously calculated  $\mathbf{P}(t_{i+1})$ —the recursion is then applied up to  $\mathbf{P}(0)$ . The same can be applied to find an approximate solution for  $\boldsymbol{\xi}(t)$ , by also considering  $\mathbf{c}(t)$ , in (4.13). Another

solution is to begin with  $\mathbf{P}(t_f)$  and use the derivative approximation backwards in time using the known values of  $\mathbf{A}(t)$ , which depends only on the desired trajectory, up to  $\mathbf{P}(0)$ . All these calculations can be done before the system starts to operate.

The design parameters of the optimal controllers are the matrices gains  $\mathbf{Q}$ ,  $\mathbf{S}$  and  $\mathbf{R}$ . The matrices  $\mathbf{Q}$  and  $\mathbf{S}$  are related to the cost of tracking a desired state. Particularly,  $\mathbf{S}$  weights the final error norm, whereas the time-varying matrices  $\mathbf{R}$  weighs the error cost along the task trajectory. Since the system input is the end-effector velocities, a proper choice of the elements of  $\mathbf{R}$  allows the designer to define an explicitly trade-off between the control effort in terms of the velocity norm and the convergence rate at the optimal geodesic trajectory.

An interesting characteristic of the optimal control design is the ability to define time-varying weights in the optimization process. For instance, we may devise a trajectory that begins far from the end effector initial position. To avoid large joint velocities when the error is expected to be large, we may assign a smaller  $\mathbf{Q}$  at the beginning of the trajectory.

## 4.4 NUMERICAL EXAMPLES AND SIMULATIONS

This section presents two set of different task conditions and scenarios devised to study and to numerically illustrate the effectiveness of the dual quaternion optimization criteria proposed in this chapter in comparison with classic controllers<sup>3</sup> used for robot manipulation. The first task was implemented numerically at Matlab without a physics engine simulation, while the second was devised and implemented in the Virtual Experimentation Platform (VREP) from Coppelia Robotics GmbH (see, [90]) using Bullet Physics Library<sup>4</sup> as the physics engine.

### 4.4.1 Numerical example: Comau SMART SiX robot using Matlab

This example demonstrates the behaviour of the dual-quaternion based controller mapped to  $\mathbb{R}^8$  manifold derived in Section 4.1. To this aim, a simulated task was devised using the six degree of freedom COMAU Smart Six manipulator with the the DQ\_robotics toolbox<sup>5</sup> and the Robotics Toolbox<sup>6</sup> in MATLAB. The task trajectory was construct considering the following periodic end-effector translation and rotation along time

$$\begin{aligned} \mathbf{t}_d(t) &= (0.99707 + 0.1 \cos(\pi t)) \hat{i} + (0.1 + 0.1 \cos(\pi t)) \hat{j} + (1.075 + 0.1 \sin(\pi t)) \hat{k}, \\ \mathbf{r}_d(t) &= \cos\left(\frac{\phi}{2}\right) + \sin\left(\frac{\phi}{2}\right) \frac{\cos(\pi t) \hat{i} + \sin(\pi t) \hat{j} + (\sin(\pi t) - 2) \hat{k}}{\sqrt{1 + (\sin(\pi t) - 2)^2}}, \end{aligned}$$

with  $\phi = 0.25 \sin(\pi t) + \pi$ . The resulting task trajectory thus stems from the coupled motion, that is,  $\underline{\mathbf{x}}_d(t) = \mathbf{r}_d(t) + \varepsilon \frac{1}{2} \mathbf{t}_d(t) \mathbf{r}_d(t)$ .

The robot initial configuration was set given the joint configuration:  $\boldsymbol{\theta}_0 = \begin{bmatrix} 0 & 0 & -\pi/2 & 0 & \pi/2 & 0 \end{bmatrix}^T$ , with the end effector placed 40 cm away from the desired trajectory. The initial configuration ensures that the desired task trajectory is well-defined within the manipulators reachable space.

<sup>3</sup>Proportional controller and proportional controller with feedforward term (for further details, see Appendix B.1).

<sup>4</sup><http://www.bulletphysics.org/>

<sup>5</sup><http://dqrobotics.sourceforge.net>

<sup>6</sup>[http://petercorke.com/Robotics\\_Toolbox.html](http://petercorke.com/Robotics_Toolbox.html)

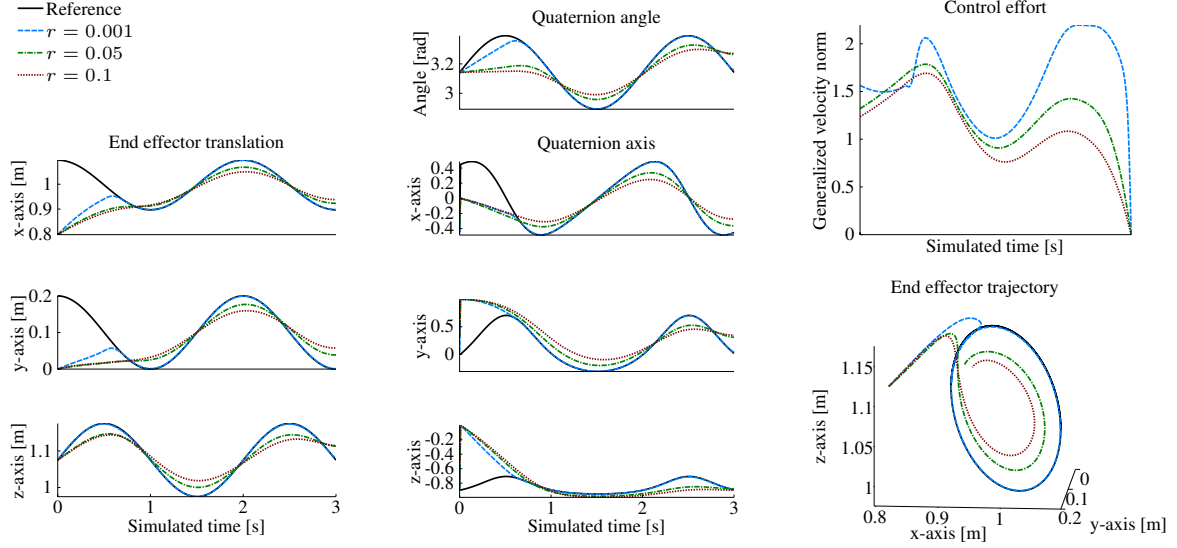


Figure 4.1: [Numerical example] End-effector translation (*left*) and orientation (*center*), the control effort (*top-right*), and end-effector trajectory (*bottom-right*); using the optimal controller from Theorem 4.1 with different control parameters. The trade-off between error and control effort is noticeable, and the end-effector motion shows no steady-state phase shift in relation to the reference.

In this numerical example, three different optimal controllers based on Theorem 4.1 were designed so that their performance can be evaluated. In order to simplify the choice of parameters, we define  $s, q, r \in \mathbb{R}$ , such that

$$\mathbf{S} = s\mathbf{I}, \quad \mathbf{Q} = q\mathbf{I}, \quad \mathbf{R} = r\mathbf{I},$$

where  $\mathbf{I}$  is an identity matrix. The choice of parameters is closely intertwined with the task specificities. For instance, we supposed that the end-time error is not of higher importance than the error in the remainder of the trajectory by setting  $s = 0$ . By knowing that the end effector starts far from the desired trajectory, we designed a trajectory error weight  $q$  that begins small and increases over time:  $q = 0.001$  for  $t \leq 0.5$ , linearly increasing to  $q = 1$  for  $t \in (0.5, 1.0]$ ,  $q = 1$  otherwise. All three controllers share the same  $s$  and  $q$ .

In order to compare control performance, we distinguished the three controllers by choosing a decreasing weight for the control effort parameter, that is  $r \in \{0.1, 0.01, 0.001\}$ . The overall behavior of the three optimal controllers can be seen in Figure 4.1. In all controllers, the choice of  $q$  allows a well-behaved initial motion. Moreover, there is no noticeable phase shift after 1.0 s, when  $q$  reaches its final value. The effect in the decreasing of  $r$  is also clearly shown in Figure 4.1, that is, a higher control effort yields smaller trajectory error.

The performance of the optimal controller with  $r = 0.001$ , in comparison with classic controllers: proportional (K) and proportional with a feedforward term (K+FF) with gain  $k = 10$  is shown in Figure 4.2. It is noticeable that whereas the K controller shows the expected phase shift in spite of the high control effort, the propose criterion with  $r = 0.001$  closely resembles the K + FF controller, but without the initial peak velocity. This allows the optimal controller from Theorem 4.1 to send smoother joint velocities when compared

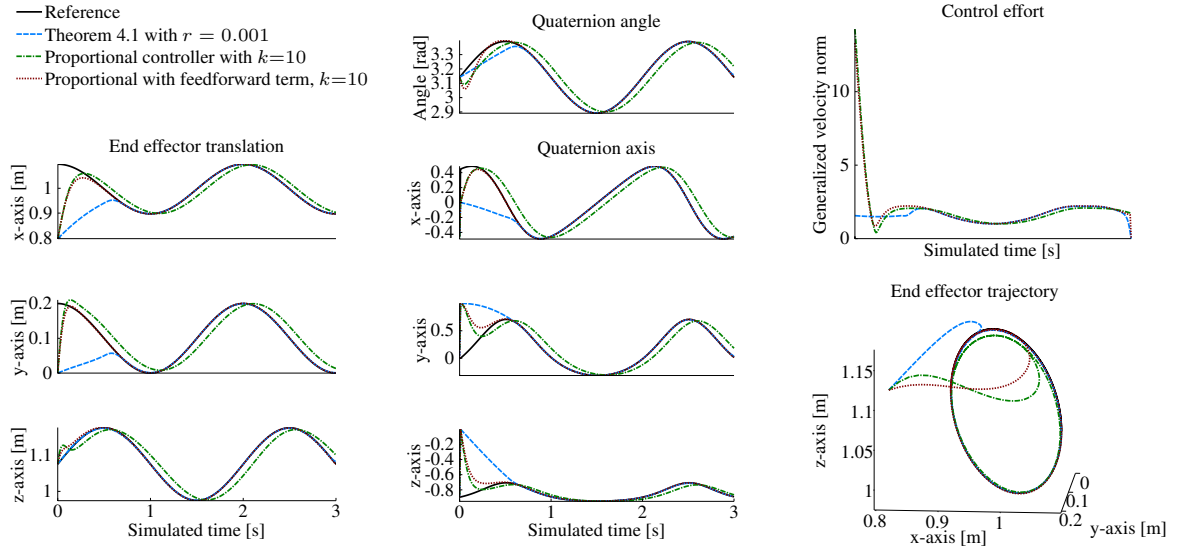


Figure 4.2: [Numerical example] End-effector translation (*left*) and orientation (*center*), the control effort (*top-right*), and end-effector trajectory (*bottom-right*); comparing the optimal quadratic controller from Theorem 4.1 with the proportional gain controllers. The initial peak velocity using the proportional controllers is noticeable. Moreover, without the prediction term, the proportional controller has an inherent phase shift in relation to the desired trajectory.

to the abrupt velocities seen in the  $K$  and  $K + FF$  controllers. It also yields smaller accelerations at the end-effector which, among other benefits, prevents damages to the manipulator and reduces the discomfort during human-robot interaction [102].

#### 4.4.2 Simulated scenario: Kuka LBR iiwa using V-REP

To better assess the effectiveness and differences between classic controllers and the optimal controllers proposed in this chapter, a task simulation was devised and implemented in the Virtual Robot Experimentation Platform (V-REP) from Coppelia Robotics GmbH—using Bullet Physics Library as the physics engine—with a KUKA LBR iiwa arm, a lightweight seven-link manipulator from Kuka Robotics. The simulated task scenario is illustrated in Figure 4.3. All V-REP simulations were performed using a 30 ms sampling time and the proposed controller was implemented using the `DQ_robotics` toolbox in C++ and using ROS.<sup>7</sup> The task trajectory defines a 5 cm radius circle along the  $XZ$ -plane with a  $\theta_0 = [0, \pi/3, 0, \pi/2, 0, \pi/3, 0, 0]$  initial joint vector configuration. The initial configuration was set such that the trajectory lies within the end-effector reachable space. To simplify the choice of parameters, the gain matrices were defined using  $s, q, r \in \mathbb{R}^+$ , such that  $S = sI, Q = qI, R = rI$ , where  $I$  is an identity matrix.

First, we compare the performance between classic controllers, the dual quaternion optimal controller based on  $\mathbb{R}^8$  mapping, Theorem 4.1, and the optimal controller in dual quaternion space from Theorem 4.3. To investigate control performance, reliability, and to minimize the possibility of simulated results outliers, the same

<sup>7</sup><http://www.ros.org/>

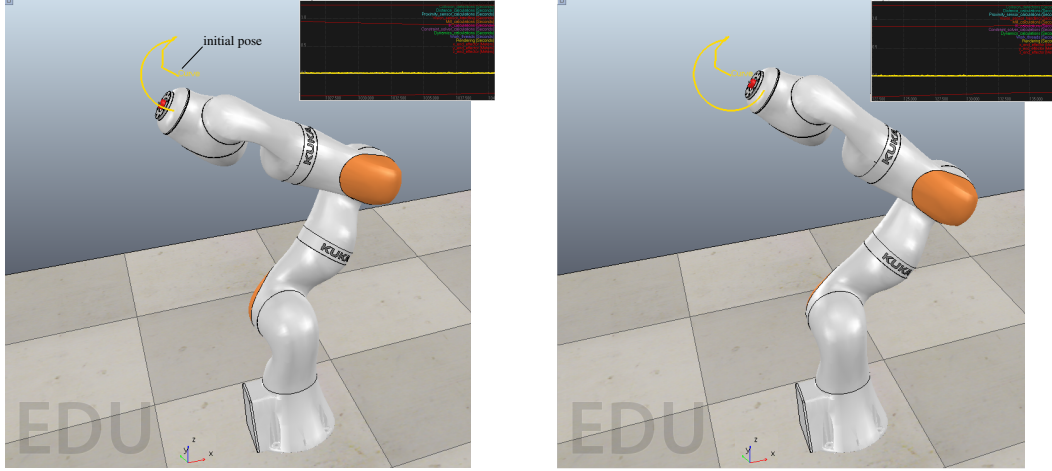


Figure 4.3: *[V-REP Simulation]* Screenshot of the simulated circular task trajectory using KUKA LBR iiwa.

circular trajectory was executed ten times with exactly the same conditions and control parameters. Classic controllers—proportional (K) and proportional with a feedforward term (K+FF)—were implemented using a feedback gain of  $k = 50$ , whereas the dual quaternion based optimal controllers—Theorems 4.1 and 4.3—were implemented with the following gains  $s = 0$ ,  $q = 20$ , and  $r = 0.01$ . Tables D.1 to D.6 in Appendix D.1 show all results for the 10 simulations for each controller. A summary of the results are presented in Table 4.1 with the mean values after ten simulations and the standard deviation for each controller.

	Proportional Controller		Proportional Feedforward		Theorem 4.1 (dq-optimal in $\mathbb{R}^8$ )		Theorem 4.3 (optimal in dq-space)	
	Mean	Std.Dev.	Mean	Std.Dev.	Mean	Std.Dev.	Mean	Std.Dev.
Error	<b>201.8</b>	325.6	<b>445.0</b>	472.1	<b>24.3</b>	4.5	<b>14.9</b>	2.7
Joint Velocity	<b>61.6</b>	0.9	<b>61.3</b>	0.9	<b>105.7</b>	13.0	<b>58.3</b>	0.4
Transl. Velocity	<b>431.0</b>	9.6	<b>430.7</b>	10.0	<b>786.7</b>	92.3	<b>396.6</b>	7.8
Rotat. Velocity	<b>191.7</b>	46.0	<b>206.3</b>	42.7	<b>712.3</b>	241.2	<b>140.1</b>	33.2
Transl. Acceleration	<b>20.85</b>	0.58	<b>20.5</b>	0.47	<b>43.0</b>	5.1	<b>19.3</b>	1.6
Rotat. Acceleration	<b>10.5</b>	2.5	<b>11.2</b>	2.1	<b>37.4</b>	10.9	<b>8.2</b>	2.1

Table 4.1: *[V-REP Simulation]* Comparison of integral norm ( $\times 10^{-3}$ ) of the trajectory error, joint velocity, and end-effector translation and rotational velocities and accelerations between classic proportional and proportional with feedforward term, and optimal controllers: Theorems 4.1 and 4.3

From Table 4.1, it is clear that the optimal controller in dual quaternion space—Theorem 4.3—provided superior results for any given criteria, that is, both in the sense of control effort and error reduction—compared to classic controllers and also compared to Theorem 4.1. In other words, the proposed optimal controller in dual quaternion space successfully reduces the control error along time with smaller control efforts—in terms of end-effector and joint configuration velocities—which, among other benefits, prevents damages to the manipulator and reduces the discomfort during human-robot interaction [102].

More importantly, Table 4.1, as well as Tables D.1 to D.6 in Appendix D.1, clearly illustrate the reliability and consistence from dual quaternion optimal controllers in contrast to the poor reliability obtained from classic controllers—particularly, considering the trajectory error along time. In other words, despite presenting some

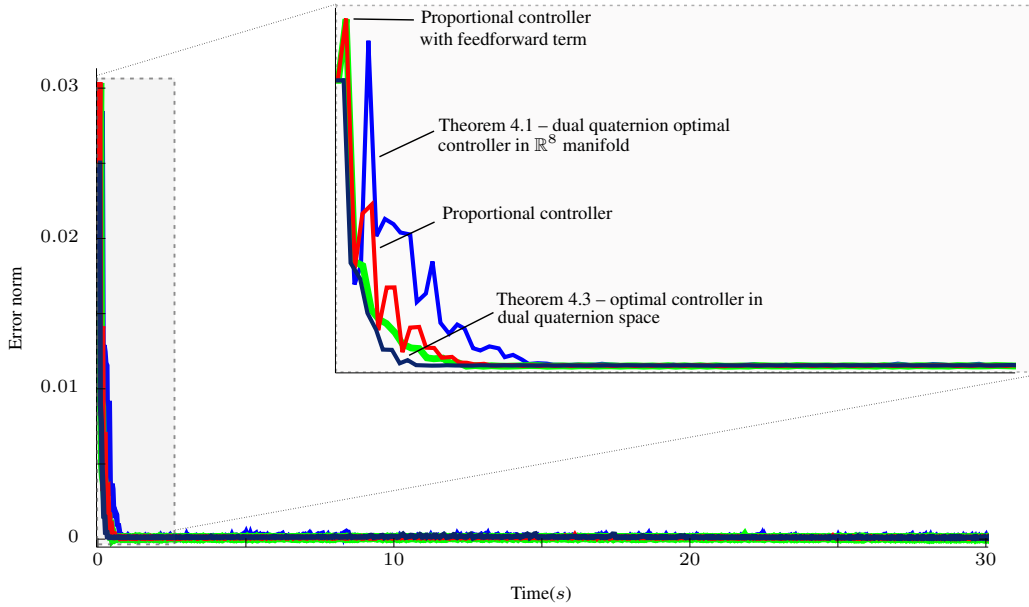


Figure 4.4: *[V-REP Simulation]* Comparison of the error norm between classic proportional (red line) and proportional with feedforward term (green line), and the dual quaternion based optimal controllers from Theorem 4.1 (blue line) and Theorem 4.3 (dark blue line).

few successful results in the sense of small trajectory errors and control effort, classic controllers may behave unexpectedly with large errors and even larger joint velocities and accelerations—which are also reflected on larger velocities and accelerations in task-space. For instance, the integral norm of the trajectory error from the K and K+FF controller may vary from 0.0131 to 0.78 and from 0.0113 to 1.0132, respectively, as shown in Table D.1 in Appendix D.1. In contrast, the error from Theorem 4.3 varies from 0.0137 to 0.0149.

Therefore, by using the proposed optimal controllers, the control design, in addition to properly set the trade-off between control effort and tracking error along the trajectory, can also expect more trustworthy results. There are no unexpected results which in turn reduces the risk of problems, improves the confidence over the controller, and increases its applicability—particularly, within human-robot interaction scenarios.

To better understand the control performance differences, the task trajectory from one of the simulations is also graphically depicted in Figures 4.4 to 4.7. The error norm evolution along time is illustrated in Figure 4.4 whereby it is easy to see the advantages that stems from using optimal controllers. The reduced error is even more relevant when we observe that the controller from Theorem 4.3 presents smaller control efforts. In other words, as depicted in Figures 4.5 and 4.6, the optimal controller in dual quaternion space considerably reduces the overall end-effector and joint configuration velocities and velocities spikes, which in turn also reflects in better acceleration behaviour as shown in Figure 4.7.

Indeed, it is clear that classic controllers are more suitable to present abrupt velocities and accelerations which may damage the manipulator and reduces the feasibility (and validity) of using a kinematic controller. The proposed optimal controllers on the other hand send smoother joint velocities with smaller accelerations at joint and task-spaces. These advantages are graphically illustrated in Figures 4.4 to 4.7 which combined with the reliability of results shown in Table 4.1 highlight the effectiveness and advantages from the proposed optimal control formalism derived in this chapter.



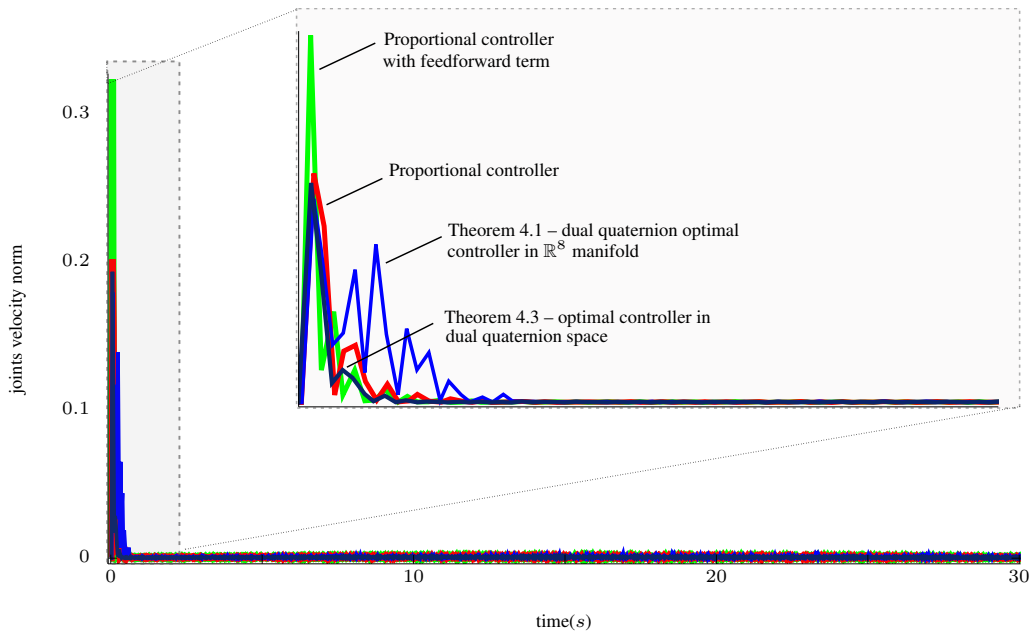


Figure 4.5: [V-REP Simulation] Comparison of the control effort as the joint velocity norm between classic proportional (red line) and proportional with feedforward term (green line), and the dual quaternion based optimal controllers from Theorem 4.1 (blue line) and Theorem 4.3 (dark blue line).

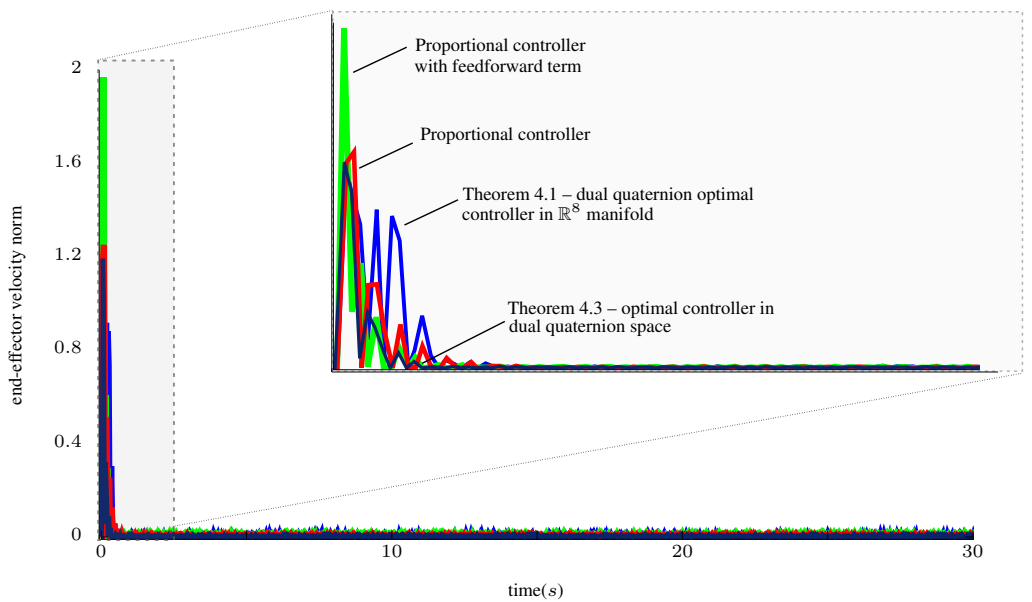


Figure 4.6: [V-REP Simulation] Comparison of the control effort in task-space, that is, the norm of the end-effector velocities between classic proportional (red line) and proportional with feedforward term (green line), and the dual quaternion based optimal controllers from Theorem 4.1 (blue line) and Theorem 4.3 (dark blue line).

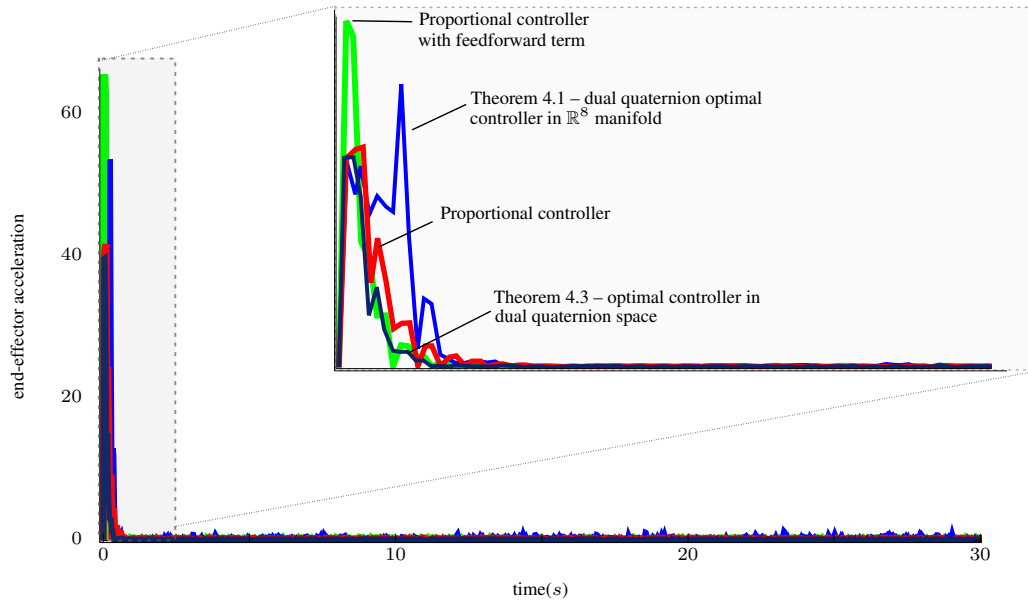


Figure 4.7: [V-REP Simulation] Comparison of the accelerations norm of the end-effector trajectory between classic proportional (red line) and proportional with feedforward term (green line), and the dual quaternion based optimal controllers from Theorem 4.1 (blue line) and Theorem 4.3 (dark blue line).

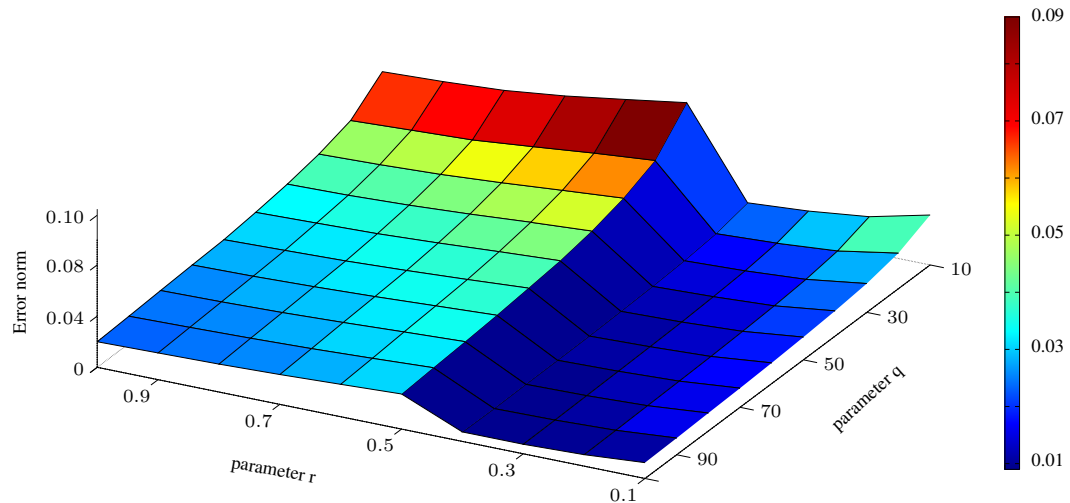


Figure 4.8: [V-REP Simulation] Trajectory error norm along time for different Theorem 4.3 dual quaternion optimal control parameters  $q$  and  $r$  for  $Q = qI$ ,  $R = rI$ , and  $S = 0$ .

## Parameter selection for optimal controller in dual quaternion space

From previous simulations, it is clear that the choice of parameters is closely related to the controller performance and control effort. The trade-off between effort and error minimization depends on the task specificities and varies according to the choice of parameters. In this sense, and in order to elucidate the influence of the control parameters with regard to the trade-off between trajectory error and control effort, we implemented the same circular trajectory for the KUKA LBR iiwa arm<sup>8</sup> with varying values for  $q$ ,  $r \in \mathbb{R}^+$ , such that  $\mathbf{Q} = q\mathbf{I}$ ,  $\mathbf{R} = r\mathbf{I}$ .

The results are illustrated in Figure 4.8. Clearly, the larger the value of  $q$ , the smaller the control error along time. Increasing the value of  $q$  reduces the trajectory error norm exponentially. Still, a reduced control error is only obtained in the presence of a smaller  $r$  since it limits the task-space velocity. Higher values of  $r$  render smaller overall velocities—as consequence, also reduces the control effort in task-space—but prevents a fast stabilization which in turn increases the overall tracking error. On the other hand, when  $r \rightarrow 0$ , the large velocities cause spikes on the trajectory which increase slightly the integral norm of the trajectory error—despite presenting a faster convergence rate.

In this sense, and considering the reliability and consistence from the proposed optimal controllers, the choice of parameters can be defined in accordance to particular task specificities and the desired trade-off between control effort and tracking error along the trajectory with higher confidence on the expected results.

## 4.5 REAL ROBOT EXPERIMENTS

This section presents practical experiments for an evaluation of the proposed optimization-based kinematic controllers at task-space using a Meka A2 compliant arm from Meka Robotics, see Figure 4.9. The motivation of using an anthropomorphic compliant arm lies in their use with collaborative robots, human-robot interaction, and the importance of evaluating existing control techniques within these scenarios. Moreover, compliant robots are inherently designed with lower stiffness, thus classic feedback controllers for stiff manipulators may behaves differently than expected and experimentation is needed. In this sense, this section, driven by the theoretical advantages of the proposed dual quaternion based optimal controllers and by the challenge of controlling a compliant robot with higher precision, presents the results from real experiments with a compliant robot manipulator.

### Task Definition

In order to demonstrate the controllers behavior under different set of parameters, two different task trajectories on the Meka A2 Arm from Meka Robotics manipulator with seven degrees of freedom (DOF) were devised: a circular trajectory around a initial configuration and a squared trajectory. The controllers were implemented using the DQ\_robotics toolbox<sup>9</sup> in C++ and using ROS<sup>10</sup> to establish communication with the real robot.

The motivation for the repetitive task trajectories lies in the need to accomplish repetitive tasks while working alongside humans. Therefore, we check the ability of the robot to follow simple trajectories. Due to an-

---

<sup>8</sup>The simulations were performed using the same configurations—Bullet Physics Library and DQ\_robotics toolbox in C++ with ROS.

<sup>9</sup><http://dqrobotics.sourceforge.net/>

<sup>10</sup><http://www.ros.org/>



Figure 4.9: [Real robot experiment] Meka A2 compliant arm with seven degrees of freedom (DOF) from Meka Robotics.

thropic arm joint limitations we considered initial robot configurations that allows the robot to execute the whole trajectory.

## Experiments using dual quaternion optimal controller based on $\mathbb{R}^8$ mapping–Theorem 4.1

First, we compare the dual quaternion optimal based controller defined in  $\mathbb{R}^8$  manifold from Section 4.1 against classic controllers, that is, proportional and proportional with feedforward term. In this part, both circle and square trajectories were implemented. The circle chosen has 10 cm radius and was drawn on the  $XZ$ -plane while maintaining  $Y$  constant. The robot initial configuration were defined by the initial joint configuration  $\theta_0 = [0, \pi/3, 0, \pi/2, 0, \pi/3, 0, 0]$ . The square trajectory was also set at the  $XZ$ -plane with 10 cm side, with  $Y$  constant and initial configuration given by  $\theta_0 = [0, \pi/4, 0, \pi/2, 0, \pi/4, 0, 0]$ . The trajectories are independent from each other and were run separately.

In order to simplify the choice of parameters for Theorem 4.1, we defined the gain matrices using  $s, q, r \in \mathbb{R}$  such that  $S = sI, Q = qI, R = rI$ , where  $I \in \mathbb{R}$  is the identity matrix. Classic controllers, that is, the proportional and proportional with feedforward term, were implemented with constant gain  $k = 50$ . Due to the lack of reliability from classic controllers—as observed from the simulations in the previous section—and to allow a fairer comparison, we executed each trajectory five times with exactly the same control proportional gain (only for K and K+FF controllers) and extracted the median value for each attribute, as the median is a robust estimator and efficient to exclude outliers. In addition, a decoupled proportional controller—which regards the rotation and translation end-effector motion separately—was implemented for the circular trajectory.

To compare performance, we implemented the dual quaternion based controller with distinguished values for the  $r$ , that is, with different weight values for the control effort,  $r \in \{0.01, 0.1, 0.5, 1\}$ . Table 4.2 shows the results for the circular trajectory and Table 4.3 shows the squared trajectory results.

The choice of  $q$  for all simulations using Theorem 4.1 allows a well-behaved initial motion. The effect in decreasing  $r$  as shown in Table 4.2 yields a higher control effort and a slight increase in  $r$  results in a smaller control effort. The influence of modifying  $r$  is also explicit in Table 4.3 for the squared trajectory. As expected,

	<u>Dual quaternion optimal controller – Theorem 4.1</u>				<u>K</u>	<u>K+FF</u>	<u>Decoup.</u>	
	Q	20	250	350	80	$k = 50$	$k = 50$	$k = 0.375$
	R	0.01	0.1	0.5	1			
Error		4.77	4.45	6.78	16.77	4.47	4.45	52.47
Control signal		7.82	8.16	6.31	5.46	8.24	8.22	22.71
Joint velocity		0.12	0.12	0.07	0.09	0.12	0.12	0.22
End-effector velocity		1.06	1.06	0.62	0.94	1.07	1.05	1.20
End-effector acceleration		23.03	22.89	19.86	21.31	23.12	26.21	27.56

Table 4.2: *[Real robot experiment]* Comparison of integral norm of the trajectory error, control signal, joint velocity, and end-effector velocities and accelerations between classic proportional and proportional with feedforward term, decoupled controller and dual quaternion based optimal controller from Theorem 4.1—experimental results obtained from the Meka A2 arm for the circular trajectory

	<u>DQ optimal controller – Theorem 4.1</u>			<u>Proportional (K)</u>	<u>FF-Prop. (K+FF)</u>
	Q	20	250	$k = 50$	$k = 50$
	R	0.01	0.1		
Error		2.47	2.23	2.63	2.63
Control signal		3.82	4.42	4.99	4.96
Joint velocity		0.06	0.07	0.09	0.09
End-effector velocity		0.51	0.58	0.68	0.68
End-effector acceleration		10.90	13.74	18.95	19.22

Table 4.3: *[Real robot experiment]* Comparison of integral norm of the trajectory error, control signal, joint velocity, and end-effector velocities and accelerations between classic proportional and proportional with feedforward term, decoupled controller and dual quaternion based optimal controller from Theorem 4.1—experimental results obtained from the Meka A2 arm for the squared trajectory

one can see that the control effort in task-space is reduced for a higher value of  $r$  with a fixed  $q$ . Meanwhile, the K and K+FF controllers have higher control signals and it cannot be directly adjusted by specific parameters. Both are bounded to the overall effect of the proportional gain  $k$ . Furthermore, classic controllers generally have larger errors even when larger control signals are applied—for instance, for the squared trajectory, the error from the K+FF controller is up to 18% higher than the error from Theorem 4.1 even with larger control efforts (control signals and joint velocities are up to 28% and 12% higher for the K+FF controller).

The control behaviour, particularly, the control effort as the norm from the joint velocities, is also graphically depicted in Figure 4.10 for the circular trajectory. It is interesting to highlight that we distinguished the real robot joint velocities along time from the control signal defined as the joint velocity reference inputs for the low level controllers of the manipulator. The motivation for distinguishing both values stems from the joints velocities limitation that we have imposed over the real robot manipulator in order to prevent damages to the robot actuators and structure. Hence, in contrast to numerical simulations, the real joint velocities are considerably lower than the ones expected from the control signal—as explicit in Figure 4.10.

In the beginning of the circular trajectory, the manipulator needs to converge to the initial pose for the circular task trajectory which yields a large initial error. The larger error in turn renders a very large control signal and joint velocities for the K and K+FF controllers due to the nature of their constant exponential

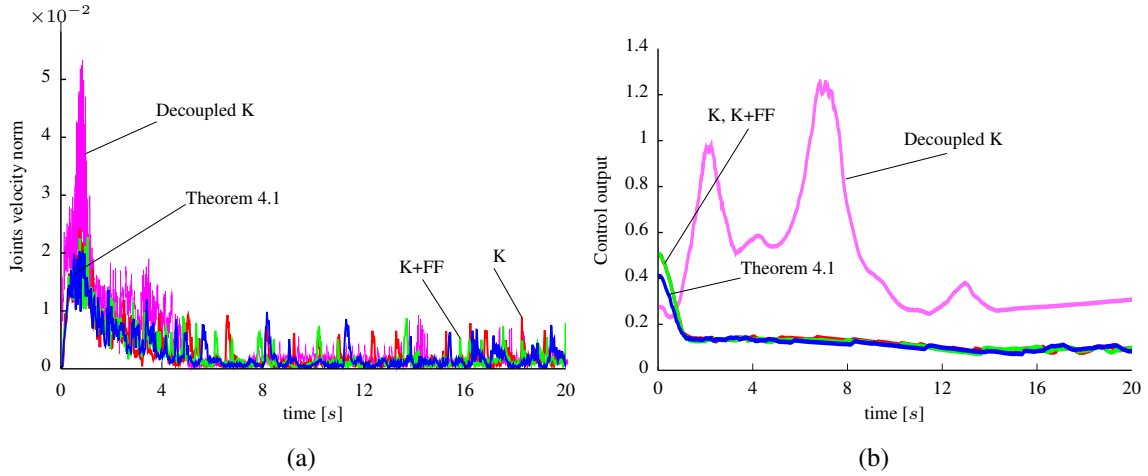


Figure 4.10: [Real robot experiment] Control effort: norm of joint velocities (a) and norm of the control signal (b) for the circular trajectory with  $r = 0.01$ ,  $q = 20$ .

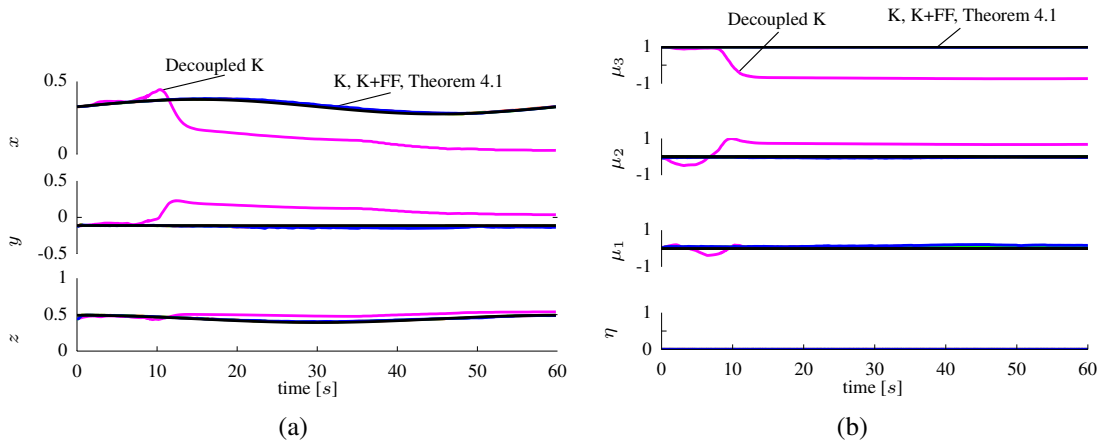


Figure 4.11: [Real robot experiment] End-effector three-dimensional translational (a) and quaternion rotational ( $\mathbf{r} = \eta + \mu_1 \hat{i} + \mu_2 \hat{j} + \mu_3 \hat{k}$ ) (b) trajectory along time for the circular trajectory with  $r = 0.5$  and  $q = 350$ .

convergence—as shown in Figure 4.10. In contrast, the proposed dual quaternion based optimal control strategy minimizes the overall trajectory error and control effort which in turn prevents such spikes while maintaining similar errors along the trajectory and smaller control effort, as shown in Figures 4.10-4.13. The decoupled proportional controller strategy is also shown in mentioned figures. They show not only higher error, control effort and velocities as seen in Table 4.2, but can also lead the robot to singular configurations which may damage the actuators and joints.

### Experiments using optimal controller in dual quaternion space—Theorem 4.3

Motivated by the theoretical properties described in Section 4.2 and by simulation results from Section 4.4, hereafter we will investigate the implementation and effectiveness of the optimal controller derived in dual quaternion space from Theorem 4.3 applied to a real robot compliant platform, the Meka A2 Arm from Meka Robotics. The proposed controller is compared with classic controllers in the literature, that is, proportional

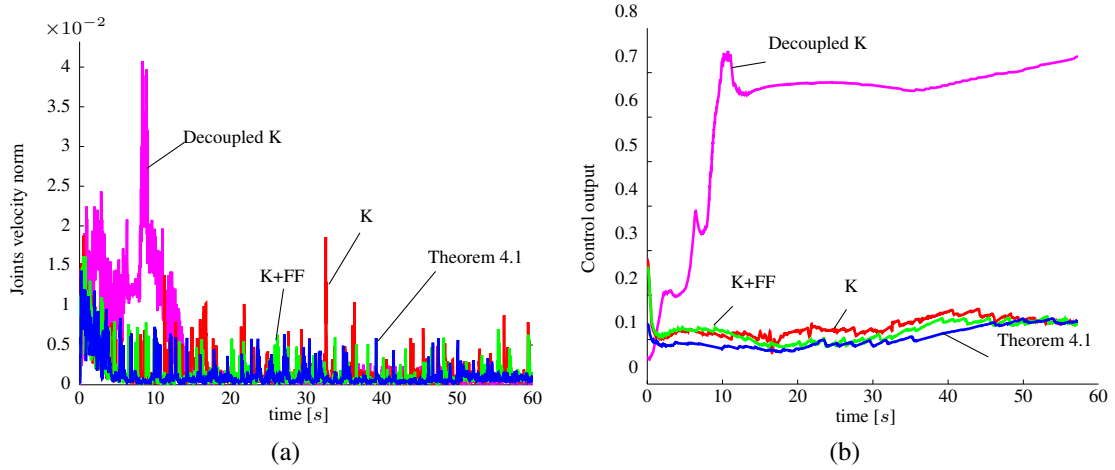


Figure 4.12: [Real robot experiment] Control effort: norm of joint velocities (a) and norm of the control signal (b) for the circular trajectory with  $r = 0.5$  and  $q = 350$ .

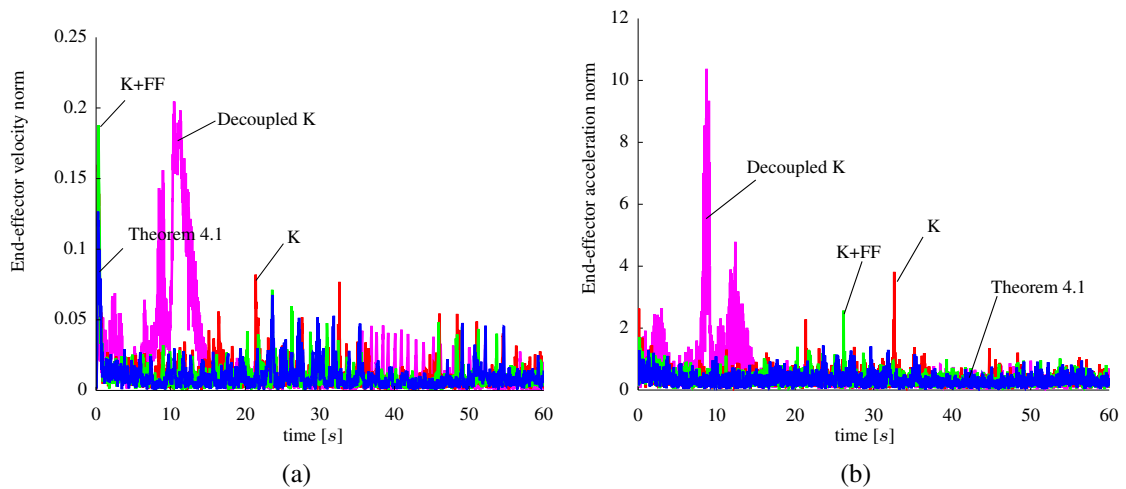


Figure 4.13: [Real robot experiment] Control effort in task-space: norm of end-effector velocities (a) and norm of its accelerations (b) for the circular trajectory with  $r = 0.5$  and  $q = 350$ .

	Proportional controller	Proportional w/ feedforward term	Theorem 4.3 (optimal in dq-space)
Error	4.863	4.854	4.386
Joint velocity	0.118	0.119	0.119
End-effector velocity	2.919	2.917	2.835
End-effector acceleration	99.564	99.686	95.621

Table 4.4: *[Real robot experiment]* Comparison of integral norm of the trajectory error, joint velocity, and end-effector velocities and accelerations between classic proportional and proportional with feedforward term, and dual quaternion based optimal controller from Theorem 4.1—experimental results obtained from the Meka A2 arm

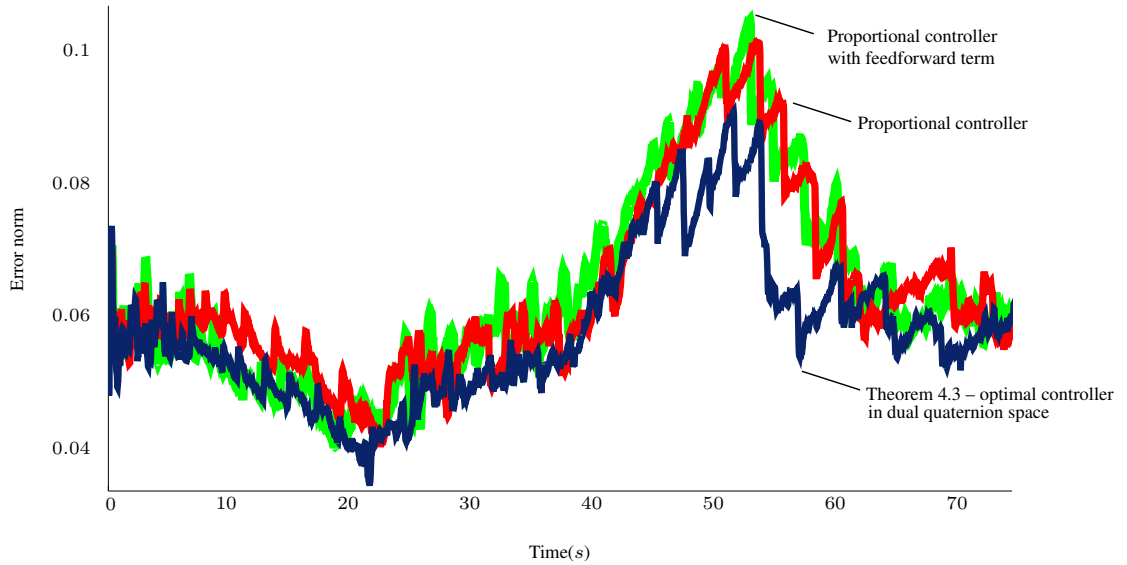


Figure 4.14: *[Real robot experiment]* Comparison of the error norm between classic proportional (red line) and proportional with feedforward term (green line) with the optimal controller in dual quaternion space from Theorem 4.3 (dark blue line).

controller and proportional controller with feedforward term. The devised task is based on the previously described circular trajectory with the same initial joint configuration  $\theta_0 = [0, \pi/3, 0, \pi/2, 0, \pi/3, 0, 0]$ , but drawing a 8 cm radius on the  $XZ$ -plane.

For practical implementation, we configured the proportional and proportional with feedforward term controllers with constant gain of  $k = 50$ . Similarly to previous experiments, they were executed five times with the same control configurations due to their lack of reliability. We extracted the median value for each attribute, as the median is a robust estimator and efficient to exclude outliers.

To compare performance with classic controllers, we implemented the dual quaternion optimal controller from Theorem 4.3 with gain matrices defined by  $S = \mathbf{0}$ ,  $Q = 35I$ ,  $R = 0.01I$ . The gains were manually selected as to obtain similar control effort in terms of the norm from the joint velocity vector. A summary of the obtained results is shown in Table 4.4. From the results, one can see that in addition of being more reliable and providing a tool to balance more conveniently the end effector error and its task-space velocity, the optimal controller has a better error performance even with smaller end-effector velocities and accelerations.



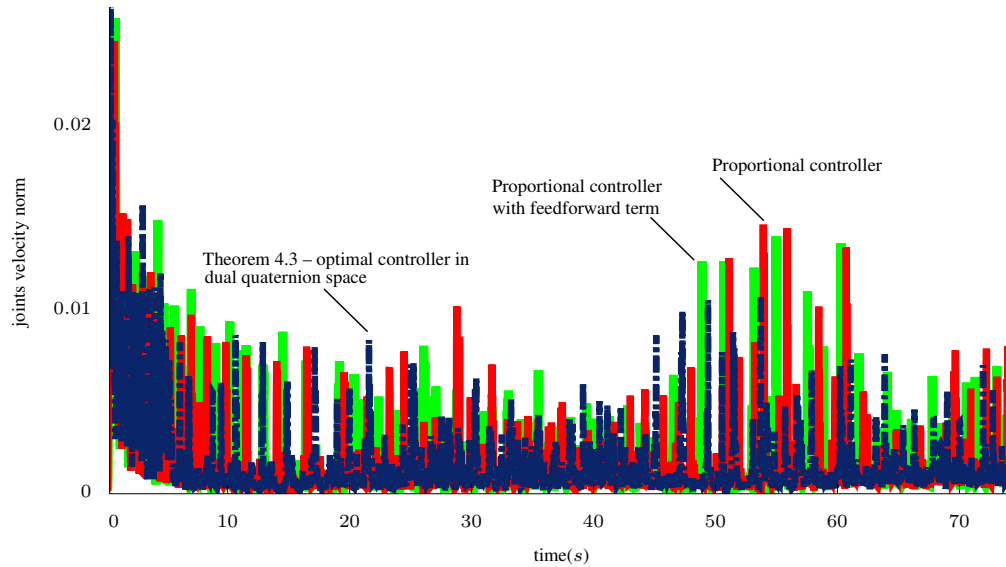


Figure 4.15: [Real robot experiment] Comparison of the control effort: joint velocity norm between classic proportional (red line) and proportional with feedforward term (green line) with the optimal controller in dual quaternion space from Theorem 4.3 (dashed dark blue line).

The differences in control performance between each controller, considering the described task trajectory, are graphically depicted in Figures 4.14 to 4.17. The task trajectory error norm along time is shown in Figure 4.14 and highlights the advantages from using an optimal controller in the sense of error reduction throughout the trajectory. The control performance is even more relevant if we observe the control effort in terms of joint velocities and task-space end-effector velocities described in Figure 4.15 and Figure 4.16, respectively. From Figure 4.15, it is clear that classic controllers are more suitable to present abrupt velocities with sharp increases in magnitude which in turn may damage the manipulator. On the other hand, the dual quaternion optimal controller from Theorem 4.3 sends smoother joint velocities to low-level controllers. In fact, the optimal controller in dual quaternion space reduces the number and the magnitude of velocity spikes in joint and task-space which also renders better behaved acceleration characteristics as shown in Figure 4.17.

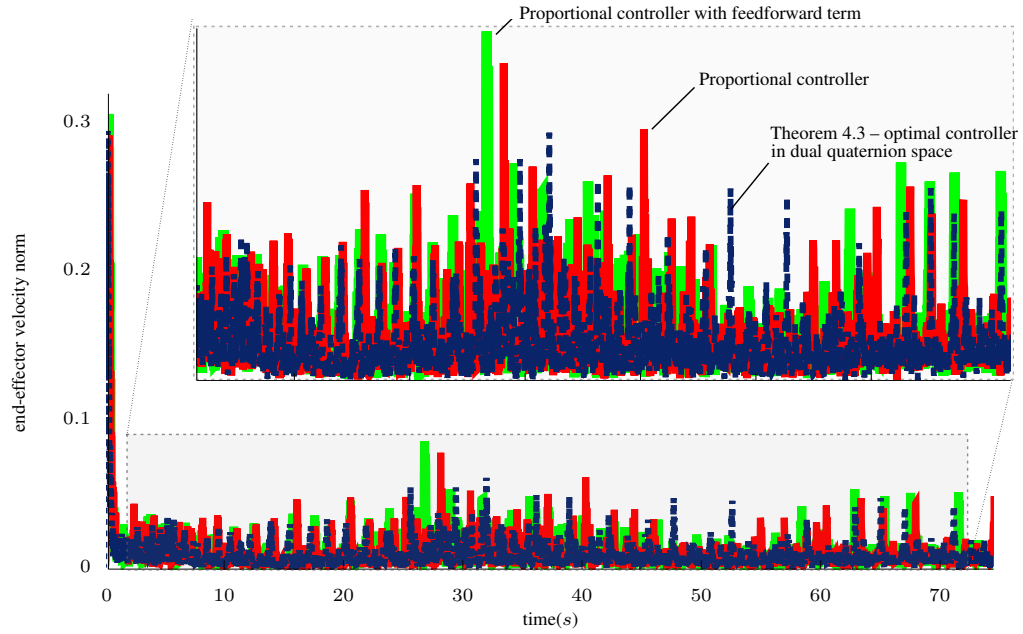


Figure 4.16: [Real robot experiment] Comparison of the control effort in task-space, that is, the norm of the end-effector velocities between classic proportional (red line) and proportional with feedforward term (green line) with the optimal controller in dual quaternion space from Theorem 4.3 (dashed dark blue line).

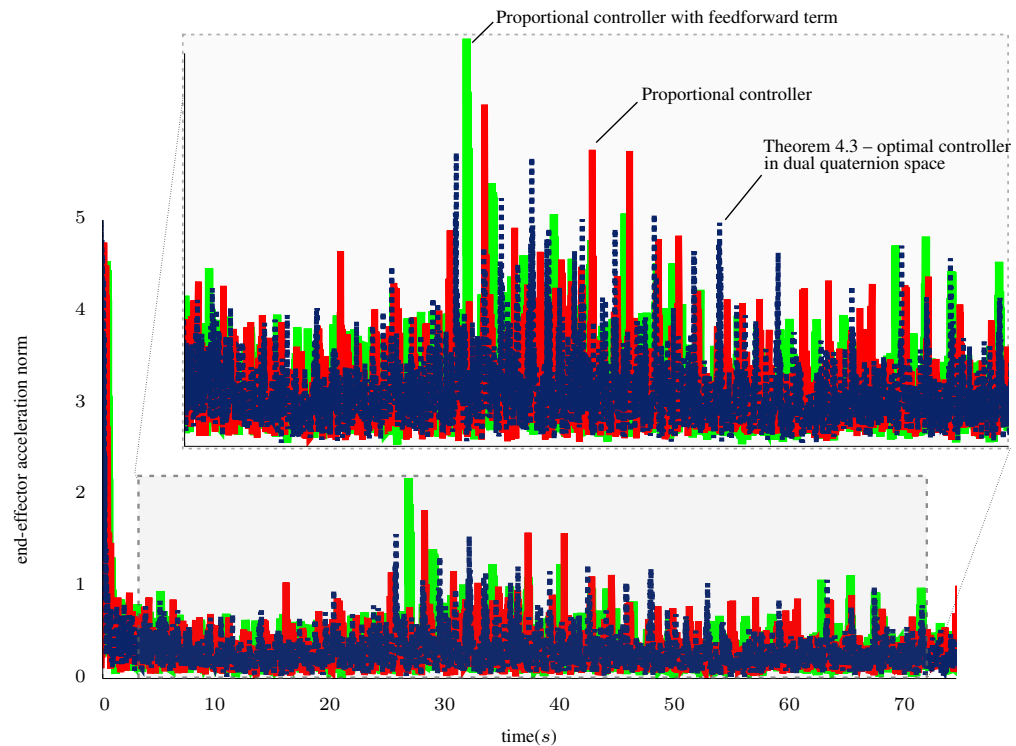


Figure 4.17: [Real robot experiment] Comparison of the accelerations norm of the end-effector trajectory between classic proportional (red line) and proportional with feedforward term (green line) with the optimal controller in dual quaternion space from Theorem 4.3 (dashed dark blue line).

# 5

## $H_\infty$ SINGULARITY AVOIDANCE TECHNIQUE USING DUAL QUATERNIONS

---

*1/r<sup>2</sup> has a nasty singularity at r = 0, but it did not bother Newton—the  
Moon is far enough – Edward Witten*

Singularities play a significant role in design and control of rigid body motion, particularly in the context of robot manipulators. The robot configuration—position and orientation—in task-space is represented in a non-Euclidean manifold which has a topological obstruction that prevents global stability using a continuous feedback, regardless the representation of rigid motion (see Chapter 6). Particularly, if a minimal representation (for instance, Euler angles for rotation) is adopted, then the topological obstruction yields a singularity, referred as representation singularity [108]. In this case, many different poses are mapped onto a single configuration within the minimal representation which fails to be well-behaved in the sense that small changes close to the singularity causes large changes in the rigid body motion.

A representation singularity is not directly related to the true motion capabilities of the manipulator structure [108]. Indeed, the unit dual quaternion framework—similarly to unit quaternions for pure rotations—provides a escape for utterly describing the coupled kinematics without representation singularities. On the other hand, the dual quaternion representation has two elements for every pose in  $SE(3)$  (see (2.21) in Subsection 2.5.1) which causes the unwinding phenomenon. A detailed description and solution for this phenomenon that stems from the topological obstruction is presented in Chapter 6.

Still, regardless the rigid motion representation, manipulator tasks are liable to kinematic singularities. Some specific joint configurations may render the differential FKM to be ill-posed—that is, the Jacobian matrix that represents the transformation mapping from the joint velocity vector to the task-space end-effector velocity loses rank—which implies in losing one or more degree-of-freedom (DOF). To study and avoid kinematic singularities of a manipulator is of great importance since at the neighborhood of these configurations several problems arise due to the rank loss [75, 109, 110]:

- Manipulator mobility is reduced, that is, some motions at the end-effector may not be feasible;
- Infinite solutions to the inverse kinematics problem may exist;
- Small velocities in the task-space may lead to large and unbounded torques in the joint-space;
- The task-space control may chatter or even provide infeasible joint velocities which degrades the control performance and endangers the manipulator;

In this context and in order to ensure proper manipulability throughout the whole end-effector task-space, this chapter addresses the problem of singularity avoidance for robot manipulators. First, we introduce existing solutions for singularity avoidance in the literature. Most of these solutions are based on the assumption of an Euclidean representation of the task-space. Therefore, they can be directly applied when using the dual quaternion based end-effector pose Jacobian ( $\mathbf{J}_{\text{vec}}$ ) that maps the  $n$ -joint velocity vector to changes in the task-space mapped to an  $\mathbb{R}^8$  manifold (see Subsection 2.7.2). Nonetheless, this is not the case for the dual quaternion Jacobian ( $\mathbf{J}_{\underline{q}}$ ) described in Subsection 2.7.3 that maps changes in the  $n$ -joint configuration to the

end-effector twist  $\omega_E$ , that is, a mapping of the form  $\mathbb{R}^n \mapsto \mathbb{H}_0 \otimes \mathbb{D}$ . It is important to emphasize that the generalization of existing techniques defined for the Euclidean space does not necessarily follow by principle of transference. Indeed, counterexamples shown in [67] illustrate examples of failures of the transfer principle outside the algebraic realm. In this sense, and to ensure a proper manipulability without singularities when using the dual quaternion Jacobian ( $\underline{J}_\omega$ ), Section 5.2 addresses solutions within the dual quaternion space for singularity avoidance of redundant and non-redundant arms. Particularly, for redundant manipulators, we prove that existing techniques based on the self-motion can be extended when using the dual quaternion Jacobian ( $\underline{J}_\omega$ ) and, for non-redundant manipulators, we propose a new singularity avoidance strategy based on the  $H_\infty$  dual quaternion controller derived in Section 3.3, suitable for the non-Euclidean task-space manifold, that explicitly regulates the trade-off between exactness of the solution and avoidance effort for inescapable singularities and non-redundant arms based on the  $H_\infty$  theory.

## 5.1 SINGULARITY CLASSIFICATION AND EXISTING AVOIDANCE TECHNIQUES

This section first provides the reader with a basic classification of different singularities that may occur in the Jacobian analysis for redundant manipulators. Afterwards, it is presented an overview of existing solutions for singularity avoidance in the literature for redundant and non-redundant manipulators.

### Why redundant manipulators?

Control requirements and assignments for a manipulator are usually defined in task-space. A arbitrary full pose transformation—position and orientation—demands six degrees of freedom to be feasible through the differential kinematics described in Chapter 2. Considering a transformation to the Euclidean space, the linear mapping requires the control of at least six joints of a  $n$ -joint serial robot manipulator structure in order to enable the inverse differential kinematics calculation.

For the case when  $n > 6$ , the manipulator is considered to be redundant. In this case, inverse differential kinematics calculation can be performed using the right pseudoinverse of the Jacobian. Due to the linear transformation from  $\mathbb{R}^n$  to  $\mathbb{R}^6$ , with  $n > 6$ , we have an infinite number of solutions to this problem. The main advantage of redundant arms over non-redundant arms is exactly the existence of multiple solutions that enable self-motion [110]. **Self-motion** (or **null motion**) are feasible movements of the links which do not disturb the end effector trajectory [109]. In this sense, singularities can be classified according to the possibility of self-motion. The occurrence of self-motion in redundant arms depends upon the existence of a nonzero vector in the kernel of the Jacobian [109, 110], which does not exist for non-redundant manipulators at regular points. In non-redundant arms, there exists no relative motion of the links which recover the manipulator to a nonsingular posture without disturbing the end-effector configuration, i.e., all singular configurations are inescapable.

The most common classification regarding singular configurations are based on the possibility of reconfiguration into a nonsingular posture using self-motion [109, 110]:

1. Self-motion does not exist (inescapable or unavoidable singularities);
2. Self-motion exists but it only allows movement along a set of singular configurations (inescapable or unavoidable singularities);

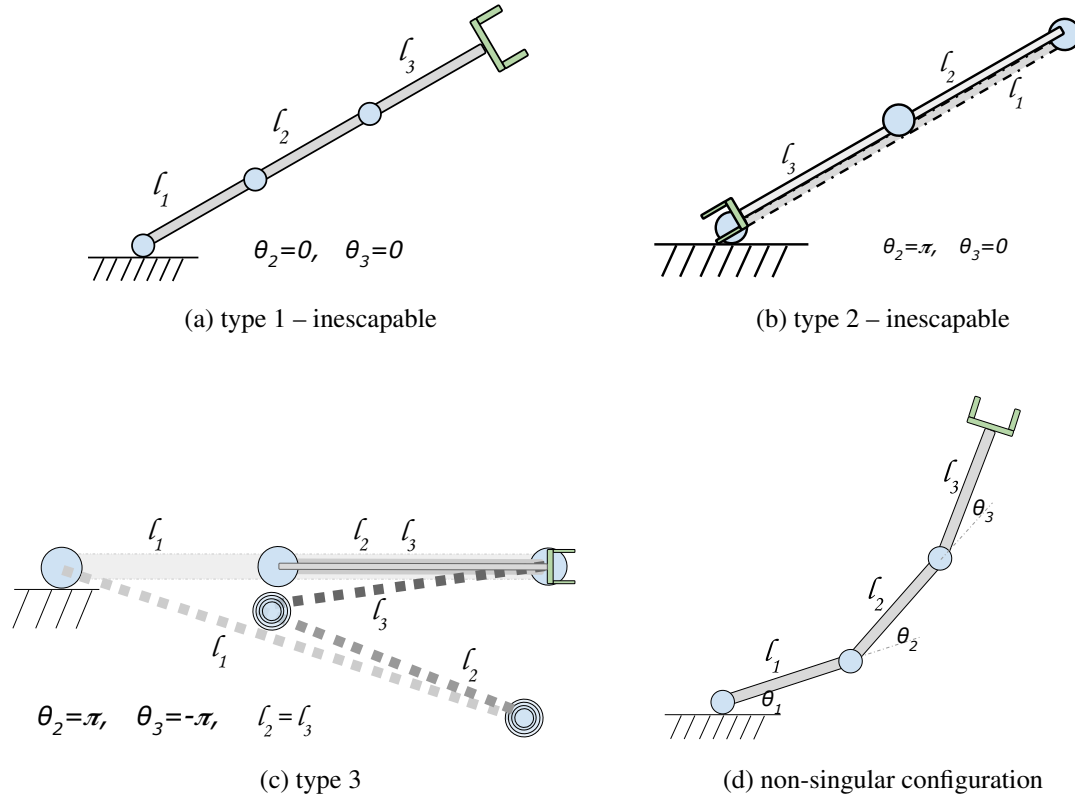


Figure 5.1: Comparison between singularities and a nonsingular configuration (d) for a 3-DOF manipulator (only 2-D position control): the boundary singularity in (a) prevents movements in self-motion since any joint will displace the end-effector pose; the joint configuration in (b) permits different joints movements without perturbing the end-effector position (that coincides with the base) but the movements are performed along the singular region; the manipulator configuration in (c) can be reconfigured via the self-motion.

3. Self-motion exists and can be used to recover the manipulator to a non-singular configuration (escapable or avoidable singularities).

A very common cause of the first type of singularity regards the case in which the end-effector position lies on its workspace boundary. In this case, the singularity is called saturation singularity (or boundary singularity) [75, 109]. In this case, there can be no relative motion of the links which does not disturb the end-effector configuration. Boundary singularities occur when the manipulator is outstretched and may be considered a less significant problem since they can be avoided on condition that the manipulator is not driven to the boundaries of its reachable workspace [75].

The second and third types of singularities are called internal singularities, since their occurrence lies inside the reachable workspace. They are generally caused by the alignment of two or more axes of motion, or else by the attainment of particular end-effector configurations. These singularities can be encountered anywhere in the reachable workspace and are particularly hard to identify. Internal singularities are divided according to whether escape by null motion is possible [109].

The types of singularities are illustrated in Figure 5.1.

## 5.1.1 Overview on singularity avoidance strategies

### 5.1.1.1 Singularity avoidance by self-motion

In redundant arms, the manipulator may recover from escapable singularities using self-motion. The idea is to optimize some manipulability function—that quantifies the proximity of a singular configuration. The optimization is projected onto the nullspace (also known as kernel) of the Jacobian matrix (see, for instance, [111–117]) which ensures that the end-effector trajectory is not influenced by the movements stemming from the nullspace optimization.

Consider a generic differential kinematics described in Euclidean space by  $\dot{\boldsymbol{x}} = \boldsymbol{J}\dot{\boldsymbol{\theta}}$ , where  $\dot{\boldsymbol{x}} \in \mathbb{R}^p$  is the decoupled angular and linear velocities of the end-effector,  $\boldsymbol{\theta} \in \mathbb{R}^n$  is the joint vector, and  $\boldsymbol{J} \in \mathbb{R}^{p \times n}$  is the Jacobian mapping. The control law using the inverse of the differential kinematics yields the following controller

$$\dot{\boldsymbol{\theta}} = \boldsymbol{J}^+ \boldsymbol{x},$$

where  $\boldsymbol{J}^+ = \boldsymbol{J}^T(\boldsymbol{J}\boldsymbol{J}^T)^{-1}$  is the right pseudoinverse of the Jacobian matrix. The attractiveness of this solution lies on the least square property of the pseudoinverse  $\boldsymbol{J}^+$  that generates minimum norm joint velocities for a given trajectory. However, [118] proved that joint velocities are only instantaneously minimized and can become arbitrarily large near singular configurations. In this sense, if  $n > p$  (more joints than the DOFs required for the task to be performed) then a more general solution for the inverse differential kinematics is

$$\dot{\boldsymbol{\theta}} = \boldsymbol{J}^+ \boldsymbol{x} + (\boldsymbol{I} - \boldsymbol{J}^+ \boldsymbol{J}) \boldsymbol{y}, \quad (5.1)$$

where  $\boldsymbol{I}$  is a  $n \times n$  identity matrix and  $\boldsymbol{y} \in \mathbb{R}^n$  is an arbitrary joint vector. Note that main task trajectory remains unchanged since  $\boldsymbol{J}(\boldsymbol{I} - \boldsymbol{J}^+ \boldsymbol{J}) \rightarrow \mathbf{0}$  which defines the nullspace.

If we combine the differential forward kinematics with (5.1), it turns out that  $(\boldsymbol{I} - \boldsymbol{J}^+ \boldsymbol{J}) \boldsymbol{y}$  represents the projection of  $\boldsymbol{y}$  onto the nullspace of  $\boldsymbol{J}$  [111]. As a consequence, if we set  $\boldsymbol{y} \triangleq \alpha \nabla y$ , where  $\alpha$  is a given scalar and  $\nabla y = \frac{\partial y}{\partial \boldsymbol{\theta}}$  is the gradient of a smooth scalar function  $y$  over  $\boldsymbol{\theta}$ , then the nullspace solution forces  $y$  to decrease.<sup>1</sup> Indeed, in the particular case where  $\boldsymbol{x} \rightarrow \mathbf{0}$ , then the solution is identical do the gradient projection method [111]. Different cost functions can be used as long as they are differentiable and expressed in terms of the joint variables (for instance, [111] exploits cost functions for joint limits avoidance). In this context, [113] introduced a online singularity avoidance technique based on the gradient of an manipulability function over the nullspace of the Jacobian of a redundant manipulator. A manipulability function quantifies the proximity of a singular configuration—usually, by means of the determinant or using the minimum singular value. The manipulability used in [113] was proposed in [119]:

$$y = \sqrt{\det \{ \boldsymbol{J}\boldsymbol{J}^T \}}. \quad (5.2)$$

It is easy to see that  $y$  is a non-negative scalar with zero value only when the Jacobian is not full rank— $\boldsymbol{J}\boldsymbol{J}^T$  not invertible. For redundant manipulators with square Jacobians, a simpler measurement could be  $y = \sqrt{\det [\boldsymbol{J}]}$ . This manipulability measure is perhaps the most common criterion for setting calculating singularity distance. The major justifications for its popularity are the fact that it is numerically simple to compute<sup>2</sup> and that its zeros coincide with the singularities of the Jacobian [120]. The gradient of the manipulability function (5.2) over  $\boldsymbol{\theta}$

<sup>1</sup>It is interesting to highlight that the gradient of  $y$  decreases only locally since the result is based on instantaneous kinematics [112]

<sup>2</sup>There is a easy solution using Cholesky decomposition of the Jacobian matrix, for further details, see [113].

described in [113] can be inferred using Jacobi's formula:

$$\nabla y = \frac{\partial \sqrt{\det\{\mathbf{J}\mathbf{J}^T\}}}{\partial \boldsymbol{\theta}} = \det\{\mathbf{J}\mathbf{J}^T\} \operatorname{tr}\left(\frac{\partial \mathbf{J}}{\partial \boldsymbol{\theta}} \mathbf{J}^+\right), \quad (5.3)$$

where the  $\operatorname{tr}(\mathbf{S})$  is the trace of a generic matrix  $\mathbf{S}$ . Hence, we can exploit the manipulator self-motion to optimize the manipulability function as to escape singularities.

The idea of optimizing a secondary task have been extended in [121] to multiple tasks—such as manipulability and distance to joint limits—switching dynamically (for further results, see [114–117]). Different solutions in this context are summarized in [115].

### 5.1.1.2 Planning singularity free trajectories

Instead of recovering from singularities, a different strategy is to consider all possible singularities before planning the desired trajectory. With a priori knowledge of joint configurations that cause kinematic singularities within the reachable workspace and considering boundary singularities, we can define different solutions for planning the trajectory avoiding such undesired configurations.

In [122–127], singularity configurations are estimated offline using artificial intelligence techniques such as genetic algorithms and artificial neural networks. Alternatively, singularity detection algorithms can also be derived from classic branch-and-prune algorithms combined with genetic algorithms and/or particular heuristics to improve classification of singularity free configurations against undesired singular poses [128–130].

Such strategies can be combined with the use of potential functions to online avoid previously known singularities [131] or with the use of path planning algorithms based on the knowledge of singularity free and singularity-in configurations. The configurations are thereafter connected solely on the singularity free workspace.

Since the overall strategies rely in planning and executing a singularity free trajectory, aforementioned methods can be used for both redundant and nonredundant manipulators.

### 5.1.1.3 Trajectory modification

With no previous knowledge of all possible existing singularities, the planned task trajectory might pass through a singularity region. In the case of non-redundant arms or inescapable singularities, there is only one feasible joint configuration for each pose in task-space. Hence, there can be no self-motion and the task trajectory must inevitably be modified in order to escape from singularities. In other words, avoidance is therefore achieved to the detriment of the planned task trajectory. In this sense, singularity avoidance relies on either offline replanning the trajectory based on the knowledge of all singularities (using aforementioned techniques) or on online modification of the differential kinematics based on the proximity to singular configurations [5, 6, 132, 133]. The strategy of modifying the differential kinematics yields a new task trajectory for the end-effector and consequently for the error along time.

#### **Singularity robust inverse: using damping factors**

In this scenario, the most classic technique is the singularity robust inverse (SRI) from [132], which introduces a damping factor to the least-square inverse. The method relies in a singularity robustness analysis by

introducing a damping factor ( $\lambda > 0$ ) to the least-square pseudoinverse, that is,

$$\mathbf{J}_{DLS}^+ = \mathbf{J}^T (\mathbf{J}^T \mathbf{J} + \lambda \mathbf{I})^{-1}.$$

The properties of the damped least-square solution may be studied using the singular value decomposition. The SVD of the Jacobian  $\mathbf{J}$ , order  $m \times n$ , can be represented in the form

$$\mathbf{J} = \sum_{i=1}^{\min(m,n)} \sigma_i \mathbf{u}_i \mathbf{v}_i^T, \quad (5.4)$$

where  $\mathbf{u}_i, \mathbf{v}_i$  denote the output and input singular vectors, and  $\sigma_i$  denotes the singular values (ordered from largest to smallest). The number of nonzero singular values is equal to the rank of  $\mathbf{J}$ . Hence, in the presence of singularities, one or more singular values will be zero. The traditional least-square inverse of  $\mathbf{J}$  can be represented in the form

$$\mathbf{J}^+ = \mathbf{J}^T (\mathbf{J}^T \mathbf{J})^{-1} = \sum_{i=1}^{\min(m,n)} \frac{1}{\sigma_i} \mathbf{v}_i \mathbf{u}_i^T. \quad (5.5)$$

Note that the singular vectors are orthogonal matrices. Therefore, if one of the singular values are zero, we will have  $\mathbf{J}^+ \rightarrow \infty$ . Using a damping factor ( $\lambda$ ) ensures a good conditioning in the whole manipulator's workspace, since

$$\mathbf{J}_{DLS}^+ = \mathbf{J}^T (\mathbf{J}^T \mathbf{J} + \lambda^2 \mathbf{I})^{-1} = \sum_{i=1}^{\min(m,n)} \frac{\sigma_i}{\sigma_i^2 + \lambda^2} \mathbf{v}_i \mathbf{u}_i^T.$$

With this new damped least-square (DLS) inverse, we may consider three scenarios:

- When  $\sigma_i \gg \lambda$ , we have  $\frac{\sigma_i}{\sigma_i^2 + \lambda^2} \approx \frac{1}{\sigma_i}$ , which is similar to ordinary least-square inverse. Thus, the DLS solution has little effect, i.e., in scenario far from singularities, it behaves similarly to ordinary least-square inverse  $\mathbf{J}_{DLS}^+$ . The norm of the DLS inverse in this case is about  $\|\mathbf{J}_{DLS}^+\|_2 \approx \|\mathbf{J}^+\|_2 \approx \frac{1}{\sigma_i} \ll \frac{1}{\lambda}$ . In this case, the original trajectory is remains unchanged;
- When  $\sigma_i$  are on the same order of  $\lambda$ , we have  $\frac{\sigma_i}{\sigma_i^2 + \lambda^2} \approx \frac{\lambda}{\lambda^2 + \lambda^2} \approx \frac{1}{2\lambda}$ . Hence, the norm of the DLS inverse,  $\|\mathbf{J}_{DLS}^+\|_2 \approx \frac{1}{2\lambda}$ , is about half of the norm obtained from the ordinary least-square solution,  $\|\mathbf{J}^+\|_2 \approx \frac{1}{\lambda}$ . In this case, the original trajectory is slightly modified as the Jacobian gets closer to the singular region;
- For  $\sigma_i$  smaller than  $\lambda$ , we have  $\frac{\sigma_i}{\sigma_i^2 + \lambda^2} \approx 0$ . Hence, it turns out that the norm of the DLS inverse tends to zero as the Jacobian gets closer to the singular region. On the other hand, the trajectory is largely different from the planned trajectory.

Figure 5.2 illustrates the norm damping effect. Summarizing, singular values on the on the order of (or smaller than)  $\lambda$ , the factor 'damps' the potentially high norm of the component solution, so that

$$\max(\|\mathbf{J}_{DLS}^+\|) \approx \frac{1}{2\lambda}.$$

The advantage of the nonnull damping factor is that it ensures continuity and good conditioning of the solution, even when  $\mathbf{J}$  loses rank ( $\sigma_i \rightarrow 0$ ). On the other hand, singularity avoidance is obtained at the expense of an increased reconstruction error due to the damping [6]. The task Jacobian is modified as it gets closer to singularities.



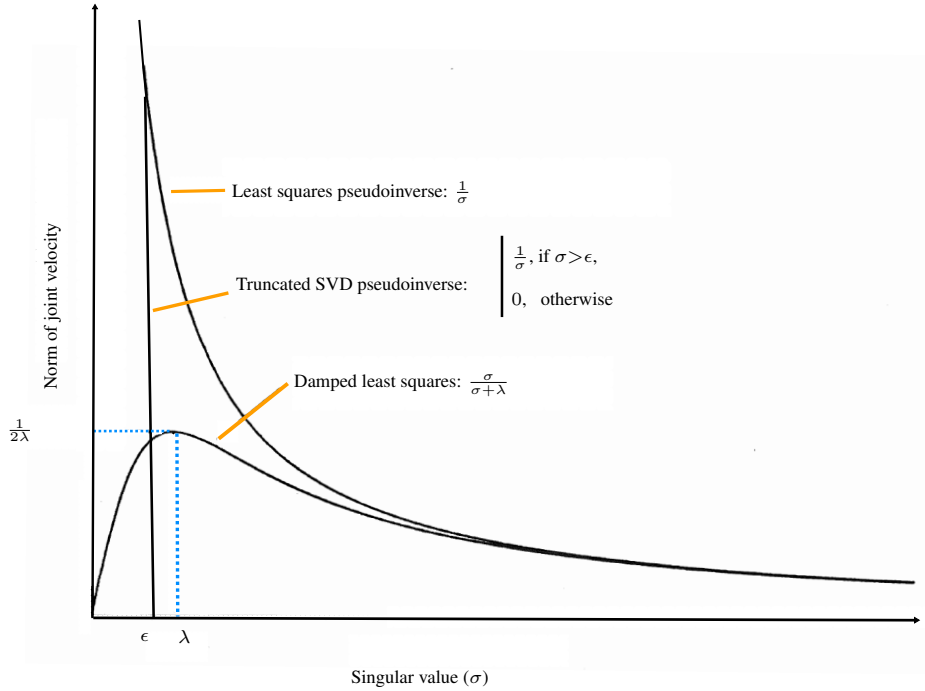


Figure 5.2: A comparison of the damped and undamped least-square solutions as a function of the singular value showing the norm of the joint velocity for a component in the direction for the singular vector associated with the plotted singular value.

The error can be reduced by both lowering the damping factor far from kinematic singularities and avoiding unnecessary damping along the feasible velocity components. In this context, an adaptive damping factor is defined in [134] based on the manipulability function of the Jacobian, and improved in [5, 6] to regard the minimum singular value of the Jacobian. In [6, 120], in addition to consider a varying damping factor that depends on the minimum singular value, they also considered the damping action only in the singularity direction through the use of the output singular vector:

$$\mathbf{J}_{SRI}^+ = \mathbf{J}^T \left( \mathbf{J}^T \mathbf{J} + \lambda_{SRI} \mathbf{u} \mathbf{u}^T \right)^{-1}$$

with an adaptive damping factor defined as

$$\lambda_{SRI} = \begin{cases} 0, & \text{if } \sigma_m \geq \epsilon, \\ \left(1 - \left(\frac{\sigma_m}{\epsilon_{SRI}}\right)^2\right) \lambda_{SRI,max}^2, & \text{if } \sigma_m < \epsilon, \end{cases}$$

where  $\sigma_m$  defines the minimum singular value from the Jacobian,  $\epsilon$  defines the size of the singular region, and  $\lambda_{max}$  sets the maximum value of the damping factor, which is used to escape the singularity.

### Truncated SVD pseudoinverse

A different solution relies in removing small terms in the minimum singular value analysis. In other words, the ordinary least-square inverse described in (5.5) is modified to accommodate the following discontinuity concerning minimum singular values:

$$\mathbf{J}^+ = \sum_{i=1}^{\min(m,n)} \frac{1}{\tilde{\sigma}_i} \mathbf{v}_i \mathbf{u}_i^T,$$

where  $\tilde{\sigma}_i$  equals the minimum singular value from (5.5) if its value is above a given threshold  $\epsilon_{\text{TSVD}}$  and zero otherwise, that is,

$$\tilde{\sigma}_i = \begin{cases} \sigma_i, & \text{if } \sigma_i \geq \epsilon_{\text{TSVD}}, \\ 0, & \text{if } \sigma_i < \epsilon_{\text{TSVD}}. \end{cases}$$

In other words, one would remove the  $i$ -nth element that corresponds to a singular value  $\sigma_i$  smaller than a given threshold. The contribution of the minimum svd  $\sigma_i$  would be null, instead of  $\infty$ . The method main advantage is the needlessness of predefined parameters, on the other hand, the method lacks continuity when the singular value becomes smaller than the given threshold which in turn causes errors and chattering as seen in Figure 5.2.

### **Direct task modification using auxiliary functions**

It is interesting to highlight that both singularity robust inverse—as well as its variations—and the truncated SVD strategies rely on modifying the pseudoinverse of the Jacobian matrix. To avoid the situation of the Jacobian rank deficiency, both techniques changes the linear mapping relation between the joint velocity vector and the task end-effector velocity space [133].

In this sense, the authors in [133], propose a method to make the task trajectory bypass the singularities and avoid the failure of the pseudoinverse of the Jacobian matrix. The basic idea is to influence the task velocity with an auxiliary function that depends on the singular direction vectors  $\mathbf{u}_S$ , that is, the set of output singular vectors from (5.4) belonging to the singular space where the corresponding minimum singular values lie below a given threshold. The auxiliary function must limit movements towards the singularity. To this aim, the authors propose a modified task velocity:

$$\partial (\text{vec } \underline{\mathbf{e}})_{\text{mod}} = \partial \text{vec } \underline{\mathbf{e}} - k \cdot \alpha \cdot (\mathbf{u}_S^T \partial \text{vec } \underline{\mathbf{e}}) \times \mathbf{u}_S,$$

where  $k$  is a characteristic function of  $\sigma_{\min}$ , i.e.,  $k = 1$  if  $\sigma_{\min}$  is below a given threshold and  $k = 0$ , otherwise. The function  $\alpha$  is the weighting function that varies from 1 to 0 according to the value of  $\sigma_{\min}$  (it assures the continuity of the function).

The method can also be seen as a disturbance along the original task which may lead to unstable situations, particularly due to the ad-hoc characteristics of the design function. The main drawback of the method concerns exactly the fact that there is no stability criterion to analyze the feasibility of the method, nor a stabilization technique to provide a suitable controller.

#### 5.1.1.4 Other singularity avoidance strategies

In [135, 136], it is proposed an hybrid approach for singularity avoidance. According to a singular minimum value manipulability function that defines the distance to singularities from the current pose, the avoidance technique relies on the switching between three different controllers: one based on the inverse of the Jacobian, one based on the pseudoinverse calculation, and one based on the inverse kinematics for the singularity region.

In [137–139], it is proposed a singularity avoidance technique based on virtual joints. The task Jacobian is augmented in order to consider virtual joints that only exist computationally, not physically, and a nullspace optimization prevents forces/velocity of the virtual joints. With the augmented Jacobian, its rank is increased which in turn allows control in the region of singularity but preventing movements in the singularity direction.

Recently, novel singularity avoidance techniques have also focused on designing algorithms to dynami-

cally estimate the inverse of the Jacobian matrix—instead of considering its pseudoinverse. In [140, 141], for instance, the dynamics of the inverse estimative stems from the error between its value and the Jacobian whereby the convergence is shown to be exponential in the case of a constant Jacobian. The main advantage of the proposed strategy is the absence of finite escapes due to convergence time of the estimator. On the other hand, as avoidance is not explicitly considered, slow convergence may still lead the arm to a singular pose.

## 5.2 DUAL QUATERNION $H_\infty$ SINGULARITY AVOIDANCE CONTROL

In preceding chapters, we derived novel results on exponential stability,  $H_\infty$  control, tracking and optimal control of the end-effector pose using dual quaternion framework which describes the rigid body coupled rotation and translation kinematics in a compact and complete way without representation singularities. Nonetheless, the proposed criteria strongly rely on the assumption that the pseudoinverse of the Jacobian matrix is well-defined at any given configuration, that is, it never meets singular points. Therefore, due to the problems that arise from the loss of degree of freedom and to ensure proper manipulability throughout the whole end-effector task-space, we are also interested in investigating robustness properties against kinematic singularities.

Herein, we are interested in a general solution that can be applied to any serial manipulator without the need of preprocessing for each application or robot manipulator. Hence, among aforementioned techniques for singularity avoidance, this section exploits the feasibility of solutions using self-motion in the case of a redundant manipulator and trajectory modification for inescapable singularities in redundant and non-redundant manipulators.

### 5.2.1 Redundant arms

Redundant arms may avoid and recover from singular poses using self-motion. As stressed in Section 5.1, a secondary task optimization can be defined in the nullspace of the Jacobian (5.1). In the context of singularity avoidance strategies, the task to optimized is the gradient a given manipulability function as in (5.2)-(5.3). Since the optimization is performed along the joint velocity vector, singularity avoidance strategies based on self-motion can be directly extended to control results herein as long as they are defined in the nullspace of the task Jacobian—in other words, as long as they have no influence on the task trajectory.

The solution when using the dual quaternion based end-effector pose Jacobian ( $\mathbf{J}_{\text{vec}}$ ) is straightforward as the Jacobian maps changes in the  $n$ -joint serial configuration to changes in the task-space mapped to an  $\mathbb{R}^8$  manifold—Subsection 2.7.2.

When using the dual quaternion Jacobian ( $\mathbf{J}_{\underline{q}}$ )—Subsection 2.7.3—we are interested in the map from the  $\mathbb{R}^n$  joint velocity to the rigid body twist of the end-effector in  $\mathbb{H}_0 \otimes \mathbb{D}$ . Still the Jacobian defines such mapping through the isomorphism from  $\mathbb{R}^6$  to  $\mathbb{H}_0 \otimes \mathbb{D}$ —Definition 2.12. In this sense, a secondary optimization can also exploit the nullspace of the task Jacobian  $\mathbf{J}_{\underline{q}}$ . The resulting movement from this optimization has no influence upon the error trajectory defined in  $\text{Spin}(3) \times \mathbb{R}^3$ . Indeed, it yields a nullvector in  $\mathbb{R}^6$  which, from the isomorphism mapping from  $\mathbb{H}_0 \otimes \mathbb{D}$  to  $\mathbb{R}^6$ , represents a null twist upon the end-effector trajectory. In this sense, classic self-motion techniques (see Section 5.1) can be straightforwardly applied within the proposed dual quaternion based framework.

## 5.2.2 Non-redundant arms and inescapable singularities

In the case of non-redundant arms or inescapable singularities, there is only feasible joint configuration for each pose in task-space and the trajectory must inevitably be modified in order to escape from singularities. Avoidance is therefore achieved to the detriment of the planned task trajectory.

Despite the large literature on trajectory modification for singularity avoidance (see Section 5.1), the requirement for task modification however contrasts with the lack of results concerning their influence upon non-Euclidean manifolds. There are no studies on the modification of the task trajectory at a non-Euclidean manifold such as the dual quaternion space. In fact, there are no results in the literature concerning any technique for singularity avoidance within dual quaternion space.

Due to the isomorphism mapping from  $\mathbb{R}^6$  to  $\mathbb{H}_0 \otimes \mathbb{D}$ , robust inverse techniques could be used to limit the norm of the pseudoinverse of the Jacobian  $\underline{\mathbf{J}}_{\underline{\mathbf{w}}}$ . Nonetheless, there is no mathematical foundation that ensures stability or justify the use of existing techniques within a dual quaternion manifold task-space.

In this sense, we define a new singularity avoidance strategy that exploits the dual quaternion  $H_\infty$  performance criterion—as well as the lack of representation singularities—to establish stability properties and bound the worst-case influence of the modification technique over the task trajectory more straightforwardly than [6].

At the vicinity of singular configurations, we introduce an induced exogenous twist acting upon the dual quaternion spatial difference, (3.46) and (3.53), such that the trajectory escapes unachievable components of the task velocity. The strategy is similar to the one proposed in [133] for Euclidean manifolds. Nonetheless, in contrast to [133], the influence of the induced signal upon the trajectory error is bounded and the robust stability and performance of the end-effector trajectory are ensured.

The design of the induced exogenous twist must be proportional to a given manipulability function. Note that the most-widely employed function  $y = \sqrt{\det \{ \mathbf{J}^T \mathbf{J} \}}$ —whereby a singular point is represented by  $y=0$  (see Section 5.1)—lacks monotonicity and, consequently, poorly quantifies the proximity to singularities. For instance, given two positive matrices  $\mathbf{A} = \text{diag}(100, 0.02)$  and  $\mathbf{B} = \mathbf{I}$ . The matrix  $\mathbf{A}$  is closer to its singularity and to lose rank, still  $\det \{ \mathbf{A} \} > \det \{ \mathbf{B} \}$ . Moreover, if we assume a time-varying matrix  $\mathbf{A}(t)$  with  $\mathbf{A}(t_1) = \mathbf{A}$  and  $\mathbf{A}(t_2) = \text{diag}(300, 0.01)$ . Clearly, the matrix  $\mathbf{A}(t)$  is moving towards the singularity—minimum singular value changes from 0.02 to 0.01—but from inspection one can see that the determinant has increased from 2 to 3. It turns out that the determinant is actually not monotonic with regard to the singularity proximity.

In this sense, we shall consider herein a more appropriate choice for manipulability based on the minimum singular value of  $\underline{\mathbf{J}}_{\underline{\mathbf{w}}}$ , i.e.,  $\sigma_m \{ \underline{\mathbf{J}}_{\underline{\mathbf{w}}} \}$ . The singular value decomposition is the most powerful tool to investigate the singularity of the robot manipulators—nonredundant or redundant [142]. Hence, the following induced twist, which ensures continuity and a good shape for the solution, is adopted

$$\mathbf{v}_{s.a.} = \varsigma(\sigma_m \{ \underline{\mathbf{J}}_{\underline{\mathbf{w}}} \}) \cdot \mathbf{u}_m \{ \underline{\mathbf{J}}_{\underline{\mathbf{w}}} \}, \quad (5.6)$$

where  $\mathbf{u}_m \{ \underline{\mathbf{J}}_{\underline{\mathbf{w}}} \}$  represents the output singular vector corresponding to the minimum singular value  $\sigma_m \{ \underline{\mathbf{J}}_{\underline{\mathbf{w}}} \}$ . The function  $\varsigma$  denotes the magnitude of the disturbance, which is given by

$$\varsigma(\sigma_m \{ \underline{\mathbf{J}}_{\underline{\mathbf{w}}} \}) = \begin{cases} \varsigma_{\max} \cdot \left( 1 - \sqrt{\frac{\sigma_m \{ \underline{\mathbf{J}}_{\underline{\mathbf{w}}} \}}{\varsigma_s}} \right), & \text{if } \sigma_m \{ \underline{\mathbf{J}}_{\underline{\mathbf{w}}} \} \leq \varsigma_s, \\ 0, & \text{otherwise.} \end{cases} \quad (5.7)$$

where  $\varsigma_{\max}$  is the maximum value for the induced twist and  $\varsigma_s$  defines the size order of the singular region

$(\sigma_m\{\underline{\mathbf{J}}\}) > \varsigma_s$  yields a null twist). The magnitude of  $\zeta(\sigma_m\{\underline{\mathbf{J}}\})$  and, consequently, the influence of the singularity avoidance disturbance is monotonically decreasing, that is, it increases as  $\sigma_m\{\underline{\mathbf{J}}\} \rightarrow 0$ .

In terms of control law, the induced vector (5.6) can be viewed as an exogenous disturbance over the task trajectory. Hence, the modified task trajectory can be defined by

$$\dot{\underline{\mathbf{x}}}_e = \left( \frac{1}{2} \sum_{i=0}^{n-1} \dot{\underline{\mathbf{j}}}_i \dot{\theta}_{s.a.,i} + \underline{\mathbf{v}}_{s.a.} \right) \underline{\mathbf{x}}_e - \frac{1}{2} \underline{\mathbf{x}}_e \underline{\boldsymbol{\omega}}_d \quad (5.8)$$

where  $\underline{\boldsymbol{\omega}}_d$  is the twist for the desired pose in inertial frame and  $\underline{\mathbf{x}}_e = \mathbf{r}_e + \frac{1}{2} \varepsilon \mathbf{p}_e \mathbf{r}_e$ . Using Theorem 3.7 and Corollary 3.1 from Section 3.3, we can bound the influence of the induced vector (5.6) over the control error while ensuring stability properties.

### Theorem 5.1 $H_\infty$ Singularity Avoidance Technique

For prescribed positive scalars  $\gamma_o, \gamma_\tau, \varsigma_{\max}$  and  $\varsigma_s$ , the task-space controller that yields joints velocities inputs

$$\begin{aligned} \dot{\theta}_{s.a.} = & \underline{\mathbf{J}}_\omega^+ \left[ \mathbf{K}_o \text{vec}_3^T(\text{Im}(\mathbf{r}_e)) \quad -\mathbf{K}_\tau \text{vec}_3^T(\mathbf{p}_e) \right]^T \\ & + \underline{\mathbf{J}}_\omega^+ \left( \frac{1}{2} \text{vec}_6(\underline{\mathbf{x}}_e \underline{\boldsymbol{\omega}}_d \underline{\mathbf{x}}_e^*) \right), \end{aligned} \quad (5.9)$$

with  $\mathbf{K}_o \geq 2\gamma_o^{-1}$  and  $\mathbf{K}_\tau \geq \sqrt{2}\gamma_\tau^{-1}$  ensures exponential stability for the closed-loop system (5.8)-(5.9) with an attenuation upper bounded,  $\gamma_o, \gamma_\tau$ , between the singularity avoidance twist and the trajectory rotational and translational errors in the  $H_\infty$  sense.

*proof.*

First, let us define a error function similarly to (3.7), that is,  $\underline{\mathbf{e}} = 1 - \underline{\mathbf{x}}_e = \mathbf{e} + \varepsilon \mathbf{e}'$ . If we address, as variable of interest, the orientation and translational errors from (5.8) considering the above-defined error definition  $\underline{\mathbf{e}}$ , that is,  $\mathcal{O}(\underline{\mathbf{e}}) \triangleq 1 - \mathbf{r}_e$ , and  $\mathcal{T}(\underline{\mathbf{e}}) \triangleq \mathbf{p}_e$ , then (5.9) equals to the task-space controller defined in (3.54)—Theorem 3.8. Hence, using exactly the same procedures from Theorem 3.7 and Corollary 3.1, the closed loop system (5.8)-(5.9) achieves exponential stability with minimum control effort and ensures  $H_\infty$  attenuation in the sense of Definition 3.3 between the end-effector pose error and the norm of the singularity avoidance twist.  $\square$

*Remark 5.1.* The differential equation (5.8) is well-posed [89, Prop. 2.1] as  $\underline{\mathbf{v}}_{s.a.}$  lies in the Lie algebra of  $\text{Spin}(3) \times \mathbb{R}^3$ .

Using (5.6) in Theorem 5.1, we can escape singular configurations while controlling the exactness of the solution in the sense of Definition 3.3, that is, the exact influence of the induced twist over the orientation and translational errors. Since  $\mathbf{u}_m\{\underline{\mathbf{J}}\}$  in (5.6) stems from an unitary matrix, we have  $\|\mathbf{u}_m\{\underline{\mathbf{J}}\}\|_2 = 1$  whereby we conclude that  $\|\underline{\mathbf{v}}_{s.a.}\|_2 \leq \varsigma_{\max}$ .

Hence, the worst-case influence from (5.6) over  $\|\mathcal{O}(\underline{\mathbf{e}})\|_2$  and  $\|\mathcal{T}(\underline{\mathbf{e}})\|_2$  is respectively attenuated with prescribed performance gains  $\gamma_o, \gamma_\tau$ , such that the trajectory errors are always smaller than  $\gamma_o \varsigma_{\max}$  and  $\gamma_\tau \varsigma_{\max}$ . Also,  $\underline{\mathbf{x}}$  converges exponentially to  $\underline{\mathbf{x}}_d$  at points removed from singularities, that is,  $\underline{\mathbf{v}}_{s.a.} \equiv 0$ . To the best of the authors knowledge, the proposed dual quaternion based  $H_\infty$  singularity-avoidance strategy is the first criterion to *explicitly* specify a maximum value for the trade-off between exactness and avoidance feasibility.

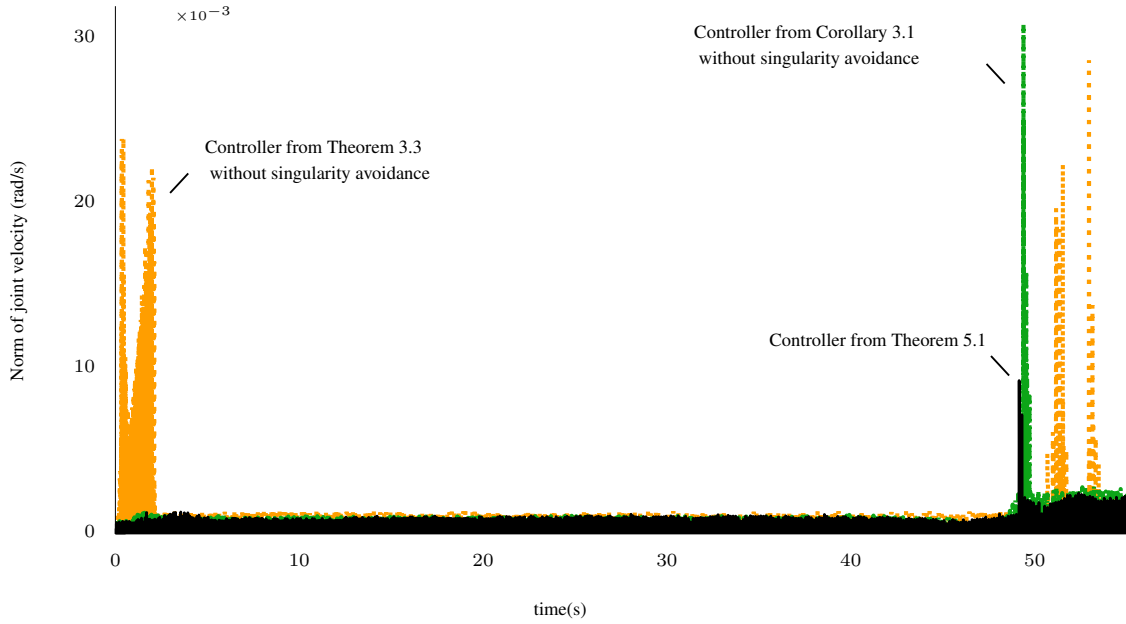


Figure 5.3: Joint velocities for a trajectory in the presence of singularities: controller from Theorem 3.3 and Corollary 3.1 without singularity avoidance consideration (green dashed and orange point-dashed lines) compared to Theorem 5.1 (solid black line).

### 5.3 SIMULATIONS

This section assesses the effectiveness and advantages of the proposed dual quaternion singularity avoidance technique for inescapable singularities based on the  $H_\infty$  criteria presented in Section 3.3. To this aim, we devise a realistic scenario similarly to the one presented in Examples 3.3 and 3.4 from Section 3.4 using the Virtual Experimentation Platform (VREP) from Coppelia Robotics GmbH (see, [90]) with Bullet Physics Library<sup>3</sup> as the physics engine, and the DQ\_Robotics toolbox<sup>4</sup> for control implementation.

In this scenario, the tracking task trajectory should lead the manipulator through multiple singularities. Initially, the desired configuration for the end-effector pose is set close to a singular configuration, which is unknown beforehand. The proposed tracking trajectory should take the arm through this unknown singularity, where the arm may lose several degrees of freedom, to a regular pose in the reachable workspace and then back to the initial pose—going through the singularity.

The lack of a proper singularity avoidance strategy and its consequences are illustrated in Figure 5.3 and compared to the proposed singularity avoidance solution in Theorem 5.1. The singularity avoidance controller was implemented using  $\zeta_{\max}=0.01$  and  $\zeta_s=10^{-5}$ . The results highlight the importance of an avoidance technique and how essential it is to prevent joint chattering and large velocities and accelerations in the vicinity of singular configurations.

Moreover, in order to compare the performance of the proposed technique with classic singularity avoidance techniques, we implemented the singularity robust inverse method with adaptive damping rate adjustment from [6]. Since the task trajectory modification from the SRI algorithm has not yet been studied within the dual quaternion space and there is no mathematical foundation that ensures stability in this context, we chose to

<sup>3</sup><http://www.bulletphysics.org/>

<sup>4</sup><http://dqrobotics.sourceforge.net>

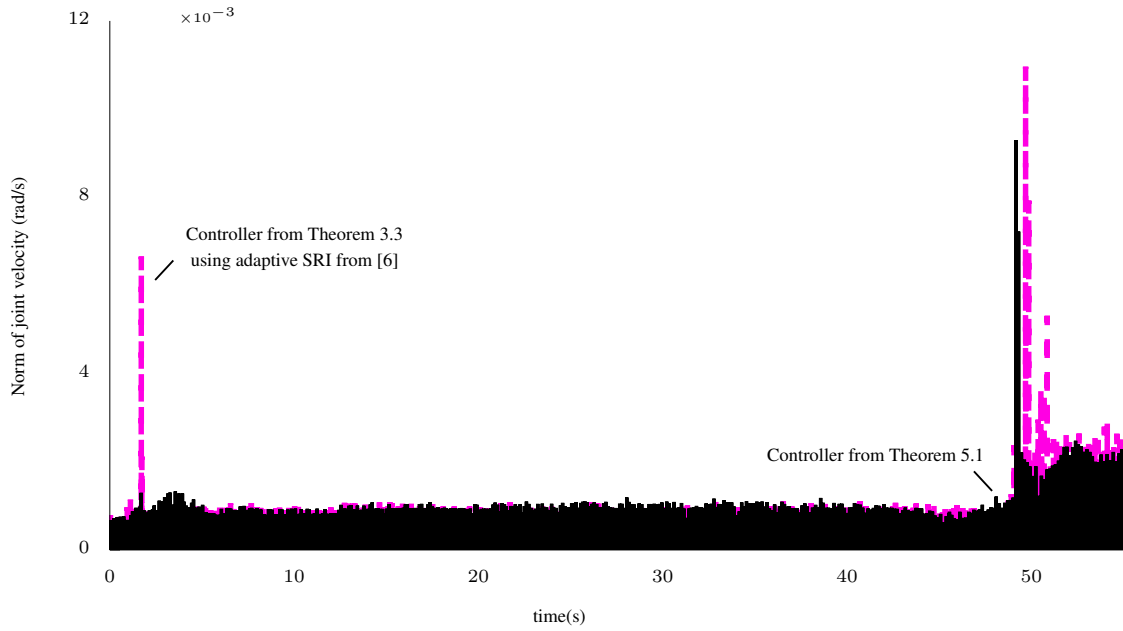


Figure 5.4: Joint velocities for a trajectory in the presence of singularities: controller from Theorem 3.3 with adaptive SRI from [5, 6] (magenta dashed line) compared to Theorem 5.1 (solid black).

implement the technique with the controller from Theorem 3.3 that is defined using the Jacobian mapping ( $\mathbf{J}_{\text{vec}}$ ) to an  $\mathbb{R}^8$  manifold. The adaptive SRI algorithm is particularly sensitive to parameters selection, thus we have tried several combinations. The parameters with better performance were  $\lambda_{\text{SRI}, \text{max}}^2 = 10^{-5}$  and  $\epsilon_{\text{SRI}} = 3 \cdot 10^{-4}$ .

The comparison is shown in Figure 5.4 and clearly illustrates that despite the adaptive SRI successful improvement compared to the lack of an avoidance method, the proposed dual quaternion based avoidance technique yields better performance results in the sense of reducing joint velocities and chattering in the vicinity of singularities.

# 6

## HYBRID ROBUST KINEMATIC CONTROL FOR GLOBAL STABILITY USING DUAL QUATERNIONS

---

When we learn how to deal effectively with systems that contain interacting groups of entities or processes of distinct characteristics, we will probably stop calling them “hybrid systems,” because at that stage the distinct character of the system’s parts will be of no importance or significance anymore and there will be no need any longer for the hybrid nature to be stressed in a name. That is, success will bring the loss of identity! This is of course only a conjecture – Panos J. Antsaklis And Anil Nerode [143]

The work and contributions presented in this thesis are based on dual quaternion representation of rigid body motion. Nonetheless, in scenarios where the state space of the dynamical system is not the Euclidean space  $\mathbb{R}^n$  but a general differentiable manifold  $\mathcal{M}$ —which is exactly the case of  $SE(3)$  and  $\text{Spin}(3) \times \mathbb{R}^3$ —some difficulties to design a stabilizing closed-loop controller may arise. In fact, if  $\mathcal{M}$  has the structure of a vector bundle over a compact manifold  $\mathcal{L}$ , then no continuous vector field on  $\mathcal{M}$ —indeed, nor in  $\mathcal{L}$ —has a globally asymptotically stable equilibrium [42]. In particular, this means that it is impossible to design a continuous feedback that globally stabilizes the pose of a rigid body, as in this case the closed-loop system state space manifold is a trivial bundle over the compact manifold  $SO(3)$ . The same topological obstruction is also present in the group of unit dual quaternions since its underlying manifold is a trivial bundle over the unit sphere  $\mathcal{S}^3$  (see Theorem 2.2).

Due to the two-to-one covering map  $\text{Spin}(3) \times \mathbb{R}^3 \rightarrow SE(3)$ , the unit dual quaternion group is endowed with a double representation for every pose in  $SE(3)$  (see (2.21) in Subsection 2.5.1)—similarly to unit quaternions [144, p. 190]. Neglecting the double covering yields to the problem of unwinding whereby solutions close to the desired pose in  $SE(3)$  may travel farther to the antipodal unit dual quaternion representing the same pose [59]. There are scarce works on unwinding avoidance in the context of pose stabilization using unit dual quaternions [52, 58–60]. All of them are based on a discontinuous sign-based feedback approach.

As shown by [43] for the particular case of  $\text{Spin}(3)$ , the discontinuous sign-based approach may however be particularly sensitive to measurement noises, and despite achieving global stability, global attractivity properties may be detracted with arbitrarily small measurement noises. As one would expect, the same happens with  $\text{Spin}(3) \times \mathbb{R}^3$ .

In  $\text{Spin}(3) \times \mathbb{R}^3$  the lack of robustness is even more relevant as the discontinuity of the controller not only affects the rotation, but may also disturb and deteriorate the trajectory of the system translation—as verified in Section 6.1. In this context, arbitrary small noises may lead to chattering, performance degradation—and in the worst case, prevent stability.

Summing up, despite the solid contributions in the literature on dual quaternion based controllers and the contributions presented in this thesis, it is important to emphasize that existing pose controllers are either stable only locally, or sensitive to arbitrarily small measurement noises. In other words, the topological constraints from  $\text{Spin}(3) \times \mathbb{R}^3$ , most of them inherited from  $SE(3)$ , still poses a challenge and there exists no result in the literature that ensures robust global stability.



In this context, using dual quaternion formalism, this chapter addresses the problem of globally stabilizing a rigid body pose. An hybrid strategy is used to design a switching control law with hysteresis in such a way that the global asymptotic stability of the closed-loop system is guaranteed and such that the controller is robust against arbitrary small perturbations. The resulting controller is written in terms of the rigid body twist within unit dual quaternion formalism. Moreover, we adapt the proposed hybrid criterion to global stability in the context of robot manipulators and using the proposed controllers from previous chapters. Last, using numerical simulations, we illustrate the problems that arise from neglecting the double cover—as unwinding and chattering—and verify the effectiveness of the proposed controller to solve the robust global pose stability problem.<sup>1</sup>

## 6.1 DUAL QUATERNION BASED DISCONTINUOUS CONTROL LAW FOR POSE STABILIZATION

Due to the topological constraint described in Theorem 2.2, there is no continuous state feedback controller on  $\underline{S}$  that can globally asymptotically stabilize the rigid body motion (2.26):

$$\dot{\underline{x}} = \frac{1}{2} \underline{\omega} \underline{x}, \quad (6.1)$$

to a rest configuration, where  $\underline{\omega} = \omega + \varepsilon(\dot{\mathbf{p}} + \mathbf{p} \times \omega)$  is the generalized twist expressed in inertial frame with  $\omega$  and  $\dot{\mathbf{p}}$  being the angular and linear velocities expressed in the inertial frame.

Indeed, the two-to-one covering map from  $\text{Spin}(3) \times \mathbb{R}^3$  to  $SE(3)$  renders a closed-loop system with two distinct equilibria  $\underline{x}_e$  and  $-\underline{x}_e$  (see (2.21) in Subsection 2.5.1). Since both  $\pm \underline{x}_e$  correspond to the same configuration in  $SE(3)$ , solutions neglecting the double cover (see, for example, [36, 49, 61–63]) may exhibit the unwinding phenomenon [42]. In this case, solutions starting arbitrarily close to the desired pose in  $SE(3)$ —represented by both stable and unstable points in  $\text{Spin}(3) \times \mathbb{R}^3$ —may travel to the farther stable point instead to the nearest unstable point (see, for example, Figure 6.5). The sole contributions in the sense of avoiding the unwinding and stabilizing (2.26) to the set  $\{\pm 1\}$  are based on a pure discontinuous control law introduced in [58–60]. In terms of the components of  $\underline{x} = \eta + \boldsymbol{\mu} + \varepsilon(\eta' + \boldsymbol{\mu}')$ , this discontinuous control law is given by<sup>2</sup>

$$\underline{\omega} = \begin{cases} -2k \left[ \text{acos}(\eta) \frac{\boldsymbol{\mu}}{\|\boldsymbol{\mu}\|} + \varepsilon(\eta \boldsymbol{\mu}' - \eta' \boldsymbol{\mu} - \boldsymbol{\mu} \times \boldsymbol{\mu}') \right], & \text{if } \eta \geq 0, \\ -2k \left[ (\text{acos}(\eta) - \pi) \frac{\boldsymbol{\mu}}{\|\boldsymbol{\mu}\|} + \varepsilon(\eta \boldsymbol{\mu}' - \eta' \boldsymbol{\mu} - \boldsymbol{\mu} \times \boldsymbol{\mu}') \right], & \text{if } \eta < 0, \end{cases} \quad (6.2)$$

where  $k$  is a proportional gain.

Albeit this control law avoids unwinding, a careful look reveals a strong sensitivity around attitudes that are up to  $\pi$  away from the desired attitude about some axis—that is,  $\eta = 0$ . In view of Theorem 2.6 of [145], one can see that such control law lacks robustness in the sense that arbitrarily small measurement noises can force  $\eta$  to stay near to 0 for initial conditions within its neighborhood. Indeed, similar to Theorem 3.2 of [43], one can even exhibit an explicit noise signal to persistently trap the system about a fixed pose, thus preventing its stability. To illustrate the sensitivity of pure discontinuous state feedback controllers, we introduce a simple

<sup>1</sup>It is important to underline that the work described in this chapter was developed in collaboration with Hugo Tadashi Kussaba, a PhD student from University of Brasilia.

<sup>2</sup>The discontinuous kinematic control law in [58–60] contains a typo that have been fixed in [52]. Different from (6.2), in [52, 58–60] the controller is expressed in terms of the logarithm of an unit dual quaternion.

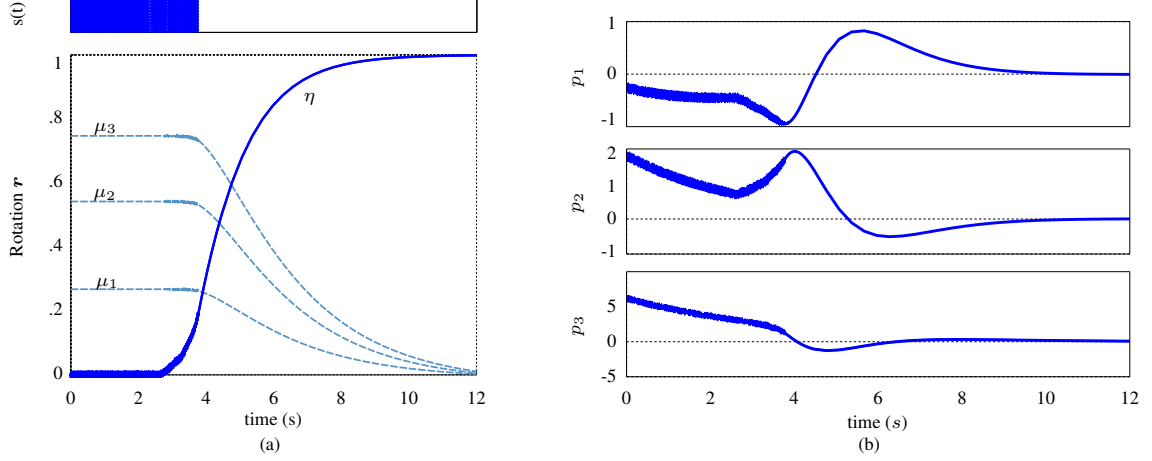


Figure 6.1: (a) Trajectory of the rotation unit quaternion  $r$  in terms of  $\eta$  and  $\mu$  (dashed line) with switches along time between the control laws in (6.2) represented by  $s(t)$ . (b) Trajectory of the three-dimensional translation elements  $p = p_1\hat{i} + p_2\hat{j} + p_3\hat{k}$ .

case study in which the trajectory of the system kinematics (6.1) is simulated using the discontinuous control law (6.2) in the presence of a small random measurement noise<sup>3</sup>—the results are shown in Figure 6.1.

The trajectory of the closed-loop system exhibits chattering in the neighborhood of the discontinuity—that lies in  $\eta = 0$ —as a result of the measurement noise. The performance degradation stems from infinitely fast switches in (6.2). Furthermore, the chattering influence over the system is not restricted to the attitude error and may also impact on the resulting trajectory of the translation, as shown in Figure 6.1(b). In this sense, the lack of robustness of a discontinuous solution may lead to chattering in orientation and to additional disturbances in the translation of the rigid motion in the presence of arbitrarily small random noises.

## 6.2 HYBRID CONTROL LAW FOR ROBUST GLOBAL RIGID BODY STABILIZATION

In this section, we address the control design problem for globally stabilizing a rigid body coupled rotational and translational kinematics with no representation singularities. The proposed solution copes with the topological constraint inherent from the  $\text{Spin}(3) \times \mathbb{R}^3$  parametrization while also ensuring robustness against measurement noises.

To avoid the unwinding phenomenon and the lack of robustness from pure discontinuous solutions, we appeal to the hybrid system formalism of [146]. A hybrid system is given by the constrained differential inclusions

$$\begin{aligned} \dot{x} &\in F(x), & x &\in C, \\ x^+ &\in G(x), & x &\in D, \end{aligned} \tag{6.3}$$

where  $x^+$  denotes the next state of the hybrid system after a jump. The flow map  $F$  and the jump map  $G$  are set-valued functions, respectively, modeling the continuous and the discrete time dynamics of the system. The

<sup>3</sup>The simulation has been performed in accordance with the procedures described in Section 6.3.

flow set  $C$  and the jump set  $D$  are the respective sets where the evolutions occur. The following concepts of set-valued analysis will also be used: a set-valued mapping  $F$  is outer semicontinuous if its graph is closed and  $F$  is locally bounded—that is, if for any compact set  $K$ , there exists  $m > 0$  such that  $F(K) \subset m\mathbb{B}$ , where  $\mathbb{B}$  is the closed unit ball in the Euclidean space of the convenient dimension [147]. For more details, the reader is referred to [146, 148].

To solve the problem of robust global asymptotic stabilization of (6.1), we propose a generalization to the hysteresis-based hybrid control law of [43] that extends the attitude stabilization to render both coupled kinematics—attitude and translation—stable. The controller is designed as a general controller for rigid body stabilization, hence it is described as a dual quaternion twist. The general purpose control law is thus proposed as

$$\underline{\omega} \triangleq h\omega_1 + \varepsilon\omega_2, \quad (6.4)$$

where  $\omega_1$  and  $\omega_2$  are pure quaternions and  $h \in \{-1, 1\}$  is a memory state with hysteresis characterized by a parameter  $\delta \in (0, 1)$ . The memory state  $h$  has its dynamics defined by

$$\begin{aligned} \dot{h} &\triangleq 0, & \text{when } (\underline{x}, h) \text{ are such that } h\eta \geq -\delta, \\ h^+ &\in \overline{\text{sgn}}(\eta), & \text{when } (\underline{x}, h) \text{ are such that } h\eta \leq -\delta, \end{aligned} \quad (6.5)$$

where  $\overline{\text{sgn}}$  is the set-valued function defined as

$$\overline{\text{sgn}}(s) \triangleq \begin{cases} \{1\}, & s > 0, \\ \{-1\}, & s < 0, \\ \{-1, 1\}, & s = 0. \end{cases}$$

In terms of the hybrid formalism (6.3), the closed loop system made by (6.1), (6.4), and (6.5) is characterized as

$$\begin{aligned} F(\underline{x}, h) &= \left( \frac{1}{2}\underline{\omega}\underline{x}, 0 \right), \\ G(\underline{x}, h) &\in (\underline{x}, \overline{\text{sgn}}(\eta)), \\ C &= \{(\underline{x}, h) \in (\text{Spin}(3) \times \mathbb{R}^3) \times \{-1, 1\} : h\eta \geq -\delta\}, \\ D &= \{(\underline{x}, h) \in (\text{Spin}(3) \times \mathbb{R}^3) \times \{-1, 1\} : h\eta \leq -\delta\}. \end{aligned} \quad (6.6)$$

Based on the dual quaternion mapping to  $\mathbb{R}^8$  defined in (2.14) and based on the Hamilton operators (2.15), the maps  $F$  and  $G$  of (6.6) induce the function  $\vec{F} : \mathbb{R}^9 \rightarrow \mathbb{R}^9$  and the set-valued mapping  $\vec{G} : \mathbb{R}^9 \rightrightarrows \mathbb{R}^9$  given by

$$\begin{aligned} \vec{F}(\vec{x}, h) &= \left( \frac{1}{2}\vec{H}(\underline{x}) \text{vec}_8(\underline{\omega}), 0 \right) \\ \vec{G}(\vec{x}, h) &\in (\vec{x}, \overline{\text{sgn}}(x_1)), \end{aligned} \quad (6.7)$$

where  $\vec{x} = (x_1, \dots, x_8) \in \mathbb{R}^8$  and  $h \in \mathbb{R}$ . Similarly, the sets  $C$  and  $D$  of (6.6) induce the subsets  $\vec{C}$  and  $\vec{D}$  of

$\mathbb{R}^9$  given by<sup>4</sup>

$$\begin{aligned}\vec{C} &= \{(\vec{x}, h_r) \in \mathbb{R}^8 \times \mathbb{R} : (\vec{x}, h_r) \in \underline{\mathcal{S}} \times \{-1, 1\} \text{ and } h_r x_1 \geq -\delta\}, \\ \vec{D} &= \{(\vec{x}, h_r) \in \mathbb{R}^8 \times \mathbb{R} : (\vec{x}, h_r) \in \underline{\mathcal{S}} \times \{-1, 1\} \text{ and } h_r x_1 \leq -\delta\}.\end{aligned}\quad (6.8)$$

The following lemma proves that the hybrid system induced by (6.1), (6.4) and (6.5) satisfies some properties which helps to prove the stability of the system and its robustness.

### Lemma 6.1

The maps  $\vec{F}$  and  $\vec{G}$  defined on (6.7) and the sets  $\vec{C}$  and  $\vec{D}$  defined on (6.8) satisfy the following properties:

1.  $\vec{C}$  and  $\vec{D}$  are closed sets in  $\mathbb{R}^9$ .
2.  $\vec{F} : \mathbb{R}^9 \rightarrow \mathbb{R}^9$  is continuous.
3.  $\vec{G} : \mathbb{R}^9 \rightrightarrows \mathbb{R}^9$  is an outer semicontinuous set-valued mapping, locally bounded and  $\vec{G}(\vec{x}, h)$  is nonempty for each  $(\vec{x}, h) \in \vec{D}$ .

*proof.*

The proof is based on Lemma 5.1 of [43]. Setting  $\delta \in (0, 1)$ , consider the continuous map  $\tau : \mathbb{R}^9 \rightarrow \mathbb{R}$  given by  $\tau(x_1, \dots, x_8, h_r) = h_r x_1 + \delta$ . The restriction of this map to  $\underline{\mathcal{S}} \times \{-1, 1\}$ ,  $\tau|_{\underline{\mathcal{S}} \times \{-1, 1\}} : \underline{\mathcal{S}} \times \{-1, 1\} \rightarrow \mathbb{R}$  is also continuous (Theorem 8 of [149]). Moreover, by the definition of the sets  $\vec{C}$  and  $\vec{D}$ , we have that

$$\begin{aligned}\vec{C} &= \tau|_{\underline{\mathcal{S}} \times \{-1, 1\}}^{-1}([0, +\infty)), \\ \vec{D} &= \tau|_{\underline{\mathcal{S}} \times \{-1, 1\}}^{-1}((-\infty, 0]).\end{aligned}$$

Since the pre-image of a closed set under a continuous mapping is closed,  $\vec{C}$  and  $\vec{D}$  are closed in  $\underline{\mathcal{S}} \times \{-1, 1\}$  (with respect to the subspace topology). We also have that  $\underline{\mathcal{S}} \times \{-1, 1\}$  is closed in  $\mathbb{R}^9$ . In fact, consider the continuous functions  $p, d : \mathbb{R}^8 \rightarrow \mathbb{R}$  given respectively by

$$\begin{aligned}p(\eta, \mu_1, \mu_2, \mu_3, \eta', \mu'_1, \mu'_2, \mu'_3) &= [\eta, \mu_1, \mu_2, \mu_3][\eta, \mu_1, \mu_2, \mu_3]^T - 1, \\ d(\eta, \mu_1, \mu_2, \mu_3, \eta', \mu'_1, \mu'_2, \mu'_3) &= [\eta, \mu_1, \mu_2, \mu_3][\eta', \mu'_1, \mu'_2, \mu'_3]^T.\end{aligned}$$

By the definition of  $p$  and  $d$ ,  $\underline{\mathcal{S}} = p^{-1}(\{0\}) \cap d^{-1}(\{0\})$ . Since  $\{0\}$  is a closed set of  $\mathbb{R}$ , the sets  $p^{-1}(\{0\})$  and  $d^{-1}(\{0\})$  are closed and their intersections are closed. Thus,  $\underline{\mathcal{S}}$  is closed in  $\mathbb{R}^8$ . Moreover, the set

<sup>4</sup>Using the vector isomorphism described in (2.14), the maps  $\vec{F}$ ,  $\vec{G}$  and the sets  $\vec{C}$  e  $\vec{D}$  are explicitly described in the vector space as

$$\begin{aligned}\vec{F}(\eta, \mu, \eta', \mu', h) &= \frac{1}{2} \begin{bmatrix} -h\omega_1^T \mu \\ h\eta\omega_1 + \omega_1 \times \mu \\ -\omega_2^T \mu - h\omega_1^T \mu' \\ \eta\omega_2 + h\eta'\omega_1 + \omega_2 \times \mu + h\omega_1 \times \mu' \\ 0 \end{bmatrix}, \\ \vec{C} &= \{(\eta, \mu, \eta', \mu', h) \in \underline{\mathcal{S}} \times \{-1, 1\} : h\eta \geq -\delta\}, \\ \vec{G}(\eta, \mu, \eta', \mu', h) &= (\eta, \mu, \eta', \mu', h, \overline{\text{sgn}}(\eta)), \\ \vec{D} &= \{(\eta, \mu, \eta', \mu', h) \in \underline{\mathcal{S}} \times \{-1, 1\} : h\eta \leq -\delta\}\end{aligned}$$

$\{-1, 1\}$  is closed in  $\mathbb{R}$ , therefore the Cartesian product  $\underline{\mathcal{S}} \times \{-1, 1\}$  is closed in  $\mathbb{R}^9$ . Since  $\underline{\mathcal{S}} \times \{-1, 1\}$  is closed in  $\mathbb{R}^9$ ,  $\vec{C}$  and  $\vec{D}$  are also closed in  $\mathbb{R}^9$ .

On the account that each component of  $\vec{F}$  is a polynomial, the map  $\vec{F}$  is continuous.

The graph of the function  $\vec{G}$  is given by  $\{(\vec{x}, h_r, z) \mid z \in \vec{G}(\vec{x}, h_r)\} = \mathbb{R}^8 \times \mathbb{R} \times \mathbb{R}^8 \times \{-1, 1\}$ . Since this set is closed, it follows by definition that  $\vec{G}$  is outer semicontinuous.<sup>a</sup> Furthermore,  $\vec{G}$  is locally bounded because given any compact set  $K \subset \mathbb{R}^9$ ,  $\vec{G}(K) \subset K \times \{-1, 1\}$  and thus  $\vec{G}(K)$  is bounded. Finally,  $\vec{G}(\vec{x}, h)$  is nonempty for every  $(\vec{x}, h) \in \vec{D}$ .

□

<sup>a</sup>The graph of a set-valued mapping  $F : X \rightrightarrows Y$  is defined by  $\{(x, y) \in X \times Y : x \in X, y \in F(x)\}$ .  $F$  is outer semicontinuous if its graph is a closed set of  $X \times Y$  [150].

### Theorem 6.1 Dual quaternion hybrid global stabilizing controller

For prescribed positive scalars  $k_1, k_2$ , and using the memory state  $h$  defined in (6.5), the proposed control law<sup>a</sup>

$$\underline{\omega} \triangleq -hk_1 \text{Im}(\mathbf{r}) - \varepsilon k_2(\mathbf{p}), \quad (6.9)$$

with  $\mathbf{r}$  and  $\mathbf{p}$  being the quaternion representation of the rigid body orientation and position, ensures the equilibrium points of the closed loop system (6.1), (6.9) to be  $\pm 1$  and the set  $\{\pm 1\}$  to be exponentially stable.

<sup>a</sup>In terms of the components of  $\underline{\mathbf{x}} = \eta + \boldsymbol{\mu} + \varepsilon(\eta' + \boldsymbol{\mu}')$ , the dual quaternion controller (6.9) can be rewritten as  $\underline{\omega} = h\boldsymbol{\omega}_1 + \varepsilon\boldsymbol{\omega}_2$ , with  $\boldsymbol{\omega}_1 = -hk_1\boldsymbol{\mu}$  and  $\boldsymbol{\omega}_2 = -k_2(\eta\boldsymbol{\mu}' - \eta'\boldsymbol{\mu} + \boldsymbol{\mu} \times \boldsymbol{\mu}')$ .

#### proof.

To study the stability of the closed loop system (6.1), (6.9), let us first find the equilibria where  $\dot{\underline{\mathbf{x}}} = 0$ . Investigating the closed-loop system (6.9)-(6.5), (6.1) in terms of the dual quaternion components

$$\dot{\underline{\mathbf{x}}} = \dot{\eta} + \dot{\boldsymbol{\mu}} + \varepsilon(\dot{\eta}' + \dot{\boldsymbol{\mu}}')$$

where

$$\begin{aligned} \dot{\eta} &= \frac{1}{2}k_1h \|\boldsymbol{\mu}\|^2, & \dot{\eta}' &= \frac{1}{2}(k_1h + k_2\eta) \langle \boldsymbol{\mu}, \boldsymbol{\mu}' \rangle, & \dot{\boldsymbol{\mu}} &= -\frac{1}{2}\eta k_1 h \boldsymbol{\mu}, \\ \dot{\boldsymbol{\mu}}' &= \frac{1}{2}[-\eta' k_1 h \boldsymbol{\mu} - \eta^2 k_2 \boldsymbol{\mu}' + \eta \eta' k_2 \boldsymbol{\mu} - \eta k_2 \boldsymbol{\mu} \times \boldsymbol{\mu}' - k_1 h \boldsymbol{\mu} \times \boldsymbol{\mu}' - k_2 \eta \boldsymbol{\mu}' \times \boldsymbol{\mu} - k_2 (\boldsymbol{\mu} \times \boldsymbol{\mu}') \times \boldsymbol{\mu}], \end{aligned} \quad (6.10)$$

turns out that the  $\dot{\underline{\mathbf{x}}} = 0$  implies  $\boldsymbol{\mu} = 0$ . From the unit sphere constraint (see, Definition 2.18), it also follows that  $\eta = \pm 1$  whereby we can find that  $\boldsymbol{\mu}' = 0$ . In this context, the constraint  $\mathcal{P}(\underline{\mathbf{q}}) \mathcal{D}(\underline{\mathbf{q}}) = 0$  in Definition 2.18 also renders  $\eta' = 0$ . Hence, the set of equilibrium points of (6.10) is the set  $\{\pm 1\}$ .

To study the stability of the set of equilibrium points  $\{\pm 1\}$ , let us regard the Lyapunov candidate function

$$V(t, \underline{\mathbf{x}}, h) = 2(1 - h\eta) + \eta'^2 + \|\boldsymbol{\mu}'\|^2. \quad (6.11)$$

Since  $\eta \in [-1, 1]$  and  $h \in \{-1, 1\}$ , one has that  $(1 - h\eta) \geq 0$ . Therefore,  $V$  is a positive semidefinite function. The condition  $V = 0$  implies  $0 \leq 2(1 - h\eta) = -\eta'^2 - \|\boldsymbol{\mu}'\|^2 \leq 0$  which yields  $\eta' = 0$ ,  $\boldsymbol{\mu}' = 0$

and  $h\eta = 1$ , that is,  $\underline{x} = \pm 1$ . Hence,  $V$  is a positive definite function. The time-derivative of (6.11) yields

$$\dot{V} = -2h\dot{\eta} + 2\eta'\dot{\eta}' + 2\langle \underline{\mu}', \dot{\underline{\mu}}' \rangle. \quad (6.12)$$

Taking the closed-loop system (6.9)-(6.5),(6.1) in terms of the dual quaternion components (6.10), and after some calculation<sup>a</sup> we have

$$\dot{V} = -h^2 k_1 \|\underline{\mu}\|^2 - \eta^2 \eta'^2 k_2 - \eta^2 \|\underline{\mu}'\|^2 k_2 \leq 0.$$

In addition,  $\dot{V} = 0$  if and only if  $\underline{x} \in \{\pm 1\}$ . Moreover,  $V$  also decreases over jumps of the closed loop system since for  $h\eta < -\delta < 0$  one has that

$$V(\underline{x}, h^+) - V(\underline{x}, h) = 4h\eta < 0.$$

Thus, asymptotically stability of the set  $\{\pm 1\}$  follows from Lemma 6.1 and by Theorem 20 of [146]. It is also important to highlight that the closed-loop differential equation is well-posed [89, Prop. 2.1] as  $\underline{\omega}$  is in the Lie algebra of  $\text{Spin}(3) \times \mathbb{R}^3$ .  $\square$

<sup>a</sup>The derivation of (6.12) follows the same procedure detailed described in Appendix C.1 if we take  $\alpha_1$  and  $\alpha_2$  to be the memory state (6.5) and the identity element, respectively, and  $\mathbf{K}_{\mathcal{O}}$  to be  $hk_1$  and  $\mathbf{K}_{\mathcal{T}}$  to be the identity  $k_2\mathbf{I}$ , with  $k_1, k_2 \in \mathbb{R}_+^*$ .

*Remark 6.1.* At a first glance one could imagine that due to the transference principle [67], the extension of rotation stabilizers (e.g., the ones of [41, 43]) to full rigid body stabilizers would be trivial, only requiring substitution of adequate variables as in (2.23) and (6.1). However, for stability analysis based on Lyapunov functions, this supposition doesn't even make sense, since a Lyapunov function is a real-valued function and never a dual-number valued function. As a consequence, stabilization in  $\text{Spin}(3) \times \mathbb{R}^3$  using dual quaternions required one independent study from the quaternion stabilization analysis in  $\text{Spin}(3)$ . The necessity of different procedures for quaternion and dual quaternion is also inferred by remembering that due to the fact that  $SO(3)$  is compact and  $SE(3)$  is not, it was required one controller design procedure for each case in [55].

Similarly to the rotation controllers proposed in [43], the proposed pose controller doesn't exhibit Zeno behavior [146]. This is shown in the next theorem.

**Theorem 6.2** Absence of Zeno behaviour

For any compact set  $K \subset \underline{\mathcal{S}} \times \{-1, 1\}$ , if  $x$  is a solution of (6.1), (6.4) and (6.5) with initial state in  $K$ , then the number of jumps is bounded.

*proof.*

Similar to Theorem 5.3 of [43].  $\square$

The stability robustness will be characterized by its resistance against  $\alpha$ -perturbations: given  $\alpha > 0$ , the

$\alpha$ -perturbation of the hybrid system given by  $\vec{F}, \vec{G}$  as in (6.7), and  $\vec{C}, \vec{D}$  as in (6.8), is given by

$$\begin{aligned}\vec{C}_\alpha &\triangleq \left\{ x \in \mathbb{R}^9 : (x + \alpha\mathbb{B}) \cap \vec{C} \neq \emptyset \right\}, \\ \vec{F}_\alpha(x) &\triangleq \overline{\text{co}} \vec{F} \left( (x + \alpha\mathbb{B}) \cap \vec{C} \right) + \alpha\mathbb{B}, \text{ for all } x \in \vec{C}_\alpha, \\ \vec{D}_\alpha &\triangleq \left\{ x \in \mathbb{R}^9 : (x + \alpha\mathbb{B}) \cap \vec{D} \neq \emptyset \right\}, \\ \vec{G}_\alpha(x) &\triangleq \left\{ v \in \mathbb{R}^9 : v \in g + \alpha\mathbb{B}, g \in \vec{G} \left( (x + \alpha\mathbb{B}) \cap \vec{D} \right) \right\}, \text{ for all } x \in \vec{D}_\alpha,\end{aligned}$$

where  $\overline{\text{co}} X$  denotes the closure of the convex hull of the set  $X$ . These perturbations, as illustrated in [146], include both measurement and modeling error.

The lack of sensitivity to these perturbations will be expressed in Theorem 6.3 bounding the Lyapunov function using a class- $\mathcal{KL}$  function.<sup>5</sup>

### Theorem 6.3 Robustness against perturbations

Let  $V$  be as in (6.11). Then there exists a class- $\mathcal{KL}$  function  $\beta$  such that for each compact set  $K \subset \underline{\mathcal{S}} \times \{-1, 1\}$  and  $\Delta > 0$  there exists  $\alpha^* > 0$  such that for each  $\alpha \in (0, \alpha^*]$ , the solutions  $x_\alpha$  from  $K$  of the perturbed system  $\mathcal{H}_\alpha = (\vec{C}_\alpha, \vec{F}_\alpha, \vec{D}_\alpha, \vec{G}_\alpha)$  satisfy

$$V(x_\alpha(t, j)) \leq \beta(V(x_\alpha(0, 0)), t + j) + \Delta, \forall (t, j) \in \text{dom } x_\alpha$$

*proof.*

We have that  $V$  is a proper indicator function<sup>a</sup> of the compact set  $\{(1, 1), (-1, -1)\}$  in  $\underline{\mathcal{S}} \times \{-1, 1\}$ . From [146, Theorem 14], there exists a class- $\mathcal{KL}$  function  $\beta$  such that for all solutions  $x$  of  $\underline{\mathcal{S}} \times \{-1, 1\}$ ,

$$V(x(t, j)) \leq \beta(V(x(0, 0)), t + j), \forall (t, j) \in \text{dom } x.$$

From this and from Lemma 6.1, the  $\mathcal{KL}$  bound on  $V(x_\alpha(t, j))$  follows now by [146, Theorem 17].  $\square$

<sup>a</sup>Following [148, p. 145], a proper indicator function of a compact set  $\mathcal{A}$  in an open set  $\mathcal{O} \supseteq \mathcal{A}$  is a continuous function on  $\mathcal{O}$  which is positive definite with respect to  $\mathcal{A}$  and such that it tends to infinity as its argument tends to infinity or to the boundary of  $\mathcal{O}$ .

*Remark 6.2.* Differently from the Lyapunov function proposed in [43] for its hybrid kinematic controller, the proposed Lyapunov function (6.11) exploits the non-compactness of  $\underline{\mathcal{S}}$  to be a proper indicator function, enabling the direct proof of Theorem 6.3.

## 6.2.1 Hybrid control law applied to robot manipulators

The hysteresis-based hybrid control solution presented herein is designed for global and exponential stabilization of general rigid body pose. Nonetheless, the criterion has been designed such that extensions to different scenarios are straightforward. Particularly, we are interested in practical applications using robot manipulators taking into account the specificities inherent to the manipulator description. In this sense, this subsection addresses the proposed hybrid control strategy in the context of robot manipulators using the dual

<sup>5</sup>A class  $\mathcal{KL}$  function is a continuous function  $\beta : \mathbb{R}_{\geq 0} \times \mathbb{R}_{\geq 0} \rightarrow \mathbb{R}_{\geq 0}$  such that for each fixed  $s$ , the function  $\beta(r, s)$  is strictly increasing and  $\beta(0, s) = 0$ ; and for each fixed  $r$ , the function  $\beta(r, s)$  is decreasing and  $\lim_{s \rightarrow \infty} \beta(r, s) = 0$ .

quaternion Jacobian ( $\underline{J}_\omega$ ) derived in Subsection 2.7.3 that maps changes in the  $n$ -joint configuration to end-effector twist  $\underline{\omega}$ .

First, recalling the result derived in Section 2.7, the  $n$ -joint serial manipulator description relies on the forward kinematics that relates the configuration of all joints to the configuration  $\underline{x}$  of the end-effector; that is,  $\underline{x} = \underline{x}_1^0 \underline{x}_2^1 \dots \underline{x}_n^{n-1}$ , and the differential forward kinematics is hence given by  $\dot{\underline{x}} = \sum_{i=0}^{n-1} \underline{x}_i^0 \dot{\underline{x}}_{i+1}^i \underline{x}_n^{i+1}$ . Because  $\underline{x}_{i+1}^i$  is a function of  $\theta_i$ , i.e.,  $\underline{x}_{i+1}^i = \underline{f}_i(\theta_i)$ , where  $\underline{f}_i : \mathbb{R} \rightarrow \text{Spin}(3) \times \mathbb{R}^3$ , we have that  $\dot{\underline{x}}_{i+1}^i = \underline{f}'_i(\theta_i) = \underline{w}_i \dot{\theta}_i \underline{f}_i(\theta_i)$  with  $\underline{w}_i \in \mathbb{H}_0 \otimes \mathbb{D}$ . Explicitly considering the dual quaternion differential FKM to be well defined within the unit dual quaternion group, we have a differential FKM described as in (2.42)-(2.48), that is,

$$\begin{aligned} \dot{\underline{x}} &= \frac{1}{2} \sum_{i=0}^{n-1} \underline{j}_i \dot{\theta}_i \underline{x} \\ &= \frac{1}{2} \text{vec}_6 \left( \underline{J}_\omega \dot{\theta} \right) \underline{x}, \end{aligned} \quad (6.13)$$

where  $\text{vec}_6 \left( \underline{J}_\omega \dot{\theta} \right)$  describes the end-effector twist in dual quaternion space,  $\theta = [\theta_0 \dots \theta_{n-1}]^T$  is the measured vector of joint variables and  $\underline{J}_\omega$  is the Jacobian, which can be found by using Algorithm 2.2.

In Section 3.3, particularly in Theorem 3.7, to solve the exponential stabilization of the dual quaternion error function defined by  $\underline{e} = \underline{1} - \underline{x}$  (for further details on the error function, see Section (3.1)), we proposed the dual quaternion task-space controller (3.47) with joint velocity inputs:

$$\dot{\theta} = \underline{J}_\omega^+ \left[ \underline{K}_\circ \text{vec}_3^T (\text{Im}(\mathcal{O}(\underline{e}))) \quad -\underline{K}_\tau \text{vec}_3^T (\mathcal{T}(\underline{e})) \right]^T$$

where  $\underline{K}_\circ, \underline{K}_\tau$  are positive definite  $3 \times 3$  matrices. The variables  $\mathcal{O}(\underline{e})$  and  $\mathcal{T}(\underline{e})$  are defined in Section 3.3 as  $\mathcal{O}(\underline{e}) = 1 - \underline{r}$  and  $\mathcal{T}(\underline{e}) = \underline{p}$  where  $\underline{r}$  and  $\underline{p}$  are the unit quaternion representation of the orientation and position of the end-effector. If  $\underline{J}_\omega \in \mathbb{R}^{6 \times n}$  is well-posed, then the closed loop differential kinematics is therefore given by

$$\begin{aligned} \dot{\underline{x}} &= \frac{1}{2} \text{vec}_6 \left[ \underline{K}_\circ \text{vec}_3^T (\text{Im}(\mathcal{O}(\underline{e}))) \quad -\underline{K}_\tau \text{vec}_3^T (\mathcal{T}(\underline{e})) \right]^T \underline{x} \\ &= \frac{1}{2} \text{vec}_6 \left[ -\underline{K}_\circ \text{vec}_3^T (\text{Im}(\underline{r})) \quad -\underline{K}_\tau \text{vec}_3^T (\underline{p}) \right]^T \underline{x}. \end{aligned} \quad (6.14)$$

In Appendix C.1, we prove that the closed-loop system is stable with exponential convergence given by  $\sigma_m\{\underline{K}_\circ\}$  and  $\sigma_m\{\underline{K}_\tau\}$ , where  $\sigma_m\{s\}$  denotes the minimum singular value from a given matrix  $s$ . Hence, taking the minimum singular value from  $\underline{K}_\circ$  and  $\underline{K}_\tau$ , the closed-loop system (6.14) yields  $\dot{\underline{x}} = -\frac{1}{2} (k_1 \text{Im}(\underline{r}) + \varepsilon k_2 \underline{p}) \underline{x}$ , where  $\underline{\omega} = -k_1 \text{Im}(\underline{r}) - \varepsilon k_2 (\underline{p})$  with  $k_1 = \sigma_m\{\underline{K}_\circ\}$  and  $k_2 = \sigma_m\{\underline{K}_\tau\}$ .

Now, if we were to take a task-space controller explicitly considering the memory state (6.5) as in (6.9) instead of the one derived in (3.47), then we can extend the proposed hybrid strategy in the context of robot manipulators. Indeed, considering a dual quaternion task-space controller given by

$$\dot{\theta} = \underline{J}_\omega^+ \left[ h \underline{K}_\circ \text{vec}_3^T (\text{Im}(\mathcal{O}(\underline{e}))) \quad -\underline{K}_\tau \text{vec}_3^T (\mathcal{T}(\underline{e})) \right]^T, \quad (6.15)$$

where  $h$  is the memory state (6.5), and taking the minimum singular value from the gain matrices, the closed-loop system (6.14) yields

$$\dot{\underline{x}} = \frac{1}{2} \underline{\omega} \underline{x},$$

where  $\underline{\omega} = -h k_1 \text{Im}(\underline{r}) - \varepsilon k_2 (\underline{p})$  with  $k_1 = \sigma_m\{\underline{K}_\circ\}$  and  $k_2 = \sigma_m\{\underline{K}_\tau\}$ . Note that the closed-loop system is exactly the same described in Theorem 6.1. Hence, the equilibrium points of the closed loop system (6.13),(6.15), is  $\pm 1$  and the set  $\{\pm 1\}$  is globally exponentially stable.



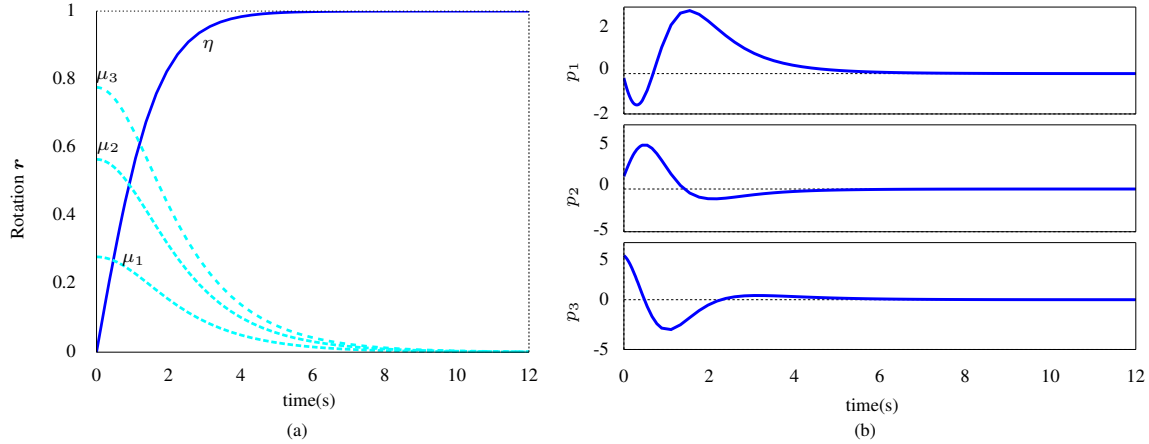


Figure 6.2: (a) Trajectory of the rotation unit quaternion  $r$  in terms of  $\eta$  and  $\mu$  (dashed line). (b) Trajectory of the three-dimensional translation elements  $p = p_1\hat{i} + p_2\hat{j} + p_3\hat{k}$ .

### 6.3 NUMERICAL SIMULATIONS

In this section, the effectiveness of the proposed hybrid technique for robust global stabilization of the rigid body motion is demonstrated under different conditions.

We first demonstrate the proposed controller global stability and robustness against measurement noises. To this aim, a simulation is performed using the hybrid feedback controller (6.4), with hysteresis parameter  $\delta=0.2$ , and the pure discontinuous controller (6.2)—using the same proportional gain  $k = 2$ . For this particular scenario, we assume an initial condition,  $\underline{x}_0=0.001 + \hat{i}0.78 + \hat{j}0.57 + \hat{k}0.28 + \varepsilon \left( -1.28 + \hat{i}1.50 - \hat{j}2.44 + \hat{k}0.77 \right)$ , located in the neighborhood of  $\eta=0$ , and a zero mean Gaussian measurement noise over  $\eta$  with a 0.1 standard deviation. Figure 6.1 illustrates the result from the discontinuous controller (6.2) whereby one can clearly see the problematic noise influence—for instance, the excess of switches causing chattering for over 3 seconds and the consequent convergence lag. In contrast, the proposed hybrid feedback controller ensures a robust performance without chattering as shown in Figure 6.2. The absence of chattering and the performance improvements are better illustrated in Figure 6.3, which presents the results from both controllers.

To illustrate the influence of the design parameter  $\delta$  over the switches along time of the closed-loop system (6.1), a set of simulations is performed using the hybrid controller (6.4) with different values for  $\delta$ . For these simulations, we assume the same initial condition, control gain, and measurement noise as defined in the former scenario. As shown in Figure 6.4(a), larger hysteresis parameters yield smaller number of switches, as one would expect. As shown in Figure 6.4(b), it is also interesting to highlight that the number of switches tend to decrease along time as  $\eta$  converges to the equilibrium.

Lastly, to elucidate the influence of the hysteresis parameter  $\delta$  with regard to the unwinding phenomenon, a different scenario is simulated using (6.4) with  $\delta=0.15$  and  $\delta=0.95$  and with a proportional gain  $k=5$ . We assume an initial state with  $\eta$  close to  $-1$  and  $h=1$ . As shown in Figure 6.5, very large values of  $\delta$  may induce the stabilization to  $\eta=1$ , which leads to needless motions and control efforts compared to the case of  $\delta=0.15$ .

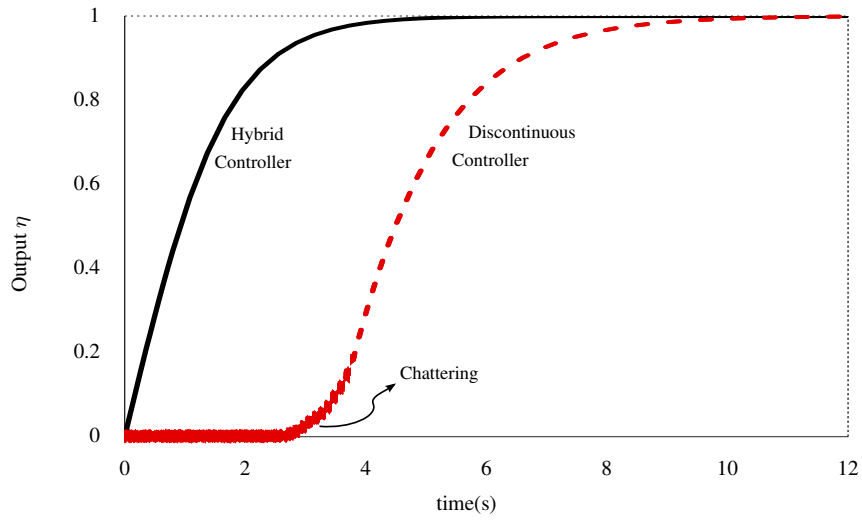


Figure 6.3: Trajectory of  $\eta$  with hybrid feedback controller (6.4) and discontinuous controller (6.2) over time.

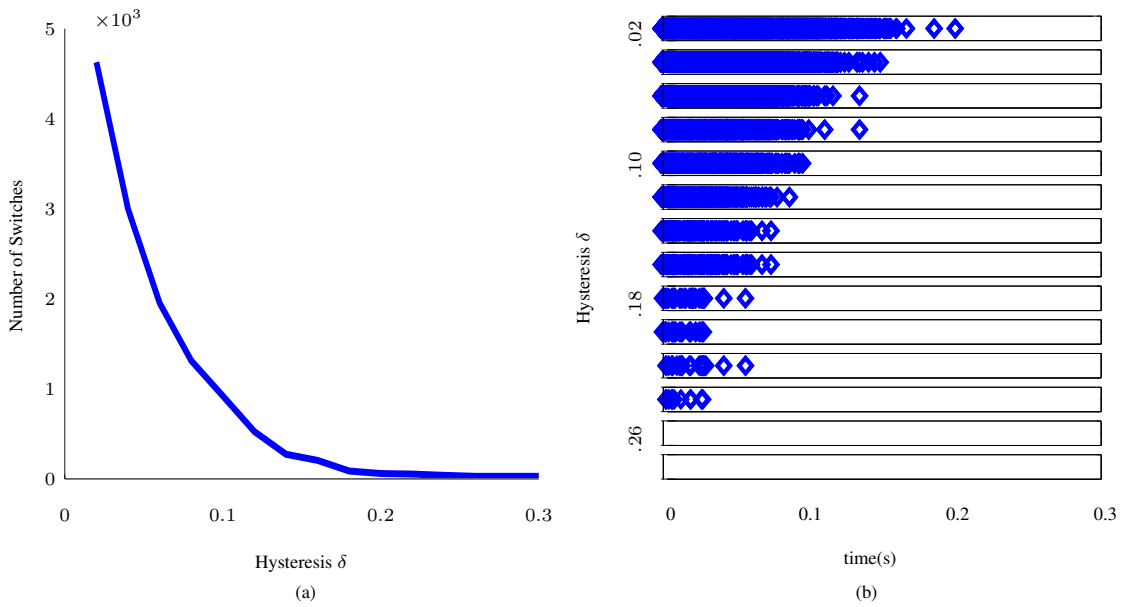


Figure 6.4: The number of switches with regard to the hysteresis parameter  $\delta$  is shown in (a), while the switches along time  $s(t)$  are illustrated in (b) for different values of  $\delta$ .

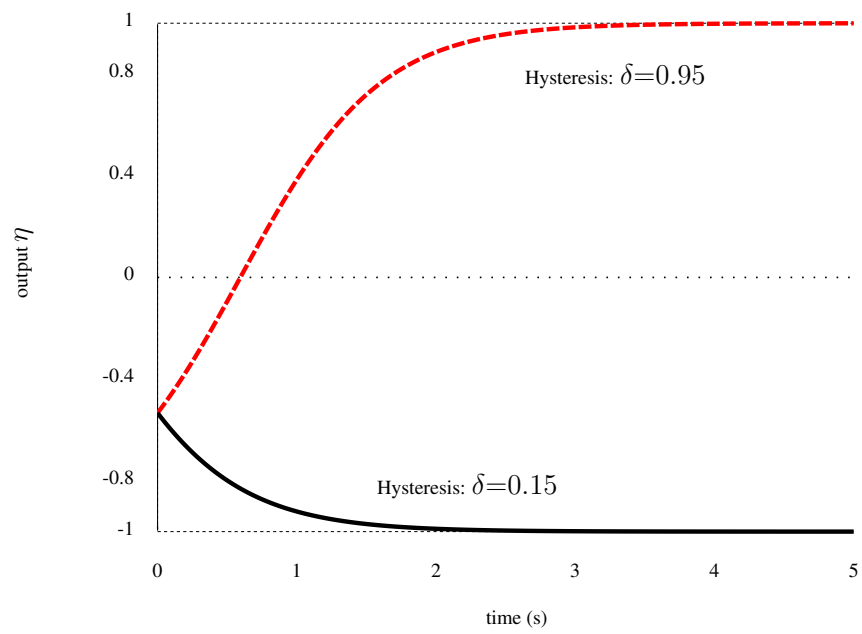


Figure 6.5: Influence of the hysteresis parameter  $\delta$  on unwinding— $\eta$  converges to the farther stable point.

# 7

## SWITCHING STRATEGY FOR FLEXIBLE TASK EXECUTION AND ITS APPLICATIONS TO BIMANUAL MANIPULATION WITHIN THE COOPERATIVE DUAL TASK-SPACE

---

In Chapter 6, we have addressed the importance of self-motion (i.e., motions of the robot links that do not disturb the end-effector configuration [109]) for kinematic singularity avoidance. Briefly, the technique lies in the optimization of a manipulability function projected on the Jacobian nullspace. The same nullspace can also be used to perform different secondary tasks (see, for instance, [117, 151–154]). In this sense, self-motion based control strategies are paramount to unfold online task flexibility and reactivity for unforeseen scenarios, such as obstacles and unknown singularities. Still, even seemingly simple problems demand a number of DOFs. For instance, controlling the end-effector orientation and position requires all degrees of freedom from a six-DOF robot manipulator, leaving no room for self-motion. In this context, this chapter focuses on a novel strategy for enlarging the use of self-motion even to redundant manipulators by relaxing the task constraints and switching to control tasks with lesser degrees of freedom whenever possible. To illustrate the importance and effectiveness of enlarging the nullspace to allow further self-motion operations, herein, this chapter concerns a two-arm manipulation operation. Due to the higher need—and also availability—of DOFs, multi-arm manipulation is indeed the main motivation for the proposed technique. Still, for the sake of simplicity, herein, we will consider a bimanual application which also illustrates both the need for further DOF and the advantages of the proposed technique.

### Cooperative Manipulation and Flexible Task Execution

Research in robotic systems has given considerably attention to the study of multi-arms systems in the past thirty years [155]. Indeed, cooperative manipulation raises a broad set of practical applications that would be restricted in a single manipulator framework, such as lifting heavy and/or large payload, complex assembly, and different tasks in an unstructured environment [155]. Nonetheless, the integration of two or more arms in a complex real robot system context is not trivial and adds significant complexity to the analysis of the resultant system [1].

In this sense, an extensive amount of research has focused on designing models and specific frameworks to cope with the complexities stemming from multi-arm manipulation. Recently, a new framework proposed in [4] has enriched the analysis and description of the cooperative task space using unit dual quaternion representation to describe rigid body motion and cooperative elements without representation singularities and without decoupling orientation and translation dynamics.

The cooperative dual task-space (CDTS) representation introduced in [4] has many advantages compared to previous techniques. The description of the cooperative space using unit dual quaternions, which is easily extendable to multi-arm manipulation and to human-robot interaction (for instance, see [156]), enlightens and eases the definition of robot objectives to be performed in the same task space. It is also more connected to the sensor space, which improves control law robustness and accuracy [157]. Using unit dual quaternions also

makes it easier to extract geometric parameters related to the bimanual manipulation [4]. In this context, the framework is indeed considerably more intuitive and attractive from the control point of view.

Integrating multi-arms in a cooperative task-space environment significantly increases the complexity of real applications, and the control technique should make sure to avoid undesirable configurations from the arms that could degrade the overall performance—e.g., joint limits, singular configuration, etc. Undesirable poses are seldom known a priori, thus it is useful to regard secondary constraints which provide more reactive solutions during execution [153]. Particularly, from the pioneer work from [111], there has been a great amount of research on solutions exploiting kinematic redundancy, that is, the additional degrees of freedom (DOF) not required by the main task. As stressed in Chapter 5, we can exploit the degrees of freedom from the nullspace of the task Jacobian to avoid kinematic singularities. Moreover, the same space can be used to perform different secondary tasks (see, for instance, [117, 151–154]). Nonetheless, very few results related to kinematic redundancy have been extended to the cooperative/multi-arm framework, despite the obvious advantages for such a complex robotic framework stemming from a reactive self-motion.

In this chapter, we extend the results from the cooperative dual task-space [4] by adding new geometric task primitives for the cooperative space, and by explicitly decoupling the free remaining motions from task primitives in order to optimize secondary constraints. The strategy alone considerably improves the cooperative dual task space applicability to real world practical problems as they yield, in conjunction with suitable controllers, to a much more robust and reactive scenario for the cooperative manipulation.

Still, the main contribution of this chapter lies on a novel proposal for task execution. Herein, we focus on bimanual task execution within the cooperative dual task-space, but the strategy is more general and can be applied to single manipulators or extended to multiple arm manipulation. The goal is to cope with highly complex task descriptions, which are common in a cooperative manipulation scenario, while enlarging the self-motion space. This is performed by relaxing control requirements within regions of interests, and thus adding additional DOF for a secondary task. To ensure stability to the desired region of interest, we propose a hysteresis-based switching control strategy which aims to reduce the complexity of the main task while maintaining the pose (i.e., position and orientation) within the valid region.

## 7.1 COOPERATIVE DUAL TASK-SPACE: DESCRIPTION AND CONTROL

This section presents the results concerning the cooperative dual task-space derived in [1] to provide the reader basic concepts and a brief background required to the main application from this chapter, namely the flexible task execution applied to bimanual manipulation. Moreover, we also introduce the concept of controllable sets in the context of the proposed task primitives and a brief analysis on task primitives stability.

Consider a two-arm robot where  $\underline{x}_1$  and  $\underline{x}_2$  represent—with respect to a common coordinate system—the dual position of left and right end-effectors, respectively, as illustrated in Figure 7.1. The relative dual position determines the configuration of the left end-effector with respect to the right one, whereas the absolute dual position corresponds to a frame located between the end-effectors [4]. The formal definition is given in the following.

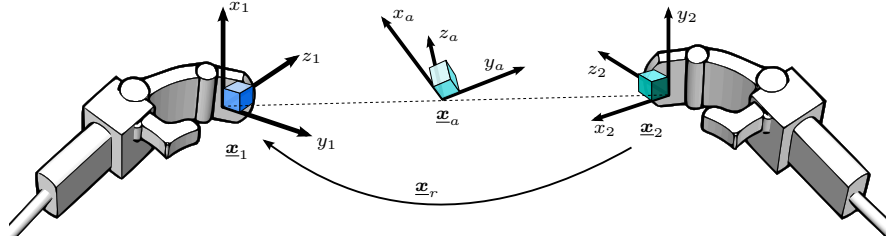


Figure 7.1: Cooperative dual task-space representation: the absolute and relative dual positions  $\underline{x}_a$  and  $\underline{x}_r$  completely describe the manipulation task [1].

**Definition 7.1.** (From [1,4]) The relative and absolute dual positions can be defined as

$$\underline{x}_r \triangleq \underline{x}_2^* \underline{x}_1 \quad (7.1)$$

$$\underline{x}_a \triangleq \underline{x}_2 \underline{x}_{r/2}, \quad (7.2)$$

where  $\underline{x}_{r/2}$  is the transformation that corresponds to half of the angle  $\phi_r$  around the axis  $\mathbf{n}_r = \hat{i}n_x + \hat{j}n_y + \hat{k}n_z$  of the quaternion  $\mathcal{P}(\underline{x}_r)$  and half of the translation between the two arms [4]. The dual quaternions  $\underline{x}_a$  and  $\underline{x}_r$  are called *cooperative variables*. The relative and absolute dual positions,  $\underline{x}_r$  and  $\underline{x}_a$ , respectively, are shown in Figure 7.1.

As shown in [1,4], the relative dual quaternion Jacobian<sup>1</sup> satisfies the relation  $\text{vec}_8 \dot{\underline{x}}_r = \mathbf{J}_{\underline{x}_r} \dot{\Theta}$ , where

$$\Theta \triangleq \begin{bmatrix} \theta_1^T & \theta_2^T \end{bmatrix}^T \quad (7.3)$$

is the vector composed of the joint variables of the first and second arms and  $\mathbf{J}_{\underline{x}_r}$  is the relative cooperative task-space Jacobian. The relative Jacobian is a function of the individual Jacobians from the first ( $\mathbf{J}_{\underline{x}_1}$ ) and second arm ( $\mathbf{J}_{\underline{x}_2}$ ) described by

$$\mathbf{J}_{\underline{x}_r} = \begin{bmatrix} \overset{+}{\mathbf{H}}(\underline{x}_2^*) \mathbf{J}_{\underline{x}_1} & \bar{\mathbf{H}}(\underline{x}_1) \mathbf{J}_{\underline{x}_2}^* \end{bmatrix}. \quad (7.4)$$

Analogously to the relative dual quaternion Jacobian, Adorno et al. [4] showed that the absolute dual quaternion Jacobian satisfies the relation

$$\text{vec}_8 \dot{\underline{x}}_a = \mathbf{J}_{\underline{x}_a} \dot{\Theta}. \quad (7.5)$$

The absolute dual quaternion based Jacobian is described by

$$\mathbf{J}_{\underline{x}_a} = \bar{\mathbf{H}}(\underline{x}_{r/2}) \mathbf{J}_{\underline{x}_{2\text{ext}}} + \overset{+}{\mathbf{H}}(\underline{x}_2) \mathbf{J}_{\underline{x}_{r/2}}, \quad (7.6)$$

where  $\mathbf{J}_{\underline{x}_{2\text{ext}}} = \begin{bmatrix} \mathbf{0}_{8 \times \dim \theta_1} & \mathbf{J}_{\underline{x}_2} \end{bmatrix}$ , with  $\dim \theta_1$  corresponding to the dimension of the joint vector  $\theta_1$ , and

$$\mathbf{J}_{\underline{x}_{r/2}} = \begin{bmatrix} \frac{1}{2} \bar{\mathbf{H}}_4(\mathbf{r}_{r/2}^*) \mathbf{J}_{\mathcal{P}(\underline{x}_r)} \\ \frac{1}{4} \left( \bar{\mathbf{H}}_4(\mathbf{r}_{r/2}) \mathbf{J}_{\mathbf{p}_r} + \overset{+}{\mathbf{H}}_4(\mathbf{p}_r) \mathbf{J}_{\mathcal{P}(\underline{x}_{r/2})} \right) \end{bmatrix}$$

<sup>1</sup>In this chapter, all presented task Jacobians describe the mapping between the joint velocities vector to an Euclidean representation of the corresponding unit dual quaternion—similarly to  $\mathbf{J}_{\text{vec}}$  described in (2.38)-(2.41). Herein, we will drop the 'vec' subscript associated to this particular mapping. The slight abuse of notation herein stems from the necessity to represent a number of different task Jacobians and to use the subscript to describe the corresponding task in a simplified manner.

	Control primitive $\mathbf{u}_{task}$	Task Jacobian
Dual position	$\underline{\mathbf{x}} = \mathbf{r} + \varepsilon (1/2) \mathbf{p}\mathbf{r}$	$\mathbf{J}_{\underline{\mathbf{x}}}$ (Eq. (7.4) and (7.5))
Cartesian position	$\mathbf{p}$	$\mathbf{J}_{\mathbf{p}}$ (Eq. (7.7))
Orientation	$\mathbf{r}$	$\mathbf{J}_{\mathcal{P}(\underline{\mathbf{x}})}$ (four upper rows of $\mathbf{J}_{\underline{\mathbf{x}}}$ )
Square distance	$\ \mathbf{p}\ ^2$	$\mathbf{J}_d$ (Eq. (7.8))

Table 7.1: Control primitives and correspondent task Jacobians.

with  $\mathbf{J}_{\mathcal{P}(\underline{\mathbf{x}}_{r/2})}$  corresponding to the four upper rows of the relative dual quaternion Jacobian  $\mathbf{J}_{\underline{\mathbf{x}}_r}$  (7.4).

**Proposition 7.1.** Consider a unit dual quaternion  $\underline{\mathbf{x}}$  with  $\text{vec}_8 \dot{\underline{\mathbf{x}}} = \mathbf{J}_{\underline{\mathbf{x}}} \dot{\boldsymbol{\theta}}$ . Let  $\mathbf{p}$  be the translation quaternion related to  $\underline{\mathbf{x}}$ , then [1]

$$\text{vec}_4 \dot{\mathbf{p}} = \mathbf{J}_{\mathbf{p}} \dot{\boldsymbol{\theta}}, \quad (7.7)$$

where  $\mathbf{J}_{\mathbf{p}} = 2\bar{\mathbf{H}}_4(\mathcal{P}(\underline{\mathbf{x}}^*)) \mathbf{J}_{\mathcal{D}(\underline{\mathbf{x}})} + 2\mathbf{H}_4^+(\mathcal{D}(\underline{\mathbf{x}})) \mathbf{J}_{\mathcal{P}(\underline{\mathbf{x}})}^*$ .

**Proposition 7.2.** Let  $\mathbf{p}$  be a translation that satisfies (7.7). The square distance Jacobian  $\mathbf{J}_d$  is the Jacobian that satisfies

$$\dot{c} = \mathbf{J}_d \dot{\boldsymbol{\theta}}, \quad (7.8)$$

where  $c \triangleq \|\mathbf{p}\|^2$  and  $\mathbf{J}_d = 2(\text{vec}_4 \mathbf{p})^T \mathbf{J}_{\mathbf{p}}$  [1].

In the context of Definition 7.1 and the geometric primitives derived from the cooperative dual task-space, the forward kinematics model (FKM) of all feasible bimanual tasks must be directly related to the kinematics from both manipulators and, consequently, they are function of the augmented joint vector  $\boldsymbol{\Theta}$  defined in (7.3). In this sense, any task primitive  $\mathbf{u}_{task}$  (e.g., relative/absolute distance, translation, orientation or pose) in the cooperative dual task space can be described as the function  $\mathbf{u}_{task} = \mathbf{f}_{task}(\boldsymbol{\Theta})$ , and the differential kinematics related to each task primitive yields

$$\text{vec}_8 \dot{\underline{\mathbf{x}}}_{task} = \mathbf{J}_{task} \dot{\boldsymbol{\Theta}}, \quad (7.9)$$

where  $\mathbf{J}_{task}$  is a predefined Jacobian that relates the augmented joint vector (7.3) with the derivative of the task primitive. The task primitives are summarized in Table 7.1.

### 7.1.1 Primitive controllable sets

Among the vast number of tasks a cooperative manipulation between two arms has to offer, we shall focus on some few geometric primitives that would be useful to most interactions: relative distance between arms, relative Cartesian position, orientation, absolute orientation and position, and combinations between relative and absolute primitives. Each task primitive requires different degrees of freedom from the two-arm system (e.g., 1 for the relative distance, 3 for the relative position, 6 for the relative pose, etc) and, as previously discussed, it would be interesting to perform such task with less degrees of freedom as possible. The idea of reducing the number of DOF used for a given task is to allow the self motion to perform secondary tasks such as collision avoidance, joint limit control, and so on.

In this sense, we define geometric controllable sets which stem from the desired task primitives on the cooperative dual space, that is, intuitive geometric spaces that are controllable from each task definition.

**Definition 7.2.** For a given set  $\mathfrak{S} \subseteq \text{Spin}(3) \times \mathbb{R}^3$ , the following proper subsets can be drawn from geometric structures of interest with regard to this set,

$$\begin{aligned}\mathfrak{R}_d(\mathfrak{S}) &= \{d \in \mathbb{R} \mid d = \|\mathcal{T}(\underline{x}_g)\|, \underline{x}_g \in \mathfrak{S}\}, \\ \mathfrak{R}_t(\mathfrak{S}) &= \{t \in \mathbb{H}_0 \mid t = \mathcal{T}(\underline{x}_g), \underline{x}_g \in \mathfrak{S}\}, \\ \mathfrak{R}_o(\mathfrak{S}) &= \{r \in \text{Spin}(3) \mid r = \mathcal{P}(\underline{x}_g), \underline{x}_g \in \mathfrak{S}\},\end{aligned}$$

where  $\mathcal{T}(\underline{x}_g) \triangleq 2\mathcal{D}(\underline{x}_g)\mathcal{P}(\underline{x}_g)^*$  is the translation corresponding to the pose  $\underline{x}_g$  and  $\mathbb{H}_0$  is the set of all pure quaternions, which is algebraically isomorphic to  $\mathbb{R}^3$  (see Definition 2.9).

In order to better specify the geometric primitives inside the CDTS, let us consider the spaces  $\mathfrak{R}_{rw}, \mathfrak{R}_{aw} \subset \text{Spin}(3) \times \mathbb{R}^3$  which correspond to the space of controllable relative poses and absolute poses, respectively. Henceforth, we will also consider regions defined by proper subsets of  $\mathfrak{R}_{rw}$  and  $\mathfrak{R}_{aw}$  that correspond to the relative/absolute distance, orientation and position.

From the relative distance primitive, it is clear that we can only control the distance of one arm with respect to the other, which results in the controllable region

$$\mathfrak{R}_1 = \{d_r \in \mathfrak{R}_d(\mathfrak{R}_{rw}) \mid d_{rm} \leq d_r \leq d_{rM}\},$$

where  $d_m$  and  $d_M$  are the boundaries of the feasible distance. Those boundaries are defined by the bimanual task to be executed. In this context, all relative distances belong to the set  $\mathfrak{R}_1$ , the radius of a ball in the set  $\mathfrak{R}_2$  that defines all relative position between arms; as a consequence  $\mathfrak{R}_1$  is clearly a proper subset of<sup>2</sup>

$$\mathfrak{R}_2 = \{t_r \in \mathfrak{R}_t(\mathfrak{R}_{rw}) \mid t_{rm} \preceq t_r \preceq t_{rM}\},$$

where  $t_{rm}$  and  $t_{rM}$  are the boundaries of the relative position. The controllable region that arises from the primitive that corresponds to the relative orientation is described by the set

$$\begin{aligned}\mathfrak{R}_3 &= \{r_r \in \mathfrak{R}_o(\mathfrak{R}_{rw}) \mid r_r = \cos(\phi/2) + \sin(\phi/2)\mathbf{n} \\ &0 \leq \langle \mathbf{m}, \mathbf{n} \rangle \leq \|\cos \beta_r\|, \|\mathbf{m}\| = 1, \phi_{rm} \leq \phi \leq \phi_{rM}\},\end{aligned}$$

where the operation  $\langle \mathbf{m}, \mathbf{n} \rangle$  is the dot product between pure quaternions  $\mathbf{m}$  and  $\mathbf{n}$  (analogous to the inner product between two vectors in  $\mathbb{R}^3$  as seen in Definition 2.9) that, together with the opening angle  $\beta_r$ , provides the solid cone in which the rotation axis  $\mathbf{n}$  lies. In addition,  $\phi_{rm}$  and  $\phi_{rM}$  are the boundaries for the feasible rotation around axis  $\mathbf{n}$ .

Analogously, the controllable sets associated with the absolute position and absolute orientation are described by  $\mathfrak{R}_4$  and  $\mathfrak{R}_5$ , that is,

$$\mathfrak{R}_4 = \{t_a \in \mathfrak{R}_t(\mathfrak{R}_{aw}) \mid t_{am} \preceq t_a \preceq t_{aM}\},$$

and

$$\begin{aligned}\mathfrak{R}_5 &= \{r_a \in \mathfrak{R}_o(\mathfrak{R}_{aw}) \mid r_a = \cos(\phi/2) + \sin(\phi/2)\mathbf{n} \\ &0 \leq \langle \mathbf{m}, \mathbf{n} \rangle \leq \|\cos \beta_a\|, \|\mathbf{m}\| = 1, \phi_{am} \leq \phi \leq \phi_{aM}\},\end{aligned}$$

<sup>2</sup>Given two translation quaternions  $t_1$  and  $t_2$ , the relation  $t_1 \preceq t_2$  implies that all elements of  $t_1$  are less than or equal to the corresponding elements of  $t_2$ .



Task primitive $\mathbf{u}_i$	Error description	Required number of DOF	Vector $\zeta$ describing the required controllable sets
Relative distance	$e_1$	1	$\zeta_1 = \begin{bmatrix} 1 & 0 & 0 & 0 & 0 \end{bmatrix}$
Relative position	$e_2$	3	$\zeta_2 = \begin{bmatrix} 1 & 1 & 0 & 0 & 0 \end{bmatrix}$
Relative orientation	$e_3$	3	$\zeta_3 = \begin{bmatrix} 0 & 0 & 1 & 0 & 0 \end{bmatrix}$
Relative pose	$e_4$	6	$\zeta_4 = \begin{bmatrix} 1 & 1 & 1 & 0 & 0 \end{bmatrix}$
Absolute position & relative distance	$e_5$	4	$\zeta_5 = \begin{bmatrix} 1 & 0 & 0 & 1 & 0 \end{bmatrix}$
Complete position	$e_6$	6	$\zeta_6 = \begin{bmatrix} 1 & 1 & 0 & 1 & 0 \end{bmatrix}$
Complete orientation	$e_7$	6	$\zeta_7 = \begin{bmatrix} 0 & 0 & 1 & 0 & 1 \end{bmatrix}$
Absolute position & relative pose	$e_8$	9	$\zeta_8 = \begin{bmatrix} 1 & 1 & 1 & 1 & 0 \end{bmatrix}$
Absolute orientation & relative pose	$e_9$	9	$\zeta_9 = \begin{bmatrix} 1 & 1 & 1 & 0 & 1 \end{bmatrix}$
Complete dual pose	$e_{10}$	12	$\zeta_{10} = \begin{bmatrix} 1 & 1 & 1 & 1 & 1 \end{bmatrix}$

Table 7.2: Summary of tasks primitives and the corresponding controllable sets

where  $\mathbf{t}_{am}$  and  $\mathbf{t}_{aM}$  are the boundaries of the absolute position whereas  $\phi_{am}$  and  $\phi_{aM}$  are the boundaries for the feasible rotation around axis  $\mathbf{n}$ . The operation  $\langle \mathbf{m}, \mathbf{n} \rangle$  together with the opening angle  $\beta_a$ , provides the solid cone in which the rotation axis  $\mathbf{n}$  lies.

The regions  $\mathfrak{R}_2 \cup \mathfrak{R}_3$  and  $\mathfrak{R}_4 \cup \mathfrak{R}_5$  define the controllable sets related to the relative pose and absolute pose in the cooperative space, respectively. Hence,  $\mathfrak{R}_2$  and  $\mathfrak{R}_3$  are proper subsets of the space of controllable relative poses  $\mathfrak{R}_{rw}$  and, similarly,  $\mathfrak{R}_4$  and  $\mathfrak{R}_5$  are proper subsets of the space of controllable absolute poses  $\mathfrak{R}_{aw}$ .

The sets  $\mathfrak{R}_i, i=\{1, \dots, 5\}$ , define the controllable regions, which can be combined and related with cooperative tasks, in such a way that we can easily define which task primitive should be controlled in order to fulfill a specific geometric task objective.

To summarize the results from the task primitives with their respective controllable sets, Table 7.2 describes the specifications for task primitive definition, error description, the required number of DOFs, and the vector description that characterizes the task required controllable sets.

## 7.1.2 Task primitive stability

In this subsection, we address the stability analysis and control design strategy for the error dynamics related to the task primitives  $\mathbf{u}_i$  presented in Table 7.2, that is,

$$\dot{e}_i = -\mathbf{J}_i \dot{\Theta}, \quad (7.10)$$

where  $i=\{1, \dots, 10\}$ , the error is defined as  $e_i = \mathbf{u}_{i,d} - \mathbf{u}_i$  with  $\dot{\mathbf{u}}_{i,d} = \mathbf{0}$ . Each  $\mathbf{J}_i$  is given as in Table 7.1 or stacked depending on the task primitive. For instance, the task primitive of the relative position is  $\mathbf{u}_2 = \text{vec}_4 \mathbf{p}_r$  and the correspondent Jacobian is  $\mathbf{J}_2 = \mathbf{J}_p$ , which in this case is calculated using (7.7) using  $\mathbf{x}_r$  and  $\mathbf{J}_{\mathbf{x}_r}$ ; for the complete dual pose,  $\mathbf{u}_{10} = \begin{bmatrix} \text{vec}_8 \mathbf{x}_r^T & \text{vec}_8 \mathbf{x}_a^T \end{bmatrix}^T$  and  $\mathbf{J}_{10} = \begin{bmatrix} \mathbf{J}_{\mathbf{x}_r}^T & \mathbf{J}_{\mathbf{x}_a}^T \end{bmatrix}^T$ .

Let us choose as Lyapunov function candidate, for each task primitive  $i$ , the positive definite quadratic function  $V_i = (1/2) e_i^T e_i$ . The time-derivative with respect to  $t$  along the trajectory (7.10) yields  $\dot{V}_i = -e_i^T \mathbf{J}_i \dot{\Theta}$ . It is clear that  $\dot{e}_i$  is a stable vector field within its particular controllable set, and the least-square solution

$\dot{\Theta} = J_i^+ K e_i$ , where  $J_i^+$  is the right pseudoinverse of  $J_i$  and  $K$  is positive definite, ensures the stability of (7.10). As a preliminary approach, we assumed a very simple error definition, but the strategy can easily be extended to invariant errors and errors defined directly at the dual quaternion space.

It is also important to highlight that the least-square solution is a particular result. Among the range of feasible solutions for (7.10), we are obviously interested to regard solutions that exploit existing redundancy from the manipulators as to perform secondary tasks. In this sense, a more general solution for (7.10), which is used to derive redundancy-based controllers, is given by [111, 158]

$$\dot{\Theta} = J_i^+ K e_i + P_i z_2, \quad (7.11)$$

where  $z_2$  is an arbitrary control input, which will be used to apply a secondary task, and  $P_i = I - J_i^+ J_i$  is the operator that projects  $z_2$  onto the nullspace of  $J_i$ .

The secondary task will be performed at the best using the self-motion of the cooperative dual space, that is, using the the movements of the links (from both manipulators) which do not disturb the configuration trajectory of the resulting main cooperative task. Therefore, the vector input  $z$  can be defined to optimize a secondary constraint using least-square, similarly to the solution of the main task.

In this context, given any secondary task  $\dot{s} = J_s \dot{\Theta}$  and the redundancy-based controller (7.11), we can easily track its dynamics along the nullspace of the first task with the input  $z_2$ , that is,

$$\dot{s} = J_s J_i^+ K e_i + J_s P_i z_2,$$

such that the minimal solution for  $\|\dot{s} - J_s \dot{\Theta}\|$ , yields

$$z_2 = (J_s P_i)^+ (\dot{s} - J_s J_i^+ K e_i). \quad (7.12)$$

*Remark 7.1.* The redundancy-controller (7.11) can be easily extended to exploit recent self-motion strategies, such as [152] to regard  $k$  levels of the hierarchical subtasks or as in [153] to regard a directional nullspace approach.

## 7.2 SWITCHING CONTROL SCHEME FOR FLEXIBLE COOPERATIVE TASK EXECUTION

This section proposes the novel switching control scheme for flexible task execution in the CDTS. The idea is to extend the results from Section 7.1, reduce control effort and provides the self-motion optimization with additional degrees of freedom by relaxing the control requirements in accordance to user-defined geometric task objectives.

### 7.2.1 Less restricted controller design

The redundancy-controller defined in (7.11) ensures stability of the primitive task variable dynamics within the task controllable set. In this sense, converging to an element within  $\mathfrak{A}_1$ , which corresponds to controlling the relative distance between arms, for example to hold a box of tools, requires the stabilization of the error  $e_1$ .

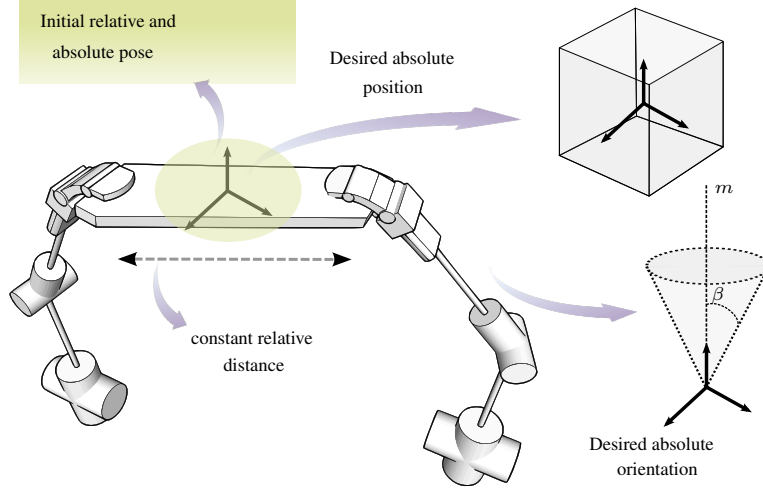


Figure 7.2: Illustration of controllable sets from primitive tasks.

Furthermore, to take the box from a point A to a drop region B, without dropping its contents, we must control the cooperative variables  $\underline{x}_a$  and  $\underline{x}_r$ , which yields an equilibrium within the controllable set  $\mathfrak{R}_2 \cup \mathfrak{R}_3 \cup \mathfrak{R}_4 \cup \mathfrak{R}_5$ .

The more complicate the main task is, the more degrees of freedom it uses, and the more difficult it is to apply the secondary constraints [153]. If the execution requires all the available DOFs, it yields a nonredundant bimanual system, and the task leaves no room for self-motion in (7.11).

In practice, however, a closer look at the task definition reveals that it usually can be satisfied even if the exact configuration has not been met, that is, it does not converge to the desired set-point but remains stable inside a surrounding region. In this context, the main idea is to define bounded geometric regions, instead of a complete pose configuration. For instance, in our example the rotation axis of the box does not need to be aligned with the  $z$ -axis from the base frame; however, it must be within a valid region around this equilibrium, particularly a region defined by a cone, as depicted in Figure 7.2.

Inside the valid region, which respects given bounds for the orientation and position, the control can be relaxed as the orientation is already satisfied. By switching to a task primitive that requires less DOF, we enlarge the self-motion space, which can be used to hold or reduce the orientation error while optimizing a secondary task. Both peripheral objectives compete for the enlarged self-motion in accordance to the proximity of the boundary region or with a given criterion defined by the secondary task.

The competition for the motion in the nullspace may be defined hierarchically [117, 152] or within a convex context as described in [154]. The latter technique will be used throughout this chapter, as it provides a better enlightenment of the competition process. Therefore, inside a valid region, the resulting controller yields

$$\dot{\Theta} = J_i^+ K e_i + \Theta_{\text{ESM}}, \quad (7.13)$$

where the enlarged self motion (ESM) dynamics is projected upon the vector input  $\Theta_{\text{ESM}}$ , such that

$$\Theta_{\text{ESM}} = \chi z_{OT} + (1 - \chi) z_{ST}, \quad (7.14)$$

with  $\chi \in [0, 1]$  being any smooth function that describes the competition scenario and yields importance to either the original primitive task  $z_{OT}$  (from Table 7.2) or to the secondary task  $z_{ST}$ , which are competing for the

nullspace motion, that is,

$$\begin{aligned} z_{OT} &= (\mathbf{J}_k \mathbf{P}_i)^+ (\dot{\mathbf{e}}_k - \mathbf{J}_k \mathbf{J}_i^+ \mathbf{K} \mathbf{e}_i), \\ z_{ST} &= (\mathbf{J}_s \mathbf{P}_i)^+ (\dot{\mathbf{s}} - \mathbf{J}_s \mathbf{J}_i^+ \mathbf{K} \mathbf{e}_i), \end{aligned} \quad (7.15)$$

where  $k \in \{2, \dots, 10\}$  is the index of the current more restricted primitive task  $\mathbf{e}_k$  (with regard to the active task  $\mathbf{e}_i$ ). In other words, the more restricted primitive task is the one that requires additional DOF from the cooperative space compared to the active primitive task  $\mathbf{e}_i$ ,  $i \in \{1, \dots, 9\}$ . The secondary task to be optimized and its corresponding Jacobian are denoted respectively by  $\dot{\mathbf{s}}$  and  $\mathbf{J}_s$ . Throughout this thesis, we shall assume a linear  $\chi$  defined within the hysteresis region with bounds corresponding to the boundaries of the valid region and the hysteresis region.

## 7.2.2 Hysteresis-based switching strategy

This subsection presents a new switching strategy that reduces the required number of DOF for a given task, thus enlarging the self-motion space, subjected to a set of geometric constraints upon the cooperative variables.

The switching rule relies on the pertinence of the current pose within sets of interest,  $\mathcal{I}$ , which are regions that respect some bounds for the orientation and/or position. These regions of interest must be designed as subsets from the primitive controllable sets  $\mathfrak{R}_i$ ,  $i = \{1, \dots, 5\}$ , as depicted in Figure 7.3.

The choice of the task primitive to be executed is therefore given in accordance to the required controllable sets to satisfy the regions of interest. As we reach a valid region, we may withdraw the controllable set requirement corresponding to that region (e.g., as pose A is driven towards pose B, in Figure 7.3). The switching therefore aims to reduce the required number of DOFs, whereas maintaining the relative and absolute configurations at the valid region. Now, if the nullspace motion from the less-restricted<sup>3</sup> controller acts as a disturbance, pushing the task variable to the boundary of the valid region, we must switch back to a more-restricted controller, in the sense of acting upon more DOF, to ensure that the trajectory will stabilize inside the valid region.

**Proposition 7.3** (Hysteresis-based switched controller). *Given a task objective defined within regions of interest  $\mathcal{I}_\ell \subseteq \mathfrak{R}_\ell$ ,  $\ell = \{1, \dots, 5\}$ , we investigate if an element  $h_\ell$  is amid  $\mathcal{I}_\ell$ , where  $h_\ell$  stems from a given parameterization from the active primitive task into the set  $\mathfrak{R}_\ell$ .*

*To ease the supervisor definition, we define a vector  $\boldsymbol{\sigma} = [\sigma_1 \ \sigma_2 \ \sigma_3 \ \sigma_4 \ \sigma_5]$  from characteristic piecewise constant functions  $\sigma_\ell \in \{0, 1\}$ , such that,*

$$\sigma_\ell = \begin{cases} 0, & \text{if } h_\ell \in \delta \mathcal{I}_\ell, \\ 1, & \text{if } h_\ell \notin \mathcal{I}_\ell, \\ \sigma_\ell, & \text{otherwise, } h_\ell \in \mathcal{I}_\ell \text{ and } h_\ell \notin \delta \mathcal{I}_\ell, \end{cases}$$

*where  $\delta \in [0, 1]$  is the hysteresis parameter which yields, with a slight abuse of notation, the subset  $\delta \mathcal{I}_\ell$  with respect to the region geometric bounds. In other words,  $\sigma_\ell = 0$  if  $h_\ell$  lies within the smaller subspace  $\delta \mathcal{I}_\ell$ , that is, if the relaxed task is being fully satisfied. On the other hand,  $\sigma_\ell = 1$  if the task lies outside the region of validity  $\mathcal{I}_\ell$  and needs to be activated to drive the pose to a valid region. The space between  $\delta \mathcal{I}_\ell$  and  $\mathcal{I}_\ell$  ensures slow switching.*

<sup>3</sup>In the sequel, to ease description, we refer to less or more-restricted controllers with respect to the number of DOF required.

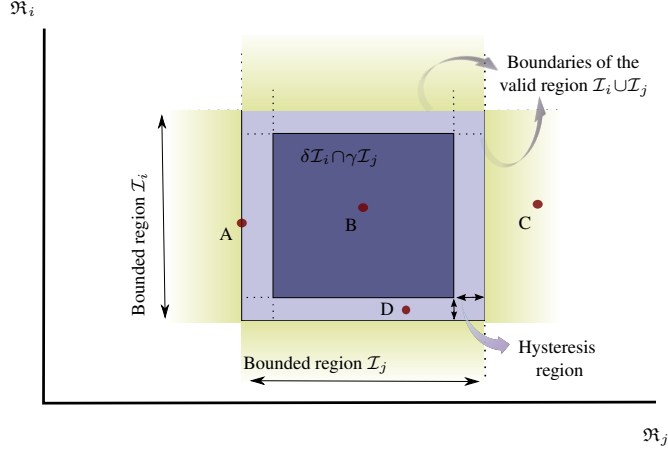


Figure 7.3: Given a task defined through the regions of interest,  $\mathcal{I}_i, \mathcal{I}_j$ , the valid region (in blue) is amid  $\mathfrak{R}_i \cup \mathfrak{R}_j$ . For example, if the initial pose satisfies only  $\mathcal{I}_i$  (as in pose C), the active task primitive must be controllable at  $\mathfrak{R}_j$ , but may relax the constraint upon  $\mathfrak{R}_i$  which can be optimized within the nullspace.

The less restricted controller (7.13)-(7.15) is switched along tasks primitives. Hence, the active task  $i$  lies within a controllable set characterized by the vector  $\zeta_i$  such that the required controllable set  $\sigma$  is a subset of the active task controllable set. Thus,

$$\begin{aligned} i &= \arg \min \text{DOF} \{e_i\}, \text{ subject to } \sigma \preceq \zeta_i, \\ k &= \arg \min \text{DOF} \{e_k\}, \text{ subject to } \zeta_i \preceq \zeta_k, \end{aligned} \quad (7.16)$$

where  $k$  is the task with higher hierarchy from the active task  $i$ ; that is, it defines the task primitive more restricted than  $e_i$  (active task with less DOF requirements). In the particular case when the task  $i$  is given by  $e_{10}$ , there is no  $k$  that satisfies (7.16), thus the peripheral task  $z_{OT}$  is null, and  $\chi \rightarrow 0$ .

The advantage of using the hysteresis-based switched controller of Proposition 7.3 is that, given the hysteresis region defined by the region designed between  $\mathcal{I}_i$  and  $\delta\mathcal{I}_i$ , as depicted in Figure 7.3 (pose D), the hysteresis strategy enforces state-dependent constraints, ensuring slow switching. This strategy eliminates the possibility of infinite switches on a finite interval, that is, it excludes chattering, or Zeno solutions [159].

Taking the worst case from the scenarios given in Table 7.2, we ought to recur to the complete cooperative task  $e_{10}$  which ensures stability<sup>4</sup> for any equilibrium in the manipulator workspace. In this sense, the switching strategy is completely controllable, as the controllable set is directly related to the sets from individual subsystems [160].

Moreover, all task primitives are derived from the dual pose  $e_{10}$  and can be regarded as a particular case from the complete dual pose task with different equilibria. Note that all equilibria from any task primitive can be assessed from  $e_{10}$  since the set of equilibria from all controllable sets are subsets of the equilibria from  $e_{10}$ . Nevertheless, stability analysis in the literature of hybrid and switched systems has generally been restricted to a single equilibrium point common to all subsystems [161]. Indeed, to the date, the literature for stability of multi-equilibria has been mostly restricted to the excel results from [161–164].

<sup>4</sup>In this chapter, we are neglecting the drawbacks from the double cover of  $\text{Spin}(3) \times \mathbb{R}^3$  over  $SE(3)$ , which may lead to unwinding effects at the end-effector [42, 43]. Nonetheless, an extension for the hybrid controller from Chapter 6 would suffice to ensure global stability.

As the stability of an equilibrium in the classic sense does not apply as the equilibrium switches during execution, a new definition is proposed in [163] to analyze the convergence to a compact set instead of an equilibrium. It can be stated as follows:

**Definition 7.3.** The switching equilibria system has a Stable Average Equilibrium if, for an arbitrary initial condition, the trajectory converges to a ball around the equilibrium with radius  $M$ , [163].

In this context, as we define a desired region for a given task objective, the center of each valid set corresponds to the equilibrium for the corresponding most-restricted task primitive. For any arbitrary pose external or at the boundary of the combined valid sets, the most restricted controller for the task primitive is activated, which ensures convergence to the valid region. Therefore, the switching strategy in Proposition 7.3 is stable in the sense of Definition 7.3 with respect to the pose at the center of the valid sets, with radius defined by the boundaries of those regions.

## 7.3 NUMERICAL EXAMPLES

To demonstrate the effectiveness of the proposed switching criterion to enlarge the self-motion space in the cooperative dual task-space, we designed in simulation a context with two seven-DOF KUKA LWR manipulators performing a cooperative manipulation, and derived the forward kinematics in the CDTS and the Jacobian matrices for primitive cooperative tasks with the aid of the with the `DQ_robotics` toolbox<sup>5</sup> and the Robotics Toolbox<sup>6</sup> in MATLAB.

In the proposed scenario, both arms must hold a box while transporting it to another location. Besides controlling the complete pose of the attached coordinate system, in a practical application the task would demand the control of the relative pose, as solely the distance control could cause undesired twists and internal forces upon the box.

Nonetheless, such phenomena could be avoided by simply enforcing a valid region for the relative position. Moreover, we could relax the description for the absolute orientation, since we just want to avoid sharp slant or obliquity.

With given requirements, a traditional cooperative framework [4] would require full dual pose control (twelve DOF), which makes more difficult to satisfy secondary tasks.

In contrast, the flexible framework could relax several constraints and enlarge the self-motion space by using switching rules proposed in Section 7.2. In this sense, besides controlling the relative distance and orientation together with the absolute position of the manipulated box, we design regions of interest for the box absolute orientation and for the relative position between arms,

$$\begin{aligned} \mathcal{I}_2 &= \{ \mathbf{t}_r \in \mathfrak{R}_2 \mid (0.95) \mathbf{t}_0 \preceq \mathbf{t}_r \preceq (1.05) \mathbf{t}_0 \} \\ \mathcal{I}_5 &= \left\{ \mathbf{r}_a \in \mathfrak{R}_5 \mid \mathbf{m} = \hat{k}, 0 \leq \langle \mathbf{m}, \mathbf{n} \rangle \leq \cos \beta_m \right\} \end{aligned} \quad (7.17)$$

<sup>5</sup><http://dqrobotics.sourceforge.net>

<sup>6</sup>[http://petercorke.com/Robotics\\_Toolbox.html](http://petercorke.com/Robotics_Toolbox.html)

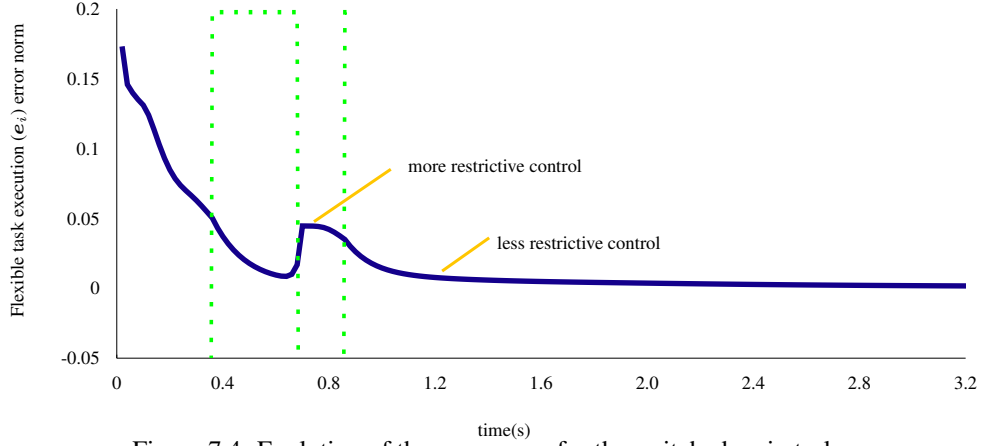


Figure 7.4: Evolution of the error norm for the switched main task  $e_i$ .

where  $\mathcal{I}_2$  define a cubic region covering the original relative position  $t_0$ , and  $\mathcal{I}_5$  define a cone with opening angle of  $\beta_m = 25^\circ$  around axis  $m$ , as depicted in Figure 7.2.

Let us regard a subtask that consists in avoiding joint limits, which is the secondary constraint to be optimized. Given the vector of joint variables  $\Theta$  for the two-arm system, the functional is given by

$$s = \sum_{i=1}^n \frac{1}{2} (\theta_i - \bar{\theta}_i)^2, \quad (7.18)$$

with  $\bar{\theta}_i = 0.5 (\theta_{i,\max} + \theta_{i,\min})$ , and differential forward kinematics given by  $\dot{s} = \mathbf{J}_s \dot{\Theta}$ , where  $\mathbf{J}_s = \nabla s = (\theta_1 - \bar{\theta}_1, \dots, \theta_n - \bar{\theta}_n)$ .

The results from the described scenario are shown in Figures 7.4 to 7.6. Besides the switching strategy, it is clear that the error  $e_i$  from the task execution converges to zero. The overshoot experienced around 0.8 s is due to the switching rule that augments the error vector with the orientation error vector.

Once the pose achieves a desired region in (7.17), the switching controller acts to enlarge the nullspace while maintaining the pose within (7.17). After the transient switches, the steady-error for the angle  $\beta$  between the rotation axis of the box and  $m$  is only  $6^\circ$ . In addition, the secondary task (7.18)—i.e., the joint limit optimization—performs considerably superior compared to the traditional cooperative framework, which yields an error about 45% higher than the proposed flexible framework. The result enlightens the importance of the new flexible framework for the exploitation of the self-motion dynamics, particularly when performing bimanual tasks.

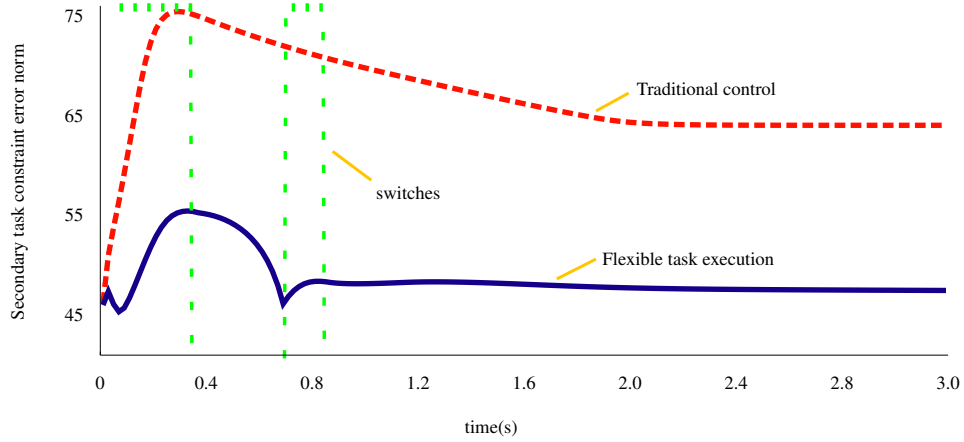


Figure 7.5: Evolution of the error norm for the secondary task (7.18) using self-motion dynamics (traditional controller in *dashed-red* and switched scheme in *solid-blue*).

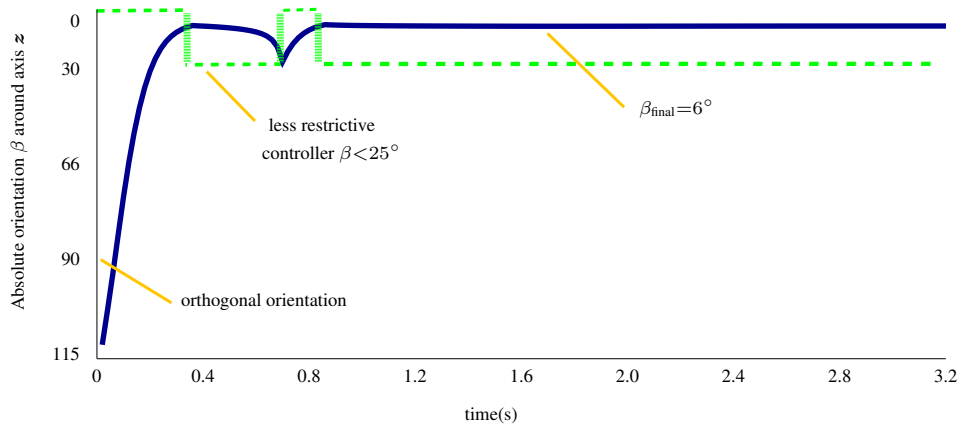


Figure 7.6: Evolution of the angle  $\beta$  for the cone in (7.17) with switching rule.



This manuscript has focused on the study of advanced kinematic control techniques in the perspective of robustness, optimality and flexibility and their applications to robot manipulators. These features have been central to this thesis and are cornerstones to support the challenges that arise from the robots of tomorrow, which are expected to perform sophisticated tasks deployed at increasingly less controlled scenarios. Moreover, since rigid body representation is paramount to the general kinematic control problem, herein we found unit dual quaternion formalism to be a rewarding alternative for representing finite rigid body transformations in space. Therefore, throughout this manuscript dual quaternion algebra has been the common tool used in proposed contributions.

Among the multiple dimensions concerning the control of robot manipulators, we first addressed their liability to modeling errors, uncertainties, and exogenous disturbances. With a detailed investigation on their sources and effects over the robot orientation and translation kinematics, we extracted an intuitive connection between their detrimental influence and performance over the task trajectory. Adapting classic  $H_\infty$  theory—suitable only for additive noises—to the algebra of dual quaternions, we derived easy-to-implement closed form  $H_\infty$  control criteria. The proposed solutions cope with robustness requirements, disturbance attenuation and performance properties with minimal control gains.

Moreover, to address the increasing requirements for manipulation accuracy in the context of compliant robots and reduced velocity profiles for multiple arms and human robot interaction, we proposed novel control strategies based on optimization theory adapted to dual quaternion space. The criteria derived herein differs from classic solutions in the sense that we focused on the optimization of task-space variables, e.g., the trajectory error with respect to the end-effector velocity. In addition to prevent drifts and overshoots, the analysis is particularly relevant in scenarios that require precise and safe interaction in contrast to convergence speed. For instance, the literature shows that, in human-robot interactions, controlled speed at task-space largely influences the human acceptance of the contact and reduces stress.

As the kinematic approach is liable to structure singularities regardless of the rigid body representation, we also addressed solutions to ensure proper manipulability throughout the whole task-space. First, we proved that classic self-motion techniques for redundant arms can be extended to the proposed dual quaternion control formalism. At the same time, we derived a novel singularity avoidance technique using the dual quaternion algebra for non-redundant arms that explicitly regulates the trade-off between the effort of avoiding inescapable singularities with respect to the error associated to the inherent trajectory modifications.

Moreover, the topological obstruction inherent to any rigid body representation that prevents global stability with a continuous control law has also been investigated. The topological restriction—that renders the unwinding phenomenon within unit dual quaternions—has been addressed using an hybrid control strategy. The criterion based on a switching control law with hysteresis ensures robust global stabilization for the closed-loop system.

Finally, a novel criterion based on switched control theory applied in a different context is introduced to enrich the self-motion of the manipulator as to cope with additional reactivity requirements from more complex control tasks. A novel concept, namely, flexible task execution was introduced to relax control specifications according to the end-effector's pose pertinence to regions of interest where fewer degrees of freedom are controlled. Hence, the task Jacobian nullspace is enlarged with additional DOFs to perform and improve

self-motion tasks. The strategy was introduced in the context of bimanual manipulation since the control of multiarms better illustrate the necessity for additional DOFs and reactivity, while the two-arm approach maintains the simplicity of the analysis.

For all the proposed approaches herein, rigorous mathematical evidence have been provided both to ensure accuracy and consistency and to provide means for proper practical applications and future comparison. Furthermore, several illustrative examples and simulations have been provided throughout this thesis to highlight the resulting criteria efficiency and reliability. Additional experiments have also been deployed in the context of multi-arm manipulation and optimization within compliant manipulators.

Substantial effort has been made to properly approach these problems in the field of kinematic control of robot manipulators using the algebra of dual quaternions and to unfold the tools for enabling sophisticated task execution. Despite the encouraging results in this thesis, there are further contributions that could be addressed in future research. Among possible improvements and further extensions, we highlight the following.

From the optimal control results within the algebra of dual quaternions presented in Chapter 7, a further step would be to consider additional optimization criteria with respect to the task-space variables. For instance, to consider minimal time optimal control by adapting classic works from [98, 100] to task-space framework with respect to optimal end-effector velocities. Additional task-space constraints such as obstacles and joint-limits could also be addressed within the control specifications.

All techniques proposed in this thesis concern non-redundant and redundant manipulators. As a consequence, a different strategy would be required for the case of underactuated manipulators. In this sense, a further contribution to be addressed would be to extend the switching control result presented in our previous work [165] to the context of stabilization at nonequilibrium points from [162]. Therein, a switching strategy is provided to stabilize the state of the system to points different from the set of subsystems equilibria. The dual quaternion formalism and the controllable sets from task primitives [1, 165] combined with the results from [162] unfolds control tools for underactuated manipulators to stabilize unreachable poses, that is, points outside the range space from available task primitives. Still at the context of our previous work [165], to incorporate a higher level switching supervisor based on automata, Petri net, or Dioid algebra theories is the natural next step towards the automation of the flexible manipulation strategy.

Moreover, to address a particular set of problems that arises from novel scenarios concerning surgical robotics and teleoperation, and that have been neglected herein, an important future contribution would be to extend our previous work [166] on networked control of quaternion based attitude subjected to unknown time-varying delays to the control analysis of a complete rigid body transformation using dual quaternion algebra. The work would be a first step towards a formal theory for the control of manipulators liable to time-delays. The analysis is also crucial for robust robotic manufacturing scenarios and service robots where bi-manual operation or human-robotic interaction with delayed human response are required.

Last, we have started some work towards extending the control results herein to filtering and estimation context within unit dual quaternion. The work in collaboration with Prof. Henrique Marra Menegaz from the University of Brasilia is a first step towards the study of a general separation principle theory within unit dual quaternion in the context of rigid body motion in robotics.

# **APPENDIX**



## RESUMO ESTENDIDO EM LÍNGUA PORTUGUESA

---

O objetivo principal deste trabalho é contribuir para a compreensão e para o avanço das técnicas de controle para robôs manipuladores a partir da exploração da álgebra de quatérnios duais. O presente trabalho fornece soluções para uma série de problemas relevantes e desafiadores para o controle cinemático de robôs manipuladores no espaço de tarefas com ênfase na precisão, robustez, otimização e flexibilidade. Estas características são essenciais para o desenvolvimento de ferramentas que permitam robôs executarem tarefas sofisticadas em cenários cada vez menos controlados.

A contínua investigação e pesquisa nas áreas de controle, cibernética e automação trouxeram o campo da robótica à beira de uma nova mudança de paradigma. O futuro da robótica está sendo estudado hoje e move-se em direção de capacitar robôs para execução de tarefas mais complexas do que as puramente repetitivas em linhas de montagem. Desta forma, os robôs tendem a participar ativamente da vida cotidiana dos seres humanos, a partir de uma interação mais fluída e robusta com outros robôs e com seres humanos em ambientes menos restritos.

Desde a revolução industrial no século 18 até os dias atuais, a relação humana com as máquinas mudou profundamente e rapidamente. Desde os primeiros robôs digitalmente operados e programáveis da Unimation nos anos cinquenta até o estado-da-arte mais recente, a robótica desempenhou—e ainda desempenha—um papel significativo nesta mudança de atitude que trouxe as máquinas para mais perto de seres humanos. Com o avanço das técnicas de controle baseadas em Lyapunov, das teorias de estimação baseadas em Kalman, e no desenvolvimento das técnicas de realimentação e cibernética de Wiener, a robótica floresceu como uma ciência voltada à compreensão e manipulação do mundo físico através de dispositivos mecânicos baseados em computador<sup>1</sup>.

Ainda há muito a ser feito em robótica e estamos muito longe do cenário futurista idealizado por Karel Čapek e Isaac Asimov<sup>2</sup>, mas a robótica é um campo com um enorme potencial transformador e capaz de mudar a forma como interagimos com o mundo e com nós mesmos. Apesar de ser um campo relativamente novo de estudo, a robótica tornou-se um campo inter e multidisciplinar de estudo, estimulando pesquisas e atraindo engenheiros de diversas áreas—como, por exemplo, controle, automação, mecânica, informática, elétrica, cibernética—cientistas, matemáticos, médicos, psicólogos, entre outros. Robôs estão atualmente presentes em diversos aspectos da construção da vida moderna, seja na fabricação industrial, na robótica de serviços, em carros autonomamente dirigidos, em braços manipuladores que auxiliam cirurgiões e outros dispositivos referentes a robótica médica, ou em plataformas robóticas para exploração aquática e planetária.

Não obstante, a maioria das aplicações que envolvem robôs—particularmente, em ambientes industriais—ainda estão usualmente limitadas pelas seguintes características: por segurança, os robôs trabalham em ambientes isolados de humanos, eles operam em ambientes que são bem estruturados e totalmente conhecidos, e são ainda condicionados a execução de tarefas simples e repetitivas.

---

<sup>1</sup>De acordo com a concepção de robótica apresentada por Thrun et al. [7]

<sup>2</sup>O termo do “robô” (do inglês, *Robot*) foi utilizado pela primeira vez na peça chamada “Robôs Universais de Rossum–RUR” (do inglês, *Rossum’s Universal Robots*) escrita pelo autor Tcheco Karel Čapek no qual ele descreve máquinas inteligentes que se assemelham a seres humanos e executam tarefas complexas e indesejáveis para seres humanos. Na década de quarenta, Asimov cunhou o termo “robótica” (do inglês, *robotics*) e postulou as famosas três leis da robótica.

Em contrapartida, espera-se que os robôs do amanhã sejam capazes de implementar e executar tarefas em ambientes cada vez menos estruturados e controlados, nos quais robustez e flexibilidade tornam-se características primordiais para o sucesso de cada operação. Neste cenário, espera-se que os robôs compreendam mudanças de ambientes e diferentes contextos, naveguem em ambientes povoados e não estruturados, e trabalhem com outros robôs e com os seres humanos. Investigando com maiores detalhes estes problemas, observa-se que mesmo problemas aparentemente simples como, por exemplo, a interpretação e medição de distância a partir de um sensor a laser, tornam-se bastante desafiadores devido à complexidade de lidarmos com ambientes realistas e as incertezas inerentes a este contexto. Estas incertezas são propagadas para problemas de decisão, planejamento e controle—exigindo respostas robustas para cada problema.

Esta tese foi motivada pelos novos desafios que surgem a partir do cenário idealizado acima e pela quantidade considerável de trabalho ainda a ser feito para alcançarmos tais características e funcionalidades. A tese foi desenvolvida no contexto do projeto *Towards Robust Robotic Manufacturing* do grupo *Model-based Embedded and Robotic Systems group* (MERS) do laboratório *Computer Science and Artificial Intelligence Laboratory* (CSAIL) da universidade Massachusetts Institute of Technology (MIT) em parceria com o grupo de pesquisa *Mechatronics, Control, and Robotics research group* (MACRO) da Universidade Federal de Minas Gerais (UFMG) e do Laboratório de Automação e Robótica (LARA) da Universidade de Brasília.

O projeto financiado pela Boeing, e a parceria pelo CNPq-MIT MISTI *Global Seed Funds*, destina-se a promoção do estado-da-arte em robótica e o desenvolvimento de ferramentas necessárias para o florescer de uma nova robótica, a robótica do amanhã. Neste contexto, espera-se que equipes de robôs atuem como pares colaborando a fim de alavancar suas diferentes habilidades na realização de tarefas complexas e elaboradas de forma robusta e eficiente em ambientes de trabalho semi-estruturados e, da mesma forma, sejam capazes de executar tarefas com auxílio humano.

Dentre as múltiplas dimensões deste projeto, o objetivo deste trabalho é contribuir para o entendimento e para o avanço das técnicas de controle para robôs manipuladores no sentido de robustez, otimização e flexibilidade—recursos essenciais para o nível esperado e necessário de desempenho e de autonomia robótica. Devido à necessidade de robôs operarem em diferentes condições e ambientes, e executarem tarefas complexas e variantes no tempo, as estratégias de controle também devem permitir reatividade. Assim, o presente trabalho foca-se em estratégias de controle cinemáticas no espaço de trabalho. Neste ponto, é essencial ressaltar que este nível de manipulação robótica ainda é um grande desafio e essencial para o florescer do cenário robótico idealizado.

A fim de estudar e projetar técnicas de controle robusto, ótimo e que permitam a flexibilização de tarefas para robôs manipuladores, esta tese explora as vantagens da álgebra de quatérnios duais para modelar e controlar a cinemática acoplada, rotação e translação, do robô manipulador no espaço de tarefas. Neste sentido, esta tese também pode ser vista como uma sequência do trabalho e da obra de Adorno [1] com referência a utilização da álgebra de quatérnios duais para a robótica. De fato, o uso de quatérnios duais unitários em robótica pode ser rastreado até as obras de [8–11], contudo apenas a partir do trabalho de Adorno uma estrutura completa para modelagem cinemática de robôs por meio de quatérnios duais unitários foi estabelecida e devidamente normalizada. Uma análise cuidadosa sobre as contribuições decorrentes do trabalho [1] lançam alguma luz sobre a mudança de paradigma promovida no sentido de representação de corpos rígidos no contexto de robótica. Desta forma, este trabalho, além de lidar com os desafios inerentes ao projeto *Towards Robust Robotic Manufacturing*, também objetiva estabelecer as bases de controle na álgebra de quatérnios duais e formalizar a teoria de controle na álgebra. Para tanto, esta tese também aborda e soluciona problemas intrínsecos à álgebra de quatérnios dual e à estrutura cinemática de robôs manipuladores—fornecendo ferramentas que permitam

tarefas complexas e sofisticadas serem realizadas de forma robusta e eficiente.

## Contribuições

A partir do formalismo de quatérnios duais unitários, esta tese apresenta soluções para uma série de problemas relevantes e difíceis que surgem no campo de controle cinemático para robôs manipuladores. Particularmente nesta tese, estamos interessados em estudar e solucionar os desafios mencionados na seção anterior que desempenham um papel importante em direção de uma robótica industrial robusta e o avanço de robôs de serviço. Além disso, os aspectos teóricos e práticos da álgebra de quatérnios duais são considerados e estudados em profundidade. Assim, esta tese também produz resultados no sentido de sistematizar técnicas de controle a partir da álgebra de quatérnios duais.

Primeiramente, o capítulo 2 fornece ao leitor um prelúdio das contribuições a fim de introduzir o leitor aos conceitos básicos e a base teórica matemática sobre transformações rígidas do corpo, sobre a álgebra de quatérnios e quatérnios duais, sobre a cinemática de braços robóticos manipuladores, e a uma base da teoria de controle utilizada. Este capítulo apresenta a estrutura necessária para entender os conceitos propostos na tese e lança uma luz sobre a importância de uma representação matemática adequada e as vantagens que derivam da utilização de quatérnios duais unitários.

Para além do capítulo de introdução e do capítulo de fundamentação, as principais contribuições da tese e sua organização são descritas da seguinte forma:

**Controle cinemático robusto no sentido  $H_\infty$  baseado em quatérnios duais** - À luz das aplicações práticas de robótica e motivado pelo problema de otimizar o desempenho do sistema em malha fechada, o Capítulo 3 investiga e defronta-se com a suscetibilidade de manipuladores robóticos com respeito a erros de modelagem e incertezas, distúrbios exógenos e, mais importante, apresenta soluções robustas com base na descrição e modelagem explícita dos requisitos de performance como problemas de controle  $H_\infty$ . Os controladores cinemáticos propostos são baseados na álgebra de quatérnios duais e são derivados de forma que o projeto de controle aborde explicitamente as diferentes fontes de incertezas e perturbações e a influência destes sobre a cinemática do efetuador (rotação e translação) no sentido  $H_\infty$ . A abordagem baseada na norma  $H_\infty$  possui a vantagem de relaxar as exigências relativas à descrição e modelagem da distribuição estatística dos ruídos—a representação destes é significativamente complexa de ser caracterizada dentro de qualquer representação de movimentos de corpos rígidos. Usando a álgebra de quatérnios duais, adaptamos técnicas clássicas de controle  $H_\infty$ —válidas apenas para análise de perturbações aditivas—a fim de derivar estratégias de controle  $H_\infty$  (de regulação e de rastreamento) de forma fechada e de fácil implementação que também incorporam requisitos de robustez, atenuação de perturbação, e propriedades de desempenho, minimizando o esforço de controle exigido. Assim, a partir dos critérios  $H_\infty$  baseados em quatérnios duais, obtemos um vínculo intuitivo e elegante entre o esforço de controle, os efeitos de desempenho sobre a trajetória do efetuador e diferentes fontes de incertezas e perturbações. A eficiência dos controladores propostos são avaliadas em cenários simulados em Matlab e no ambiente de experimentação virtual V-REP (do inglês, *Virtual Robot Experimentation Platform*) da empresa Coppelia Robotics GmbH.

**Rastreamento de trajetória ótimo baseado em quatérnios duais** - A fim de capacitar o manipulador robótico para diferentes perfis de operação e equilibrar de forma mais eficiente a precisão de manipulação com esforço de controle, particularmente no contexto de robôs complacentes, o Capítulo 4 aborda o problema de projeto de controladores no espaço de tarefas de robô manipuladores a partir de quatérnios duais unitários e no contexto da teoria de controle ótimo. Novas estratégias de controle no espaço de tarefas são propostas a a fim

de encontrar uma trajetória ótima para o efetuador no espaço de quatérnios duais, fornecendo uma ferramenta para equilibrar de forma mais conveniente o erro do efetuador com sua velocidade no espaço de operação. O controlador ótimo estende os resultados dos controladores baseados na álgebra de quatérnios duais propostos—compartilhando as vantagens de inerentes da representação—e fornece ao projetista um conjunto mais intuitivo de índices de performance, e amplia a gama de aplicações do formalismo de quatérnios duais em robótica. Em contraste a técnicas clássicas de controle ótimo, a otimização proposta foca em variáveis do espaço de tarefas do manipulador, simplificando consideravelmente a implementação do controlador. Como consequência, objetivamos um controlador ótimo para a velocidade do efetuador no espaço de tarefas. Esta análise é essencial ao lidarmos com tarefas avançadas de manipulação—como, por exemplo, a manipulação em ambientes perigosos ou não estruturados e manipulação com múltiplos braços—que exigem interação com maior precisão e segurança em contraste com a velocidade de convergência. Este é o caso por exemplo, da interação entre homem-robô na qual a velocidade do efetuador influencia largamente a aceitação humana ao contato e reduz o estresse e desconforto que surgem a partir da interação. A velocidade controlada no espaço de tarefas também evita derrapagens e sobrepessos causados por grandes requisitos de acelerações nos controladores de baixo nível do manipulador. Por fim, a fim de ilustrar a eficiência e a confiabilidade dos critérios ótimos propostos baseados em quatérnios duais, apresentamos um conjunto de exemplos numéricos e simulações em diferentes cenários e avaliamos os controladores experimentalmente em um manipulador complacente (Meka A2).

**Prevenção de singularidades cinemática pelo critério  $H_\infty$  descrito em quatérnios duais** - A fim de assegurar capacidades de manipulação adequadas em toda a área de trabalho do efetuador, o Capítulo 5 investiga o problema de prevenção de singularidades de robôs manipuladores. As singularidades desempenham um papel significativo na concepção e controle de corpos rígidos, em particular, no contexto de robôs manipuladores. A abordagem baseada em quatérnios duais unitários—de forma semelhante ao grupo de quatérnios para rotação pura—oferece uma solução para o modelamento cinemático completo acoplado (rotação mais translação) sem singularidades de representação. Não obstante, independentemente da representação movimento rígido, as tarefas de manipulação a partir de um braço manipulador são susceptíveis a singularidades cinemáticas onde configurações específicas das juntas tornam a cinemática direta diferencial mal-posta o que implica consequentemente na perda de um ou mais graus de liberdade. O estudo e a prevenção de singularidades cinemáticas de um manipulador é de grande importância uma vez que na vizinhança destas configurações podem surgir vários problemas devido à perda de posto matricial da Jacobiana. Contudo, dado que a maioria das soluções de prevenção de singularidades cinemáticas na literatura assumem que o espaço de tarefas é representado por um espaço Euclidiano, nos focamos em fornecer ferramentas que possam ser utilizadas e prevenir singularidades cinemáticas dentro espaço de quatérnios duais. No caso de manipuladores redundantes, provamos que as técnicas existentes com base no movimento no espaço nulo da Jacobiana (isto é, movimentos projetadas no seu espaço nulo) podem ser estendidos no formalismo de quatérnios duais proposto e nas Jacobianas aqui derivadas e, no caso de manipuladores não-redundantes, propomos uma nova estratégia de prevenção de singularidades utilizando critérios e o controlador  $H_\infty$  derivado na álgebra de quatérnios duais. Assim, a solução proposta, além de ser adequada para o espaço de operação não-Euclidiano, regula explicitamente a compensação entre a exatidão do rastreamento de tarefas e o esforço de prevenção de singularidades inevitáveis (e para braços não-redundantes) com base na teoria  $H_\infty$ .

**Estabilidade global robusta baseada em controle híbrido utilizando a álgebra de quatérnios duais** - As abordagens discutidas acima e as contribuições propostas nesta tese são baseadas em quatérnios duais unitários para a representação acoplada e compacta da cinemática de rotação e translação da movimentação do manipulador sem singularidades de representação. No entanto, qualquer representação adequada para movimento

de corpos rígidos apresenta uma obstrução topológica para a estabilização global por meio de um controlador contínuo. A representação por meio de quatérnios duais unitários não é uma exceção. De fato, cada pose (orientação e translação) de um corpo rígido pode ser representado por um par de quatérnios duais unitários antipodais o que por sua vez causa o fenômeno conhecido como *unwinding*—no qual um corpo rígido próximo à pose desejada pode convergir para o ponto antipodal mais distante que por sua vez representa a mesma pose. Neste contexto e utilizando o formalismo de quatérnios duais unitários, o Capítulo 6 aborda o problema da estabilização global da pose de um corpo rígido. Uma estratégia híbrida de controle é utilizada na derivação de um controlador chaveado baseado em histerese de modo que a estabilidade assintótica global do sistema em malha fechada é assegurada, e de tal forma que o controlador seja robusto contra pequenas perturbações arbitrárias. O controlador resultante é descrito em termos de transformações de corpos rígidos dentro da álgebra de quatérnios duais. Ademais, utilizando simulações numéricas ilustramos os problemas decorrentes de negligenciar a cobertura dupla—como, por exemplo, *unwinding* e vibrações indesejadas—e verificamos a eficácia do controlador proposto no sentido de solucionar o problema de estabilização robusta global da pose de um efetuador robótico.

### **Flexibilização de tarefas baseada na álgebra de quatérnios duais aplicada para manipulação bimanual -**

Além de estudar o problema de controle cinemático no espaço de tarefas a partir da álgebra de quatérnios duais no sentido de otimizar a trajetória de uma tarefa e incrementar a robustez do manipulador quanto a incertezas, a perturbações, as singularidades cinemáticas e, até mesmo, a obstruções topológicas inerentes a representações de corpos rígidos, neste trabalho investigamos também um novo paradigma de execução de tarefas robóticas. O contexto deste novo paradigma surge da necessidade de um nível adicional de reatividade para o manipulador em cenários dinâmicos. Em tarefas modernas de manipulação, além de satisfazer uma trajetória também estamos interessados em satisfazer restrições secundárias como, por exemplo, evitar singularidades, limites de juntas, obstáculos, entre outras poses indesejadas—usualmente, não conhecidas a priori. Neste sentido, movimentos no espaço nulo da tarefa principal são primordiais para a flexibilização e reatividade do manipulador quanto a cenários imprevistos, permitindo a realização de movimentos nas juntas do manipulador serial que não perturbem a trajetória principal do efetuador. Não obstante, mesmo problemas aparentemente simples podem exigir todos os graus de liberdade disponíveis no manipulador, não deixando espaço para movimentos no espaço nulo. Neste contexto, o capítulo 7 apresenta uma nova estratégia que permite o alargamento do espaço nulo sobre a Jacobiana da tarefa principal, relaxando especificações de controle de acordo com a pertinência da pose do efetuador em regiões de interesse—nas quais são necessários menos graus de liberdade. A fim de ilustrar a eficácia da estratégia proposta referente à ampliação do espaço nulo permitindo a execução de mais tarefas projetadas no espaço nulo da Jacobiana, consideramos o contexto de manipulação cooperativa com dois braços. O contexto de múltiplos braços manipuladores melhor ilustra a necessidade de mais graus de liberdade para execução de tarefas, contudo a execução de tarefas bimanual mantém o problema simples o suficiente para destacar as vantagens da técnica proposta.

Por fim, é essencial ressaltar que os resultados propostos são validados por uma exploração matemática rigorosa a fim de garantir precisão e síntese adequada para aplicações práticas. Assim, o trabalho formaliza a teoria de controle na álgebra de quatérnios duais e aprimora o estado-da-arte de controle para manipuladores—contribuindo com o esforço contínuo para o desenvolvimento da robótica do futuro.



# B

## SUMMARY OF DUAL QUATERNION BASED CONTROLLERS

This appendix provides the reader with a summary of control strategies proposed in this thesis for robot manipulators which are ready to be implemented. Moreover, we also revise classic control solutions—herein—described within dual quaternion algebra.

The solutions proposed in this thesis for the kinematic control of robot manipulators are basically based on the spatial difference between the current pose  $\underline{x}$  and desired pose  $\underline{x}_d$  defined within unit dual quaternions by

$$\underline{x}_e = \underline{x}\underline{x}_d^* = \mathbf{r}_e + \varepsilon \frac{1}{2} \mathbf{p}_e \mathbf{r}_e, \quad (\text{B.1})$$

where  $\mathbf{r}_e$  denote the orientation error in  $\text{Spin}(3)$  and  $\mathbf{p}_e$  the position error in  $\mathbb{H}_0$ . Hence,  $\underline{x}_e$  is a function of the form  $\underline{x}_e : (\text{Spin}(3) \times \mathbb{R}^3) \times (\text{Spin}(3) \times \mathbb{R}^3) \rightarrow \text{Spin}(3) \times \mathbb{R}^3$ . From the spatial difference, we also define an invariant dual quaternion error function of the form  $\underline{e} : \text{Spin}(3) \times \mathbb{R}^3 \mapsto \mathbb{H} \otimes \mathbb{D}$ , given by

$$\underline{e} = 1 - \underline{x}_e = \mathbf{e} + \varepsilon \mathbf{e}'. \quad (\text{B.2})$$

In this sense, when  $\underline{x}$  converges to  $\underline{x}_d$ , the dual quaternion error function  $\underline{e} \rightarrow 0$ . Analogously, to stabilize  $\underline{e}$  to 0 yields the end-effector convergence to the desired pose.

### B.1 CLASSIC CONTROL SOLUTIONS

The characteristics of classic controllers and their application in the context of robot manipulators can be summarized as follows:

#### Proportional controllers – K controllers

Classic proportional control strategies exponentially reduce the error between the current state of a general linear system and a given desired state. In the context of robot manipulators, they can be seen as the result of a least square minimization which locally minimizes<sup>1</sup> the required control effort—defined as the joint velocity vector norm—based on the task-space differential kinematics. For the simulations presented throughout this thesis, we will consider the following proportional controller (also called K-controllers herein)

$$\begin{cases} \mathbf{K} = k\mathbf{I}, & k \in \mathbb{R}^+ \\ \dot{\boldsymbol{\theta}} = \mathbf{N}^+ \mathbf{K} \text{vec}_8 \underline{e}, \end{cases}$$

where  $\dot{\boldsymbol{\theta}}$  is the task-space controller that yields the joint velocity input, and the error is defined in (B.2) with differential kinematics given by  $\dot{e} = -\mathbf{N}\dot{\boldsymbol{\theta}}$ . The matrix  $\mathbf{N}^+$  is the pseudo-inverse of the Jacobian  $\mathbf{N} = \overline{\mathbf{H}}(\underline{x}_d^*) \mathbf{J}_{\text{vec}}$  for a given representation based on the analytical dual quaternion based Jacobian, which can be found by using Algorithm 2.1, and using the Hamilton operator described in (2.15) and the  $\text{vec}_8$  mapping described in (2.14).

<sup>1</sup>It is important to emphasize that the joint velocity is minimized only locally since the result is based on instantaneous kinematics [112]

### Proportional controllers with feedforward term – K-FF controllers

Note that proportional controllers neglect the influence of a moving reference—that is, this class of controllers ignores the context when the end-effector is tracking a desired trajectory instead of a fixed point. To better address this particular context, a classic control solution is to add a feedforward term to the proportional controller (K+FF), that is,

$$\begin{cases} \mathbf{K} = k\mathbf{I}, & k \in \mathbb{R}^+ \\ \dot{\boldsymbol{\theta}} = \mathbf{N}^+(\mathbf{K} \text{vec}_8 \underline{\mathbf{e}} - \mathbf{e}_{ff}), \end{cases}$$

where the feedforward term  $\mathbf{e}_{ff}$  stems from the differential kinematics when  $\dot{\underline{\mathbf{x}}}_d \neq \mathbf{0}$ . For instance,  $\mathbf{e}_{ff} = \text{vec}_8(\underline{\mathbf{x}}\dot{\underline{\mathbf{x}}}_d^*)$  for a dual quaternion based error mapped to  $\mathbb{R}^8$  manifold where the differential kinematics is given by  $\dot{\underline{\mathbf{e}}} = -\mathbf{N}\dot{\boldsymbol{\theta}} - \text{vec}_8(\underline{\mathbf{x}}\dot{\underline{\mathbf{x}}}_d^*)$ .

## B.2 DUAL QUATERNION BASED $H_\infty$ CONTROL SOLUTIONS

### Dual quaternion based $H_\infty$ controller in $\mathbb{R}^8$ manifold

Considering the analytical dual quaternion based end-effector Jacobian  $\mathbf{J}_{\text{vec}}$  described in (2.38)-(2.41) and the influence of different sources of uncertainties and exogenous disturbances over the system, the differential kinematics of the robotic manipulator is given by (3.10):

$$\text{vec}_8 \dot{\underline{\mathbf{x}}} = \mathbf{J}_{\text{vec}} \dot{\boldsymbol{\theta}} + \mathbf{B} \text{vec}_8 \underline{\mathbf{v}}$$

where  $\boldsymbol{\theta} = [\theta_0 \dots \theta_{n-1}]^T$  is the measured vector of joint variables,  $\mathbf{J}_{\text{vec}}$  is the analytical dual quaternion based Jacobian, which can be found by using Algorithm 2.1,  $\mathbf{B}$  is a known matrix concerning  $\underline{\mathbf{x}}$  and  $\underline{\mathbf{v}}$  is the dual quaternion that describes both the uncertainties and the exogenous disturbances, whose influence we want to minimize. Note that  $\underline{\mathbf{v}}$  actually belongs to the set of pure dual quaternions  $\mathbb{H}_0 \otimes \mathbb{D}$  which in turn is isomorphic to  $\mathbb{R}^6$ .

In accordance to Theorem 3.3, a dual quaternion based  $H_\infty$  controller can be stated as following.

*For a prescribed  $\gamma > 0$ , a task-space  $H_\infty$  controller that stabilizes the error dynamics  $\text{vec}_8 \dot{\underline{\mathbf{e}}} = -\mathbf{N}\dot{\boldsymbol{\theta}} - \mathbf{B}_v \underline{\mathbf{v}}$ , whereas ensuring disturbance attenuation properties in the sense of Definition 3.1, is given by*

$$\dot{\boldsymbol{\theta}} = \mathbf{N}^+ \bar{\mathbf{K}} \text{vec}_8 \underline{\mathbf{e}},$$

*where  $\mathbf{N}^+$  is the pseudo-inverse of  $\mathbf{N} = \bar{\mathbf{H}}(\underline{\mathbf{x}}_d^*) \mathbf{J}_{\text{vec}}$ ,  $\mathbf{B}_v = \bar{\mathbf{H}}(\underline{\mathbf{x}}_d^*) \mathbf{B}$ , and*

$$\bar{\mathbf{K}} = \frac{1}{\gamma} \left( \mathbf{B}_v \mathbf{B}_v^T + \left[ \frac{\sqrt{2}}{4} \mathbf{B}_v^T \mathbf{B}_v \right] \mathbf{I} \right) \frac{\alpha}{\sqrt{\mathbf{B}_v^T \mathbf{B}_v \sqrt{2}}}, \quad (\text{B.3})$$

*is the minimum norm control gain for any scalar  $\alpha > 1$ . The norm of  $\bar{\mathbf{K}}$  is given by  $\|\bar{\mathbf{K}}\|_2 = \frac{1}{\gamma} \alpha \sqrt{\frac{1}{2}(1+\sqrt{8}) \mathbf{B}_v^T \mathbf{B}_v}$ .*

Further details concerning the above controller can be found in Theorem 3.3 and in Subsection 3.2.1.

The discrete-time tracking controller alternative for the proposed  $H_\infty$  controller—considering the discretization error—that also minimizes the norm of the control gain is derived in Theorem 3.6.

*For a prescribed performance parameter  $\gamma > 0$ , a control strategy with minimum norm for the control gain that ensures  $H_\infty$  tracking performance  $\gamma$  for the system (3.25) with exogenous disturbances and errors in the sense of Definition 3.2 is given by*

$$\boldsymbol{\theta}[k+1] = \boldsymbol{\theta}[k] + \mathbf{N}^+ \left( (\mathbf{I} - \overline{\mathbf{K}}) \text{vec}_8 \underline{\mathbf{e}}[k] + \text{vec}_8 \underline{\mathbf{x}}_{trk}[k] \right), \quad (\text{B.4})$$

where  $\mathbf{N}^+$  is the pseudo-inverse of  $\mathbf{N} = \overline{\mathbf{H}}(\underline{\mathbf{x}}_d^*[k+1]) \mathbf{J}_{\text{vec}}$  with  $\mathbf{B}_v = \overline{\mathbf{H}}(\underline{\mathbf{x}}_d^*[k+1]) \mathbf{B}$ , the feedforward term is given by  $\text{vec}_8 \underline{\mathbf{x}}_{trk}[k] = \overline{\mathbf{H}}(\underline{\mathbf{x}}_d^*[k+1] - \underline{\mathbf{x}}_d^*[k]) \text{vec}_8 \underline{\mathbf{x}}[k]$ , and the minimum control gain by

$$\overline{\mathbf{K}} = \alpha \sqrt{\mathbf{P}^{-1} - \gamma^{-2} \mathbf{B}_v \mathbf{B}_v^T} \sqrt{\mathbf{P} - \mathbf{I}}, \quad (\text{B.5})$$

with

$$\mathbf{P} = \gamma \sqrt{\mathbf{B}_v \mathbf{B}_v^T}^{-1}. \quad (\text{B.6})$$

Note that Theorems 3.4 and 3.5 are particular cases of the above dual quaternion based discrete-time  $H_\infty$  controller. For further details, the reader is referred to Subsection 3.2.2.

## $H_\infty$ Controller in dual quaternion space

Considering the dual quaternion Jacobian  $\mathbf{J}_\omega$  described in (2.42)-(2.48) and the influence of different sources of uncertainties and exogenous disturbances over the system, the differential kinematics of the robotic manipulator is given by (3.4):

$$\dot{\underline{\mathbf{x}}} = \frac{1}{2} \left( \text{vec}_6 \left( \mathbf{J}_\omega \dot{\boldsymbol{\theta}} \right) \underline{\mathbf{x}} + \underline{\mathbf{v}}_w \underline{\mathbf{x}} + \underline{\mathbf{v}}_c \underline{\mathbf{x}} \right)$$

where  $\text{vec}_6 \left( \mathbf{J}_\omega \dot{\boldsymbol{\theta}} \right)$  describes the end-effector twist in dual quaternion space based on the isomorphic mapping (2.12),  $\mathbf{J}_\omega$  is the twist Jacobian which can be found by using Algorithm 2.2. Moreover,  $\underline{\mathbf{v}}_w$  models the twist uncertainties and disturbances over the end-effector and  $\underline{\mathbf{v}}_c$  stems from the pose configuration uncertainties—for further details, the reader is referred to Section 3.1. As stressed in Chapter 3, the differential equation is well-posed as  $\underline{\mathbf{v}}_w = \mathbf{v}_w + \varepsilon \mathbf{v}'_w$  and  $\underline{\mathbf{v}}_c \triangleq \mathbf{v}_c + \varepsilon \mathbf{v}'_c$ —with  $\mathbf{v}_w, \mathbf{v}'_w, \mathbf{v}_c, \mathbf{v}'_c \in \mathbb{H}_0$ —is in the Lie algebra of  $\text{Spin}(3) \ltimes \mathbb{R}^3$ .

To address the detrimental influence of the uncertainties and disturbances in the  $H_\infty$  sense explicitly in dual quaternion space, we assume that  $\mathbf{v}_w, \mathbf{v}'_w, \mathbf{v}_c, \mathbf{v}'_c \in L_2[0, \infty)$  and introduce as variable of interest the orientation and translational errors from (3.44) defined respectively as

$$\mathcal{O}(\underline{\mathbf{e}}) \triangleq \mathbf{1} - \mathbf{r}_e,$$

$$\mathcal{T}(\underline{\mathbf{e}}) \triangleq \mathbf{p}_e,$$

where the dual quaternion error  $\underline{\mathbf{e}}$  is described in (B.2) with orientation and translation errors described by the spatial difference as in (B.1).

Hence, according to Theorem 3.8, a dual quaternion  $H_\infty$  tracking controller can be stated as following.

For prescribed positive performance scalar parameters  $\gamma_{o1}, \gamma_{o2}, \gamma_{\tau1}, \gamma_{\tau2}$ , the task-space controller yielding joint velocity inputs

$$\dot{\theta} = \underline{\mathbf{J}}_{\omega}^+ \left[ \mathbf{K}_o \text{vec}_3^T (\text{Im} (\mathcal{O}(\underline{\mathbf{e}}))) \quad -\mathbf{K}_{\tau} \text{vec}_3^T (\mathcal{T}(\underline{\mathbf{e}})) \right]^T + \underline{\mathbf{J}}_{\omega}^+ (\text{vec}_6 (\underline{\mathbf{x}}_e \underline{\omega}_d \underline{\mathbf{x}}_e^*)),$$

with feedforward term  $\text{vec}_6 (\underline{\mathbf{x}}_e \underline{\omega}_d \underline{\mathbf{x}}_e^*)$  based on the desired end-effector twist  $\underline{\omega}_d$  described in (3.52), and control gains  $\mathbf{K}_o \geq \sqrt{2} \sqrt{\gamma_{o1}^{-2} + \gamma_{o2}^{-2}} \mathbf{I}$  and  $\mathbf{K}_{\tau} \geq \sqrt{\gamma_{\tau1}^{-2} + \gamma_{\tau2}^{-2}} \mathbf{I}$  ensures exponential  $H_{\infty}$  tracking performance with disturbance rejection in the sense of Definition 3.3 with minimum norm control gain for the closed-loop system  $\dot{\underline{\mathbf{x}}}_e = \frac{1}{2} \left( \text{vec}_6 (\underline{\mathbf{J}}_{\omega} \dot{\theta}) + \underline{\mathbf{v}}_w + \underline{\mathbf{v}}_c \right) \underline{\mathbf{x}}_e - \frac{1}{2} \underline{\mathbf{x}}_e \underline{\omega}_d$  with error described by (B.2).

Note that Theorem 3.7 and Corollary 3.1 are particular cases of the above dual quaternion  $H_{\infty}$  controller. For further details, the reader is referred to Section 3.3.

Moreover, it is interesting to highlight that the dual quaternion based  $H_{\infty}$  solutions derived in Chapter 3 can be straightforwardly combined with the results from Chapters 5 and 6 to ensure robustness to kinematic singularities—inherent to the kinematic structure of manipulators—and to the topological obstruction—inherent to any representation of the rigid body coupled transformation.

For instance, a solution for the dual quaternion  $H_{\infty}$  tracking problem that ensures robust global exponential stability and singularity avoidance through self-motion can be directly extracted from Sections 3.3, 5.2 and 6.2.1:

For prescribed positive performance scalar parameters  $\gamma_{o1}, \gamma_{o2}, \gamma_{\tau1}, \gamma_{\tau2}$ , the task-space controller yielding joint velocity inputs

$$\begin{aligned} \dot{\theta} = & \underline{\mathbf{J}}_{\omega}^+ \left[ h \mathbf{K}_o \text{vec}_3^T (\text{Im} (\mathcal{O}(\underline{\mathbf{e}}))) \quad -\mathbf{K}_{\tau} \text{vec}_3^T (\mathcal{T}(\underline{\mathbf{e}})) \right]^T \\ & + \underline{\mathbf{J}}_{\omega}^+ (\text{vec}_6 (\underline{\mathbf{x}}_e \underline{\omega}_d \underline{\mathbf{x}}_e^*)) + (\mathbf{I} - \underline{\mathbf{J}}_{\omega}^+ \underline{\mathbf{J}}_{\omega}) \mathbf{y}, \end{aligned}$$

where  $h \in \{-1, 1\}$  is the memory state defined in (6.5) with hysteresis—characterized by a parameter  $\delta \in (0, 1)$ , such that,  $\dot{h} = 0$  when  $h\eta \geq -\delta$  and  $h^+ \in \overline{\text{sgn}}(\eta)$ , otherwise—ensures exponential  $H_{\infty}$  tracking performance with disturbance rejection in the sense of Definition 3.3 with minimum norm control gains defined by  $\mathbf{K}_o \geq \sqrt{2} \sqrt{\gamma_{o1}^{-2} + \gamma_{o2}^{-2}} \mathbf{I}$  and  $\mathbf{K}_{\tau} \geq \sqrt{\gamma_{\tau1}^{-2} + \gamma_{\tau2}^{-2}} \mathbf{I}$  for the closed-loop system  $\dot{\underline{\mathbf{x}}}_e = \frac{1}{2} \left( \text{vec}_6 (\underline{\mathbf{J}}_{\omega} \dot{\theta}) + \underline{\mathbf{v}}_w + \underline{\mathbf{v}}_c \right) \underline{\mathbf{x}}_e - \frac{1}{2} \underline{\mathbf{x}}_e \underline{\omega}_d$  with error described by (B.2).

Moreover, since  $(\mathbf{I} - \underline{\mathbf{J}}_{\omega}^+ \underline{\mathbf{J}}_{\omega}) \mathbf{y}$  represents the projection of  $\mathbf{y}$  onto the nullspace of  $\underline{\mathbf{J}}_{\omega}$ , setting  $\mathbf{y} \triangleq \alpha \nabla y$ , where  $\alpha$  is a given scalar and  $\nabla y = \frac{\partial y}{\partial \theta}$  is the gradient of a smooth scalar function  $y$  over  $\theta$ , then the nullspace solution forces  $y$  to decrease. For singularity avoidance, we can set  $\nabla y = \det \left\{ \underline{\mathbf{J}}_{\omega} \underline{\mathbf{J}}_{\omega}^T \right\} \text{tr} \left( \frac{\partial \underline{\mathbf{J}}_{\omega}}{\partial \theta} \underline{\mathbf{J}}_{\omega}^+ \right)$  which optimizes the manipulability function as to escape singularities.

Note that main task trajectory remains unchanged since  $\underline{\mathbf{J}}_{\omega} (\mathbf{I} - \underline{\mathbf{J}}_{\omega}^+ \underline{\mathbf{J}}_{\omega}) \rightarrow \mathbf{0}$  which defines the nullspace. The idea of optimizing a secondary task have been extended in [121] to multiple tasks—such as manipulability and distance to joint limits—switching dynamically (for further results, see [114–117]). Different solutions in this context are summarized in [115].

In the case of non-redundant manipulators or inescapable singularities, the solution for the dual quaternion  $H_\infty$  tracking problem that ensures robust global exponential stability and singularity avoidance can be obtained using the above strategies with the avoidance solution derived in Subsection 5.2.2.

*For prescribed positive performance scalar parameters  $\gamma_{o1}, \gamma_{o2}, \gamma_{\tau1}, \gamma_{\tau2}$ , the task-space controller yielding joint velocity inputs*

$$\dot{\boldsymbol{\theta}} = \underline{\mathbf{J}}_{\boldsymbol{\omega}}^+ \left[ h \mathbf{K}_o \text{vec}_3^T (\text{Im}(\mathcal{O}(\underline{\mathbf{e}}))) \quad - \mathbf{K}_\tau \text{vec}_3^T (\mathcal{T}(\underline{\mathbf{e}})) \right]^T + \underline{\mathbf{J}}_{\boldsymbol{\omega}}^+ (\text{vec}_6(\underline{\mathbf{x}}_e \boldsymbol{\omega}_d \underline{\mathbf{x}}_e^*)),$$

where  $h \in \{-1, 1\}$  is the memory state defined in (6.5), ensures exponential  $H_\infty$  tracking performance with disturbance rejection in the sense of Definition 3.3 with minimum norm control gains defined by  $\mathbf{K}_o \geq \sqrt{2} \sqrt{\gamma_{o1}^{-2} + \gamma_{o2}^{-2}} \mathbf{I}$  and  $\mathbf{K}_\tau \geq \sqrt{\gamma_{\tau1}^{-2} + \gamma_{\tau2}^{-2}} \mathbf{I}$  for the modified closed-loop system (5.8) that explicitly considers the induced twist  $\mathbf{v}_{s.a.} = \varsigma(\sigma_m\{\underline{\mathbf{J}}_{\boldsymbol{\omega}}\}) \cdot \mathbf{u}_m\{\underline{\mathbf{J}}_{\boldsymbol{\omega}}\}$ , where  $\sigma_m\{\underline{\mathbf{J}}_{\boldsymbol{\omega}}\}$  is the minimum singular value of  $\underline{\mathbf{J}}_{\boldsymbol{\omega}}$  and  $\mathbf{u}_m\{\underline{\mathbf{J}}_{\boldsymbol{\omega}}\}$  the corresponding output singular vector, and

$$\varsigma(\sigma_m\{\underline{\mathbf{J}}_{\boldsymbol{\omega}}\}) = \begin{cases} \varsigma_{\max} \cdot \left( 1 - \sqrt{\frac{\sigma_m\{\underline{\mathbf{J}}_{\boldsymbol{\omega}}\}}{\varsigma_s}} \right), & \text{if } \sigma_m\{\underline{\mathbf{J}}_{\boldsymbol{\omega}}\} \leq \varsigma_s, \\ 0, & \text{otherwise.} \end{cases}$$

where  $\varsigma_{\max}$  is the maximum value for the induced twist and  $\varsigma_s$  defines the size order of the singular region ( $\sigma_m\{\underline{\mathbf{J}}_{\boldsymbol{\omega}}\} > \varsigma_s$  yields a null twist).

It is also interesting to emphasize that the aforementioned control strategies can be combined in different manners in accordance to the task requirements.

### B.3 DUAL QUATERNION BASED OPTIMAL CONTROL SOLUTIONS

Motivated by the problem of optimizing the task-space trajectory of general serial-link manipulator described in time  $t \in [0, t_f]$  and its velocity at the task-space, Chapter 4 presented solutions both in  $\mathbb{R}^8$  manifold and within dual quaternion space.

#### Optimal Dual Quaternion Based Controller in $\mathbb{R}^8$ Manifold

Summarizing the optimal control strategy proposed in Section 4.1 for the dual quaternion error trajectory mapped to an  $\mathbb{R}^8$  manifold, we reached to the following cost function

$$F = \frac{1}{2} \text{vec}_8 \underline{\mathbf{e}}^T(t_f) \mathbf{S} \text{vec}_8 \underline{\mathbf{e}}(t_f) + \frac{1}{2} \int_{t_0}^{t_f} (\text{vec}_8 \underline{\mathbf{e}}^T(\tau) \mathbf{Q} \text{vec}_8 \underline{\mathbf{e}}(\tau) + \mathbf{u}^T(\tau) \mathbf{R} \mathbf{u}(\tau)) d\tau \quad (\text{B.7})$$

where  $\mathbf{S}, \mathbf{Q}, \mathbf{R} \in \mathbb{R}^{8 \times 8}$  are gain matrices satisfying  $\mathbf{S} \geq 0$ ,  $\mathbf{Q}(t) \geq 0$  and  $\mathbf{R}(t) > 0$ , and  $\mathbf{u}$  is the end-effector velocity mapped  $\mathbb{R}^8$  manifold.

The matrix  $\mathbf{S}$  is the weight of the final error norm, while the time-varying matrices  $\mathbf{Q}$  and  $\mathbf{R}$  respectively weigh the error cost along the trajectory and the control effort in terms of end-effector velocity norm. The

constrained optimization of (B.7) leads to an optimal feedback without excessive expenditure of control energy while keeping the error  $\text{vec}_8 \underline{e}(t)$  near zero [103].

Considering the analytical dual quaternion based end-effector Jacobian  $\mathbf{J}_{\text{vec}}$  described in (2.38)-(2.41), the optimal control tracking solution mapped to an  $\mathbb{R}^8$  is stated in Theorem 4.1 as follows.

*For prescribed gain matrices  $\mathbf{S}, \mathbf{Q}, \mathbf{R} \in \mathbb{R}^{8 \times 8}$  satisfying  $\mathbf{S} \geq 0$ ,  $\mathbf{Q}(t) \geq 0$  and  $\mathbf{R}(t) > 0$ , the task-space controller yielding joint velocity inputs*

$$\dot{\boldsymbol{\theta}} = \mathbf{N}^+ \mathbf{R}^{-1} (\mathbf{P} \text{vec}_8 \underline{e} + \boldsymbol{\xi}),$$

*where  $\mathbf{N}^+$  is the pseudo-inverse of  $\mathbf{N} = \bar{\mathbf{H}}(\underline{\mathbf{x}}_d) \mathbf{C}_8 \mathbf{J}_{\text{vec}}$ , minimizes the quadratic cost function (B.7). In other words, the optimal controller defines the optimal trajectory along (4.3), i.e.,  $\text{vec}_8 \dot{\underline{e}} = \mathbf{A} \text{vec}_8 \underline{e} - \mathbf{N} \dot{\boldsymbol{\theta}} + \mathbf{c}$ , for the cost function (B.7). The Lagrangian matrices  $\mathbf{P}$  and  $\boldsymbol{\xi}$  are derived from (4.13):*

$$\begin{cases} \dot{\mathbf{P}} &= -\mathbf{P}\mathbf{A} - \mathbf{A}^T \mathbf{P} + \mathbf{P}\mathbf{R}^{-1} \mathbf{P} - \mathbf{Q} \\ \dot{\boldsymbol{\xi}} &= -\mathbf{A}^T \boldsymbol{\xi} + \mathbf{P}\mathbf{R}^{-1} \boldsymbol{\xi} - \mathbf{P}\mathbf{c}, \end{cases}$$

*where  $\mathbf{A} = \bar{\mathbf{H}}(\underline{\mathbf{x}}_d^* \dot{\underline{\mathbf{x}}}_d)$ ,  $\mathbf{c} = -\text{vec}_8(\underline{\mathbf{x}}_d^* \dot{\underline{\mathbf{x}}}_d)$ , and  $\mathbf{C}_8 = \text{diag}(1, -1, -1, -1, 1, -1, -1, -1)$ .*

A solution for the nonlinear Riccati equation that describes the dynamics of the Lagrangian matrices  $\mathbf{P}$  and  $\boldsymbol{\xi}$  can be obtained by Euler based discretization of  $\mathbf{P}(t)$  and  $\boldsymbol{\xi}(t)$ . Hence, given the known value of  $\mathbf{P}(t_f)$ , an algebraic Riccati equation solver can be employed to find  $\mathbf{P}(t_{f-1})$ . Using a backward algorithm, we can then apply the same solver to find the value of  $\mathbf{P}(t_i)$  using previously calculated  $\mathbf{P}(t_{i+1})$ —the recursion is then applied up to  $\mathbf{P}(0)$ . The same can be applied to find an approximate solution for  $\boldsymbol{\xi}(t)$ , by also considering  $\mathbf{c}(t)$ , in (4.13).

## Optimal Quadratic Controller in Dual Quaternion Space

Considering the spatial difference in  $\text{Spin}(3) \times \mathbb{R}^3$  between the current and desired end-effector pose, that is,  $\underline{\mathbf{x}}_e = \underline{\mathbf{x}}_d^*$  and the dual quaternion Jacobian  $\mathbf{J}_{\underline{\omega}}$  described in (2.42)-(2.48), the differential kinematics of the end-effector trajectory error yields

$$\dot{\underline{\mathbf{x}}}_e = \frac{1}{2} \text{vec}_6 \left( \mathbf{J}_{\underline{\omega}} \dot{\boldsymbol{\theta}} \right) \underline{\mathbf{x}}_e - \frac{1}{2} \underline{\mathbf{x}}_e \underline{\boldsymbol{\omega}}_d, \quad (\text{B.8})$$

where  $\underline{\boldsymbol{\omega}}_d$  being the twist of the desired pose in inertial frame,  $\text{vec}_6 \left( \mathbf{J}_{\underline{\omega}} \dot{\boldsymbol{\theta}} \right)$  describes the end-effector twist in dual quaternion space based on the isomorphic mapping (2.12) and  $\mathbf{J}_{\underline{\omega}}$  is the twist Jacobian which can be found by using Algorithm 2.2.

To address the optimal trajectory tracking problem in dual quaternion space, we exploited the results from Theorem 4.2 which yields exponential convergence of the translational and rotational errors. Hence, the optimal control tracking solution in dual quaternion space follows from the cost function (4.5):

$$F = \frac{1}{2} e^T(t_f) \mathbf{S} e(t_f) + \frac{1}{2} \int_{t_0}^{t_f} \left( e^T(\tau) \mathbf{Q} e(\tau) + \mathbf{u}^T(\tau) \mathbf{R} \mathbf{u}(\tau) \right) d\tau \quad (\text{B.9})$$

where  $e = \left[ \text{vec}_3^T \{ \text{Im}(\mathbf{r}_e) \} \quad \text{vec}_3^T \{ \mathbf{p}_e \} \right]^T$ ,  $\mathbf{u}$  defines the end-effector twist given its rigid body description within unit dual quaternions as described in Section 4.2, and  $\mathbf{S}, \mathbf{Q}, \mathbf{R} \in \mathbb{R}^{6 \times 6}$  are gain matrices satisfying  $\mathbf{S} \geq 0$ ,  $\mathbf{Q}(t) \geq 0$  and  $\mathbf{R}(t) > 0$ . Moreover, the gain matrices are defined as  $3 \times 3$  block diagonal matrices.

The matrix  $\mathbf{S}$  is the weight of the final error norm, while the time-varying matrices  $\mathbf{Q}$  and  $\mathbf{R}$  respectively weigh the error cost along the trajectory and the control effort in terms of end-effector velocity norm. As long as  $\underline{\mathbf{J}}_{\omega}$  is well conditioned, an increase in  $\mathbf{R}$  will lead to an overall decrease in joint velocities. The optimization of B.9 leads to an optimal feedback in unit dual quaternion tangent space without excessive expenditure of control energy while optimizing the exponential convergence of the dual quaternion error function.

The optimization result in dual quaternion space from the cost function is stated in Theorem 4.3.

*For prescribed gain matrices  $\mathbf{S}, \mathbf{Q}, \mathbf{R}$  composed of pairs of  $3 \times 3$  block diagonal matrices and satisfying  $\mathbf{S} \geq 0$ ,  $\mathbf{Q}(t) \geq 0$  and  $\mathbf{R}(t) > 0$ , the task-space controller yielding joint velocity inputs*

$$\dot{\boldsymbol{\theta}} = \underline{\mathbf{J}}_{\omega}^+ \left[ -\mathbf{R}^{-1} \mathbf{P}(t) \mathbf{e} + \text{vec}_6(\underline{\mathbf{x}}_e \underline{\boldsymbol{\omega}}_d \underline{\mathbf{x}}_e^*) \right],$$

*defines an optimal quadratic controller for the system (4.17), that is, B.8, with positive definite matrix  $\mathbf{P}$  being derived from (4.32), that is,*

$$\dot{\mathbf{P}} = \mathbf{P} \mathbf{R}^{-1} \mathbf{P} - \mathbf{Q}.$$

Since  $\mathbf{S}, \mathbf{Q}, \mathbf{R}$  are constrained to be block diagonal, then it is needless to prove that  $\mathbf{P}$  also needs to be block diagonal. Furthermore, a solution for the nonlinear Riccati equation that describes the dynamics of the Lagrangian matrices  $\mathbf{P}$  can be obtained by Euler based discretization of  $P(t)$  and using an algebraic Riccati equation solver employed backwardly.

Similarly to the proposed  $H_{\infty}$  solutions, the dual quaternion optimal control strategies can be straightforwardly combined with the results from Chapter 6 to ensure robust global stability—escaping from the unwinding phenomenon inherent to the  $\text{Spin}(3) \times \mathbb{R}^3$  topological obstruction that prevents global asymptotic stability with a continuous controller.

*For prescribed gain matrices  $\mathbf{S}, \mathbf{Q}, \mathbf{R}$  composed of pairs of  $3 \times 3$  block diagonal matrices and satisfying  $\mathbf{S} \geq 0$ ,  $\mathbf{Q}(t) \geq 0$  and  $\mathbf{R}(t) > 0$ , the task-space controller yielding joint velocity inputs*

$$\dot{\boldsymbol{\theta}} = \underline{\mathbf{J}}_{\omega}^+ \left[ -\text{diag}(h\mathbf{I}, \mathbf{I}) \mathbf{R}^{-1} \mathbf{P}(t) \mathbf{e} + \text{vec}_6(\underline{\mathbf{x}}_e \underline{\boldsymbol{\omega}}_d \underline{\mathbf{x}}_e^*) \right],$$

*where  $\mathbf{I}$  is a  $3 \times 3$  identity matrix and  $h \in \{-1, 1\}$  is the memory state defined in (6.5) with hysteresis—characterized by a parameter  $\delta \in (0, 1)$ , such that,  $\dot{h} = 0$  when  $h\eta \geq -\delta$  and  $h^+ \in \overline{\text{sgn}}(\eta)$ , otherwise—defines an optimal quadratic controller for the system (4.17), that is, B.8, with positive definite matrix  $\mathbf{P}$  being derived from (4.32), that is,*

$$\dot{\mathbf{P}} = \mathbf{P} \mathbf{R}^{-1} \mathbf{P} - \mathbf{Q}.$$

The singularity avoidance strategy from Chapter 5 can also be imposed to the dual quaternion optimal

tracking controller, however it will inherently modify the optimization result.

## B.4 SWITCHING STRATEGY FOR FLEXIBLE TASK EXECUTION

In Chapter 7, we focused on bimanual task execution within the cooperative dual task-space, but the strategy is more general and can be applied to single manipulators or extended to multiple arm manipulation. The goal of the strategy is to cope with highly complex task descriptions, which are common in a cooperative manipulation scenario, while enlarging the self-motion space. This is performed by relaxing control requirements within regions of interests, and thus adding additional DOF for a secondary task. To ensure stability to the desired region of interest, we propose a hysteresis-based switching control strategy which aims to reduce the complexity of the main task while maintaining the pose (i.e., position and orientation) within the valid region.

A manipulator task is hence described by task primitives. A summary of the task primitive definition, error description, the required number of DOFs, and the vector description that characterizes the task required controllable sets is presented in Table 7.2.

Inside the valid region, which respects given predefined bounds, the control can be relaxed as pertinence to a valid region is satisfied. By switching to a task primitive that requires less DOF, we enlarge the self-motion space, which can be used to hold or reduce the end-effector task primitive within the valid region while optimizing a secondary task. Both peripheral objectives compete for the enlarged self-motion in accordance to the proximity of the boundary region or with a given criterion defined by the secondary task. For further details, the reader is referred to Chapter 7.

The switching strategy is defined as follows.

*Given a task objective defined within regions of interest  $\mathcal{I}_\ell \subseteq \mathfrak{R}_\ell$ ,  $\ell = \{1, \dots, 5\}$ , we investigate if an element  $h_\ell$  is amid  $\mathcal{I}_\ell$ , where  $h_\ell$  stems from a given parameterization from the active primitive task into the set  $\mathfrak{R}_\ell$ .*

*To ease the supervisor definition, we define a vector  $\sigma = [\sigma_1 \ \sigma_2 \ \sigma_3 \ \sigma_4 \ \sigma_5]$  from characteristic piecewise constant functions  $\sigma_\ell \in \{0, 1\}$ , such that,*

$$\sigma_\ell = \begin{cases} 0, & \text{if } h_\ell \in \delta\mathcal{I}_\ell, \\ 1, & \text{if } h_\ell \notin \mathcal{I}_\ell, \\ \sigma_\ell, & \text{otherwise, } h_\ell \in \mathcal{I}_\ell \text{ and } h_\ell \notin \delta\mathcal{I}_\ell, \end{cases}$$

*where  $\delta \in [0, 1]$  is the hysteresis parameter which yields, with a slight abuse of notation, the subset  $\delta\mathcal{I}_\ell$  with respect to the region geometric bounds. In other words,  $\sigma_\ell = 0$  if  $h_\ell$  lies within the smaller subspace  $\delta\mathcal{I}_\ell$ , that is, if the relaxed task is being fully satisfied. On the other hand,  $\sigma_\ell = 1$  if the task lies outside the region of validity  $\mathcal{I}_\ell$  and needs to be activated to drive the pose to a valid region. The hysteresis region between  $\delta\mathcal{I}_\ell$  and  $\mathcal{I}_\ell$  ensures slow switching.*

*The resulting switched controller is defined as*

$$\dot{\Theta} = J_i^+ K e_i + \Theta_{ESM}, \quad (\text{B.10})$$



where the active task  $e_i$  lies within a controllable set characterized by the vector  $\zeta_i$  such that the required controllable set  $\sigma$  is a subset of the active task controllable set ( $e_i$  is the task with less DOF requirements satisfying the required controllable set  $\sigma$ ). Thus,

$$\begin{aligned} i &= \arg \min \text{DOF} \{e_i\}, \text{ subject to } \sigma \preceq \zeta_i, \\ k &= \arg \min \text{DOF} \{e_k\}, \text{ subject to } \zeta_i \preceq \zeta_k, \end{aligned} \quad (\text{B.11})$$

where  $k \in \{2, \dots, 10\}$  is the index of the current more restricted primitive task  $e_k$  (with regard to the active task  $e_i$ ). In other words, the more restricted primitive task is the one that requires additional DOF from the cooperative space compared to the active primitive task  $e_i$ ,  $i \in \{1, \dots, 9\}$ .

The enlarged self motion (ESM) dynamics is projected upon the vector input  $\Theta_{\text{ESM}}$ , such that

$$\Theta_{\text{ESM}} = \chi z_{OT} + (1 - \chi) z_{ST}, \quad (\text{B.12})$$

with  $\chi \in [0, 1]$  being any smooth function that describes the competition scenario and yields importance to either the original primitive task  $z_{OT}$  (from Table 7.2) or to the secondary task  $z_{ST}$ , which are competing for the nullspace motion, that is,

$$\begin{aligned} z_{OT} &= (\mathbf{J}_k \mathbf{P}_i)^+ (\dot{e}_k - \mathbf{J}_k \mathbf{J}_i^+ \mathbf{K} e_i), \\ z_{ST} &= (\mathbf{J}_s \mathbf{P}_i)^+ (\dot{s} - \mathbf{J}_s \mathbf{J}_i^+ \mathbf{K} e_i), \end{aligned} \quad (\text{B.13})$$

where the secondary task to be optimized and its corresponding Jacobian are denoted respectively by  $\dot{s}$  and  $\mathbf{J}_s$ . In the particular case when the task  $i$  is given by  $e_{10}$ , there is no  $k$  that satisfies (B.11), thus the peripheral task  $z_{OT}$  is null, and  $\chi \rightarrow 0$ .

# C

## GENERAL PROOFS AND DEFINITIONS

This appendix provides the reader with detailed proof of theorems, lemmas and derivations used herein.

### C.1 GENERAL LYAPUNOV CANDIDATE FUNCTION DERIVATIVE

In Section 3.3, particularly, in Theorem 3.7, we proposed a Lyapunov candidate function of the form<sup>1</sup>

$$V(t, \underline{\mathbf{x}}) = \|\underline{\mathbf{x}}(t)\| = \alpha_1 \|\underline{\mathbf{1}} - \underline{\mathbf{x}}(t)\|_2^2 + \alpha_2 \|\underline{\mathbf{x}}'(t)\|_2^2, \quad (\text{C.1})$$

where  $\underline{\mathbf{x}} = \underline{\mathbf{x}} + \varepsilon \underline{\mathbf{x}}' = \underline{\eta} + \underline{\boldsymbol{\mu}} + \varepsilon (\underline{\eta}' + \underline{\boldsymbol{\mu}}')$  and  $\alpha_1, \alpha_2$  are strictly positive scalars. The time-derivative of this general Lyapunov candidate function yields<sup>2</sup>

$$\dot{V}(t, \underline{\mathbf{x}}) = -2\alpha_1 \dot{\underline{\eta}} + 2\alpha_2 \underline{\eta}' \dot{\underline{\eta}}' + 2\alpha_2 \langle \underline{\boldsymbol{\mu}}', \dot{\underline{\boldsymbol{\mu}}}' \rangle. \quad (\text{C.2})$$

To investigate the exponential stability in the absence of exogenous disturbances of the closed-loop system, let us first recall the end-effector differential kinematics represented within dual quaternion space:

$$\begin{aligned} \underline{\mathbf{x}} &= \underline{\mathbf{r}} + \varepsilon \frac{1}{2} \underline{\mathbf{p}} \underline{\mathbf{r}}, \\ \dot{\underline{\mathbf{x}}} &= \frac{1}{2} \text{vec}_6 \left( \underline{\mathbf{J}} \dot{\underline{\boldsymbol{\theta}}} \right) \underline{\mathbf{x}}, \end{aligned}$$

and the dual quaternion task-space controller defined in (3.47), that is,

$$\dot{\underline{\boldsymbol{\theta}}} = \underline{\mathbf{J}}^+ \left[ \mathbf{K}_\mathcal{O} \text{vec}_3^T (\text{Im}(\mathcal{O}(\underline{\mathbf{e}}))) \quad -\mathbf{K}_\mathcal{T} \text{vec}_3^T (\mathcal{T}(\underline{\mathbf{e}})) \right]^T$$

where  $\mathbf{K}_\mathcal{O}, \mathbf{K}_\mathcal{T}$  are positive definite  $3 \times 3$  matrices,  $\underline{\mathbf{e}} = \underline{\mathbf{1}} - \underline{\mathbf{x}}$ , and  $\mathcal{O}(\underline{\mathbf{e}})$  and  $\mathcal{T}(\underline{\mathbf{e}})$  are defined as  $\mathcal{O}(\underline{\mathbf{e}}) = \underline{\mathbf{1}} - \underline{\mathbf{r}}$  and  $\mathcal{T}(\underline{\mathbf{e}}) = \underline{\mathbf{p}}$ . If  $\underline{\mathbf{J}} \in \mathbb{R}^{6 \times n}$  is well-posed, then the closed loop differential kinematics is therefore given by

$$\dot{\underline{\mathbf{x}}} = \frac{1}{2} \text{vec}_6 \left[ \mathbf{K}_\mathcal{O} \text{vec}_3^T (\text{Im}(\mathcal{O}(\underline{\mathbf{e}}))) \quad -\mathbf{K}_\mathcal{T} \text{vec}_3^T (\mathcal{T}(\underline{\mathbf{e}})) \right]^T \underline{\mathbf{x}}. \quad (\text{C.3})$$

*Remark C.1.* Note that, in addition to Theorem 3.7, the first order derivative (C.2) also appears in the proof of Theorem 6.1, Section 6.2. Indeed, if we take  $\alpha_1$  to be the memory state (6.5) and  $\alpha_2$  to be the identity element, then (C.2) yields exactly the same derivative from (6.12) (note that, although having the same derivative, the Lyapunov function associated with Theorem 6.1 is different from C.1 and positiveness is proven in Section 6.2 even considering  $\alpha_1$  as the memory state). Moreover, if we regard  $\mathbf{K}_\mathcal{O}$  to be  $hk_1$  (where  $h$  is the memory state (6.5)) and  $\mathbf{K}_\mathcal{T}$  to be the identity  $k_2 \mathbf{I}$ , with  $k_1, k_2 \in \mathbb{R}_+^*$ , then the closed loop considered in Theorem 6.1 is exactly the same to (C.3).

Expressing (C.3) in terms of the dual quaternion components yields

$$\dot{\underline{\mathbf{x}}} = \dot{\underline{\eta}} + \dot{\underline{\boldsymbol{\mu}}} + \varepsilon (\dot{\underline{\eta}}' + \dot{\underline{\boldsymbol{\mu}}}')$$

<sup>1</sup>Particularly, in Theorem 3.7, we regarded a Lyapunov candidate function of the form  $V(t, \underline{\mathbf{e}}) = \|\underline{\mathbf{e}}(t)\| = \alpha_1 \|\underline{\mathbf{e}}(t)\|_2^2 + \alpha_2 \|\underline{\mathbf{e}}'(t)\|_2^2$ , where  $\underline{\mathbf{e}}(t) = \underline{\mathbf{1}} - \underline{\mathbf{x}}(t)$ . Please note that the function is exactly the same of the one described in (C.1) with a simple variable change.

<sup>2</sup>To ease the description and for brevity, the time indexes herein.

with

$$\begin{aligned}\dot{\eta} &= -\frac{1}{2}\langle \mathbf{h}_1, \boldsymbol{\mu} \rangle, & \dot{\eta}' &= -\frac{1}{2}(\langle \mathbf{h}_1, \boldsymbol{\mu}' \rangle + \langle \mathbf{h}_2, \boldsymbol{\mu} \rangle), \\ \dot{\boldsymbol{\mu}}' &= \frac{1}{2}(\eta' \mathbf{h}_1 + \eta \mathbf{h}_2 + \mathbf{h}_1 \times \boldsymbol{\mu}' + \mathbf{h}_2 \times \boldsymbol{\mu}),\end{aligned}$$

where  $\mathbf{h}_1 = \text{vec}_3(\mathbf{K}_\circ \text{vec}_3 \text{Im}(\mathcal{O}(\underline{e})))$  and  $\mathbf{h}_2 = -\text{vec}_3(\mathbf{K}_\tau \text{vec}_3(\mathcal{T}(\underline{e})))$ . Replacing (C.3) within the Lyapunov derivative yields

$$\begin{aligned}\dot{V}(t, \underline{\mathbf{x}}) &= 2(\alpha_1 \frac{1}{2} \langle \mathbf{h}_1, \boldsymbol{\mu} \rangle - \alpha_2 \frac{1}{2} \eta' (\langle \mathbf{h}_1, \boldsymbol{\mu}' \rangle + \langle \mathbf{h}_2, \boldsymbol{\mu} \rangle)) \\ &\quad + 2\alpha_2 (\frac{1}{2} \langle \boldsymbol{\mu}', (\eta' \mathbf{h}_1 + \eta \mathbf{h}_2 + \mathbf{h}_1 \times \boldsymbol{\mu}' + \mathbf{h}_2 \times \boldsymbol{\mu}) \rangle) \\ &= \alpha_1 \langle \boldsymbol{\mu}, \mathbf{h}_1 \rangle - \alpha_2 (\eta' \langle \boldsymbol{\mu}', \mathbf{h}_1 \rangle + \eta' \langle \boldsymbol{\mu}, \mathbf{h}_2 \rangle) + \alpha_2 \langle \boldsymbol{\mu}', \eta' \mathbf{h}_1 \rangle \\ &\quad + \alpha_2 \langle \eta \boldsymbol{\mu}', \mathbf{h}_2 \rangle + \alpha_2 \langle \boldsymbol{\mu}', (\mathbf{h}_1 \times \boldsymbol{\mu}') \rangle + \alpha_2 \langle \boldsymbol{\mu}', (\mathbf{h}_2 \times \boldsymbol{\mu}) \rangle \\ &= \langle \alpha_1 \boldsymbol{\mu}, \mathbf{h}_1 \rangle + \alpha_2 \langle \eta \boldsymbol{\mu}' - \eta' \boldsymbol{\mu}, \mathbf{h}_2 \rangle + \alpha_2 \langle \boldsymbol{\mu}, \boldsymbol{\mu}' \times \mathbf{h}_2 \rangle \\ &= \alpha_1 \langle \boldsymbol{\mu}, \mathbf{h}_1 \rangle + \alpha_2 \langle -\eta' \boldsymbol{\mu} + \eta \boldsymbol{\mu}' + (\boldsymbol{\mu} \times \boldsymbol{\mu}'), \mathbf{h}_2 \rangle.\end{aligned}\tag{C.4}$$

Considering minimum singular value from from  $\mathbf{K}_\circ$  and  $\mathbf{K}_\tau$ , that is,  $\sigma_m\{\mathbf{K}_\circ\}$  and  $\sigma_m\{\mathbf{K}_\tau\}$ ,

$$\begin{aligned}\dot{V}(t, \underline{\mathbf{x}}) &= \alpha_1 \langle \boldsymbol{\mu}, \sigma_m\{\mathbf{K}_\circ\} \text{Im}(\mathcal{O}(\underline{e})) \rangle \\ &\quad - \alpha_2 \langle \eta \boldsymbol{\mu}' - \eta' \boldsymbol{\mu} + \boldsymbol{\mu} \times \boldsymbol{\mu}', \sigma_m\{\mathbf{K}_\tau\} \mathcal{T}(\underline{e}) \rangle.\end{aligned}$$

Noting that  $\frac{1}{2}\mathcal{T}(\underline{e}) = \eta \boldsymbol{\mu}' - \eta' \boldsymbol{\mu} + \boldsymbol{\mu} \times \boldsymbol{\mu}'$ ,  $\text{Im}(\mathcal{O}(\underline{e})) = -\boldsymbol{\mu}$ , we have  $\dot{V}(t, \underline{\mathbf{x}}) \leq V_1$ , where

$$\begin{aligned}V_1 &\triangleq \alpha_1 \sigma_m\{\mathbf{K}_\circ\} \langle \boldsymbol{\mu}, -\boldsymbol{\mu} \rangle \\ &\quad - 2\alpha_2 \sigma_m\{\mathbf{K}_\tau\} \langle \eta \boldsymbol{\mu}' - \eta' \boldsymbol{\mu} + \boldsymbol{\mu} \times \boldsymbol{\mu}', \eta \boldsymbol{\mu}' - \eta' \boldsymbol{\mu} + \boldsymbol{\mu} \times \boldsymbol{\mu}' \rangle \\ &= -\alpha_1 \sigma_m\{\mathbf{K}_\circ\} \langle \boldsymbol{\mu}, \boldsymbol{\mu} \rangle - 2\alpha_2 \sigma_m\{\mathbf{K}_\tau\} (\eta^2 \langle \boldsymbol{\mu}', \boldsymbol{\mu}' \rangle \\ &\quad + \eta'^2 \langle \boldsymbol{\mu}, \boldsymbol{\mu} \rangle + \langle \boldsymbol{\mu} \times \boldsymbol{\mu}', \boldsymbol{\mu} \times \boldsymbol{\mu}' \rangle - 2\eta \eta' \langle \boldsymbol{\mu}, \boldsymbol{\mu}' \rangle + 0 + 0) \\ &= -\alpha_1 \sigma_m\{\mathbf{K}_\circ\} \langle \boldsymbol{\mu}, \boldsymbol{\mu} \rangle - 2\alpha_2 \sigma_m\{\mathbf{K}_\tau\} (\eta^2 \langle \boldsymbol{\mu}', \boldsymbol{\mu}' \rangle \\ &\quad + \eta'^2 \langle \boldsymbol{\mu}, \boldsymbol{\mu} \rangle + \langle \boldsymbol{\mu}, \boldsymbol{\mu} \rangle \langle \boldsymbol{\mu}', \boldsymbol{\mu}' \rangle - \langle \boldsymbol{\mu}, \boldsymbol{\mu}' \rangle^2 - 2\eta \eta' \langle \boldsymbol{\mu}, \boldsymbol{\mu}' \rangle).\end{aligned}$$

From the unit dual quaternion group constraint (2.18), we have that,  $\eta \eta' + \langle \mathbf{u}, \mathbf{u}' \rangle = 0$ , which in turn yields

$$\begin{aligned}V_1 &= -\alpha_1 \sigma_m\{\mathbf{K}_\circ\} \|\boldsymbol{\mu}\|_2^2 - 2\alpha_2 \sigma_m\{\mathbf{K}_\tau\} \left( \eta^2 \|\boldsymbol{\mu}'\|_2^2 \right. \\ &\quad \left. + \eta'^2 \|\boldsymbol{\mu}\|_2^2 + \|\boldsymbol{\mu}\|_2^2 \|\boldsymbol{\mu}'\|_2^2 - (-\eta \eta')^2 - 2\eta \eta' (-\eta \eta') \right) \\ &= -\alpha_1 \sigma_m\{\mathbf{K}_\circ\} \|\boldsymbol{\mu}\|_2^2 - 2\alpha_2 \sigma_m\{\mathbf{K}_\tau\} \left( \eta^2 \|\boldsymbol{\mu}'\|_2^2 \right. \\ &\quad \left. + \eta'^2 (1 - \eta^2) + (1 - \eta^2) \|\boldsymbol{\mu}'\|_2^2 + (\eta \eta')^2 \right) \\ &= -\alpha_1 \sigma_m\{\mathbf{K}_\circ\} \frac{1}{2} (\|\boldsymbol{\mu}\|_2^2 + \|\boldsymbol{\mu}'\|_2^2) - 2\alpha_2 \sigma_m\{\mathbf{K}_\tau\} (\|\boldsymbol{\mu}'\|_2^2 \\ &\quad + \eta'^2 (1 - \eta^2) + \eta^2 \eta'^2) \\ &= -\frac{\alpha_1 \sigma_m\{\mathbf{K}_\circ\}}{2} (1 - \eta^2 + \|\boldsymbol{\mu}\|_2^2) - 2\alpha_2 \sigma_m\{\mathbf{K}_\tau\} (\eta'^2 + \|\boldsymbol{\mu}'\|_2^2).\end{aligned}$$

For  $\eta \in [0, 1]$ , it is easy to see that  $(1 - \eta)^2 \leq (1 - \eta^2)$ . Hence,

$$\begin{aligned}\dot{V}(t, \underline{\mathbf{x}}) &\leq V_1 \leq -\frac{\alpha_1 \sigma_m\{\mathbf{K}_\circ\}}{2} \left( (1 - \eta)^2 + \|\boldsymbol{\mu}\|_2^2 \right) \\ &\quad - 2\alpha_2 \sigma_m\{\mathbf{K}_\tau\} \left( \eta'^2 + \|\boldsymbol{\mu}'\|_2^2 \right),\end{aligned}$$

which in turn, yields (3.49).

## C.2 LYAPUNOV CANDIDATE FUNCTION DERIVATIVE IN THE PRESENCE OF DISTURBANCES

In Appendix C.1, we described how to obtain the time-derivative of the Lyapunov candidate function from Theorem 3.7 along the closed-loop system (C.3) in the absence of exogenous disturbances. Nonetheless, if we explicitly regard the influence of  $\underline{v}_w = \mathbf{v}_w + \varepsilon \mathbf{v}'_w$  and  $\underline{v}_c = \mathbf{v}_c + \varepsilon \mathbf{v}'_c$  in the end-effector differential kinematics (3.46), the Lyapunov derivative (C.4) yields

$$\dot{V}(t, \underline{\mathbf{e}}) = \alpha_1 \langle \boldsymbol{\mu}, \mathbf{h}_1 \rangle + \alpha_2 \langle \eta \boldsymbol{\mu}' - \eta' \boldsymbol{\mu} + \boldsymbol{\mu} \times \boldsymbol{\mu}', \mathbf{h}_2 \rangle,$$

where  $\mathbf{h}_1, \mathbf{h}_2 \in \mathbb{H}_0$ , with  $\mathbf{h}_1 = \underline{\text{vec}}_3(\mathbf{K}_O \text{vec}_3 \text{Im}(\mathcal{O}(\underline{\mathbf{e}}))) + \mathbf{v}_w + \mathbf{v}_c$  and  $\mathbf{h}_2 = -\underline{\text{vec}}_3(\mathbf{K}_T \text{vec}_3(\mathcal{T}(\underline{\mathbf{e}}))) + \mathbf{v}'_w + \mathbf{v}'_c$ . Taking  $\frac{1}{2}\mathcal{T}(\underline{\mathbf{e}}) = \eta \boldsymbol{\mu}' - \eta' \boldsymbol{\mu} + \boldsymbol{\mu} \times \boldsymbol{\mu}'$  and using the isomorphism from  $\mathbb{H}_0$  and  $\mathbb{R}^3$ , we have

$$\begin{aligned} \dot{V}(t, \underline{\mathbf{e}}) &= \alpha_1 \langle \boldsymbol{\mu}, \underline{\text{vec}}_3(\mathbf{K}_O \text{vec}_3 \text{Im}(\mathcal{O}(\underline{\mathbf{e}}))) + \mathbf{v}_w + \mathbf{v}_c \rangle \\ &\quad + \frac{\alpha_2}{2} \langle \mathcal{T}(\underline{\mathbf{e}}), -\underline{\text{vec}}_3(\mathbf{K}_T \text{vec}_3(\mathcal{T}(\underline{\mathbf{e}}))) + \mathbf{v}'_w + \mathbf{v}'_c \rangle, \end{aligned}$$

which is equivalent to (3.50)

# D TABLE OF RESULTS

## D.1 TABLE FROM V-REP SIMULATION USING DUAL QUATERNION OPTIMAL CONTROL THEORY—SUBSECTION 4.4.2

Simulation	Proportional Controller $k = 50$	Proportional Feedforward $k = 50$	Theorem 4.1 (dq-optimal in $\mathbb{R}^8$ ) $s = 0, q = 20, r = 0.01$	Theorem 4.3 (optimal in dq-space)
1	0.0134	0.6914	0.0194	0.0137
2	0.7525	0.0117	0.0216	0.0140
3	0.5765	0.9969	0.0324	0.0144
4	0.0152	0.2207	0.0273	0.0147
5	0.0131	1.0132	0.0290	0.0149
6	0.0144	0.0197	0.0209	0.0138
7	0.7800	0.0125	0.0264	0.0138
8	0.0140	0.7704	0.0213	0.0137
9	0.0145	0.0231	0.0289	0.0139
10	0.0134	0.0113	0.0193	0.0143

Table D.1: Integral norm of the end-effector trajectory error

Simulation	Proportional Controller $k = 50$	Proportional Feedforward $k = 50$	Theorem 4.1 (dq-optimal in $\mathbb{R}^8$ ) $s = 0, q = 20, r = 0.01$	Theorem 4.3 (optimal in dq-space)
1	0.063	0.060	0.086	0.058
2	0.060	0.060	0.109	0.058
3	0.061	0.062	0.136	0.058
4	0.062	0.060	0.096	0.058
5	0.062	0.062	0.110	0.058
6	0.060	0.060	0.094	0.058
7	0.061	0.060	0.110	0.057
8	0.060	0.061	0.103	0.058
9	0.062	0.059	0.111	0.058
10	0.061	0.062	0.098	0.058

Table D.2: Integral norm of the joint velocity vector

Simulation	Proportional Controller $k = 50$	Proportional Feedforward $k = 50$	Theorem 4.1 (dq-optimal in $\mathbb{R}^8$ ) $s = 0, q = 20, r = 0.01$	Theorem 4.3 (optimal in dq-space)
1	0.424	0.438	0.651	0.391
2	0.438	0.439	0.840	0.389
3	0.443	0.425	1.000	0.389
4	0.443	0.417	0.725	0.410
5	0.426	0.417	0.789	0.399
6	0.434	0.439	0.709	0.389
7	0.421	0.437	0.777	0.404
8	0.439	0.419	0.793	0.389
9	0.432	0.435	0.804	0.407
10	0.416	0.422	0.727	0.389

Table D.3: Integral norm of the end-effector translational velocity

Simulation	Proportional Controller $k = 50$	Proportional Feedforward $k = 50$	Theorem 4.1 (dq-optimal in $\mathbb{R}^8$ ) $s = 0, q = 20, r = 0.01$	Theorem 4.3 (optimal in dq-space)
1	0.151	0.238	0.395	0.110
2	0.235	0.238	0.513	0.110
3	0.239	0.208	1.086	0.114
4	0.235	0.135	0.675	0.191
5	0.139	0.148	1.041	0.178
6	0.218	0.237	0.624	0.115
7	0.145	0.236	0.825	0.175
8	0.237	0.143	0.530	0.110
9	0.222	0.240	1.016	0.179
10	0.144	0.204	0.593	0.127

Table D.4: Integral norm of the end-effector rotation velocity

Simulation	Proportional	Proportional	Theorem 4.1	Theorem 4.3
	Controller	Feedforward	(dq-optimal in $\mathbb{R}^8$ )	(optimal in dq-space)
	$k = 50$	$k = 50$	$s = 0, q = 20, r = 0.01$	
1	21.254	21.270	36.152	18.397
2	21.024	19.622	45.026	18.496
3	20.267	20.530	55.927	19.473
4	20.701	20.189	39.991	18.764
5	21.575	20.667	42.243	20.920
6	20.186	19.872	39.877	19.048
7	21.779	20.583	42.607	17.335
8	20.854	20.578	44.632	18.467
9	20.905	20.720	41.209	17.875
10	20.959	20.955	39.573	21.975

Table D.5: Integral norm of the end-effector translational acceleration

Simulation	Proportional	Proportional	Theorem 4.1	Theorem 4.3
	Controller	Feedforward	(dq-optimal in $\mathbb{R}^8$ )	(optimal in dq-space)
	$k = 50$	$k = 50$	$s = 0, q = 20, r = 0.01$	
1	8.607	13.020	12.129	6.277
2	12.050	12.724	12.904	6.455
3	11.87	11.707	15.526	6.488
4	14.534	7.660	13.647	11.79
5	7.815	8.292	14.945	10.966
6	11.362	12.146	13.433	6.780
7	8.176	12.411	14.253	10.198
8	11.823	8.198	12.988	6.247
9	13.576	12.888	15.184	10.372
10	7.933	11.963	13.139	7.590

Table D.6: Integral norm of the end-effector rotation acceleration

# E

## BASIC ALGEBRAIC STRUCTURES

This appendix provides the reader with a quick glance of definitions and properties of some algebraic structures that are used throughout this manuscript.

**Definition E.1 (Group).** [167, p.31] A **group**  $(G, \diamond, \epsilon)$  is defined by a set  $G$ , a single binary operation  $\diamond : G \times G \mapsto G$  (named the *group operation*), and a element  $\epsilon \in G$  (named the *operation identity* or the *identity element*) that satisfies the following axioms:

**G1 [Associative]** For all  $a, b, c \in G$  we have

$$(a \diamond b) \diamond c = a \diamond (b \diamond c);$$

**G2 [Identity Operation]** For all  $x \in G$ , we have

$$x \diamond \epsilon = \epsilon \diamond x = x;$$

**G3 [Inverse Element]** For all  $x \in G$ , there exists an inverse element in  $G$  (denoted by  $x^{-1}$ ) such that

$$x \diamond x^{-1} = x^{-1} \diamond x = \epsilon.$$

**(G4) [Closure]** Some authors, e.g., [35, p.24] defines the group with this additional axiom – For all  $a, b \in G$ , we have

$$a \diamond b \in G.$$

*Remark E.1.* The axiom **G4** from Definition E.1 is already implied by the definition of the codomain of function  $\diamond$ .

To simplify notation, groups are usually defined only by the pair  $(G, \diamond)$ , and sometimes even only by the set  $G$ . The follow properties are valid for all groups:

**Proposition E.1.** *The identity of the group is unique.*

*proof.*

The proof is established by contradiction. Supposing that  $\epsilon_2 \neq \epsilon$  is another identity of  $G$ , we have that  $\epsilon_2 = \epsilon_2 \diamond \epsilon = \epsilon$ . □

**Proposition E.2.** *For all  $g \in G$ , there exists an unique inverse element  $g^{-1}$ .*

*proof.*

It is easy to proof the uniqueness using the axioms **G1** and **G2** from Definition E.1. For absurd, let us assume that  $\hat{g}$  and  $g^{-1}$  are inverses for  $g$ , then  $\hat{g} = \epsilon \diamond \hat{g} = (g^{-1} \diamond g) \diamond \hat{g} = g^{-1} \diamond (g \diamond \hat{g}) = g^{-1} \diamond \epsilon = g^{-1}$ . Thus,  $\hat{g} = g^{-1}$  must hold. □



Groups whose operation behave nicely with regard to commutativity have a special name.

**Definition E.2** (Group Homomorphism). [167, p.58] A map  $\phi : (G, \diamond, \epsilon) \mapsto (H, \circ, e)$  between group is called a **group homomorphism** if it satisfies:

**H1** For all  $a, b \in G$ , we have  $\phi(a \diamond b) = \phi(a) \circ \phi(b)$ .

If the map is surjective, we call it an **epimorphism** and denote it by  $G \xrightarrow{\phi} H$ ; if the map is injective, we call it a **monomorphism** and denote by  $G \xrightarrow{\phi} H$ ; and if the map is bijective we call it an **isomorphism** and denote by  $G \xleftrightarrow{\phi} H$ ;

**Proposition E.3.** If  $\phi : (G, \diamond, \epsilon) \mapsto (H, \circ, e)$  is a homomorphism, then  $\phi(\epsilon) = e$  and  $\phi(g^{-1}) = \phi^{-1}(g)$  for all  $g \in G$ .

*proof.*

Since  $\phi$  is a homomorphism we have:  $\phi(\epsilon \diamond \epsilon) = \phi(\epsilon) = \phi(\epsilon) \circ \phi(\epsilon)$ . From  $H$  being a group, we have by **G3** from Definition E.1 that:  $e = \phi(\epsilon) \circ \phi^{-1}(\epsilon) = \phi(\epsilon) \circ \phi(\epsilon) \circ \phi^{-1}(\epsilon) = \phi(\epsilon)$ .  $\square$

**Definition E.3.** Two groups  $G$  and  $H$  are **isomorphic** if there exists an isomorphism between  $G$  and  $H$ . If this occurs, we denote  $G \simeq H$  to indicate that they are isomorphic.

**Definition E.4** (Subgroup). [167, p.31] A subgroup  $(H, \diamond, \epsilon_H)$  of  $(G, \diamond, \epsilon_G)$  is a subset of  $G$  that is also a group under the same group operation – we use the notation  $H \leq G$  to indicate that  $H$  is a subgroup of  $G$ .

A group  $(G, \otimes)$  is called an **Abelian<sup>a</sup> group** if for all  $a, b \in G$  the following property is valid:

$$a \otimes b = b \otimes a. \quad (\text{E.1})$$

<sup>a</sup>In homage to the mathematician Niels Henrik Abel who studied the relationship between some groups and impossibility of solving quintic equations by radicals.

**Definition E.5 (Ring).** A ring is a 3-uple  $(R, \oplus, \otimes)$ , where  $R$  is a set and  $\oplus, \otimes : G \times G \rightarrow G$  are functions such that  $(R, \oplus)$  is an Abelian group and  $(R, \otimes)$  is almost a group, in the sense that satisfies only properties **G1** and **G2** from Definition E.1. The identity of  $(R, \oplus)$  is usually denoted by  $0_R$  and entitled as the **additive identity**. The identity of  $(R, \otimes)$  is denoted by  $1_R$  and called **multiplicative identity**.

There is also a need to satisfy a compatibility condition between  $\oplus$  and  $\otimes$ , the so called **distributive property**:

$$a \oplus (b \otimes c) = (a \oplus b) \otimes (a \oplus c).$$

*Remark E.2.* In the “unorthodox” literature,  $(R, \otimes)$  doesn’t need to follow property **G2** from Definition E.1 to be a ring. To the orthodox, this is called **rng** (intentionally without the letter “i”) and to the heterodox, our definition is called an **unital ring** or **ring with unity**.

An archetype of ring is the ring of integers with  $\oplus$  being the usual sum and  $\otimes$  being the usual multiplication of arithmetic.

**Definition E.6 (Field).** A field  $\mathbb{F}$  is a ring  $(\mathbb{F}, \oplus, \otimes)$  where  $(\mathbb{F} - \{0_{\mathbb{F}}\}, \otimes)$  is also a group.

**Definition E.7 (Vector Space).** A vector space  $V$  over a field  $\mathbb{F}$  is the 3-uple  $(V, +, \cdot)$  such that  $V$  and the functions  $\oplus : V \times V \rightarrow V$  (known as **addition between vectors**) and  $\otimes : \mathbb{F} \times V \rightarrow V$  (known as **product by scalar**) satisfies the following properties:

1.  $(V, \oplus)$  is an Abelian group.
2. The scalar product must distribute with the addition between vectors, that is, for all  $v, w \in V$  and  $\alpha \in \mathbb{F}$ :

$$\alpha \cdot (v + w) = \alpha \cdot v + \alpha \cdot w.$$

3. The operation of  $\oplus$  in  $\mathbb{F}$  must distribute with the scalar product also, that is, for all  $\alpha, \beta \in \mathbb{F}$  and  $v \in V$ :

$$(\alpha \oplus \beta) \cdot v = \alpha \cdot v + \beta \cdot v$$

4. There is a kind of associative property between the scalar product and the operation  $\otimes$  of  $\mathbb{F}$ , that is, for all  $\alpha, \beta \in \mathbb{F}$  and  $v \in V$ :

$$\alpha \cdot (\beta \cdot v) = (\alpha \otimes \beta) \cdot v.$$

5. The multiplicative identity of  $\mathbb{F}$  must satisfy for all  $v \in V$ :

$$1_{\mathbb{F}} \cdot v = v.$$

If the field can be implied by context, it is common to not mention it. A vector space may be equipped with a well-behaved function that measures the size of the vector, in the sense that a vector can be greater or smaller than other vectors.

**Definition E.8** (Normed Vector Space). A normed vector space is a vector space equipped with a function  $\|\cdot\| : V \rightarrow \mathbb{R}$  denominated as **norm** such that the following are satisfied:

1. The norm must be **positive definite**, that is, for all  $x \in V$

$$\|x\| \geq 0, \text{ and } \|0_V\| = 0.$$

2. The norm must be compatible with the scalar product in the sense that for all  $\alpha \in \mathbb{F}$  and  $x \in V$  we have

$$\|\alpha x\| = |\alpha| \|x\|.$$

3. The **triangle inequality** must hold, i.e.: for all  $x, y \in V$ ,

$$\|x + y\| \leq \|x\| + \|y\|.$$

The vector space may also have a richer structure equipping it with an operation of multiplication between the vectors.

**Definition E.9** (Algebra over a field<sup>a</sup>). An algebra  $\mathcal{A}$  over a field  $\mathbb{F}$  is a vector space over the same field equipped with a bilinear function  $\square : \mathcal{A} \times \mathcal{A} \rightarrow \mathcal{A}$ , where **bilinear** means that the function must obey the following properties:

1. For all  $x, y, z \in \mathcal{A}$  and  $\alpha, \beta \in \mathbb{F}$  we have:

$$(\alpha \cdot x + \beta \cdot y) \square z = \alpha \cdot (x \square z) + \beta \cdot (y \square z) \text{ and } z \square (\alpha \cdot x + \beta \cdot y) = \alpha \cdot (z \square x) + \beta \cdot (z \square y).$$

<sup>a</sup>The concept of algebra over a field should not be confused with the more general concept of abstract algebra. For instance, in abstract algebra, a set is an algebraic structure with one or more operations and axioms but not necessarily forms an algebra over a field.

Some algebras over a field are related to Lie Groups, the so-called Lie Algebras. Their connection with Lie Groups will be shown later.

**Definition E.10** (Lie Algebra). A Lie Algebra  $\mathfrak{g}$  is an algebra over a field such that its multiplication between vectors, entitled by **Lie Bracket** and usually denoted by  $[\cdot, \cdot]$ , satisfies the following additional identities:

1. (**Skew-symmetry** or **Alternating**) For every  $x \in \mathfrak{g}$ ,

$$[x, x] = 0_{\mathbb{F}}$$

2. (**Jacobi Identity**) For every  $x, y, z \in \mathfrak{g}$ ,

$$[x, [y, z]] + [y, [z, x]] + [z, [x, y]] = 0_{\mathbb{F}}$$

Familiar examples are the Euclidean space  $\mathbb{R}^3$  with the multiplication given by the cross product and  $\mathbb{F}^{n \times n}$  with the **commutator** between matrices  $A, B \in \mathbb{F}^{n \times n}$  given by  $[A, B] = AB - BA$ .

## E.1 ALGEBRAIC PROPERTIES FROM MOST USED SETS AND GROUPS

This thesis exploits the geometric properties from different sets and groups. The following table summarizes the most important (according to their use in this thesis) sets that—excluding the zero element  $0^1$ —forms groups under multiplication over the reals. Moreover, the corresponding nonzero groups are also smooth differentiable manifolds and, thus, Lie groups.

---

<sup>1</sup>Particularly, in the case of dual quaternions—and its subsets—the group is defined for elements with nonzero primary part.

Sets	Underlying		Basis <sup>a</sup>	Compatness		Algebraic Properties			Ring
	Unit Group	Unit Group		Division	Associative	Commutative	Commutative		
Real numbers	$\mathbb{R}$	-	$\{1\}$	⊗	✓	✓	✓	✓	✓
Complex numbers	$\mathbb{C}$	-	$\{1, \hat{i}\}$	⊗	✓	✓	✓	✓	✓
Dual numbers	$\mathbb{D}$	-	$\{1, \varepsilon\}$	⊗	⊗	✓	✓	✓	✓
Quaternions	$\mathbb{H}$	-	$\{1, \hat{i}, \hat{j}, \hat{k}\}$	⊗	✓	✓	⊗	⊗	✓
Unit Quaternions	$\mathcal{S}^3$	Spin(3)	$\{1, \hat{i}, \hat{j}, \hat{k}\}$	✓	<sub>b</sub>	✓	⊗	⊗	⊗
Pure Quaternions	$\mathbb{H}_0$	-	$\{1, \hat{i}, \hat{j}, \hat{k}\}$	⊗	✓	✓	⊗	⊗	✓
Dual Quaternions	$\mathbb{H} \otimes \mathbb{D}$	-	$\{1, \hat{i}, \hat{j}, \hat{k}, \varepsilon\}$	⊗	⊗	✓	⊗	⊗	✓
Unit Dual Quaternions	$\underline{\mathcal{S}}$	Spin(3) $\times$ $\mathbb{R}^3$	$\{1, \hat{i}, \hat{j}, \hat{k}, \varepsilon\}$	⊗	<sub>c</sub>	✓	⊗	⊗	⊗
Pure Dual Quaternions	$\mathbb{H}_0 \otimes \mathbb{D}$	-	$\{1, \hat{i}, \hat{j}, \hat{k}, \varepsilon\}$	⊗	⊗	✓	⊗	⊗	✓

Table E.1: Summary of algebraic properties from sets and unit groups used in this thesis

<sup>a</sup>Basis of the algebra over the reals.

<sup>b</sup>In the context of abstract algebra, the algebraic structure of unit quaternions is equipped with the division operation (and also with an inverse element since the unit constraint removes the zero element). Nonetheless, this should not be confused with the most common concept of division ring since the usual sum operation is unfeasible within  $\mathcal{S}^3$ .

<sup>c</sup>In the context of abstract algebra, the algebraic structure of unit dual quaternions is equipped with the division operation since the set ensures a nonzero primary part. Nonetheless, this should not be confused with the most common concept of division ring since the usual sum operation is unfeasible within  $\underline{\mathcal{S}}$ .

# F PUBLICATIONS

---

Some part of this thesis has already been published in the following papers:

## PEER-REVIEWED JOURNALS

**L.F.C. Figueredo**, B.V. Adorno, and J.Y. Ishihara, "Robust  $H_\infty$  Kinematic control of manipulator robots using dual quaternion representation", Transaction on Robotics, 2016 (to be submitted).

H.T. Kussaba, **L.F.C. Figueredo**, J.Y. Ishihara, and B.V. Adorno, "Hybrid Kinematic Control for Rigid Body Stabilization using Dual Quaternions", Journal of the Franklin Institute, 2016 (submitted for publication).

## PEER-REVIEWED CONFERENCES

M.M. Marinho, **L.F.C. Figueredo** and B.V. Adorno, "A Dual Quaternion Linear-Quadratic Optimal Controller for Trajectory Tracking", IEEE/RSJ International Conference on Intelligent Robots and Systems, IROS 2015, September 2015.

**L.F.C. Figueredo**, B.V. Adorno, J.Y. Ishihara, and G.A. Borges, "Switching Strategy for Flexible Task Execution using the Cooperative Dual Task SPace Framework", IEEE/RSJ International Conference on Intelligent Robots and Systems, IROS 2014, September 2014.

**L.F.C. Figueredo**, B.V. Adorno, J.Y. Ishihara, and G.A. Borges, "Robust kinematic control of manipulator robots using dual quaternion representation", IEEE International Conference on Robotics and Automation, ICRA2013, May 2013.

Other publications during the period of the thesis, but related to different topics:

## PEER-REVIEWED JOURNALS

**L.F.C. Figueredo**, J.Y. Ishihara, G.A. Borges, and A. Bauchspiess, "Robust  $H_\infty$  Output Tracking Control for a Class of Nonlinear Systems with Time-Varying Delays", *Circuits, Systems, and Signal Processing*, Vol. 33, n. 5, pp. 1451-1471, 2014.

**L.F.C. Figueredo**, J.Y. Ishihara, G.A. Borges, and A. Bauchspiess, "Delay-Dependent Robust Stability Analysis for Time-Delay T-S Fuzzy Systems with Nonlinear Local Models", *Journal of Control, Automation and Electrical Systems (former Controle & Automação)*, Vol. 24, n. 1-2, pp. 11-21, 2013.

## PEER-REVIEWED CONFERENCES

J.V.C. Vilela, **L.F.C. Figueredo**, J.Y. Ishihara and G.A. Borges, "Quaternion-based  $H_\infty$  attitude tracking control of rigid bodies with time-varying delay in attitude measurements", 55th IEEE Conference on Decision and Control, CDC 16, Dec. 2016.

J.V.C. Vilela, **L.F.C. Figueredo**, J.Y. Ishihara and G.A. Borges, "Quaternion-based Kinematic  $H_\infty$  attitude control subjected to input time-varying delays", 54th IEEE Conference on Decision and Control, CDC 15, Dec. 2015.

J.V.C. Vilela, **L.F.C. Figueredo**, J.Y. Ishihara and G.A. Borges, "An improved stability criterion of networked control systems with dynamic controllers in the feedback loop", 53th IEEE Conference on Decision and Control, CDC 14, Dec. 2014.

**L.F.C. Figueredo**, F.B. Cavalcanti, J.Y. Ishihara, G.A. Borges, and A. Bauchspiess, "Novel stabilization technique for the  $H_\infty$  control of systems with time-varying input delay", American Control Conference, ACC 2013, Jun. 2013.

**L.F.C. Figueredo**, J.Y. Ishihara, G.A. Borges, and A. Bauchspiess, "A delay-fractioning approach to stability analysis of networked control systems with time-varying delay", 50th IEEE Conference on Decision and Control, CDC 11, Dec. 2011.

**L.F.C. Figueredo**, J.Y. Ishihara, G.A. Borges, and A. Bauchspiess, "Delay-Dependent Robust  $H_\infty$  Output Tracking Control for Uncertain Networked Control Systems", Proceedings of the 18th IFAC World Congress, IFAC WS 2011, Aug. 2011.

**L.F.C. Figueredo**, J.Y. Ishihara, G.A. Borges, and A. Bauchspiess, "Estabilidade de sistemas fuzzy Takagi-Sugeno com atrasos variantes no tempo", X Simpósio Brasileiro de Automação Inteligente, SBAI 2011, Sep. 2011. (Best Session Paper).

# G SYSTEM DEMONSTRATIONS - AWARDS

---

## *Outstanding System Demonstration – Honorable Mention ICAPS 2014 (June, 2014)*

Title: "*Best Intent Recognition and Temporal Relaxation in Human Robot Assembly*";

Conference: *24th International Conference on Automated Planning and Scheduling – ICAPS 2014*;

Authors: Sean Burke, Enrique Fernandez, **Luis F. C. Figueredo**, Andreas Hofmann, Christopher Hofmann, Erez Karpas, Steve Levine, Pedro Santana, Peng Yu, and Brian Williams;

\* Link for the awarded list: <http://icaps14.icaps-conference.org/index/awards.html>

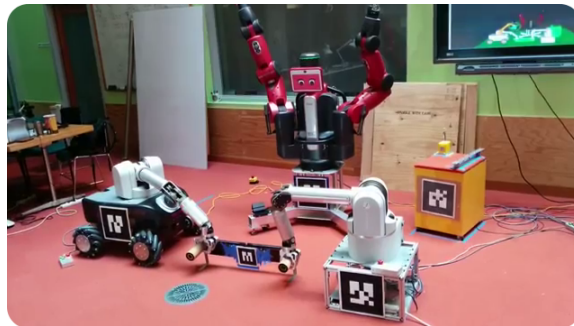


Figure G.1: *Outstanding System Demonstration – Honorable Mention ICAPS 2014 (June, 2014)*.



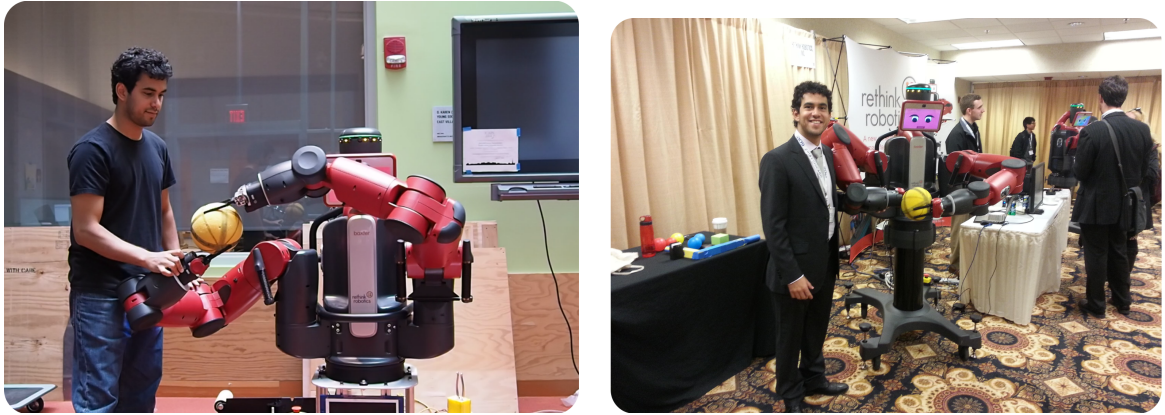


Figure G.2: Winner of Rethink Robotics Contest for IROS 2014 (Sept, 2014)

### ***Winner of Rethink Robotics Contest for IROS 2014 (Sept, 2014)***

Title: "*Cooperative Manipulation using Cooperative Dual Task Space*";

Conference: *IEEE/RSJ International Conference on Intelligent Robots and Systems – IROS 2014*;

Authors: **Luis Felipe da Cruz Figueredo**;

\* Link for the awarded project: [http://sdk.rethinkrobotics.com/wiki/IROS\\_2014](http://sdk.rethinkrobotics.com/wiki/IROS_2014)

\* Project had also been used by the Rethink Robotics for a short course on teleoperation with Baxter at the NERVE (New England Robotics Validation and Experimentation) group at the University of Massachusetts Lowell<sup>1</sup>

---

<sup>1</sup><http://nerve.uml.edu/ros-2014/>

## Bibliography

---

- [1] B. V. Adorno, “Two-arm Manipulation: From Manipulators to Enhanced Human-Robot Collaboration,” PhD thesis, Laboratoire d’Informatique, de Robotique et de Microélectronique de Montpellier (LIRMM) - Université Montpellier 2, Montpellier, France, 2011.
- [2] K. J. Åström and R. M. Murray, *Feedback Systems: An Introduction for Scientists and Engineers*, 2nd ed. Princeton University Press, 2010.
- [3] G. V. M. da Silva, *Controlo Não Linear*. Escola Superior de Tecnologia de Setúbal, 2003.
- [4] B. V. Adorno, P. Fraisse, and S. Druon, “Dual position control strategies using the cooperative dual task-space framework,” in *IEEE/RSJ International Conference on Intelligent Robots and Systems*, Taipei, Oct. 2010, pp. 3955–3960.
- [5] O. Egeland, J. Sagli, I. Spangelo, and S. Chiaverini, “A damped least-squares solution to redundancy resolution,” in *Robotics and Automation, 1991. Proceedings., 1991 IEEE International Conference on*, 1991, pp. 945–950 vol.1.
- [6] S. Chiaverini, “Singularity-robust task-priority redundancy resolution for real-time kinematic control of robot manipulators,” *IEEE Transactions on Robotics and Automation*, vol. 13, no. 3, pp. 398–410, Jun. 1997.
- [7] S. Thrun, W. Burgard, and D. Fox, *Probabilistic Robotics (Intelligent Robotics and Autonomous Agents)*. The MIT Press, 2005.
- [8] T. Connolly and F. Pfeiffer, “Cooperating manipulator control using dual quaternion coordinates,” in *IEEE Conference on Decision and Control*, Lake Buena Vista, 1994, pp. 2417–2418.
- [9] J. R. Dooley and J. M. McCarthy, “Spatial rigid body dynamics using dual quaternion components,” in *Proceedings of 1991 IEEE International Conference on Robotics and Automation*, 1991, pp. 90–95.
- [10] —, “On the geometric analysis of optimum trajectories for cooperating robots using dual quaternion coordinates,” in *Proceedings of 1993 IEEE International Conference on Robotics and Automation*, May 1993, pp. 1031–1036 vol.1.
- [11] C. Perrier, P. Dauchez, and F. Pierrot, “Towards the Use of Dual Quaternions for Motion Generation of Non-Holonomic Mobile Manipulators,” in *IEEE/RSJ International Conference on Intelligent Robots and Systems*, 1997, pp. 1293–1298.
- [12] D. M. Burton, *The History of Mathematics: An Introduction*, 7th ed. McGraw-Hill, 2010.
- [13] I. Yaglom, *Complex numbers in geometry*. Academic Press, Translated by E. J. F. Primrose, 1968.
- [14] P. J. Nahin, *An Imaginary Tale: The Story of  $\sqrt{-1}$* . Princeton University Press, 2007.
- [15] J. C. K. Chou, “Quaternion kinematic and dynamic differential equations,” *IEEE Transactions on Robotics and Automation*, vol. 8, no. 1, pp. 53–64, Feb 1992.
- [16] W. Clifford, *Preliminary Sketch of Biquaternions*. Proc. London Mathematical Society, 1873.

- [17] B. Felzenszwalb, *Álgebras de Dimensão Finitas*. Rio de Janeiro, Brasil: Instituto de Matemática Pura e Aplicada, 1979.
- [18] W. R. Hamilton, “On quaternions, or on a new system of imaginaries in algebra: Copy of a letter from Sir William R. Hamilton to John T. Graves, esq. on quaternions,” *Journal of Mechanical Design - Transactions of ASME*, vol. 25, no. 3, pp. 489–495, 1844.
- [19] J. McCarthy, *Introduction to Theoretical Kinematics*. MIT Press, 1990.
- [20] T. A. Ell and S. J. Sangwine, “Quaternion involutions and anti-involutions,” *Computers & Mathematics with Applications*, vol. 53, no. 1, pp. 137 – 143, 2007.
- [21] H. Anton, *Elementary linear algebra*. John Wiley & Sons, 2010.
- [22] E. Study, “Von den bewegungen und umlegungen,” vol. 39, no. 4, pp. 441–565, 1891.
- [23] J. M. Selig, *Geometric Fundamentals of Robotics*, 2nd ed. Springer-Verlag New York Inc., 2005.
- [24] L. Silberstein, *The representation of physical motions by various types of quaternions (translated to english from the original Elektromagnetische Grundgleichungen in bivectorieller Behandlung by L. Silberstein in 1907)*, T. by D. H. Delphenich, Ed. Annalen Phys., 2012.
- [25] P. Jitka, “Application of dual quaternions algorithm for geodetic datum transformation,” *Journal of Applied Mathematics*, vol. 4, no. 2, pp. 225–237, 2011.
- [26] B. Akyar, “Dual quaternions in spatial kinematics in an algebraic sense,” *Turk. J. Math*, vol. 32, pp. 373–391, 2008.
- [27] M. Spong, S. Hutchinson, and M. Vidyasagar, *Robot modeling and control*. John Wiley & Sons, 2006.
- [28] J. Wen and K. Kreutz-Delgado, “The attitude control problem,” *IEEE Transactions on Automatic Control*, vol. 36, no. 10, pp. 1148—1162, 1991.
- [29] M. D. Shuster, “A survey of attitude representations,” *The Journal of the Astronautical Sciences*, vol. 41, no. 4, pp. 439–517, 1993.
- [30] N. A. Chaturvedi, A. K. Sanyal, and N. H. McClamroch, “Rigid-body attitude control,” *IEEE Control Systems*, vol. 31, no. 3, pp. 30–51, June 2011.
- [31] C. D. Meyer, *Matrix Analysis and Applied Linear Algebra*. SIAM, 2000.
- [32] A. Baker, *An Introduction to Lie Group Theory*, 1st ed., ser. Undergraduate Mathematics Series. Springer-Verlag, 2002.
- [33] ———, “An introduction to matrix groups and their applications,” University of Glasgow, Glasgow, Tech. Rep., 2000.
- [34] A. Givental, *Linear Algebra and Differential Equations*, ser. Berkeley Mathematics Lecture Notes. American Mathematical Society, 2001.
- [35] R. M. Murray, Z. Li, and S. S. Sastry, *A Mathematical Introduction to Robotic Manipulation*. CRC, 1994.

- [36] X. Wang and C. Yu, "Unit-dual-quaternion-based PID control scheme for rigid-body transformation," in *Proceedings of the 18th IFAC World Congress*, Milano, 2011, pp. 9296–9301.
- [37] J. Kuipers, *Quaternions and Rotation Sequences: A Primer with Applications to Orbits, Aerospace, and Virtual Reality*. Princeton University Press, 1999.
- [38] M. Moakher, "Means and averaging in the group of rotations," *SIAM journal on matrix analysis and applications*, vol. 24, no. 1, pp. 1–16, 2002.
- [39] B. Wie and P. M. Barba, "Quaternion feedback for spacecraft large angle maneuvers," *Journal of Guidance, Control, and Dynamics*, vol. 8, no. 3, pp. 360–365, 1985.
- [40] P. Tsiotras, "New Control Laws For The Attitude Stabilization Of Rigid Bodies," in *IFAC Symposium on Automatic Control in Aerospace*, 1992, pp. 316—321.
- [41] F. Bullo, R. M. Murray, and A. Sarti, "Control on the sphere and reduced attitude stabilization," California Institute of Technology, Technical Report Caltech/CDS 95–005, Jan. 1995.
- [42] S. P. Bhat and D. S. Bernstein, "A topological obstruction to continuous global stabilization of rotational motion and the unwinding phenomenon," *Systems & Control Letters*, vol. 39, no. 1, pp. 63–70, 2000.
- [43] C. G. Mayhew, R. G. Sanfelice, and A. R. Teel, "Quaternion-based hybrid control for robust global attitude tracking," *IEEE Transactions on Automatic Control*, vol. 56, no. 11, pp. 2555–2566, Nov. 2011.
- [44] O. P. Agrawal, "Hamilton operators and dual-number-quaternions in spatial kinematics," *Mechanism and Machine Theory*, vol. 22, no. 6, pp. 569–575, 1987.
- [45] J. Funda and R. Paul, "A computational analysis of screw transformations in robotics," *IEEE Transactions on Robotics and Automation*, vol. 6, no. 3, pp. 348–356, 1990.
- [46] J. Gallier and J. Quaintance, *Notes on Differential Geometry and Lie Groups*, 2016.
- [47] S. M. LaValle, *Planning Algorithms*. Cambridge University Press, 2006.
- [48] O. Bottema and B. Roth, *Theoretical kinematics*. New York: North-Holland Pub. Co., 1979.
- [49] X. Wang, D. Han, C. Yu, and Z. Zheng, "The geometric structure of unit dual quaternion with application in kinematic control," *Journal of Mathematical Analysis and Applications*, vol. 389, no. 2, pp. 1352–1364, May 2012.
- [50] Y. Wu, X. Hu, D. Hu, T. Li, and J. Lian, "Strapdown inertial navigation system algorithms based on dual quaternions," *IEEE Transactions On Aerospace And Electronic Systems*, vol. 41, no. 1, pp. 110–132, 2005.
- [51] X. Wang and H. Zhu, "On the comparisons of unit dual quaternion and homogeneous transformation matrix," *Advances in Applied Clifford Algebras*, vol. 24, pp. 213–229, 2014.
- [52] X. Wang and C. Yu, "Unit dual quaternion-based feedback linearization tracking problem for attitude and position dynamics," *Systems & Control Letters*, vol. 62, no. 3, pp. 225–233, Mar. 2013.
- [53] M.-j. Kim, M.-s. Kim, and S. Y. Shin, "A compact differential formula for the first derivative of a unit quaternion curve," *The Journal of Visualization and Computer Animation*, vol. 7, no. 1, pp. 43–57, 1996.

- [54] J. Luh, M. Walker, and R. Paul, "Resolved-acceleration control of mechanical manipulators," *IEEE Transactions on Automatic Control*, vol. 25, no. 3, pp. 468–474, Jun. 1980.
- [55] F. Bullo and R. Murray, "Proportional derivative (PD) control on the euclidean group," Division of Engineering and Applied Science, California Institute of Technology, Technical Report Caltech/CDS 95–010, 1995.
- [56] N. A. Aspragathos and J. K. Dimitros, "A Comparative Study of Three Methods for Robot Kinematics," *IEEE Transactions on Systems, Man, and Cybernetics, Part B: Cybernetics*, vol. 28, no. 2, pp. 135–145, 1998.
- [57] K. Daniilidis, "Hand-eye calibration using dual quaternions," *The International Journal of Robotics Research*, vol. 18, pp. 286–298, 1999.
- [58] D. Han, Q. Wei, and Z. Li, "A Dual-quaternion Method for Control of Spatial Rigid Body," in *IEEE International Conference on Networking, Sensing and Control*, no. 5, 2008.
- [59] D.-P. Han, Q. Wei, and Z.-X. Li, "Kinematic control of free rigid bodies using dual quaternions," *International Journal of Automation and Computing*, vol. 5, no. 3, pp. 319–324, 2008.
- [60] D. Han, Q. Wei, Z. Li, and W. Sun, "Control of Oriented Mechanical systems: A Method Based on Dual Quaternion," in *IFAC World Congress, 17th*, Seoul, 2008, pp. 3836–3841.
- [61] X. Wang and C. Yu, "Feedback linearization regulator with coupled attitude and translation dynamics based on unit dual quaternion," in *IEEE International Symposium on Intelligent Control - Part of 2010 IEEE Multi-Conference on Systems and Control*, 2010, pp. 2380–2384.
- [62] X. Wang, C. Yu, and Z. Lin, "A dual quaternion solution to attitude and position control for rigid-body coordination," *IEEE Transactions on Robotics*, vol. 28, no. 5, pp. 1162–1170, 2012.
- [63] H.-L. Pham, V. Perdereau, B. V. Adorno, and P. Fraise, "Position and orientation control of robot manipulators using dual quaternion feedback," in *IEEE/RSJ International Conference on Intelligent Robots and Systems*, Taipei, Oct. 2010, pp. 658–663.
- [64] L. F. C. Figueredo, B. V. Adorno, J. Y. Ishihara, and G. Borges, "Robust kinematic control of manipulator robots using dual quaternion representation," in *IEEE International Conference on Robotics and Automation (ICRA)*, 2013, pp. 1949–1955.
- [65] J. M. Lee, *Introduction to Smooth Manifolds*, 2nd ed., ser. Graduate Texts in Mathematics. Springer-Verlag New York, Inc., 2013.
- [66] J. E. Hurtado, *Kinematic and Kinetic Principles*, 2012.
- [67] D. Chevallier, "On the transference principle in kinematics: its various forms and limitations," *Mechanism and Machine Theory*, vol. 31, no. 1, pp. 57–76, Jan. 1996.
- [68] D. E. Whitney, "Resolved Motion Rate Control of Manipulators and Human Prostheses," *Man-Machine Systems, IEEE Transactions on*, vol. 10, no. 2, pp. 47–53, Jun. 1969.
- [69] W. Khalil and E. Dombre, *Modeling, Identification and Control of Robots*. Butterworth-Heinemann, 2004.

- [70] E. Dombre and W. Khalil, *Robot Manipulators: Modeling, Performance Analysis and Control*. Wiley-ISTE, 2007.
- [71] K. Ogata, *Ingenieria de control moderna*, 3rd ed. Prentice-Hall, 1998.
- [72] H. K. Khalil, *Nonlinear Systems*, 2nd ed. Prentice-Hall, 1996.
- [73] P. Shcherbakov, “Alexander Mikhailovitch Lyapunov: On the centenary of his doctoral dissertation on stability of motion,” *Automatica*, vol. 28, no. 5, pp. 865 – 871, 1992.
- [74] I. M. F. Ghiggi, “Controle de sistemas com atrasos no tempo na presença de atuadores saturantes,” Ph.D. dissertation, Universidade Federal do Rio Grande do Sul, 2008.
- [75] B. Siciliano, L. Sciavicco, L. Villani, and G. Oriolo, *Robotics: modelling, planning and control*. Springer Verlag, 2009.
- [76] J. N. Pires, *Industrial Robots Programming: Building Applications for the Factories of the Future*. New York: Academic Press, 2007.
- [77] M. Schilling, “Universally manipulable body models – dual quaternion representations in layered and dynamic MMCs,” *Autonomous Robots*, vol. 30, no. 4, pp. 399–425, 2011.
- [78] B. V. Adorno, A. P. L. Bó, and P. Fraisse, “Kinematic modeling and control for human-robot cooperation considering different interaction roles,” *Robotica*, vol. 33, no. 2, pp. 314–331, 2015.
- [79] G. Zames, “Feedback and optimal sensitivity: Model reference transformations, multiplicative seminorms, and approximate inverses,” *Automatic Control, IEEE Transactions on*, vol. 26, no. 2, pp. 301–320, 1981.
- [80] J. Doyle and G. Stein, “Multivariable feedback design: Concepts for a classical/modern synthesis,” *Automatic Control, IEEE Transactions on*, vol. 26, no. 1, pp. 4 – 16, 1981.
- [81] C. Scherer, “The riccati inequality and state-space  $H_\infty$ -optimal control,” Ph.D. dissertation, University of Würzburg, Germany, 1990.
- [82] V. Arsigny, X. Pennec, and N. Ayache, “Bi-invariant Means in Lie Groups. Application to Left-invariant Polyaffine Transformations,” INRIA, Research Report RR-5885, 2006.
- [83] D. Simon, *Optimal State Estimation: Kalman,  $H_\infty$ , and Nonlinear approaches*. Wiley-Interscience, 2006.
- [84] R. T. Stefani, B. Shanian, C. J. Savant Jr., and G. H. Hostetter, *Design of feedback control systems*, 4th ed., ser. The Oxford Series in Electrical and Computer Engineering. Oxford University Press, 2002.
- [85] L. F. C. Figueredo, J. Y. Ishihara, G. A. Borges, and A. Bauchspiess, “Delay-dependent robust  $H_\infty$  output tracking control for uncertain networked control systems,” in *Proceedings of the 18th IFAC World Congress*, 2011, pp. 3256–3261.
- [86] J. T. Spooner, M. Maggiore, R. Ordóñez, and K. M. Passino, *Stable Adaptive Control and Estimation for Nonlinear Systems: Neural and Fuzzy Approximator Techniques*. Wiley-Interscience, 2002.
- [87] M. Hou, G. Duan, and M. Guo, “New versions of barbalat’s lemma with applications,” *Journal of Control Theory and Applications*, vol. 8, no. 4, pp. 545–547, 2010.

- [88] J. R. Magnus and H. Neudecker, "Matrix differential calculus with applications to simple, hadamard, and kronecker products," *Journal of Mathematical Psychology*, vol. 29, no. 4, pp. 474 – 492, 1985.
- [89] Y. L. Sachkov, "Control theory on Lie groups," *Journal of Mathematical Sciences*, vol. 156, no. 3, pp. 381–439, 2009.
- [90] E. Rohmer, S. P. N. Singh, and M. Freese, "V-rep: a versatile and scalable robot simulation framework," in *IEEE/RSJ Int. Conf. on Intelligent Robots and Systems*, 2013.
- [91] H. Pan and M. Xin, "Nonlinear robust and optimal control of robot manipulators," *Nonlinear Dynamics*, vol. 76, no. 1, pp. 237–254, 2014.
- [92] M. Negm, "Application of optimal preview and adaptive controllers for robotics manipulator with control input constraints," in *Proceedings of the IEEE International Symposium on Industrial Electronics*, vol. 2, 1999, pp. 853–860 vol.2.
- [93] F. Lin and R. Brandt, "An optimal control approach to robust control of robot manipulators," *IEEE Transactions on Robotics and Automation*, vol. 14, no. 1, pp. 69–77, Feb 1998.
- [94] F. Lin, *Robust Control Design*. New York: Wiley, 2007.
- [95] R.-J. Wai, C.-H. Tu, and K.-Y. Hsieh, "Design of intelligent optimal tracking control for robot manipulator," in *2003 IEEE/ASME International Conference on Advanced Intelligent Mechatronics*, vol. 1, July 2003, pp. 478–483 vol.1.
- [96] S. Dutta and L. Behera, "Policy iteration based near-optimal control scheme for robotic manipulator with model uncertainties," in *IEEE International Symposium on Intelligent Control*, Aug 2013, pp. 358–363.
- [97] O. Egeland and E. Lunde, "Trajectory generation for manipulators using linear quadratic optimal tracking," in *IEEE International Conference on Robotics and Automation*, Apr 1988, pp. 376–381 vol.1.
- [98] M. Galicki and D. Ucinski, "Time-optimal motions of robotic manipulators," *Robotica*, vol. 18, no. 6, pp. 659–667, 2000.
- [99] J. Bobrow, S. Dubowsky, and J. Gibson, "Time-optimal control of robotic manipulators along specified paths," *The International Journal of Robotics Research*, vol. 4, no. 3, pp. 3–17, 1985.
- [100] M. Zefran, "Review of the literature on time-optimal control of robotic manipulators, Report No. MS-CIS-94-30," Technical report, University of Pennsylvania, Department of Computer and Information Science,, May 1994.
- [101] A. Mertens, C. Brandl, I. Blotenberg, M. Ludtke, T. Jacobs, C. Brohl, M. P. Mayer, and C. M. Schlick, "Human-robot interaction: Testing distances that humans will accept between themselves and a robot approaching at different speeds," in *Ambient Assisted Living*, ser. Advanced Technologies and Societal Change, R. Wichert and H. Klausing, Eds. Springer Berlin Heidelberg, 2014, pp. 269–286.
- [102] P. A. Lasota, G. F. Rossano, and J. A. Shah, "Toward safe close-proximity human-robot interaction with standard industrial robots," in *IEEE International Conference on Automation Science and Engineering*, 2014.
- [103] A. Locatelli, *Optimal Control: An Introduction*. Birkhäuser Basel, 2001.

- [104] J. Wyatt, “Lagrange multipliers, constrained maximization, and the maximum entropy principle,” University Lecture Notes, June 2004.
- [105] R. M. Murray, “Optimization-based control,” in *Feedback Systems*, K. J. Åström and R. M. Murray, Eds. Princeton Univ. Press, 2010.
- [106] V. Garber, “Optimum intercept laws for accelerating targets.” *AIAA Journal*, vol. 6, no. 11, pp. 2586–2591, Nov 1968.
- [107] P. Ghiglini, J. L. Forshaw, and V. J. Lappas, “OQTAL: Optimal quaternion tracking using attitude error linearization,” *IEEE Transactions on Aerospace and Electronic Systems*, vol. 51, no. 4, pp. 2715–2731, Oct 2015.
- [108] B. Siciliano and O. Khatib, *Springer Handbook of Robotics*. Secaucus, NJ, USA: Springer-Verlag New York, Inc., 2007.
- [109] N. Bedrossian, “Classification of singular configurations for redundant manipulators,” in *IEEE International Conference on Robotics and Automation*, may 1990, pp. 818–823.
- [110] J. Seng, K. O’Neil, and Y. Chen, “Escapability of singular configuration for redundant manipulators via self-motion,” in *IEEE/RSJ International Conference on Intelligent Robots and Systems*, aug 1995, pp. 78–83.
- [111] A. Liegeois, “Automatic supervisory control of the configuration and behavior of multibody mechanisms,” *IEEE Transactions on Systems, Man, and Cybernetics*, vol. 7, no. 12, pp. 868–871, 1977.
- [112] B. Siciliano, “Kinematic control of redundant robot manipulators: A tutorial,” *Journal of Intelligent and Robotic Systems*, vol. 3, no. 3, pp. 201–212, 1990.
- [113] G. Marani, J. Kim, J. Yuh, and W. K. Chung, “A real-time approach for singularity avoidance in resolved motion rate control of robotic manipulators,” in *IEEE International Conference on Robotics and Automation*, no. May, 2002, pp. 1–6.
- [114] —, “Algorithmic singularities avoidance in task-priority based controller for redundant manipulators,” in *Proceedings IEEE/RSJ International Conference on Intelligent Robots*, vol. 4, 2003, pp. 3570–3574.
- [115] J. Kim, G. Marani, W. K. Chung, and J. Yuh, “Task reconstruction method for real-time singularity avoidance for robotic manipulators,” *Advanced Robotics*, vol. 20, no. 4, pp. 453–481, Jan. 2006.
- [116] J. Kim, G. Marani, W. K. Chung, J. Yuh, and S.-R. Oh, “Dynamic task priority approach to avoid kinematic singularity for autonomous manipulation,” in *IEEE/RSJ International Conference on Intelligent Robots and Systems*, 2002, pp. 1942–1947.
- [117] J. Kim, G. Marani, W. K. Chung, and J. Yuh, “A general singularity avoidance framework for robot manipulators: task reconstruction method,” in *IEEE International Conference on Robotics and Automation*, April 2004.
- [118] J. Baillieul, J. Hollerbach, and R. Brockett, “Programming and control of kinematically redundant manipulators,” in *The 23rd IEEE Conference on Decision and Control*, Dec 1984, pp. 768–774.
- [119] T. Yoshikawa, “Manipulability of robotic mechanisms,” *The International Journal of Robotics Research*, vol. 4, no. 2, pp. 3–9, 1985.



- [120] A. Maciejewski and C. Klein, "Numerical filtering for the operation of robotic manipulators through kinematically singular configurations," *Journal of Robotic Systems*, vol. 5, no. 6, pp. 527–552, 1988.
- [121] D. N. Nenchev and Z. M. Sotirov, "Dynamic task-priority allocation for kinematically redundant robotic mechanisms," in *Intelligent Robots and Systems '94. 'Advanced Robotic Systems and the Real World', IROS '94. Proceedings of the IEEE/RSJ/GI International Conference on*, vol. 1, Sep 1994, pp. 518–524 vol.1.
- [122] Y. Su, C. Zheng, and B. Duan, "Singularity analysis of a 6 DOF Stewart platform using genetic algorithm," in *IEEE International Conference on Systems, Man, and Cybernetics*, 2002.
- [123] Y. Su, B. Duan, B. Peng, and R. Nan, "Singularity analysis of fine-tuning Stewart platform for large radio telescope using genetic algorithm," *Mechatronics*, vol. 13, no. 5, pp. 413–425, Jun. 2003.
- [124] R. V. Mayorga and P. Sanongboon, "Inverse kinematics and geometrically bounded singularities prevention of redundant manipulators: An Artificial Neural Network approach," *Robotics and Autonomous Systems*, vol. 53, no. 3-4, pp. 164–176, Dec. 2005.
- [125] ———, "An Artificial Neural Network Approach for Inverse Kinematics Computation and Singularities Prevention of Redundant Manipulators," *Journal of Intelligent and Robotic Systems*, vol. 44, no. 1, pp. 1–23, Feb. 2006.
- [126] A. T. Hasan, N. Ismail, a.M.S. Hamouda, I. Aris, M. Marhaban, and H. Al-Assadi, "Artificial neural network-based kinematics Jacobian solution for serial manipulator passing through singular configurations," *Advances in Engineering Software*, vol. 41, no. 2, pp. 359–367, Feb. 2010.
- [127] S. S. Parsa, H. M. Daniali, and R. Ghaderi, "Optimization of parallel manipulator trajectory for obstacle and singularity avoidances based on neural network," *The International Journal of Advanced Manufacturing Technology*, vol. 51, no. 5-8, pp. 811–816, Apr. 2010.
- [128] J. Kotlarski, R. de Nijs, H. Abdellatif, and B. Heimann, "New interval-based approach to determine the guaranteed singularity-free workspace of parallel robots," in *IEEE International Conference on Robotics and Automation*, May 2009, pp. 1256–1261.
- [129] O. Bohigas, D. Zlatanov, L. Ros, M. Manubens, and J. M. Porta, "Numerical computation of manipulator singularities," in *IEEE International Conference on Robotics and Automation*, May 2012, pp. 1351–1358.
- [130] J.-P. Merlet, "A Formal-Numerical Approach for Robust In-Workspace Singularity Detection," *IEEE Transactions on Robotics*, vol. 23, no. 3, pp. 393–402, Jun. 2007.
- [131] D. Oetomo and M. H. Ang Jr, "Singularity robust algorithm in serial manipulators," *Robotics and Computer-Integrated Manufacturing*, vol. 25, no. 1, pp. 122–134, Feb. 2009.
- [132] Y. Nakamura and H. Hanafusa, "Inverse Kinematic Solutions With Singularity Robustness for Robot Manipulator Control," *Journal of Dynamic Systems, Measurement, and Control*, vol. 108, no. 3, p. 163, 1986.
- [133] C. Qiu, Q. Cao, and S. Miao, "An on-line task modification method for singularity avoidance of robot manipulators," *Robotica*, vol. 27, no. 4, p. 539, Sep. 2009.

- [134] T. Liu and S. Tsay, "Singularity of robotic kinematics: a differential motion approach," *Mechanism and Machine Theory*, vol. 25, no. 4, pp. 439–448, 1990.
- [135] J. Tan and N. Xi, "Hybrid system design for singularityless task level robot controllers," in *IEEE International Conference on Robotics and Automation*, no. April, 2000.
- [136] J. Tan, N. Xi, and Y. Wang, "A singularity-free motion control algorithm for robot manipulators—a hybrid system approach," *Automatica*, vol. 40, no. 7, pp. 1239–1245, Jul. 2004.
- [137] D. V. Phong and N. Q. Hoang, "Singularity-free simulation of closed loop multibody systems by using null space of Jacobian matrix," *Multibody System Dynamics*, vol. 27, no. 4, pp. 487–503, Dec. 2012.
- [138] S. Yahya, M. Moghavvemi, and H. A. F. Mohamed, "Improvement of singularity avoidance for three dimensional planar manipulators by increasing their degrees of freedom," in *International Symposium on Computer, Consumer and Control*, Jun. 2012, pp. 568–572.
- [139] D. Oetomo and M. Ang, "Singularity robust manipulator control using virtual joints," in *IEEE International Conference on Robotics and Automation*, vol. 3, no. May, 2002, pp. 2418–2423.
- [140] L. V. Vargas, A. C. Leite, and R. R. Costa, "Kinematic control of robot manipulators using filtered inverse," in *Mediterranean Conference on Control and Automation (MED)*, vol. 1, no. 4, 2013, pp. 27–33.
- [141] —, "Overcoming kinematic singularities with the filtered inverse approach," in *IFAC World Congress, 19th*, vol. 19, 2014, pp. 8496–8502.
- [142] A. A. Maciejewski and C. A. Klein, "The singular value decomposition: Computation and applications to robotics," *The International Journal of Robotics Research*, vol. 8, no. 6, pp. 63–79, 1989.
- [143] P. J. Antsaklis and A. Nerode, "Hybrid control systems: An introductory discussion to the special issue," *IEEE Transactions on Automatic Control*, vol. 43, no. 4, pp. 457–460, Apr 1998.
- [144] J. Stillwell, *Naive Lie theory*. Springer, 2008.
- [145] R. G. Sanfelice, M. J. Messina, S. Emre Tuna, and A. R. Teel, "Robust hybrid controllers for continuous-time systems with applications to obstacle avoidance and regulation to disconnected set of points," in *Proceedings of the 2006 American Control Conference*, 2006, pp. 3352–3357.
- [146] R. Goebel, R. G. Sanfelice, and A. R. Teel, "Hybrid dynamical systems," *IEEE Control Systems Magazine*, vol. 29, no. 2, pp. 28–93, 2009.
- [147] R. T. Rockafellar and R. J.-B. Wets, *Variational analysis*, 2nd ed. Springer, 2004.
- [148] R. Goebel, R. G. Sanfelice, and A. R. Teel, *Hybrid Dynamical Systems: modeling, stability, and robustness*. Princeton University Press, 2012.
- [149] W. Basener, *Topology and Its Applications*, ser. Pure and Applied Mathematics: A Wiley Series of Texts, Monographs and Tracts. Wiley, 2013.
- [150] C. G. Mayhew, R. G. Sanfelice, and A. R. Teel, "Quaternion-based hybrid control for robust global attitude tracking," *IEEE Transactions on Automatic Control*, vol. 56, no. 11, pp. 2555–2566, 2011.
- [151] C. Samson, M. L. Borgne, and B. Espiau, *Robot Control: The Task Function Approach*. Oxford University Press, 1991.

- [152] P. Baerlocher and R. Boulic, “An inverse kinematics architecture enforcing an arbitrary number of strict priority levels,” *The Visual Computer*, vol. 20, no. 6, pp. 402–417, 2004.
- [153] N. Mansard and F. Chaumette, “Directional redundancy for robot control,” *IEEE Transactions on Automatic Control*, vol. 54, no. 6, pp. 1179 – 1192, 2009.
- [154] A. Cherubini and F. Chaumette, “A redundancy-based approach for obstacle avoidance in mobile robot navigation,” in *IEEE/RSJ International Conference on Intelligent Robots and Systems*, Oct. 2010, pp. 5700–5705.
- [155] F. Caccavale and M. Uchiyama, *Handbook of Robotics - ch. 29. Cooperative Manipulators*. Springer, 2008.
- [156] B. V. Adorno, A. P. L. Bó, and P. Fraisse, “Kinematic modeling and control for human-robot cooperation considering different interaction roles,” *Robotica*, vol. FirstView, no. February, pp. 1–18, Feb. 2014.
- [157] B. Espiau, F. Chaumette, and P. Rives, “A new approach to visual servoing in robotics,” *IEEE Transactions on Robotics and Automation*, vol. 8, no. 3, pp. 313–326, 1992.
- [158] H. Hanafusa, T. Yoshikawa, and Y. Nakamura, “Analysis and control of articulated robot arms with redundancy,” in *8th Triennial World Congress of IFAC*, 1981, pp. 1927–1932.
- [159] P. Hespanha, “Logic-Based Switching Algorithms in Control by Logic-Based Switching Algorithms in Control,” Ph.D. dissertation, Yale University, 1998.
- [160] S. Ge, Z. Sun, and T. Lee, “Reachability and controllability of switched linear discrete-time systems,” *Automatic Control, IEEE Transactions on*, vol. 46, no. 9, pp. 1437–1441, Sep 2001.
- [161] T. Alpcan and T. Basar, “A stability result for switched systems with multiple equilibria,” *Dynamics of Continuous, Discrete and Impulsive Systems Series A: Mathematical Analysis*, vol. 17, no. 6, pp. 949–958, 2010.
- [162] P. Bolzern and W. Spinelli, “Quadratic stabilization of a switched affine system about a nonequilibrium point,” in *Proceedings of the American Control Conference*, vol. 5, June 2004, pp. 3890–3895 vol.5.
- [163] S. Mastellone, D. Stipanovic, and M. Spong, “Stability and convergence for systems with switching equilibria,” in *46th IEEE Conference on Decision and Control*, Dec 2007, pp. 4013–4020.
- [164] E. Navarro-Lopez and D. Laila, “Group and total dissipativity and stability of multi-equilibria hybrid automata,” *Automatic Control, IEEE Transactions on*, vol. 58, no. 12, pp. 3196–3202, Dec 2013.
- [165] L. F. C. Figueredo, B. V. Adorno, J. Y. Ishihara, and G. A. Borges, “Switching strategy for flexible task execution using the cooperative dual task-space framework,” in *IEEE/RSJ International Conference on Intelligent Robots and Systems*, 2014, pp. 1703–1709.
- [166] J. V. C. Vilela, L. F. C. Figueredo, J. Y. Ishihara, and G. A. Borges, “Quaternion-based  $H_\infty$  kinematic attitude control subjected to input time-varying delays,” in *2015 54th IEEE Conference on Decision and Control (CDC)*, Dec 2015, pp. 7066–7071.
- [167] N. Jacobson, *Basic Algebra I*, 2nd ed. W.H. Freeman and Company, 1985.